

JULIA FADJUKOV

# Electrical Communication and its Physiological Relevance in Retinal Pigment Epithelium



JULIA FADJUKOV

# Electrical Communication and its Physiological Relevance in Retinal Pigment Epithelium

ACADEMIC DISSERTATION

To be presented, with the permission of  
the Faculty of Medicine and Health Technology  
of Tampere University,  
for public discussion in the B1100 auditorium  
of the Pinni B building, Kanslerinrinne 1, Tampere,  
on 31 March 2023, at 13 o'clock.

ACADEMIC DISSERTATION  
Tampere University, Faculty of Medicine and Health Technology  
Finland

*Responsible  
supervisor  
and Custos*

Docent Soile Nymark  
Tampere University  
Finland

*Supervisor*

Docent Teemu Ihalainen  
Tampere University  
Finland

*Pre-examiners*

Professor  
Aparna Lakkaraju  
University of California, San  
Francisco  
USA

Professor  
Petri Ala-Laurila  
University of Helsinki  
Finland

*Opponent*

Professor  
Christophe Ribelayga  
University of Houston  
USA

The originality of this thesis has been checked using the Turnitin OriginalityCheck service.

Copyright ©2023 author

Cover design: Roihu Inc.

ISBN 978-952-03-2823-8 (print)

ISBN 978-952-03-2824-5 (pdf)

ISSN 2489-9860 (print)

ISSN 2490-0028 (pdf)

<http://urn.fi/URN:ISBN:978-952-03-2824-5>



Carbon dioxide emissions from printing Tampere University dissertations have been compensated.

PunaMusta Oy – Yliopistopaino  
Joensuu 2023

“Science has taught me that everything is more complicated than we first assume,  
and that being able to derive happiness from discovery is a recipe  
for a beautiful life.”

*-Hope Jabren, the author of Lab girl*



# ACKNOWLEDGEMENTS

The research presented in this thesis has been carried out during 2016–2023 in the Biophysics of the Eye research group at the Faculty of Medicine and Health Technology, Tampere University, and the former Department of Biomedical Sciences and Engineering, Tampere University of Technology, Tampere, Finland. For funding, I wish to thank Silmä- ja kudospankkisäätiö foundation, Finnish Cultural Foundation, Academy of Finland, Emil Aaltonen Foundation, Intrumentariumin tiedesäätiö Foundation, Tamperelaisen tutkimuksen tukisäätiö Foundation, TUT on World Tour mobility grant, and the Doctoral Program of Tampere University.

This thesis, my first step in a hopefully long journey into discovering how our vision works, would have been impossible without numerous people who deserve a huge thank you. First and foremost, I would like to thank my supervisor Adjunct Professor Soile Nymark, for everything she has taught me. Soile, your incredible attention to detail, action potential -like reaction time and willingness to allow your group members to pursue their own interests- are attributes I wish to carry forward to my future career. I will always warmly remember all the conference trips we shared, the ‘sidukka’ we still have never had, and our long discussions about academic life and beyond. I also want to thank my second supervisor Adjunct Professor Teemu Ihalainen, for his support throughout this thesis. You are an absolute wizard with confocal microscopy (and a continuous supply of high-class memes), and your passion for basic research has always inspired me. Soile and Teemu, you have shaped me into the scientist I am today. I could not have asked for better mentors, and I will continue to do my best to make you proud.

I am genuinely grateful to my steering group members for their efforts to bring this journey to its end. Professor Jari Hyttinen is kindly acknowledged for teaching me the value of networking and providing his engineering expertise in this thesis. I also wish to thank Professor Silvia Finnemann for her expertise on phagocytosis and for always having the time to discuss our work. Your intellect never stops to amaze me, and it was an honor having you visit our lab. I sincerely hope we stay in touch.

Furthermore, I wish to thank Professor Heli Skottman and Professor Maija Vihinen-Ranta, and all the members of their labs for providing us with their expertise

on stem cells and electron microscopy. I am also grateful to Professor Petri Ala-Laurila and Professor Aparna Lakkaraju for their insightful revisions that helped me improve this thesis. Lastly, I must extend this gratitude to Finland's wider vision research community, especially Professor Kristian Donner, for organizing the excellent Rodieck seminars that shaped my scientific curiosity and passion for this field.

Learning things for a living is incredible but sharing them with amazing co-workers is a privilege. I wish to thank my past and present colleagues at Tampere University, Tampere University of Technology, and the University of Tampere. Specifically, I am grateful to Aapo Tervonen, Toni Montonen, Viivi Karema-Jokinen, and Noora Nevala for their friendship. Aapo, our cycling trips solved most of my career problems, and I wanted to thank you for your support in writing this thesis. Because of you, I originally joined Soile's group, and I owe you everything. Toni, my bro-of-honor, I miss our daily heated arguments, your exceptional expertise on microscopes, and your ability to steer any conversation into weird places. Viivi, your ability to balance home and work inspires all female early career researchers. I will miss having someone as eager to nerd over endurance sports as I am.

Noora, my emotional support pony, you carried me through the last years of this thesis. I am so glad I got the chance to get to know you better, and your baking will be sorely missed! I also want to thank all the members of our current D222 office gang Jenni Partinen, Sanna Korpela, and Heidi Peussa. You guys were always there when I needed you the most; you made me laugh uncontrollably, forget failed experiments, and proofread various works along the way. You guys are incredibly talented, and I cannot wait to see what you do next. I am also grateful to Nemanja Milicevic, IElina Mäntylä, and Bobin Abraham for all the fruitful discussions and advice on pursuing a successful postdoctoral position. Lastly, I kindly thank the brilliant technicians Outi Heikkilä and Elina Lehtinen for being so helpful and saving me numerous times with all the last-minute orders and ideas.

Furthermore, I would like to thank Professor Gregory Schwartz for the opportunity to visit his research group at Northwestern University, USA, in 2018. Greg, your willingness to let a person studying RPE use your rigs all summer speaks for your enthusiasm for research and discovery. I am very grateful and honored to get a second chance to learn as much from you as possible in the coming years. In addition, I wish to thank everyone in Schwartz lab for making me feel so welcomed. Especially the talented lab manager Susan Wohlgenant, whose help made the short project possible. I also wish to thank now-alumni Sophia Wienbar. There are not



many people with whom you can spend nearly 24/7 in the dark doing something technically demanding and walk out as better friends, but I am glad I found one of them. Finally, I want to thank my gracious host Euan Parnell. You and Meg made Chicago feel much closer to home.

As much as I love science, life exists outside of Academia, and my life is better because of the people who are part of it. Rosa, Mona, and Suvi, your friendship means the world to me. I appreciate your patience during this thesis. I also want to thank my friend and coach, Arttu Peltola. Running has become an integral part of my creative process and problem-solving, and I would never have realized how much I enjoy it without your help.

Mom, you have believed in me since day one and taught me the value of working hard to achieve one's dreams. Jarno & Sari and Marko & Hannele, being an aunt to Ukko, Aune, and Milja is the most incredible honor I have ever received. Mervi & Hannu, joining the Fadjukov family has made me feel as if I now have two sets of supportive parents instead of one, for which I am grateful. Most importantly, I want to thank my dearest husband, Miika, for always being there for me. I am in awe of your work ethic and your always in-mint-condition style. Your love and support made all of this happen. Science sometimes takes me far, but by your side is where I will always feel most at home.

Julia Fadjukov  
Tampere, March 7, 2023



# ABSTRACT

Retinal pigment epithelium (RPE) is a tissue that preserves the health and functionality of its closely associated neural tissue, the retina. Many of the essential functions of RPE, including the renewal of light-sensing retinal photoreceptors, are regulated by ion channels. Yet, the involved ionic mechanisms, the extent of membrane potential dynamics, and the intercellular communication are not entirely understood. In this thesis, I studied the voltage-gated ion channels and electrical coupling of RPE in both human embryonic stem cell-derived and mouse RPE.

Voltage-gated sodium channels ( $\text{Nav}$ ), while best known for their role in action potential generation, are expressed in several non-excitabile cell types such as macrophages and astrocytes. Yet, these channels had not been considered to exist in native RPE, although they had occasionally been detected in cell culture. This thesis demonstrates that stem cell-derived and mouse RPE exhibit several subtypes of  $\text{Nav}$  channels and that their earlier dismissal was due to cell isolation procedures. Our electrophysiological recordings showed that these identified  $\text{Nav}$  channels are functional. The main channel subtypes  $\text{Nav}1.4$ – $\text{Nav}1.6$  and  $\text{Nav}1.8$  were found to localize in the cell-cell junctions or apical membrane in RPE.

As the conventional method to carry out electrophysiological recordings in RPE is to use single cells, the electrical connectivity had not been characterized in mammalian RPE, despite the importance of gap junctions in ocular development. In this thesis, we showed that the major connexin ( $\text{Cx}$ ) isoform was  $\text{Cx}43$  which was found to form both gap junctions and apical hemichannels. The electrophysiological recordings demonstrated that the electrical connectivity was relatively low despite the extensive network of gap junctions in RPE. Yet, it was modifiable by gap junction blockers or by inhibiting a specific kinase known as cyclin-dependent kinase 5 ( $\text{Cdk}5$ ).

The significance of  $\text{Nav}$  channels and gap junctions to RPE physiology was investigated by focusing on the renewal of photoreceptor outer segments, where phagocytosis by RPE plays a key role. The results demonstrated that  $\text{NaV}$  subtypes  $\text{NaV}1.4$  and  $\text{NaV}1.8$  localize with the outer segments during phagocytosis. Moreover, inhibiting the activity of  $\text{Nav}$  channels with pharmacological modulators or short hairpin RNA (shRNA) significantly impaired phagocytosis efficiency.

Furthermore, Nav channels were found to localize to the forming phagocytic cups in the apical membrane and the ingested phagosomes together with an endosomal marker Rab7. The results obtained in this thesis imply that Nav channels have versatile roles in phagocytosis.

In addition to Nav channels, Cx43 localized adjacent to outer segments during phagocytosis, and the results indicate that gap junctions are internalized during the process. This translocation of gap junctions was shown to be regulated by phosphorylation, particularly by kinases such as Cdk5 and protein kinase C. The results obtained in this thesis imply that Cx43 is involved in the formation of phagocytic cups. As phagocytosis is known to be under circadian control, and Cdk5 has previously been shown to regulate this cycle, it is plausible that Cdk5 helps to control the rhythm of photoreceptor renewal.

Our results highlight the complexity of RPE physiology and its ion channel machinery. The findings add to the growing body of evidence demonstrating that Nav channels' role is much more diverse than action potential generation. The results show that RPE can generate fast changes in voltage and rapidly modify its cell-cell connectivity across the epithelium. Gaining a deeper understanding of the involvement of ionic mechanisms in phagocytosis could help us to understand the phagocytosis pathway both in the healthy and diseased eye. Ultimately, this work highlights that RPE's role in its interaction with the neural retina is far more active than was previously thought.

# TIIVISTELMÄ

Verkkokalvon pigmenttiepiteeli (eng. retinal pigment epithelium, RPE) tekee tiivistä yhteistyötä verkkokalvon kanssa turvatakseen näköaistin toiminnan. Useita RPE:n tärkeitä tehtäviä, kuten valoa aistivien näköaistinsolujen uusiutumista, säädellään ionikanavien avulla. Näiden kanavien toimintaa ja RPE:n kykyä säädellä kalvopotentiaaliaan ei kuitenkaan vielä täysin ymmärretä. Tässä väitöskirjatyössä tutkittiin jänniteherkkien ionikanavien toimintaa sekä RPE:n sähköistä kytkeytyvyyttä käyttäen mallina ihmisen alkion kantasoluista erilaistettuja RPE-soluja sekä hiiren RPE-kudosta

Jänniteherkät natriumkanavat (Nav) tunnetaan parhaiten osallisuudestaan aktiopotentiaalien synnyssä hermosoluissa, mutta näiden kanavien tiedetään esiintyvän myös useissa muissa solutyypeissä, kuten makrofageissa ja astrosyyteissä, joissa aktiopotentiaaleja ei lähtökohtaisesti muodostu. Nav kanavien ei kuitenkaan uskottu esiintyvän RPE-kudoksessa huolimatta siitä, että niitä on toisinaan havaittu RPE-soluviljelmissä. Tämä väitöskirjatyö osoitti, että sekä kantasoluista erilaistetuissa RPE-soluissa että hiiren RPE-soluissa ilmenee useita Nav-kanavaperheen alatyyppejä. Samalla havaittiin, että aikaisempi virheellinen johtopäätös aiheutui tutkimusten suorittamisesta yksittäisillä soluilla toiminnallisen kudoksen sijaan. Tässä työssä osoitettiin myös löydettyjen Nav-kanavatyypien toiminnallisuus sähköfysiologisilla mittauksilla. Merkittävimpien kanavatyypien (Nav1.4–Nav1.6 sekä Nav1.8) havaittiin sijoittuvan solu-soluliitoksiin tai RPE:n apikaaliselle solukalvolle.

RPE-solujen sähköfysiologisia mittauksia on tyyppillisesti tehty yksittäisistä eristetyistä soluista. Tästä johtuen RPE-solujen sähköistä kytkeytyvyyttä ei ole selvitetty nisäkkäillä, vaikka tiedetään, että aukkoliitoksilla on tärkeitä tehtäviä silmän kehityksessä. Tämä väitöskirjatyö osoitti, että solujen merkittävin aukkoliitosproteiini (engl. Connexin, Cx) on Cx43, jonka havaittiin muodostavan sekä aukkoliitoksia että puolikkaita hemikanavia solujen apikaalisella pinnalla. Sähköfysiologiset mittaukset osoittivat, että RPE:n laajasta aukkoliitosten verkostosta huolimatta RPE-solujen välinen kytkeytyvyys on suhteellisen alhainen. Kytkeytyvyyttä voitiin kuitenkin säädellä aukkoliitosten farmakologisilla estäjillä, tai estämällä tietyn Cdk5 (engl. cyclin-dependent kinase 5) kinaasi-entsyymin toimintaa.

Nav-kanavien ja aukkoliitosten merkitystä RPE:n fysiologiassa tutkittiin keskittymällä näköaistinsolujen kalvojen uusiutumiseen, jossa RPE:n solusyönte eli fagosytoosi on merkittävässä roolissa. Tulokset osoittivat, että fagosytoosin aikana Nav-alatyypit Nav1.4 ja Nav1.8 esiintyvät lähellä näköaistinsolujen kalvopartikkeleita. Nav-kanavien toiminnan estäminen farmakologisesti tai geneettisesti (engl. short hairpin RNA, shRNA) vähensi merkittävästi fagosytoosin tehokkuutta. Lisäksi näiden kanavien havaittiin paikantuvan sekä apikaalipinnalle muodostuviin fagosytoosi-kuppeihin, että jo sisään otettuihin fagosomeihin yhdessä endosomien markkeriproteiinien (engl. rat sarcoma virus-related protein, Rab7) kanssa. Nämä tulokset antavat viitteitä siitä, että Nav-kanavilla olisi monipuolisia tehtäviä fagosytoosin aikana.

Nav-kanavien lisäksi myös Cx43:n havaittiin esiintyvän näköaistinsolujen kalvopartikkelien kanssa fagosytoosissa ja tulokset antavat viitteitä siitä, että aukkoliitoksia otetaan solujen sisälle prosessin aikana. Fosforylaation havaittiin säätelevän tätä aukkoliitosten siirtymää ja erityisesti Cdk5-, ja proteiinkinaasi C-entsyymeillä oli merkittävä rooli tässä säätelyssä. Tämän työn tulokset osoittivat, että Cx43 liittyy fagosytoosikuppien muodostukseen sekä solujen aktiini-tukirangan uudelleen järjestymiseen. Fagosytoosin säätelyn tiedetään perustuvan vuorokausirytmiiin ja mielenkiintoista on, että Cdk5-kinaasin on osoitettu vaikuttavan tähän rytmiiin. On siis mahdollista, että Cdk5 auttaa myös fagosytoosin ajoituksen säätelyssä.

Kokonaisuutena työni osoittaa RPE:n fysiologian ja sen ionikanavakoneiston säätelyn monimutkaisuuden. Nav-kanavien roolin on havaittu olevan huomattavasti monipuolisempi kuin aktiopotentiaalien muodostus hermosoluissa ja tuloksemme vahvistavat tätä käsitystä. Yksi työni yllättävimmistä ja merkittävimmistä tuloksista oli, että RPE voi säädellä kalvojännitettään ja epiteelikudoksen solujen välistä viestintäänsä nopeasti. Tarkemmat tiedot tämän ionisignaloinnin roolista fagosytoosissa lisäävät ymmärrystämme prosessista, joka on merkittävä näkökyvyillemme. Yhteenvetona tämä työ osoittaa, että RPE:n rooli yhteistyössä verkkokalvon kanssa on paljon aktiivisempi kuin on aikaisemmin luultu.

# CONTENTS

1	Introduction .....	19
2	Literature review .....	21
2.1	The vertebrate eye .....	21
2.2	The retina and retinal pigment epithelium are intimately associated .....	23
2.2.1	Phagocytosis of photoreceptor outer segments .....	25
2.3	Electrical signaling in RPE .....	30
2.3.1	Electrical characteristics of RPE tissue .....	30
2.3.2	How the resting membrane potential is established and regulated .....	31
2.3.3	Various voltage-gated ion channel families are found in RPE .....	32
2.3.4	Voltage-gated sodium channels (Nav) .....	34
2.3.5	Gap junctions .....	37
2.4	Circadian rhythm in the eye .....	41
2.4.1	How the rhythm is set .....	41
2.4.2	Circadian changes in gap junctional coupling .....	43
2.4.3	Circadian regulation of disk shedding and phagocytosis .....	44
2.5	Ionic mechanisms in the regulation of phagocytosis .....	46
3	Aims .....	50
4	Materials and methods .....	51
4.1	Ethics declaration (I, II, III) .....	51
4.2	hESC and iPSC derived RPE differentiation (I, II, II) .....	51
4.3	Animal handling (I, II, III) .....	52
4.4	Patch clamp experiments (I, II, III) .....	52
4.5	Phagocytosis assay for cultured and mouse RPE .....	54
4.6	Sample preparation for microscopy imaging .....	55
4.6.1	Immunocytochemistry (I, II, III) .....	55
4.6.2	Pre-embedding and cryosections .....	56
4.6.3	Fixed samples and live imaging .....	56
4.6.4	Electron microscopy .....	58
4.7	Western blot (I, II) .....	59
4.8	Pharmacology .....	60
4.9	Statistical analysis .....	60

5	Summary of the Results.....	62
5.1	Discovery of Nav channels and characterization of gap junctions in RPE (Study I and II).....	62
5.1.1	Several subtypes of Nav channels function in RPE .....	62
5.1.2	Cx43 is the major isoform in RPE, and electrical connectivity is low at baseline (Study II) .....	65
5.2	The role of Nav channels and gap junctions in phagocytosis .....	67
5.2.1	Nav channels and gap junctions translocate during POS phagocytosis (Study I, III).....	67
5.2.2	Nav1.4 translocation is inhibited by Nav blockers, Cx43 translocation is regulated by PKC and Cdk5 (Study I, III) .....	70
5.2.3	Inhibition of Nav channel activity and gap junction translocation decreases the efficiency of phagocytosis (Study I, III).....	72
6	Discussion.....	74
6.1	RPE cells are capable of fast electrical signaling.....	74
6.2	The electrical connectivity of RPE cells can be dynamically modified .....	77
6.3	Voltage-gated sodium channels and gap junctions are involved in the phagocytosis pathway .....	79
6.4	Are voltage-gated sodium channels and gap junctions in the RPE regulated by the circadian rhythm? .....	82
6.5	Future perspectives.....	84
7	Summary and Conclusions.....	86
8	References.....	87



# ABBREVIATIONS

AICS	Allen Institute for Cell Science
AKT	Protein kinase B
Anx2	annexin II
ATP	Adenosine triphosphate
BK	Big potassium
BEST-1	Bestrophin-1
BMAL1	Brain and muscle aryl hydrocarbon receptor nuclear translocator-like transcription factor
CAMKII	Calcium/calmodulin-dependent protein kinase II
cAMP	Cyclic adenosine monophosphate
CaV	Voltage-gated Ca <sup>2+</sup> channel
CK1	casein kinase 1
CD36	Cluster of differentiation 36, platelet glycoprotein-4
CDK5	Cyclin-dependent kinase 5
CNGC	Cyclic-nucleotide-gated channel
CLC	Voltage-gated Cl <sup>-</sup> channel
CLOCK	(Circadian Locomotor Output Cycles Kaput) transcription factor
CRALBP	retinaldehyde binding protein 1
Cry	Cryptochrome
Cx	Connexin (Protein)
DA	Dopamine
DBP	D-site-Binding Protein
E-box	Enhancer box
EEA1	Early Endosome Antigen 1
EGF	Epidermal growth factor
ERK1/2	Extracellular signal-regulated kinase 1/2
FAK	Focal adhesion kinase
GAPDH	glyceraldehyde 3-phosphate dehydrogenase
GJA1	Cx43 (gene)
GMP	Guanosine monophosphate
GTP	Guanosine triphosphate

hESC	human embryonic stem cell
hiPSC	human induced pluripotent stem cell
IP <sub>3</sub>	Inositol trisphosphate
KCNQ	M-type, K <sub>v</sub> 7
Kir	Inwardly rectifying K <sup>+</sup> channel
K <sub>v</sub>	Voltage-gated K <sup>+</sup> channel
MAPK	Mitogen-activated protein kinase
mEGFP	monomeric enhanced green fluorescent protein
MerTK	Mer receptor tyrosine kinase
MFGES8	Milk fat globule-EGF factor 8
MREG	Melanoregulin
mRNA	Messenger RNA
myoII	myosin II
Nav	Voltage-gated sodium channel (protein)
Per	Period
PI3K	Phosphoinositide 3-kinase
PKA	Protein kinase A
PKC	Protein kinase C
PLC	Phospholipase C
POS	Photoreceptor outer segment
Rab	Ras-related protein
Rac1	Ras-related C3 botulinum toxin substrate 1
Ras	Rat sarcoma virus
RCS	Royal College of Surge
RNA	Ribonucleic acid
RPE	Retinal pigment epithelium
RPE65	Retinoid isomerohydrolase
RT	Room temperature
SCN	Voltage-gated sodium channel (gene)
Src	Tyrosine kinase oncoprotein
TEP	Transepithelial electrical potential
TER	Transepithelial electrical resistance
Tyk2	Tyrosine kinase 2
REV-ERB	Retinoic acid-related orphan nuclear receptor
ROR	Retinoic acid-related orphan receptors
ZO-1	Zonula occludens-1

# ORIGINAL PUBLICATIONS

This dissertation is based on the following original peer-reviewed publications and a submitted manuscript, referred to as Study I–III in the text. The original publications are reproduced at the end of this thesis with the permission of the copyright holders.

Publication I Johansson JK\*, Karema-Jokinen VI, Hakanen S, Jylhä A, Uusitalo H, Vihinen-Ranta M, Skottman H, Ihalainen TO, Nymark S. Sodium channels enable fast electrical signaling and regulate phagocytosis in the retinal pigment epithelium. *BMC biology*. 2019 Dec;17(1):1–9.

Publication II Fadjukov J, Wienbar S, Hakanen S, Aho V, Vihinen-Ranta M, Ihalainen TO, Schwartz GW, Nymark S. Gap junctions and connexin hemichannels both contribute to the electrical properties of retinal pigment epithelium. *Journal of General Physiology*. 2022 Mar 11;154(4).

Publication III Fadjukov J\*\*, Wienbar S\*\*, Nemanja Milićević, Hakanen S, Vihinen-Ranta M, Ihalainen TO, Schwartz GW, Nymark S. CDK5 activity in retinal pigment epithelium contributes to gap junction phosphorylation and dynamics during photoreceptor outer segment phagocytosis. Manuscript.

\* Fadjukov, née Johansson

\*\*Authors contributed equally

# AUTHOR CONTRIBUTIONS

- Publication I Conception, design of the study, data acquisition, analysis, and interpretation, was performed by Johansson with contribution from Nymark. Karema-Jokinen contributed independently to the research related to genetic manipulation and its data analysis. Johansson and Karema-Jokinen both contributed to the electron microscopy sample preparation. Johansson and Nymark wrote the manuscript with contributions from all authors.
- Publication II Conception and design of the study and data interpretation were performed by Fadjukov with help from Nymark. The computational model was built by Wienbar and Schwartz. The experimental work and data analysis were conducted primarily by Fadjukov and Wienbar. All authors contributed to the writing and approved the final manuscript.
- Publication III Fadjukov and Wienbar contributed to experimental design as well as data acquisition and analysis together with Nymark. All authors contributed to the writing of the manuscript, with Fadjukov and Wienbar as primarily responsible.

# 1 INTRODUCTION

Vision is a fundamental sense, enabling us to appreciate the world we live in and allowing us to respond to the variation and challenges our environment presents. The visual system is also an attractive field of study because of its natural stimulus, the light, and because our eyes are the only directly accessible part of the central nervous system. The structure and organization of the retina have been extensively studied for over a century, and electrophysiological investigations on its functionality began decades ago. Many of those ground-breaking studies (Rabin 2013; Bae et al. 2018; Goetz et al. 2022;; Kuffler 1953; Baden et al. 2016; and reviewed by Sanes and Masland 2015 and Kerschensteiner 2022) have enabled us to discover the highly ordered subclasses of neurons that are packed into this relatively small piece of tissue and the circuitries that the neurons form. Yet, we still do not fully understand how vision works, which underlines the complexity of information processing that the retina encompasses.

To maintain viability, structural integrity, and excitability of the retina, it needs support from its closely associated tissue, the retinal pigment epithelium (RPE) (Bok 1993; Steinberg 1985). Many detrimental visual disorders originate from disruptions in the structure or functions of RPE. Among these disorders, age-related macular degeneration is considered the leading cause of vision loss in the elderly population in developed countries (Somasundaran et al. 2020). Deciphering the physiological mechanisms that govern and enable the numerous tasks of RPE is therefore crucial for understanding retinal functions and the molecular mechanisms underlying retinal pathologies.

The first electrophysiological studies of RPE in 1988 (Fox, Pfeffer, and Fain 1988) demonstrated that the physiology of this tissue is versatile and complex (Wimmers, Karl, and Strauss 2007). Yet, the electrical properties of RPE are not entirely understood, particularly in terms of its membrane potential dynamics and cell-cell communication. In this thesis, I aimed to improve our knowledge of the physiology of RPE by focusing on its voltage-gated ion channels and gap junctions. I used human embryonic stem cell-derived RPE and mouse RPE as model systems to reach this objective. My studies demonstrated that this non-excitabile tissue,

remarkably, shows a diversity of voltage-gated sodium channels and an ability to modulate its electrical coupling. Moreover, the data showed that both ionic mechanisms are essential regulators for one of the critical tasks of RPE – the turnover of membrane material of the light-sensing retinal photoreceptors. The findings suggest that mature RPE cells have the cellular machinery to electrically communicate with these retinal sensory neurons. Overall, the results indicate that RPE can rapidly modulate its physiology to fulfill its versatile roles as an interactive partner in vision.

## 2 LITERATURE REVIEW

### 2.1 The vertebrate eye

The eyes of all vertebrate species share a common structural plan resembling a pinhole camera. Incoming light enters the eye through the pupil. It is focused on the interior eye by the cornea and the lens to form an inverted image to the retina. Light distribution information is eventually conveyed as neural code to the higher visual centers of the brain via the optic nerve (Willoughby et al. 2010; Hoon et al. 2014). The interior eye (Figure 1) is comprised of the neural retina that captures and transduces the light into electrical signals, its underlying retinal pigment epithelium (RPE), and a vascular structure known as the choroid (Willoughby et al. 2010). The RPE is connected to the choroid via a supportive extracellular matrix, Bruch's membrane (Murali et al. 2020). These structures help to provide both oxygen and nutrients to the outer retinal layers (Willoughby et al. 2010).

Processing of visual information begins with the conversion of light to electrical signals. The neural retina is a complex and highly organized multi-layered structure formed by six broad classes of neurons and their supportive cells, the Müller glia (Hoon et al. 2014; Wu 2010; Willoughby et al. 2010). These neuronal classes include the light-sensing photoreceptors that typically are rods and cones in vertebrates. The two photoreceptor types can be separated by their morphology, type of photopigment (opsins), retinal distribution, density, and synaptic connections. The rod and cone systems are also targeted for different features of vision. The rod system is universally much more sensitive but offers less acuity, while the cone system provides higher spatial resolution at the expense of sensitivity. Accordingly, cones mediate daytime (photopic) vision and help us to distinguish colors, while rods dominate at low light levels (scotopic vision). Both rods and cones contribute at intermediate (mesoscopic) light levels (Mustafi, Engel, and Palczewski 2009; Ingram, Sampath, and Fain 2016; Peichl 2005; Tikidji-Hamburyan et al. 2017). In mammals, the ratio of rods and cones is species-dependent but tends to correlate with the daily activity pattern. Generally, the proportion of rods is higher in nocturnal animals (Peichl 2005). The ratio is also dependent on retinal origin, for instance, in humans

the density of cones is much higher in the central retina known as the macula (Mustafi, Engel, and Palczewski 2009; Okano et al. 2012).

Both rods and cones have a distinctive single structural cilium known as the outer segment (OS) that accommodates a stack of 1,000 – 2000 membrane disks and a very high concentration (3–5mM) of the visual pigment (Palczewski 2006). In rods, these disks are autonomous and isolated by a plasma membrane. In contrast, in cones, the outer segment is formed of a continuous, deeply invaginated membrane that does not close to create individual disks. The orientation along the light path and the substantial visual pigment density of the outer segments help to increase the probability of light absorption by photoreceptors (Genovese, Reisert, and Kefalov 2021; Bowmaker and Dartnall 1980 and reviewed by Palczewski 2006; Hubbell and Bownds 1979). The visual transduction cascade is initiated when a chromophore known as retinal, covalently attached to the photopigment formed by opsin protein, absorbs photons. This absorption leads to isomerization of the chromophore to all-trans configuration and conformational changes in the opsin protein. Ultimately, the subsequent biochemical cascade prompts the closure of cation-conducting cyclic nucleotide-gated channels (CNGCs) at the photoreceptor outer segment membrane and a hyperpolarizing membrane potential change (Farahbakhsh, Hideg, and Hubbell 1993; Hoon et al. 2014; Fu and Yau 2007). The resulting electrical signals are then processed by retinal neurons in the inner retina. These neurons are not in this thesis's scope but include bipolar cells, horizontal cells, amacrine cells, and ganglion cells that form many functionally overlapping circuits. The individual layers of the retina are comprised of the cell bodies (nuclear layers) and connective synapses (plexiform layers) of its neurons, and its general organization has been well-conserved among various vertebrate species (Hoon et al. 2014; Nag and Wadhwa 2012, reviewed by Willoughby et al. 2010).



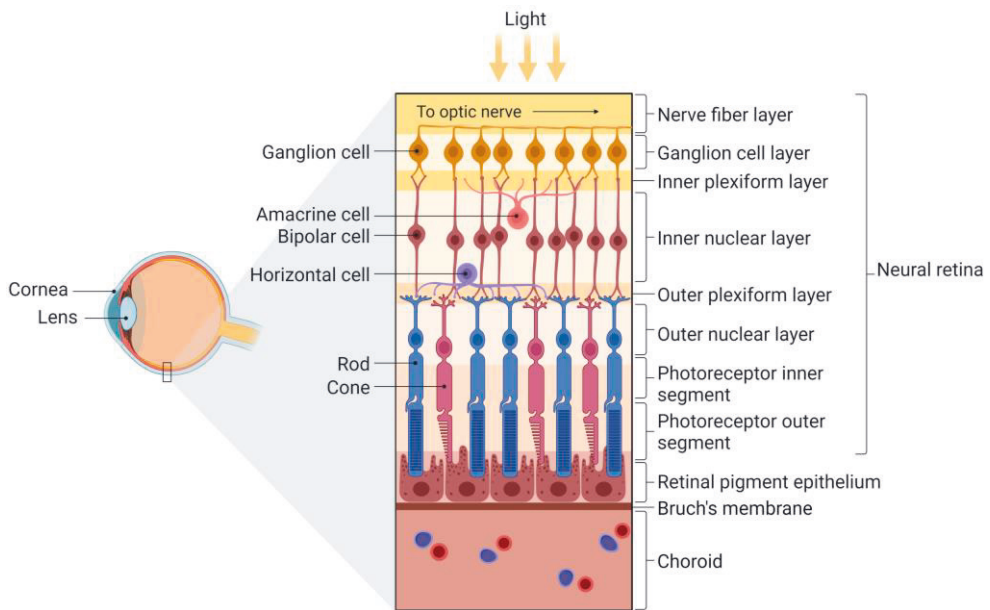


**Figure 1.** A schematic illustration of the typical structure of the vertebrate eye. Light is focused on the interior eye by the lens and the cornea. The retina comprises several classes of neurons that form its different layers. Photoreceptors are in contact with the retinal pigment epithelium, which in turn is supported by the vascular structure known as the choroid. The extracellular matrix known as Bruch's membrane connects the epithelium and the choroid. Adapted from "Structure of the Retina" by BioRender.com (2022). Retrieved from <https://app.biorender.com/biorender-templates>.

## 2.2 The retina and retinal pigment epithelium are intimately associated

The RPE and retina are derived from the neuroectoderm that lines the optic vesicle during embryogenesis. This close association is preserved in the adult eye as the epithelium extends across the whole length of the retina, and the two tissues can be separated by a space as narrow as 10–20 nm (Steinberg and Wood 1974). This space is known as the subretinal space or interphotoreceptor matrix, comprised of organized proteoglycans, glycoproteins, fluids, ions, and metabolites (Ishikawa, Sawada, and Yoshitomi 2015). The RPE is a single continuous monolayer of heavily pigmented cells whose functions are vital for the maintenance and survival of photoreceptors (reviewed in Strauss, 2005 and summarized in figure 2). A defect in any of its functions can lead to retinal degeneration and even blindness (Strauss 2005). These functions range from serving as a protective barrier, secretory

epithelium, and a professional phagocyte, and they are enabled by the unique structure and localization of this tissue (Steinberg 1985, reviewed by Lakkaraju et al. 2020). RPE cells are highly polarized (Caceres and Rodriguez-Boulan 2020), and their apical microvilli are intertwined with photoreceptors' light-sensing outer segments. The cells are bound together by a complex of three junctions (adherens, gap, and tight junctions) whose functions are interlinked (Hartsock and Nelson 2008; Mellman and Nelson 2008). Tight junctions limit the flow of fluids and solutes (discussed in chapter 2.2.1) and enable RPE to serve as part of the outer blood-retinal barrier (for review, see Lawrence J. Rizzolo 2007). Furthermore, tight junctions help to establish polarity and separate protein composition between the apical and basal sides. Along with adherens junctions, they help regulate cell shape and proliferation and strengthen the bonds between neighboring cells (Lawrence J. Rizzolo 2007; Lawrence J. Rizzolo et al. 2011). Gap junctions are discussed in chapter 2.3.5.

RPE actively participates in the visual transduction cascade by regenerating the photopigments. The visual chromophores (now all-trans-retinol) diffuse to RPE through the subretinal space, where they are re-isomerized from the all-trans configuration into 11-cis-retinal. The chromophores are then transported back to photoreceptors to maintain their excitability (Strauss 2005; Bok 1990). Moreover, RPE cells show polarized expression of  $\text{Na}^+/\text{K}^+$ -ATPase and various other pumps and channels that help to stabilize the ionic homeostasis of subretinal space and to preserve photoreceptor health (Wimmers, Karl, and Strauss 2007). RPE also helps to prevent retinal photo-oxidation and improves image resolution by absorbing scattered excess light by its pigment granules or melanosomes (Sparrow, Hicks, and Hamel 2010; Weingeist 1982) and buffer the changes in subretinal  $\text{K}^+$  concentration following light detection (Shahi et al. 2017). RPE cells help to renew the outer segments of photoreceptors to combat the build-up of photo-oxidative radicals caused by light exposure, (Lakkaraju et al. 2020; Young and Bok 1969; Mazzoni, Safa, and Finnemann 2014) that is discussed in detail in chapter 2.2.1.

Photoreceptor function requires an intricate balance of proteins, lipids, and metabolites, which, if disrupted, can result in retinal degeneration. RPE serves as a selective membrane between the choroidal blood supply and the neural retina. RPE cells transport nutrients such as glucose (To and Hodson 1998; Swarup et al. 2019) and fatty acids and can secrete growth and immunosuppressive factors. They help maintain the structural integrity and function of the photoreceptors and preserve the eye's immune privilege (Strauss 2005). Lastly, metabolic end products (Hamann et al. 2003), water, and ions produced by intraocular pressure and the sizeable metabolic

turnover of retinal neurons can be transported from the subretinal space to the bloodstream (Strauss 2005).

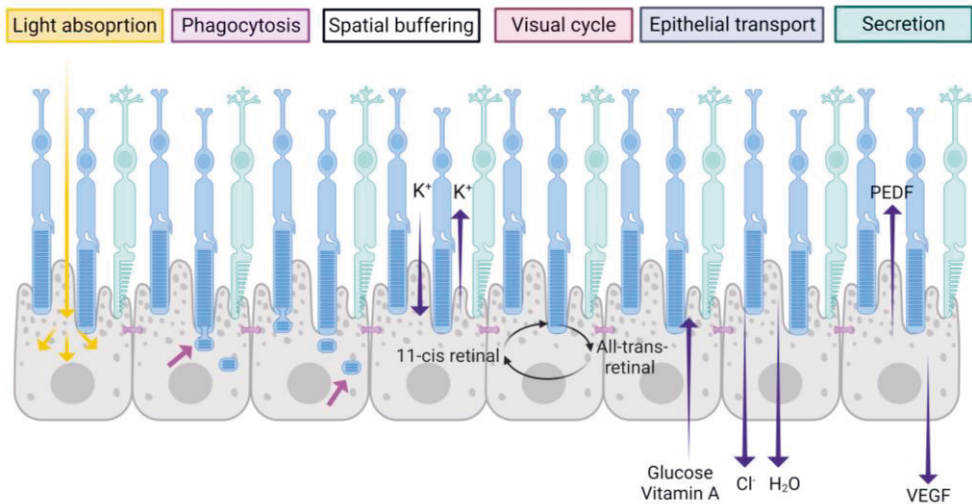


**Figure 2.** A schematic illustration of the integrative functions between photoreceptors and the underlying RPE enveloping the outer segments. The epithelium absorbs excess light, provides spatial buffering, transports nutrients and water, and secretes growth factors such as pigment epithelium-derived factor (PEDF) and vascular Endothelial Growth Factor (VEGF) (the black arrows demonstrate the direction of movement). In addition, RPE recycles the visual pigment and helps the photoreceptors to renew their membranes through phagocytosis (purple arrows). The illustration was created with BioRender.com by re-creating with modifications from (Strauss 2005).

## 2.2.1 Phagocytosis of photoreceptor outer segments

The turnover of photoreceptor outer segments (POS) is one of the most extensively studied cases of specialized phagocytosis (Nguyen-Legros and Hicks 2000; M. O. Hall, Bok, and Bacharach 1969; Young 1978; Young and Bok 1969; Mao and Finnemann 2013; for a review see Kwon and Freeman 2020), yet many unresolved questions remain regarding its regulation. Photoreceptor renewal presents an enormous metabolic load for RPE cells. It is estimated that depending on species and retinal location, every RPE cell serves a range of 20–45 photoreceptors, and the entire POS population is renewed every two weeks (Strauss 2005; Kwon and Freeman 2020). This renewal is under circadian regulation and occurs daily (discussed in chapter 2.4.3). The peak time of phagocytosis is species-dependent, but

generally, for rods, it occurs at light onset and for cones at light offset (LaVail 1976, 1980; Young and Bok 1969; Ailis L. Moran et al. 2022). Moreover, RPE cells are considered largely postmitotic in the adult retina and thus do not typically divide, making them the most active phagocytes in the body (Nandrot and Finnemann 2006).

To maintain the constant length of the POS, outer segments are constantly formed at their base, while the aged disks containing the highest amounts of radicals and photo-damaged proteins and lipids are removed at the OS tips (Young and Bok 1969). The formation of new disks requires a balanced cycle of actin polymerization and disassembly to flatten and expand the disks and finally enclose them (reviewed by Spencer et al. 2020). The membrane turnover was initially discovered with autoradiography labeling and thus did not reveal the renewal of cones due to the continuous structure of their OS. While OS renewal is known to occur for cones, much less is currently known about their interaction with RPE (Anderson, Fisher, and Steinberg 1978; Jonnal et al. 2010; Steinberg 1974). RPE cells bind and degrade the POS through a complicated molecular pathway (summarized in figure 3). Studies have shown that preceding the peak of POS phagocytosis, the OS tips display higher concentrations of phosphatidylserine (PtdSer), the classical “eat me” signal for phagocytosis (Ruggiero et al. 2012). In apoptosis, this switch in lipid composition is believed to be regulated by enzymes such as flippases (Ailis L. Moran et al. 2022; K. Segawa et al. 2014). Interestingly, as the PtdSer accumulates, the RPE microvilli extend and can reach even half-way up (approximately 15  $\mu\text{m}$ ) the POS length (Kwon and Freeman 2020). The exposed PtdSer can then be bound by CD36 receptors on the apical surface of RPE (S. C. Finnemann and Silverstein 2001) or be trapped by secreted molecules such as Growth Arrest Specific 6 (Gas6), Protein S (ProtS) (Michael O. Hall et al. 2005), and milk fat globule-EGF factor 8 (MFG-E8) (Hanayama et al. 2002; Ruggiero et al. 2012). These molecules also serve as ligands for the phagocytosis receptors found in the apical membrane of RPE (Ruggiero et al. 2012).

The binding of POS via phagocytosis receptor  $\alpha\text{v}\beta\text{5}$  integrin (S. C. Finnemann et al. 1997) initiates downstream signaling pathways and is regulated by kinases such as phosphoinositide 3-kinases (PI3K), protein kinase C (PKC) and serine/threonine kinase 1 (AKT), but the underlying mechanisms are not entirely understood (Bulloj, Duan, and Finnemann 2013; S. C. Finnemann and Rodriguez-Boulan 1999; M. O. Hall, Abrams, and Mittag 1991). It should be noted that while individual phagosomes tend only to have diameters of 1-2  $\mu\text{m}$ , a single RPE cell must engulf 30 or more phagosomes at once. Thus, the process requires a substantial reorganization of F-

actin and the delivery of a new membrane (Kwon and Freeman 2020). It is also important to state that while recognition and binding of POS are necessary for phagocytosis, they alone are not sufficient to induce engulfment. This evidence was discovered with Royal College of Surgeons (RCS) line rats that lack the second essential phagocytosis receptor Mer receptor tyrosine kinase (MerTK). RPE cells from this line can bind POS similarly to control, but only a limited number of them are internalized (Chaitin and Hall 1983). MerTK ligands are also sufficient to induce POS ensheathment, while the addition of MFG8 has been shown to cause accumulation of unensheathed POS at the RPE apical surface (Almedawar et al. 2020).

The process of particle engulfment has been extensively studied in macrophages. It is thought to depend on the formation of actin-mediated pseudopods that are fused to envelop the particle. In macrophages, membrane fusion requires the orchestrated activity of multiple proteins, such as cadherins and catenins, which form complexes that lead to the formation of radial actin bundles. The resulting adherens junctions help to fuse the advancing pseudopods. To date, it is uncertain whether a similar process occurs in RPE (Kevany and Palczewski 2010). The activation of MerTK occurs via phosphorylation through integrin-associated focal adhesion kinase (FAK) activation (Nandrot et al. 2004; Silvia C. Finnemann 2003). In addition to FAK, integrin activates a member of the GTPase family Ras-related C3 botulinum toxin substrate 1 (Rac1) that is involved in phagocytic cup formation via F-actin rearrangement (Mao and Finnemann 2012). F-actin is also recruited downstream of activated MerTK as it generates docking sites for Src homology 2 (SH2) proteins such as PI3K (Shelby et al. 2013; Bulloj, Duan, and Finnemann 2013). Inhibition of PI3K has also been shown to have a role in F-actin rearrangement independent of AKT. The inhibition of PI3K leads to increased levels of F-actin in the phagocytic cups (Bulloj, Duan, and Finnemann 2013), possibly because PI3K regulates the modifications of phospholipids which in turn can help to activate Rac1 (Kwon and Freeman 2020).

Furthermore, MerTK has been shown to regulate the redistribution of myosin II (myoII) that, alongside annexin AII (Anx2), possibly controls the formation or closure of the phagocytic cups (Strick, Feng, and Vollrath 2009; Bulloj, Duan, and Finnemann 2013). Myosin recruitment has also been shown to be regulated by AKT (Lakkaraju et al. 2020). Lastly, proteolytic cleavage of MerTK from the cell surface could act as a negative feedback loop to limit POS binding (Law et al. 2015). The POS ingestion rate is also regulated by intracellular cyclic adenosine monophosphate cAMP, possibly increasing the POS engulfment by stimulating both  $\beta$ -adrenergic and A2 adenosine receptors (M. O. Hall, Abrams, and Mittag 1993; Gregory,

Abrams, and Hall 1994). To date, most of the studied regulatory proteins are localized to RPE, but more recent studies have shown that specific proteins found on cone OS can also regulate the rate of phagocytosis. Specifically, the lack of ciliary proteins kinesin family member 17 (Lewis et al. 2018) or Ras-related protein 28 (Rab28) (Ailís L. Moran et al. 2022; Carter et al. 2020) has been shown to decrease the number of phagosomes found in RPE in zebrafish.

Once RPE has internalized the POS, they undergo gradual acidification by vacuolar-type H<sup>+</sup>-ATPase while migrating to the basal side through the endo/lysosomal pathway (Lakkaraju et al. 2020; Deguchi et al. 1994). These maturation steps of the phagosomes involve switches in the associated Rab proteins, such as Rab5 to Rab7, that mediate membrane fusion events and microtubule-based movement. Of these proteins, Rab5 and another protein Early Endosome Antigen 1 (EEA1), are generally considered markers for early endosomal events (Kwon and Freeman 2020). The motility of phagosomes is regulated by kinesin motor proteins and their associated kinesin-1 light chain 1 (Jiang et al. 2015; Esteve-Rudd et al. 2018). Proteases responsible for the stepwise digestion of rhodopsin include proteins such as caveolin-1 (Sethna et al. 2016), cathepsin S and D, as well as lysosomal protein melanoregulin (MREG) (Mazzoni, Safa, and Finnemann 2014; Bosch, Horwitz, and Bok 1993). Eventually, some of the molecular content of digested POS, such as retinal and fatty acids, can be recycled back to photoreceptors (Strauss 2005). The complete removal of ingested POS material is crucial; otherwise, the oxidized proteins and lipids may accumulate as granules known as lipofuscin (Caceres and Rodriguez-Boulan 2020). As some level of accumulation occurs through healthy aging, it is crucial to understand how the phagocytosis process is regulated and how the pathologies originate (Kwon and Freeman 2020). In addition to the proteins described in this chapter, various ion channels, especially Ca<sup>2+</sup> channels, are considered important for the pathway. These are discussed in more detail in chapter 2.5.

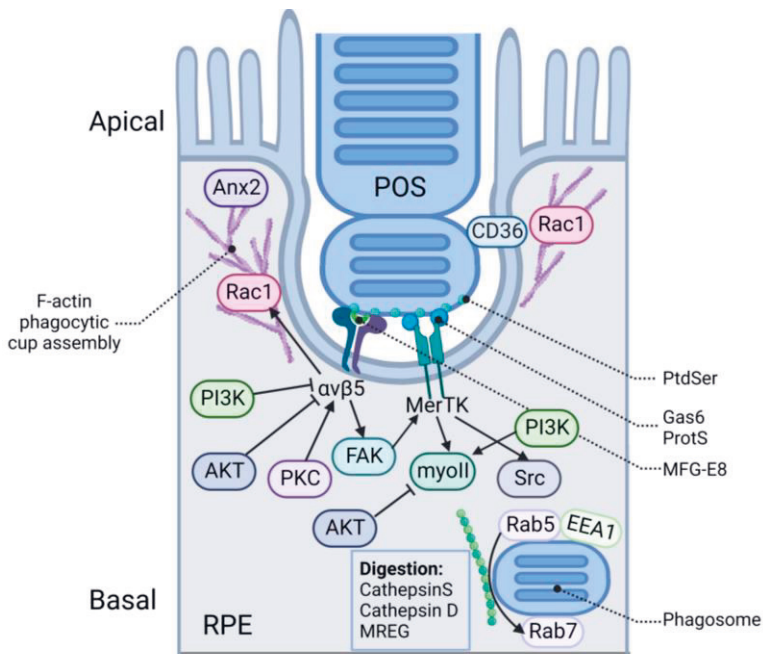


**Figure 3.** A schematic illustration of the molecular pathway of POS phagocytosis. The POS are bound by integrin  $\alpha\text{v}\beta 5$  through its ligand (MFG-E8) and exposed PtdSer residues. The internalization step involves the reorganization of the actin cytoskeleton through Rac1 and Anx2 and the activation of MerTK, which has its own ligand (Gas6, ProtS). The ingested phagosomes are transported via motor proteins (myoII) to the basal side while being degraded in a stepwise manner through endo/lysosomal pathways regulated by Rab, EEA1, and Cathepsin proteins. Details for the roles of individual proteins acting downstream of  $\alpha\text{v}\beta 5$  and MerTK are provided in the main text. The illustration was re-drawn with modifications based on (Mazzoni, Safa, and Finnemann 2014; Strauss 2005; Kwon and Freeman 2020; Müller and Finnemann 2020) and created with BioRender.com. Abbreviations: POS: photoreceptor outer segment, PtdSer: phosphatidylserine, MFG-E8: milk fat globule-EGF factor 8, Rac1: ras-related C3 botulinum toxin substrate 1, Anx2: annexin II, MerTK: Mer receptor tyrosine kinase, Gas6: Growth Arrest Specific 6, ProtS: Protein S, myoII: myosin II, Rab: ras-related protein, EEA1: early Endosome Antigen 1, CD36: a cluster of differentiation 36, PI3K: phosphoinositide 3-kinase, FAK: focal adhesion kinase, AKT: protein kinase B, Src: Tyrosine kinase oncoprotein, MREG: melanoregulin.

## 2.3 Electrical signaling in RPE

### 2.3.1 Electrical characteristics of RPE tissue

All epithelia can be classified as leaky or tight depending on how readily ions can cross between the cells (paracellular) relative to their transport through the cells (transcellular). In RPE, the paracellular transport is regulated by tight junctions that also define the baseline tightness of the epithelial barrier (for a review, see Lawrence J. Rizzolo 2007). The transepithelial ion transport can be modeled conceptually by imagining the apical and basolateral sides as two electrically coupled membranes that are arranged in series, while tight junctions form the boundary that separates them. This model connects tight junctions parallel to the transepithelial ion movement. The barrier function of RPE can be investigated by measuring a property known as transepithelial electrical resistance (TER). The TER values obtained from RPE cells are species-dependent but generally range from 135 to 600  $\Omega \times \text{cm}^2$ . Regardless, TER is an effective measurement of RPE monolayer maturity and polarization. It is often used to assess the barrier properties of RPE cells *in vitro*, as the value increases overtime from enucleation (in the case of primary RPE) and after cell plating (Lawrence J. Rizzolo et al. 2011; Fernandez-Godino, Garland, and Pierce 2016). Typically, for cultured RPE, TER values exceeding 200  $\Omega \times \text{cm}^2$  are considered a reliable marker for barrier integrity.

All polarized epithelia maintain a difference in membrane voltage between the apical and basolateral sides. This potential difference is known as transepithelial electrical potential (TEP), which results from varying spatial distribution of ion pumps, channels, and leak conductances that maintain the ion gradients across the tissue (Cao et al. 2018; Tran et al. 2013; Lawrence J. Rizzolo et al. 2011; Miller and Steinberg 1977). These ionic gradients also control the movement of ions from the subretinal space toward the choroid and vice versa. Accordingly, the values of TEP change when the membrane permeability changes ( $\text{TEP} = V_{\text{Basolateral}} - V_{\text{apical}}$ ). Typically, the values of TEP in epithelia range between 1–10 mV (Saw et al. 2022). In RPE, the values vary depending on the species. For example, a TEP of 1.6 mV has been reported for canine RPE and 8.0 mV for bovine RPE (Lawrence J. Rizzolo et al. 2011). In such experiments, TEP is measured by placing an electrode on each side of the tissue while the reference is set to the subretinal space, meaning that the basolateral membrane potential is more depolarized (Immel and Steinberg 1986;



Griff and Steinberg 1984). TEP has been shown to change in response to aging or pathological states such as age-related macular degeneration (Cao et al. 2018).

### 2.3.2 How the resting membrane potential is established and regulated

The various functions of RPE are tightly associated with changes in ion channel activities that permit rapid, highly selective, and regulated movement of ions. Therefore, electrophysiological investigations of RPE are crucial for understanding the mechanisms that enable the tissue to support visual function. The movement of ions across the cellular membrane is driven by differences in ion concentrations and charge between the inside and outside of the cell, known as the electrochemical gradient. Each type of ion moves down its electrochemical gradient, and the net movement ceases at its subjective reversal potential. Reported values for the resting membrane potential are often more depolarized for cultured RPE cells ( $\sim -30\text{mV}$ ) (Kokkinaki, Sahibzada, and Golestaneh 2011; Tao and Kelly 1996), but *in situ* and in freshly isolated cells, values of  $\sim -60\text{ mV}$  have been reported for many species (Quinn and Miller 1992; Y. Segawa and Hughes 1994; Botchkin and Matthews 1994).  $\text{Na}^+$  and  $\text{Ca}^{2+}$  ions have higher concentrations on the extracellular side, and the electrochemical gradient is driven towards the cell interior at the resting membrane potentials.  $\text{K}^+$  ions, on the other hand, exhibit opposite electrochemical gradients, and their movement is driven towards the extracellular space (Wimmers, Karl, and Strauss 2007; Dvoriashyna et al. 2020). The apical membrane of RPE exhibits a large  $\text{K}^+$  conductance enabled by its Kir channel family (discussed in chapter 2.3.3) (Joseph and Miller 1991). With their negative reversal potential and high membrane permeability at rest, these ions also maintain the hyperpolarized resting membrane potential in non-excitable cells.  $\text{Cl}^-$  concentration gradient is towards the intracellular side. Yet, as its reversal potential is close to the typical resting membrane potential of RPE, the direction of the flow is not as straightforward as it is with the other ions and can fluctuate depending on the physiological state (Dvoriashyna et al., 2020; Wimmers et al., 2007).

Various transporters establish and maintain these electrochemical gradients that can move ions against their electrochemical gradients by hydrolyzing ATP or by exchanging or co-transporting the ion with another ion carried down its electrochemical gradient (Wimmers, Karl, and Strauss 2007; Neverisky and Abbott 2015). In RPE, the steep gradient for  $\text{Na}^+$  is maintained by the electrogenic  $\text{Na}^+/\text{K}^+$ -

ATPase, which, unlike in many other epithelial tissues, is localized predominantly to the apical rather than basolateral membrane (Okami et al. 1990; L. J. Rizzolo 1990; Griff, Shirao, and Steinberg 1985; Miller and Steinberg 1977). This unique localization of  $\text{Na}^+/\text{K}^+$ -ATPase may be caused by the reversed polarity of other cytoskeleton-associated proteins in RPE, such as ankyrin (Gundersen, Orłowski, and Rodriguez-Boulan 1991) and by the presence of  $\text{Na}^+/\text{K}^+$ -ATPase subunit  $\beta_2$  (Lobato-Álvarez et al. 2016).

Small changes in  $\text{Ca}^{2+}$  ion concentration can significantly affect cell functions. Since this ion has a high affinity for proteins, its binding can induce conformational changes that lead to changes in protein functionality. Furthermore,  $\text{Ca}^{2+}$  can act as a second messenger in multiple signaling cascades. Therefore, its intracellular concentration is usually kept very low, and its changes tend to be very localized within the cell (Clapham 2007). Cells achieve this by actively sequestering  $\text{Ca}^{2+}$  to intracellular stores. In RPE, the total intracellular  $\text{Ca}^{2+}$  concentration is typically 15 mmol/l which is considerably higher than in other cells, of which a large proportion is stored in melanosomes (Hess 1975; Wimmers, Karl, and Strauss 2007).  $\text{Na}^+/\text{Ca}^{2+}$  exchanger maintains RPE's low cytosolic  $\text{Ca}^{2+}$  concentration (Fijisawa, Ye, and Zadunaisky 1993; Loeffler and Mangini 1998) and  $\text{Ca}^{2+}$ -ATPase (Kennedy and Mangini 1996), which both help to transport  $\text{Ca}^{2+}$  out the cytoplasm. The high intracellular concentration of  $\text{K}^+$  is generated by  $\text{Na}^+/\text{K}^+$ -ATPase and another apical cotransporter,  $\text{Na}^+/\text{K}^+/\text{2Cl}^-$ .

### 2.3.3 Various voltage-gated ion channel families are found in RPE

Voltage-gated ion channels are responsible for generating electrical signals in cells and are thus an integral part of physiology. These channels share common structural features (an example of  $\text{Nav}$  channels can be found in figure 4) but differ functionally by their voltage-dependent activation, inactivation, permeability to various ions, and pharmacological characteristics (W. A. Catterall 1995; Wimmers, Karl, and Strauss 2007). Once activated, these channels facilitate the movement of ions across the cell membrane along an electrochemical gradient. Depending on the ions, they can be classified as voltage-gated potassium ( $\text{K}_V$ ), calcium ( $\text{Ca}_V$ ), chloride (CLC), and sodium channels ( $\text{Na}_V$ ) (de Lera Ruiz and Kraus 2015). To date, several different ion channel families have been identified in RPE (reviewed in Wimmers, Karl, and

Strauss 2007; Reichhart and Strauss 2014). The characterization of these ion channels has been made possible by patch clamp recordings described in chapter 4.4.

K<sup>+</sup> channels comprise one of the most prominent families of ion channels in RPE, and inwardly and outwardly rectifying currents have been reported (Wimmers, Karl, and Strauss 2007; Korkka, Skottman, and Nymark 2022; Pattnaik and Hughes 2012; Wollmann et al. 2006; Pinto and Klumpp 1998). Many members of this family have been identified in RPE, including delayed rectifier channels, M-type (KCNQ, K<sub>v</sub>7), and A-type channels (Korkka, Skottman, and Nymark 2022; Pattnaik and Hughes 2012). Inwardly rectifying K<sup>+</sup> channels (Kir) have also been found in RPE and are known to support subretinal K<sup>+</sup> homeostasis, but this family is not traditionally included in voltage-gated channels (Kumar and Pattnaik 2014). In RPE, K<sub>v</sub> channels are found on both apical and basolateral membranes. They have been linked to the generation of membrane potential and buffering of K<sup>+</sup> in the subretinal space (Shahi et al. 2017), as well as control of cell volume and transport of ions and water (Wimmers, Karl, and Strauss 2007; Grunnet et al. 2003).

CLC channels have been identified in the RPE in cell membranes, or intracellular organelles such as endosomes (Wimmers, Karl, and Strauss 2007; Korkka et al. 2018; Weng et al. 2002; Hanke-Gogokhia et al. 2021), and they have been implicated in various processes such as cell division and migration (Zhao et al. 2017), POS phagocytosis, secretion of growth factors (Mamaeva et al. 2021), preservation of the subretinal homeostasis (Hanke-Gogokhia et al. 2021) and possibly fluid transport (Wimmers, Karl, and Strauss 2007). The CLC channel family opens in response to hyperpolarization and conducts inwardly rectifying currents (Wimmers, Karl, and Strauss 2007).

Cav channels form a versatile family defined by physiological and pharmacological characteristics (William A. Catterall 2011). To date, both slow (L-type) and fast inactivating (T-type) currents have been identified in RPE, and both types activate in response to membrane depolarization. The localization of Cav channels depends on the channels subtype and has also been shown to change during RPE maturation (Müller et al. 2014; Korkka et al. 2019; Wimmers, Coeppicus, et al. 2008). Cav channels have been implicated in various tasks of RPE, such as phagocytosis and growth factor secretion (Müller et al. 2014; Korkka et al. 2019). The family of Nav channels and their presence in RPE are discussed in chapter 2.3.4.

### 2.3.4 Voltage-gated sodium channels (Nav)

The family of Nav channels consists of nine different subtypes, Nav1.1–Nav1.9, as well as the non-voltage-sensitive Na<sub>x</sub> channel (Noda and Hiyama 2015; de Lera Ruiz and Kraus 2015), and they can be classified according to their sensitivity range to Nav channels blocker tetrodotoxin (TTX) (de Lera Ruiz and Kraus 2015). In excitable cells, the so-called TTX-sensitive group requires nanomolar levels of TTX (Nav1.1–Nav1.4, Nav1.6, and Nav1.7), whereas the TTX-resistant group (Nav1.5, Nav1.8, and Nav1.9) requires the blocker in micromolar concentrations. The Nav subtypes vary in their expression pattern among different tissues. They are most recognized for initiating and propagating action potentials in electrically excitable cells, including neurons and cardiac myocytes (W. A. Catterall 2000b, 1995; Hodgkin and Huxley 1952). However, the Nav family has recently been identified in several non-excitable cell types (for a review, see Black and Waxman 2013). In addition to being crucial for membrane potential depolarization during action potential generation, Na<sup>+</sup> is vital in the transport processes of various molecules such as amino acids, sugars, and neurotransmitters. The steep Na<sup>+</sup> gradient enables the secondary active transport processes of these molecules. Thus, Na<sup>+</sup> homeostasis is vital for cellular function and physiology (Wimmers, Karl, and Strauss 2007).

#### *Structure and function of Nav channels*

The mammalian Nav channels are large multimeric membrane-spanning complexes comprised of a pore-forming  $\alpha$  subunit (260 kDa) and one or two closely associated  $\beta$  subunits (30–40 kDa) that modulate channel gating and cell-cell interaction through adhesion (F. H. Yu and Catterall 2003; Malhotra et al. 2000; Isom et al. 1992; de Lera Ruiz and Kraus 2015; Beneski and Catterall 1980). The  $\alpha$  subunit is organized into four similar domains (I–IV), each including six  $\alpha$ -helical transmembrane segments (S1–S6). These segments form the voltage sensor (S4), selectivity filter, and the pore of the Nav channel (S5 and S6) (William A. Catterall 2010; Yarov-Yarovoy, Baker, and Catterall 2006; Guy and Seetharamulu 1986) (Figure 4). The resulting structure is highly dynamic and transitions between closed, open-conducting, and nonconducting inactive states (de Lera Ruiz and Kraus 2015; Hodgkin and Huxley 1952; W. A. Catterall 2000b; Armstrong 1981). At hyperpolarized membrane potentials, the probability of the Nav channel opening is low. Upon depolarization, the S4 helices move outward, enabling a conformational change in the channel

structure that opens its pore allowing the channel to conduct  $\text{Na}^+$  ions (William A. Catterall 2014). Typically, these channels inactivate and close within milliseconds. However, persistent  $\text{Na}_V$  current and action potential backpropagation can also be mediated in some cases, such as in neural dendrites (de Lera Ruiz and Kraus 2015; W. A. Catterall 2000b; Armstrong 1981). The inactivation and activation of the  $\text{Na}_V$  current can also be modulated by phosphorylation, by kinases such as protein kinase A (PKA) and protein kinase C (PKC) that primarily target the intercellular loop between domains I and II (Scheuer 2011; Berendt, Park, and Trimmer 2010).

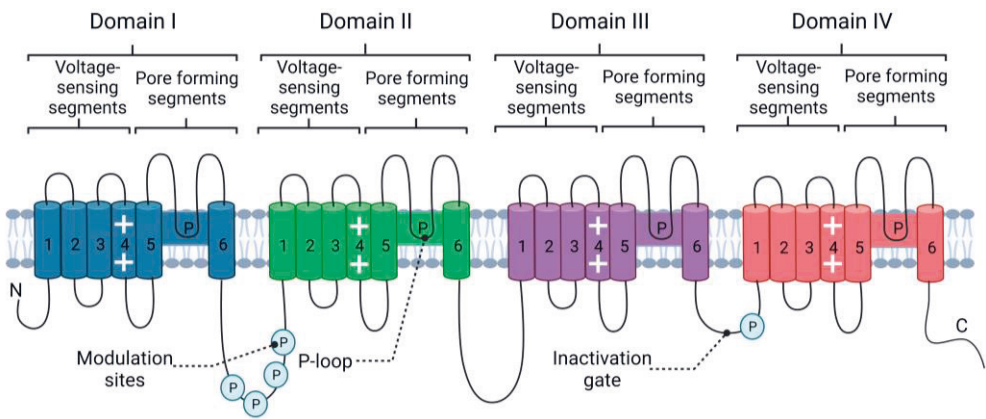


**Figure 4.** A schematic illustration of the classical structure of  $\text{Na}_V$  channels. The channels are assembled from four domains (I–IV), each comprised of six helical segments creating the voltage-sensing and pore-forming parts of the ion channel together with the pore-loops (P-loops). The plus signs correspond to positively charged residues of S4. The inactivation gate closes the ion channel, and the inactivation can be modulated by phosphorylation (encircled P). The illustration was modified from (W. A. Catterall 2000b; de Lera Ruiz and Kraus 2015) with BioRender.com.

### *Noncanonical roles of $\text{Na}_V$ channels*

$\text{Na}_V$  channels have been found in a wide range of non-excitabile cells, including astrocytes, cancer cells, fibroblasts, and odontoblasts, and their roles have been reviewed by (Black and Waxman 2013). In addition to the  $\alpha$  subunits,  $\beta$  subunits have also been found in some cell types (Oh and Waxman 1994). At large, the estimated density of  $\text{Na}_V$  channels in non-excitabile cells ( $<1 \mu\text{m}^{-2}$ ) is remarkably lower than in excitabile cells ( $2\text{--}75 \mu\text{m}^{-2}$ ) (Black and Waxman 2013). One known

exception to this is spinal cord astrocytes that, at least *in vitro*, have much higher densities of Nav channels and can generate responses resembling action potentials when cells are hyperpolarized enough to remove their resting inactivation (Sontheimer and Waxman 1992). However, the density and expression of Nav channels can also be influenced by the external milieu and developmental or physiological state of the cells, and such changes can also occur after pathological challenges (Thio and Sontheimer 1993; Thio, Waxman, and Sontheimer 1993; Paez et al. 2009; Macfarlane and Sontheimer 1998; Chatelier et al. 2012). Thus far, some non-excitabile cell types have only been shown to express one Nav channel subtype, while other cells, such as astrocytes, have been shown to express multiple types (Reese and Caldwell 1999; Zsiros et al. 2009; Chatelier et al. 2012; Black and Waxman 2013). In addition to the plasma membrane, Nav channels have been identified in intracellular membranes surrounding specific cellular organelles (Black and Waxman 2013).

In non-excitabile cells, Nav channels regulate various functions, including phagocytosis, migration, metastatic activity, and bioactive molecule release. The involvement of Nav channels has been investigated with pharmacological inhibitors or genetic modifications, yet the underlying molecular mechanisms are not understood in detail (Black and Waxman 2013). For instance, in astrocytes and oligodendrocyte precursor cells, the activity of Nav channels has been suggested to serve as a feedback loop to maintain the activity of Na<sup>+</sup>/K<sup>+</sup>-ATPase (Sontheimer et al. 1994) or to reverse Na<sup>+</sup>/Ca<sup>2+</sup> exchange (Kirischuk, Kettenmann, and Verkhratsky 1997; Tong et al. 2009). On the other hand, in macrophages and melanoma cells, the control of cell motility through F-actin remodeling has been linked to the release of Na<sup>+</sup> from intracellular stores and its subsequent uptake in mitochondria (Carrithers et al. 2009). In retinal Müller glia, rapid fluctuations in membrane potential have been suggested to mediate the activation of Ca<sub>v</sub> channels to promote the vascular endothelial growth factor (VEGF) induced release of glutamate. Yet, the mechanisms behind Nav activation in these cells are not understood (Linnertz et al. 2011).

#### *Previous knowledge of Nav channels in RPE*

Despite the growing body of evidence demonstrating the relevance of Nav channels in non-excitabile cells (Black and Waxman 2013) and the acknowledged importance of controlled Na<sup>+</sup> homeostasis in RPE, the presence of these channels has remained ambiguous in this tissue (Wimmers, Karl, and Strauss 2007). To date, Nav currents

have only been recorded in sub-confluent RPE cultures (Sakai and Saito 1997; Botchkin and Matthews 1994; Wen, Lui, and Steinberg 1994), resulting in the interpretation that their expression results from neuroepithelial differentiation occurring in RPE *in vitro* (Reichhart and Strauss 2014; Miyagishima et al. 2016; Wimmers, Karl, and Strauss 2007). This dissertation refutes this notion and demonstrates the presence and functionality of Nav channels in RPE. These findings will be covered in the results and discussion (**Study I**).

### 2.3.5 Gap junctions

#### *Structure and function of gap junctions*

Gap junctions are intercellular channels that allow the direct passage of small ions and molecules (1–1.5 kDa) between neighboring cells (D. A. Goodenough, Goliger, and Paul 1996). This cell-cell communication is considered vital for a broad array of physiological events, including cell synchronization, proliferation, differentiation, and maintenance of tissue homeostasis (Meşe, Richard, and White 2007; White and Paul 1999; Y. W. Zhang et al. 2001; Hervé and Derangeon 2013). Moreover, in macrophages, gap junctions have been suggested to regulate phagocytosis, but the findings have been conflicting (Anand et al. 2008; Dosch et al. 2019; Glass et al. 2013). In vertebrates, these channels are assembled of proteins known as connexins (Cx) that form hexameric structures known as hemichannels that are docked together to create the complete channel (D. A. Goodenough, Goliger, and Paul 1996; Daniel A. Goodenough and Paul 2009; Willecke et al. 2002; Pogoda et al. 2016) (Figure 5A). In addition to mediating cellular communication, Cx proteins have been shown to have channel-independent roles, for example, in regulating cell growth (Van Campenhout et al. 2020). Hemichannels can also function independently in various cell types, such as promoting paracrine signaling and cell survival (Orellana 2016; D'hondt et al. 2014; Daniel A. Goodenough and Paul 2003, 2009; D. A. Goodenough, Goliger, and Paul 1996).

Cx proteins differ in their expression pattern between tissues (D. A. Goodenough, Goliger, and Paul 1996). Of the 21 closely related members in the human genome, Cx43 is the most ubiquitously expressed isoform (reviewed by Willecke et al. 2002; Söhl and Willecke 2003). Lack of Cx43 is fatal shortly after birth

in mice (Reaume et al. 1995). Like other membrane proteins, Cx proteins are synthesized in the endoplasmic reticulum. Their assembly can occur before or after transport to the Golgi apparatus, depending on the type of Cx isoform. Once oligomerized, hemichannels are trafficked to the plasma membrane via mechanisms such as secretory pathways or microtubule-based vesicle targeting (Lauf et al. 2002; Johnson et al. 2002; Shaw et al. 2007) and incorporated into gap junction plaques, typically at their peripheral regions (Kirichenko, Skatchkov, and Ermakov 2021; Gaietta et al. 2002). Cx proteins are comprised of two extracellular domains that help to dock the opposing cells, four helical and hydrophobic transmembrane domains, as well as three cytoplasmic domains that connect the transmembrane domains and are involved in molecule selectivity (Meşe, Richard, and White 2007; Pogoda et al. 2016; Willecke et al. 2002) (Figure 5B). When gap junctions are degraded, the Cx proteins are separated from the central parts of the plaques to form double-membraned structures known as annular gap junctions. It has also been suggested that this internalization could occur through endocytosis from a single membrane although the underlying mechanisms are not resolved (Solan and Lampe 2016). Once internalized, gap junctions are degraded through endosomal and lysosomal pathways (Laird, Puranam, and Revel 1991; Kirichenko, Skatchkov, and Ermakov 2021) and at least in some conditions such as autophagy, ubiquitination has also been shown to regulate gap junction turnover (J. G. Laing and Beyer 1995; James G. Laing and Beyer 1995).

### *Regulation of gap junctions*

Unlike many other membrane proteins, gap junctions have half-lives of only 1–3 h and thus need to be continuously replaced (Falk, Kells, and Berthoud 2014; Laird, Puranam, and Revel 1991; P. D. Lampe 1994; Musil, Beyer, and Goodenough 1990). Therefore, controlling gap junction-mediated connectivity requires careful regulation of Cx trafficking, channel assembly, degradation, and gap junctional gating (Daniel A. Goodenough and Paul 2009; Segretain and Falk 2004). This intercellular communication can be regulated across multiple levels and timescales by changes in membrane voltage, cellular pH, and post-translational modifications such as phosphorylation (Daniel A. Goodenough and Paul 2009; Pogoda et al. 2016). The effect of phosphorylation on channel conductance is highly specific, as modifications on different residues by the same kinases can have contrary effects on channel gating (Paul D. Lampe and Lau 2004). The most significant phosphorylation targets in Cx proteins are the residues located at its C-terminal end (Figure 5B). For Cx43, some



of the best-studied kinases include tyrosine kinase oncoprotein (Src), mitogen-activated protein kinase (MAPK), PKA, PKC, casein kinase 1 (CK1) reviewed in (Paul D. Lampe and Lau 2004) and cyclin-dependent kinase 5 (Cdk5) (Qi et al. 2016) (Table 1). While Cdk5 has been primarily studied in the nervous system (Qi et al. 2016; Liu et al. 2008), recent reports have shown that it regulates numerous physiological and pathological functions in other cell types, such as pancreatic cells and neutrophils (Contreras-Vallejos, Utreras, and Gonzalez-Billault 2012). This dissertation describes new information regarding the role of Cdk5 in gap junction regulation in RPE (**Study III**).

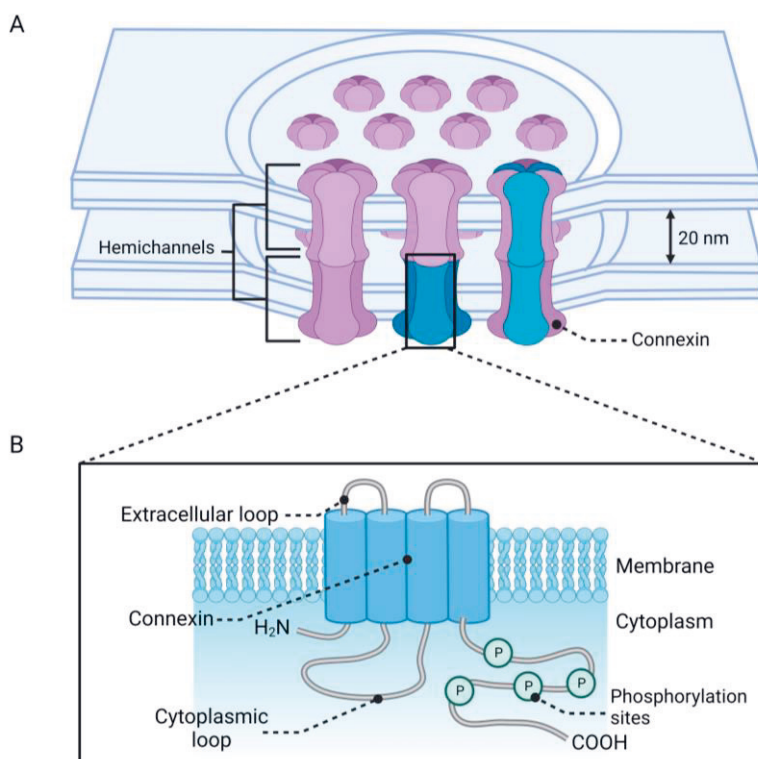


**Figure 5.** A) Schematic illustration of the classical structure of gap junctions that are comprised of two hemichannels or connexons that are docked together from opposing membranes. Homotypic or heterotypic gap junctions are comprised of identical or different types of connexin proteins, respectively. Each hemichannel is formed by six connexin proteins, and they can also serve roles independent of gap junctions. B) The connexin proteins are assembled from four transmembrane domains, two extracellular loops, and three cytoplasmic domains (N- and C-terminal ends and a cytoplasmic loop). The gating of the resulting channel can be modified by various mechanisms, including phosphorylation (encircled P). The illustration was modified from (Söhl, Maxeiner, and Willecke 2005; Leithe, Mesnil, and Aasen 2018) and created with BioRender.com.

**Table 1.** List of known phosphorylation sites, responsible kinases, and their effects on Cx43.

Sites	Kinase	Effect	Reference
Y247	<sup>1</sup> Src, <sup>2</sup> Tyk2	Disassembly, increased turnover	<sup>1</sup> (Lin et al. 2001), <sup>2</sup> (Hanjun Li et al. 2016)
S244	Clk2?	Auxiliary binding to 14-4-3?	(R. Y.-C. Huang et al. 2011; Park et al. 2006)
S255	<sup>1,2</sup> MAPK, <sup>3,4,5</sup> CDK1 (mitosis specific)	Gating, cellular communication downregulation	<sup>1</sup> (Warn-Cramer et al. 1996), <sup>2</sup> (Warn-Cramer et al. 1998), <sup>3</sup> (Leithe, Mesnil, and Aasen 2018), <sup>4</sup> (Xie et al. 1997), <sup>5</sup> (P. D. Lampe et al. 1998)
S257	CaMKII	Unknown	(R. Y.-C. Huang et al. 2011)
S262	<sup>1,2</sup> MAPK <sup>3,4,5</sup> CDK1 (mitosis specific) <sup>6</sup> PKC	Gating, cellular communication downregulation	<sup>1</sup> (Solan and Lampe 2008), <sup>2</sup> (Norris et al. 2008), <sup>3</sup> (Leithe, Mesnil, and Aasen 2018), <sup>4</sup> (Xie et al. 1997), <sup>5</sup> (P. D. Lampe et al. 1998), <sup>6</sup> (Srisakuldee et al. 2009)
Y265	<sup>1</sup> MAPK, <sup>2,3</sup> Src, <sup>4</sup> Tyk2	Interaction with IP <sub>3</sub> , Increases overall Cx43 but decreases gap junctions, cellular communication downregulation	<sup>1</sup> (Warn-Cramer et al. 1996), <sup>2</sup> (Toyofuku et al. 2001), <sup>3</sup> (Lin et al. 2001), <sup>4</sup> (Hanjun Li et al. 2016)
S279/S282	<sup>1,2</sup> MAPK, <sup>3</sup> Cdk5	Gating, inhibition of membrane targeting, degradation	<sup>1</sup> (Warn-Cramer et al. 1996), <sup>2</sup> (Warn-Cramer et al. 1998), <sup>3</sup> (Qi et al. 2016)
S296/S297	CaMKII	Unknown	(Axelsen et al. 2006; R. Y.-C. Huang et al. 2011)
S306	CaMKII	Gating	(Axelsen et al. 2006; R. Y.-C. Huang et al. 2011; Procida et al. 2009)
S314	CaMKII	Unknown	(R. Y.-C. Huang et al. 2011)
Y313	Src	Interaction with gap junction stabilizing protein Drebrin	(Zheng et al. 2019)
S325/328/330	CKI	Assembly	(Cooper and Lampe 2002)
S364	PKA	Increased trafficking and assembly	(TenBroek et al. 2001; Shah, Martinez, and Fletcher 2002; Paulson et al. 2000)
S365	Src	Assembly, turnover	(Solan et al. 2007; Solan and Lampe 2020; Yogo et al. 2002)
S368	PKC	Assembly, permeability, Cx43 endocytosis, and degradation	(P. D. Lampe 1994; Berthoud et al. 1993; Rivedal, Yamasaki, and Sanner 1994; P. D. Lampe et al. 2000)
S369	Akt	Assembly, interaction with regulatory protein 14-3-3	(Park et al. 2007; Yogo et al. 2002)
S372	<sup>1</sup> PKC, <sup>2</sup> CAMKII	Maintained electrical coupling	<sup>1</sup> (Sáez et al. 1997), <sup>2</sup> (R. Y.-C. Huang et al. 2011)
S373	<sup>1</sup> Akt, <sup>2</sup> PKA	Gap junction size, interaction with ZO-1 and regulatory protein 14-3-3	<sup>1</sup> (Park et al. 2007; Yogo et al. 2002; Dunn and Lampe 2014; Chen et al. 2008), <sup>2</sup> (Yogo et al. 2002)

Abbreviations: S: Serine, Y: Tyrosine, Src: Tyrosine kinase oncoprotein, Tyk2: Tyrosine kinase 2, Clk2: Dual specificity protein kinase, MAPK: Mitogen-activated protein kinase, CDK: Cyclin-dependent kinase, PKC: Protein kinase C, PKA: Protein kinase A, CaMKII: Calcium/calmodulin-dependent protein kinase II, CKI: Casein kinase 1, Akt: Protein kinase B, IP<sub>3</sub>: Inositol trisphosphate, ZO-1: Zonula occludens-1.

## *Previous knowledge of gap junctions in RPE*

Previous studies have suggested that RPE cells, like many other epithelia (Kretz, Maass, and Willecke 2004; Ey et al. 2009; Aasen and Kelsell 2009), primarily express Cx43 isoform, but low levels of Cx36 and Cx46 have also been identified (Malfait et al. 2001; Milićević et al. 2021; Janssen-Bienhold, Dermietzel, and Weiler 1998). In RPE, *in vitro* models using an immortalized ARPE-19 cell line have demonstrated that gap junctions play roles in cell differentiation and viability (Hutnik et al. 2008; Kojima et al. 2008; Losso, Truax, and Richard 2010). In addition, during eye development, transient Cx43 gap junctions and hemichannels have been identified between RPE and the neuroblastic retina that may transmit signaling molecules such as ATP (Tibber, Becker, and Jeffery 2007; Pearson et al. 2005). Therefore, gap junctions are considered necessary for the correct pacing of retinal organogenesis and purinergic regulation of retinal proliferation, which are both mediated by RPE (Tibber, Becker, and Jeffery 2007; Pearson et al. 2005). Despite their importance, much less is known about the roles of gap junctions in mature RPE. Furthermore, studies detailing the physiological coupling of RPE cells have focused on dye coupling studies (Hutnik et al. 2008; Akanuma et al. 2018) or microelectrode recordings from non-mammalian species (Hudspeth and Yee 1973). This dissertation unravels the electrical connectivity and its dynamics in mammalian RPE and resolves the function and regulation of gap junctions during POS phagocytosis. These findings will be covered in the results and discussion (**Study II and III**).

## 2.4 Circadian rhythm in the eye

### 2.4.1 How the rhythm is set

Circadian oscillators are internalized timing systems that exist in almost all living organisms and are sustained even without external cues (Takahashi 2017). In mammals, the master pacemaker of this clock can be found in the suprachiasmatic nucleus of the hypothalamus, which controls the timing in other organs. Some of the other organs serve as peripheral oscillators. The mammalian retina is unique among these peripheral oscillators. Its rhythms appear independent from the master clock (Terman, Remé, and Terman 1993), and its phase can be set directly by light exposure (G. Tosini and Menaker 1996). The light-dark cycle is the most predictable

periodic environmental cue and ensures that the intrinsic circadian clock does not drift out of a 24 h phase (Aschoff and Pohl 1978). This entrainment occurs via specific ganglion cell types expressing a visual pigment known as melanopsin and, as a result, are intrinsically photosensitive. These neurons project to the suprachiasmatic nucleus via the retinohypothalamic tract (Hattar et al. 2002; Berson, Dunn, and Takao 2002). The circadian organization of the retina is complex, and contribution from multiple of its cell types is integrated (Jaeger et al. 2015) to help the retina to prepare and actively respond to the alternating cycles of solar day and night (Douglas G. McMahon, Iuvone, and Tosini 2014; Ko 2020). This rhythm can be regulated by neuromodulators dopamine and melatonin, which have antiphase circadian cycles. Dopamine levels peak during the day and decrease at night, while melatonin levels are lowest during the day and highest at night (Adachi, Nogi, and Ebihara 1998; Iuvone et al. 1978; Hamm and Menaker 1980).

While a significant portion (~5–20 %) of genes in any particular tissue have been discovered to show rhythmic expression, the molecular mechanisms underlying the circadian clock are governed by specific clock genes that generate feedback loops. In mammals, this pathway (shown in figure 6) involves transcription factors CLOCK and BMAL1 that periodically enhance the expression of various clock genes, including Period (Per) and Cryptochrome (Cry) genes, by binding to their enhancer elements (E-boxes). The resulting Period–protein complex (PER) and CRY proteins suppress their expression. In mice, their accumulation is highest in the afternoon or evening (for reviews, see Takahashi 2017; Takahashi et al. 2008). The second feedback loop involves the transcription and translation of other proteins known as the retinoic acid-related orphan receptors (ROR) and retinoic acid-related orphan nuclear receptors (REV–ERB). Their expression, in turn, provides either positive or negative regulation on the expression of CLOCK and BMAL1, demonstrating the complexity of these interlocking feedback loops (Ko, Shi, and Ko 2009; Douglas G. McMahon, Iuvone, and Tosini 2014; Cox and Takahashi 2019). The rhythmic expression of the core clock genes can then drive the expression of many other clock-controlled genes, including D-site-Binding Protein (DBP), in a tissue-specific manner which causes the rhythm of physiological processes (Cox and Takahashi 2019). Ultimately this can regulate synaptic communication, neurotransmitter release, and metabolism to reconfigure retinal circuits and physiology and can even influence cell survival and growth (Douglas G. McMahon, Iuvone, and Tosini 2014; Gianluca Tosini et al. 2008). The circadian control of the retina is regulated by multiple of its cell types, and their rhythm, in turn, can be regulated by neuromodulator dopamine and hormone melatonin that have antiphase circadian

cycles (Adachi, Nogi, and Ebihara 1998; Ribelayga and Mangel 2010; Ko, Shi, and Ko 2009).

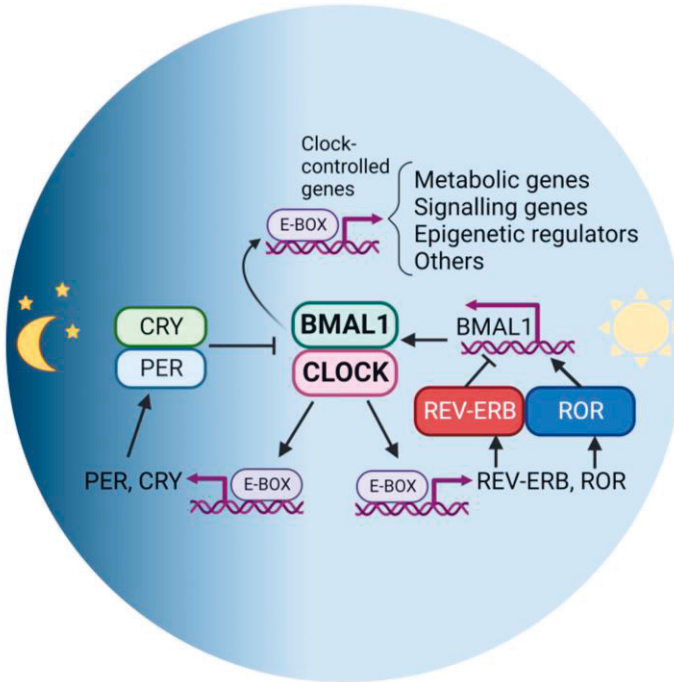


**Figure 6.** Schematic illustration of the core molecular clock machinery in mice. The mechanism consists of autoregulatory feedback loops that drive clock-controlled gene expression. The core clock consists of a complex of transcription factors CLOCK and BMAL1 that drive the expression of repressor proteins PER and CRY by binding to regulatory E-boxes. The accumulation of PER and CRY is highest during the late afternoon and evening, and at night they interact with CLOCK-BMAL1 to suppress their own transcription. The other feedback loop involves the transcription and translation of ROR and REV-ERB, which can either repress or activate the expression of CLOCK and BMAL1. The illustration was modified from (Lee 2021) under the terms of the Creative Commons license and created with BioRender.com. Abbreviations: CLOCK: (Circadian Locomotor Output Cycles Kaput) transcription factor, BMAL1: Brain and muscle aryl hydrocarbon receptor nuclear translocator-like transcription factor, CRY: cryptochrome, PER: period, E-box: enhancer elements, ROR: retinoic acid-related orphan receptors, REV-ERB: retinoic acid-related orphan nuclear receptors,

## 2.4.2 Circadian changes in gap junctional coupling

Gap junctions have been recognized as important regulators of the retinal circuitry, and these connections can be dynamically regulated by changing ambient light levels

and circadian rhythms (Bloomfield and Völgyi 2009; Raviola and Gilula 1973). Previous studies in species such as goldfish, rabbits, and mice have shown that coupling between photoreceptors is much more significant at night (Mangel et al., 1994; Wang and Mangel, 1996; Ribelayga et al., 2008; Ribelayga and Mangel, 2010). This modulation is achieved by lowered dopamine release to limit the activation of its receptors, subsequently increasing the levels of cAMP. cAMP opens the gap junctions between rods and cones (Mangel et al. 1994; Wang and Mangel 1996; Ribelayga, Cao, and Mangel 2008). At dark-adapted conditions, the regulatory sites of the Cx isoform of photoreceptors, Cx36 (or Cx35 in fish), are also more heavily phosphorylated by PKA (Z. Zhang et al. 2015; Hongyan Li et al. 2013; Hongyan Li, Chuang, and O'Brien 2009). In addition to dopamine, the purine adenosine, whose levels are highest at night, has also been shown to affect rod-cone coupling and Cx36 phosphorylation (Ribelayga and Mangel 2005; Hongyan Li et al. 2013). Ultimately, these changes in the circuitry allow dim rod signals to reach cones, possibly improving the reliability of rod signals and the detection of large dim objects at night (Ribelayga, Cao, and Mangel 2008). Conversely, modulating rod-cone coupling helps to relay sensitivity in mesoscopic conditions when rods are becoming saturated (DeVries and Baylor 1995). It is currently unknown whether this rhythm regulates gap junctions in RPE. New insight into this question and the related experimental findings are covered in the results and discussion (**Study II and III**).

### 2.4.3 Circadian regulation of disk shedding and phagocytosis

The rhythm of POS renewal can be maintained under constant darkness (LaVail 1976; Grace, Chiba, and Menaker 1999) or light (Besharse and Hollyfield 1979), and the rhythm is maintained even after the optic nerve or suprachiasmatic nucleus has been ablated (Teirstein, Goldman, and O'Brien 1980; Terman, Remé, and Terman 1993). These findings suggest the timing of POS phagocytosis persists even without the influence of the central clock. Yet, once the optic nerve has been severed, the rhythm can no longer be shifted, suggesting that some elements of the master clock regulation are also required (Teirstein, Goldman, and O'Brien 1980). Interestingly, it is still unresolved whether phagocytosis rhythm is regulated by the retinal or RPE circadian clock or a combination of both (Baba, Goyal, and Tosini 2022). In addition to the retina, a functional circadian clock has been found in RPE (Baba et al. 2010; Baba, DeBruyne, and Tosini 2017). While some studies have suggested that RPE

could be capable of light detection (Peirson et al. 2004), the present consensus is that its rhythm is entrained by retinal dopamine, which could serve as the synchronization signal between the photoreceptors and the RPE. However, the underlying molecular mechanisms are poorly understood (Baba, DeBruyne, and Tosini 2017). Melatonin has also been suggested; however, studies in mice have demonstrated that a lack of its receptors only advances the phagocytosis peak by a few hours and does not remove it entirely (Laurent et al. 2017). The rhythmic disk renewal has also been shown in C57BL/6 mice incapable of melatonin synthesis, albeit with dampened peaks (Grace, Chiba, and Menaker 1999).

One suggested downstream mechanism for dopamine is that it could drive the transcription of *Period* via an extracellular signal-regulated kinase 1/2 (ERK1/2) signaling pathway (Baba, Goyal, and Tosini 2022). Studies with mice deficient in specific subtypes of dopamine receptors have been shown to lack the burst of POS phagocytosis. These mice have dysregulated integrin pathways, while clock gene expression has not been affected (Goyal et al. 2020). Lack of integrin  $\alpha v \beta 5$  or its ligand MFG-E8 (Nandrot et al. 2004; Nandrot and Finnemann 2008) has also been shown to remove the phagocytosis burst. In addition to dopamine, cytosolic  $Ca^{2+}$  rhythms and histaminergic or cholinergic signaling have been suggested to regulate diurnal phagocytosis rhythm (Ikarashi et al. 2017; Morioka et al. 2018). The rhythm has also been shown to be controlled by clock genes such as *Bmal1* (DeVera et al. 2022) *Per* and *REV-ERB $\alpha$*  and by the POS themselves (Milićević et al. 2021, 2019).

It is important to note that it is still under speculation how detrimental the loss of the specific daily burst is to vision. Studies with mice lacking integrin  $\alpha v \beta 5$  have shown lipofuscin accumulation and progressive vision loss, although with relatively late onset (Nandrot and Finnemann 2006). Yet, this pathology has not been found when the peak is lost due to dopaminergic receptors (Goyal et al. 2020) or MFG-E8 (Nandrot and Finnemann 2008). On the other hand, loss of *Bmal1* has been suggested to affect rod viability (Baba et al. 2018), and deficiency of either *MerTK* or its ligands has been shown to result in retinal degeneration in both mice and rats (Bok and Hall 1971; Burstyn-Cohen et al. 2012; Duncan et al. 2003). These detriments could highlight the importance of integrin  $\alpha v \beta 5$  and *MerTK* for phagocytosis regulation or suggest that unknown compensatory feedback mechanisms exist in the molecular pathway. The findings emphasize the crucial role of integrin in phagocytosis rhythm regulation. In fact, removing this receptor also impairs the activation of FAK, *MerTK*, and *Rac1* and prevents the rhythmic exposure of phosphatidylserine residues (Mao and Finnemann 2012; Ruggiero et al. 2012; Mazzoni, Safa, and Finnemann 2014). Alternatively, the lack of obvious retinal

pathologies could be explained by the remaining or elevated basal phagocytosis level that could help compensate for the lacking burst (Nandrot et al. 2004; Ko, Shi, and Ko 2009; Strauss 2005; Ailis L. Moran et al. 2022). It has also been suggested that more subtle defects in phagocytosis rates are insufficient to result in apparent pathologies over the relatively short lifespan of mice (Mazzoni, Safa, and Finnemann 2014). Ultimately, these studies highlight the complexity of regulating this essential task of RPE.

## 2.5 Ionic mechanisms in the regulation of phagocytosis

While much of the POS phagocytosis pathway has already been discovered, the involvement of ion channels and gap junctions in the process is relatively unknown. Most of our current knowledge comes from pharmacological studies showing that modulating ion channels such as L-type and T-type Cav, bestrophin-1, and transient receptor potential channels or gap junctions influence the phagocytosis efficiency (Müller et al. 2014; Korkka et al. 2019; Zielicka, Williams, and Moss 2015). Yet, the upstream mechanisms that enable their activation and the downstream mechanisms explaining how these channels are linked to the phagocytosis pathway are largely speculative or unknown.

In addition to entraining the circadian rhythm and coinciding with the onset of POS phagocytosis, light has been shown to modulate ion transport in RPE. The concentration of  $K^+$  has been shown to change with light exposure (Oakley, Flaming, and Brown 1979) (Figure 7). In the absence of light, the subretinal concentration of  $K^+$  is approximately 5 mM, and these ions enter the RPE cells via  $Na^+/K^+$ -ATPase (Miller and Steinberg 1982; la Cour, Lund-Andersen, and Zeuthen 1986). After light exposure, the subretinal space  $K^+$  concentration decreases to 2 mM due to the closure of cyclic-nucleotide-gated channels (CNGC) of photoreceptors hyperpolarizing RPE membrane potential (Oakley 1987). This change leads to an increased  $K^+$  efflux from RPE, which is combined with a delayed short hyperpolarization of the basolateral membrane and a decreased basolateral  $K^+$  conductance (Joseph and Miller 1991; Griff and Steinberg 1984). Hence, the decrease in subretinal  $K^+$  is buffered with a decreased transepithelial  $K^+$  transport and substantial apical  $K^+$  conductance. The increased apical  $K^+$  efflux is likely mediated by Kir channels (Bialek, Joseph, and Miller 1995; Joseph and Miller 1991;



Steinberg and Miller 1973; Reichhart and Strauss 2014).  $\text{Na}^+/\text{K}^+ / 2\text{Cl}^-$  co-transporter could also mediate volume control (Russell 2000).

The light-induced decrease in subretinal  $\text{K}^+$  also inhibits  $\text{Na}^+/\text{K}^+ / 2\text{Cl}^-$  co-transporter and  $\text{Na}^+/\text{HCO}_3^-$  co-transporter. The resulting drop of  $\text{HCO}_3^-$  inhibits the basolateral  $\text{Cl}^-/\text{HCO}_3^-$  exchanger. Thus inhibition of the transporters results in decreased intracellular  $\text{Cl}^-$  concentration, causing cytosol acidification and cell shrinkage (Wimmers, Karl, and Strauss 2007). In addition, light illumination is thought to cause the retina to release a so-called light peak substance that would bind receptors on the apical membrane of RPE and lead to an increase in intracellular  $\text{Ca}^{2+}$ . This substance is currently unknown, but it has been speculated to be ATP that would bind to purinergic receptors and cause a release of  $\text{Ca}^{2+}$  from intracellular stores via phospholipase C (PLC) and inositol trisphosphate ( $\text{IP}_3$ ). The L-type  $\text{Ca}_v$  channels are also thought to contribute to increased intracellular  $\text{Ca}^{2+}$ . The increased  $\text{Ca}^{2+}$  could, in turn, activate  $\text{Ca}^{2+}$ -dependent  $\text{Cl}^-$  channels (Wimmers, Karl, and Strauss 2007; Reichhart and Strauss 2014; Reichhart and Strauß 2020).

As POS phagocytosis rhythm is sustained even in the absence of light, light is unlikely the only factor that links ion channels to phagocytosis. In fact, various ion channels have been shown to regulate the circadian rhythm of POS phagocytosis. Studies with knockdown mice have shown that a lack of a specific subtype of  $\text{Ca}_v$  channels ( $\text{Ca}_v1.3$ ) or  $\text{Ca}^{2+}$ -dependent  $\text{K}^+$  channels (maxiK, BK) (Müller et al. 2014) reduces the phagocytosis burst or shift its phase.  $\text{Ca}_v1.3$  mRNA level has also been shown to vary depending on the time of the day. However, its levels were significantly higher outside the peak hours of phagocytosis (8 h after light onset) (Müller et al. 2014). The involvement of L-type  $\text{Ca}_v$  channels has also been linked to integrin  $\alpha v\beta 5$  and MerTK as their stimulation activates the channels (Karl et al. 2008). MerTK is also thought to cause an increase in intracellular  $\text{Ca}^{2+}$  via release from intracellular stores (Reichhart and Strauß 2020). Furthermore, local changes in intracellular  $\text{Ca}^{2+}$  have been observed after POS binding (Kindzelskii et al. 2004), while significant pharmacological increases in intracellular  $\text{Ca}^{2+}$  can prevent POS internalization (M. O. Hall, Abrams, and Mittag 1991). Lastly, studies in other cell types have shown that multiple proteins, such as Anx2 (Koerdts and Gerke 2017), and steps in the phagocytosis pathway, including actin cytoskeleton remodeling and vesicle fusion (for a review, see (Nunes and Demarex 2010)), have shown to be  $\text{Ca}^{2+}$ -dependent. Thus, it is likely that  $\text{Ca}^{2+}$  is vital for both the binding and internalization of POS.

The uptake of POS and large amounts of membrane material requires RPE cells to regulate their volume. This regulation has been linked to chloride channels,

including Bestrophin-1, which would be activated by the increased intracellular  $\text{Ca}^{2+}$ . Bestrophin-1 could also activate volume-regulated  $\text{Cl}^-$  channels (Reichhart and Strauß 2020). In addition,  $\text{Cl}^-$  has been speculated to be involved in later stages of phagocytosis as several CLC channels can be found in endosomes and lysosomes and could, therefore also acidify internalized phagosomes (Wimmers, Karl, and Strauss 2007).

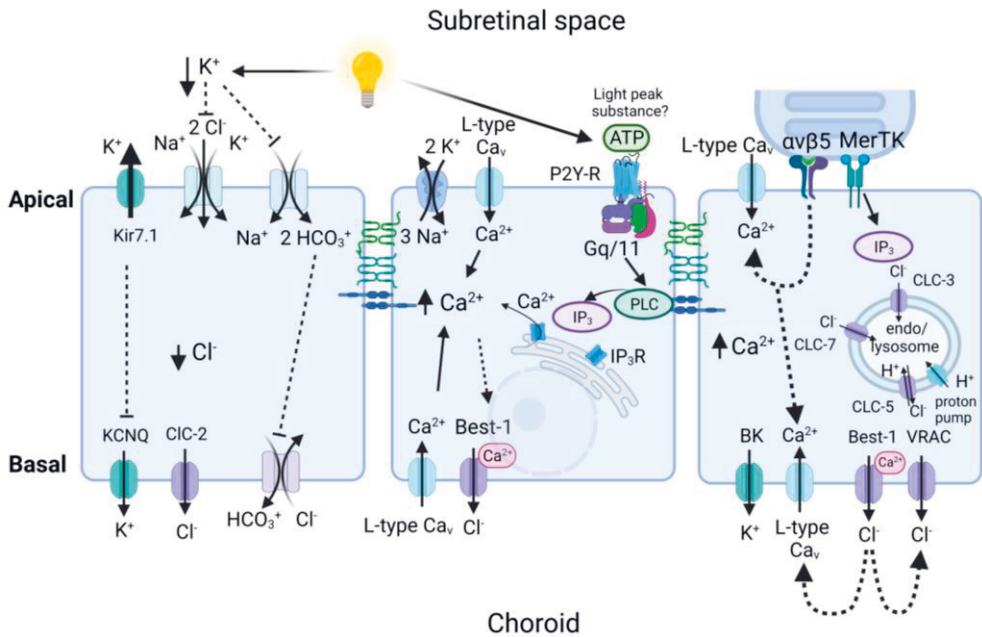


**Figure 7.** A schematic illustration of the effect of light exposure and phagocytosis on RPE's apical and basal transport mechanisms. Left: Illumination causes a decrease in subretinal  $K^+$  that is compensated by an increased apical  $K^+$  conductance through Kir7.1 and decreased basolateral  $K^+$  conductance through KCNQ and possibly Kir7.1 channels. Decreased subretinal  $K^+$  also decreases the activity of the  $Na^+/K^+/2Cl^-$ - and  $Na^+/HCO_3^-$ -cotransporters. The decreased intracellular  $HCO_3^-$  then inhibits the  $Cl^-/HCO_3^-$ - exchanger. These changes lead to a net  $Cl^-$  flux across the basolateral membrane towards the choroid. Middle: After light exposure, the retina is thought to release a currently unknown light-peak substance that can bind to receptors on the apical membrane in RPE. It is speculated that this might occur via a P2Y-R that would lead to a release of  $Ca^{2+}$  from the intracellular stores via IP<sub>3</sub>R and PLC. This release and activated L-type  $Ca^{2+}$  channels would lead to an increase in intracellular  $Ca^{2+}$  that could, in turn, activate  $Ca^{2+}$ -dependent  $Cl^-$  channels (Best-1). Ultimately, this would increase transepithelial  $Cl^-$  transport. Right: Ligation of phagocytosis receptors  $\alpha\beta 5$  and MerTK lead to an increase in intracellular  $Ca^{2+}$  via L-type  $Ca_v$  channels and intracellular stores. This increase can activate  $Cl^-$  channels to mediate volume control in phagocytosis. CCl channels also help to acidify endosomes and lysosomes, and likely phagosomes. Illustration modified from (Wimmers, Karl, and Strauß 2007; Reichhart and Strauß 2020) and created with BioRender.com. Abbreviations: Kir: Inwardly rectifying  $K^+$  channel, KCNQ: M-type  $K_v$  channel, PLC: phospholipase C, IP<sub>3</sub>R: inositol trisphosphate receptor, P2Y-R: purinergic receptor, Best1: Bestrophin-1, BK: big potassium, VRAC: volume-regulated anion channel, CCL: voltage-dependent  $Cl^-$  channels, MerTK: Mer receptor tyrosine kinase,  $Ca_v$ : voltage-gated  $Ca^{2+}$  channel.

## 3 AIMS

The fundamental question in RPE research is how RPE communicates with the electrically active neural retina. Specifically, is RPE a passive partner responding to biochemical cues, or does it have the machinery for active electrical communication? In this doctoral dissertation, this question is studied with methods conventional to neuroscience using the models that best resemble the physiological status of RPE *in vivo*: human stem cell-derived RPE and mouse RPE monolayers. The overarching objective was to improve our understanding of RPE physiology. The specific aims are outlined below.

**1. To investigate the presence and functionality of voltage-gated sodium channels in RPE (Study I).**

Voltage-gated Nav channels had previously been identified in various non-excitable cells, but their existence in mature RPE had not been resolved.

**2. To characterize the electrical connectivity of RPE (Study II and III).**

RPE cells had previously been shown to express gap junction proteins, but their electrical connectivity had not been characterized in mammals. Due to the extensive Cx labeling and previous knowledge regarding ocular development, we hypothesized that coupling coefficients would be high in RPE.

**3. To determine the roles of voltage-gated sodium channels and gap junctions in phagocytosis of photoreceptor outer segments (Study I and III).**

Several ion channels in RPE have been shown to regulate phagocytosis and its circadian timing. As the process requires synchronization, activation of multiple channels, and precise temporal control, the hypothesis was that fast-activating sodium channels and intercellular communication mediating gap junctions are involved in the phagocytosis process.

## 4 MATERIALS AND METHODS

### 4.1 Ethics declaration (I, II, III)

The hESC lines of Study **I–III** were obtained through close collaboration with Prof. Heli Skottman's group at Tampere University, Finland. The National Authority Fimea has approved the study with human embryos (Dnro 1426/32/300/05 and Fimea/2020/003758) conducted at Tampere University. The research was conducted under the supportive statements of the Ethical Committee of the Pirkanmaa Hospital District to derive, culture, and differentiate hESC lines for research purposes (Skottman/R05116). New cell lines were not derived in this thesis. All animals used in the mouse studies were treated following the ARVO Statement for the Use of Animals in Ophthalmic and Vision Research using protocols approved and monitored by the Animal Experiment Board of Finland and the Animal Care and Use Committee at Northwestern University.

### 4.2 hESC and iPSC derived RPE differentiation (I, II, III)

The human embryonic stem cell (hESC) lines Regea08/023, Regea08/017, and Regea11/013 were cultured and spontaneously differentiated according to previously established protocols (Vaajasaari et al. 2011; Skottman 2010; Viheriälä et al. 2021) and as described in **Study I–III**. Once enriched, the differentiated and pigmented cells were replated for maturation in hanging culture inserts (1.0  $\mu\text{m}$  pore size, EMD Millipore, MA, USA) coated either with collagen IV (10  $\mu\text{g}/\text{cm}^2$ ) or with collagen IV and laminin (1.8  $\mu\text{g}/\text{cm}^2$ , Biolamina, Sweden). The cells were cultured at +37 °C in 5%  $\text{CO}_2$  in Knock-Out Dulbecco's modified Eagle's medium supplemented with the following: 15% Knock-Out serum replacement (KO-SR), 2 mM GlutaMax, 0.1 mM 2-mercaptoethanol (Life Technologies, Carlsbad, CA), 1% Minimum Essential Medium nonessential amino acids, and 50 U/mL penicillin/streptomycin (from Cambrex BioScience, Walkersville, MD, USA). The medium was changed three times a week. At 8–14 weeks, the monolayers typically showed transepithelial resistance values (TER) of over 200  $\Omega \text{ cm}^2$  and were used for

experiments. The mono-allelic endogenously mEGFP-tagged GJA1 WTC human induced pluripotent stem cell (hiPSC) line AICS-0053-016 (Allen Cell Collection, Coriell Institute, Camden, NJ, USA), hereby referred to as mEGFP-tagged Cx43 hiPSC-RPE, was differentiated and cultured as above.

### 4.3 Animal handling (I, II, III)

All mice were on a mixed C57/Bl6 background and between 4–10 weeks. Both male and female mice were included in **Study I–III**, and the animals were housed in a 12 h light/dark cycle. Animals were euthanized with CO<sub>2</sub> inhalation and/or cervical dislocation. For immunocytochemistry, the eyes were enucleated and bisected along the equator and then sectioned in Ames' solution buffered with 10 mM HEPES (Sigma-Aldrich, MA, USA) (pH 7.4). The retina was gently removed from the eyecup, leaving the RPE firmly attached to the eyecup preparation.

For electrophysiological experiments, the mouse RPE dissections were conducted under IR light (940 nm). After the dissection procedure, a piece of the eyecup containing the RPE and choroid was mounted apical side up on a poly-d-lysine-coated 12-mm glass coverslip (BioCoat Cellware, Corning, NY, USA), which was secured under a slice anchor (Warner Instruments, MA, USA) to the recording chamber. Further animal handling and RPE dissection details can be found in **Study I–III**.

### 4.4 Patch clamp experiments (I, II, III)

The electrophysiological properties of RPE were investigated to assess the functionality and subtype composition of the expressed Nav channels and to analyze the electrical connectivity of RPE. Ionic currents were recorded from mature hESC-derived RPE or mouse RPE monolayers using the standard patch clamp technique in whole-cell configuration either in voltage clamp or current clamp mode (Figure 8). When coupling coefficients were analyzed, two adjacent RPE cells or pairs of varying intercellular distance were recorded simultaneously.

In voltage clamp recordings, the patch pipettes were filled with an internal solution which pH  $\sim$  7.2 was adjusted with CsOH, and osmolarity was set to  $\sim$  290 mOsm. In current clamp recordings, patch pipettes were filled with an internal

solution which pH  $\sim$ 7.15 was adjusted with KOH, and osmolarity was set to  $\sim$  277 mOsm. The resistance of all patch pipettes was 5–7 M $\Omega$  (Sutter Instruments, CA, USA). The components for each internal solution are described in table 2. During all recordings, the cells were superfused with Ames' solution (Sigma-Aldrich or US Biological Life Sciences, MA, USA) at either 2.5 ml or 9 ml per min. The solution was buffered in **Study I** with 10 mM HEPES and supplemented with 10 mM NaCl and 5 mM TEA-Cl and in **Study II–III** by carbonation and warmed to 32 °C. Mouse RPE tissue was illuminated using infrared light (950 nm).

**Table 2.** Internal solutions for patch clamp measurement used in Studies I, II, and III

Component	Voltage clamp (in mM)	Current clamp (in mM)
K-aspartate	-	125
CsCH <sub>3</sub> SO <sub>3</sub>	83	-
CsCl	25	
TEA-Cl	10	
EGTA	5.5	2
CaCl <sub>2</sub>	0.5	1
MgCl <sub>2</sub>	-	1
ATP-Mg	4	4
GTP-Na	0.1	-
Tris-GTP	-	0.5
HEPES	10	10
NaCl	5	
KCl	-	10

The recordings were performed with Axopatch 200B or MultiClamp 700B patch clamp amplifiers connected via AD/DA Digidata 1440 converter to an acquisition computer (all from Molecular Devices, CA, USA). The selection criteria for analyzed recordings was set to having the cell access resistance below 30 M $\Omega$  and membrane resistance above 150 M $\Omega$ . From the voltage clamp data, peak current values were plotted against applied voltages to obtain the current-voltage (IV)-curve. The steady-state inactivation curve was analyzed by plotting a normalized test pulse peak current against a series of prepulse voltages, and the data was fit with the Boltzmann equation. The recovery from inactivation was investigated using two subsequent pulses and plotting the peak of the second pulse current against the pulse interval time. From the current clamp data, input resistance was analyzed as the ratio of change in the membrane potential versus the applied current. Coupling coefficients were analyzed from paired recordings as the ratio of membrane potential change in the coupled cell to that in the current injected cell (See **Study II** for details). Series

resistance was not compensated. The patch clamp data were analyzed with pClamp (10.2 or 10.7 release, Molecular Devices) or Matlab software (R2018b release, Mathworks, MA, USA).

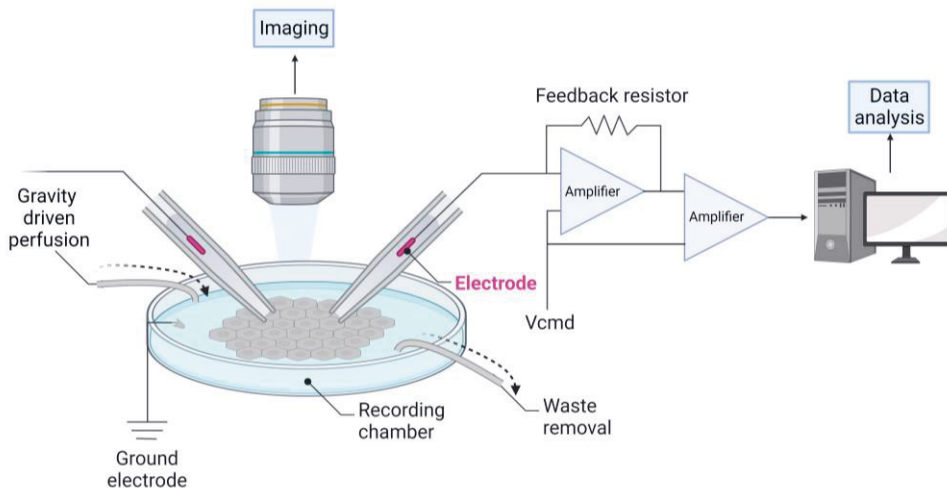


**Figure 8.** A schematic illustration of the patch clamp set up. The samples are placed in a recording chamber and continuously perfused with extracellular solution from a gravity-driven reservoir while a pump removes the solution from the chamber. The cells are visualized with an inverted (**Study I**) or upright (**Study II and III**) microscope connected to a camera and a computer. In whole cell configuration, a high-resistance seal (gigaseal) is formed with the cell membrane through a glass micropipette filled with intracellular solution and connected with an electrode holder to the electrode wire. The cell membrane enclosed within the micropipette tip is then ruptured by suction. When the recordings are performed in voltage clamp mode (**Study I**), the transmembrane voltage is controlled, and the transmembrane current required to maintain the transmembrane voltage is measured. This recording mode involves an electronic feedback system that compares the recorded membrane potential to the command voltage ( $V_{cmd}$ ). In current clamp mode, a known current pulse is applied to the cell, and the membrane voltage change is measured. Here, recordings were performed from individual cells in the RPE monolayer (**Study I and II**) or simultaneously from multiple cells (**Study II and III**). The recorded current or membrane potential changes are analyzed and further processed during the data analysis. The illustration was created with modifications from (Okada n.d.) with BioRender.com.

## 4.5 Phagocytosis assay for cultured and mouse RPE

Phagocytosis assays were performed to investigate the potential roles of  $Na_V$  channels and Cx43 in this process. The purification of porcine POS particles was carried out under red light or minimal light exposure according to previously



published protocols (Mao and Finnemann 2013; Vaajasaari et al. 2011) described in detail in **Study I–III**. The eyecups were obtained from a slaughterhouse and dissected in HEPES buffered Ames' solution to gently remove the retina from each eye. The collected retinas were agitated in 0.73 M sucrose phosphate buffer, filtered, and then separated with ultracentrifugation (112,400 x g for 48 min at +4 °C, Optima ultracentrifuge, Beckman Coulter, Inc., Brea, CA, USA). The obtained POS layer was purified by centrifugation (3000 x g for 10 min) and suspended in 73 mM sucrose phosphate buffer. In the phagocytosis experiments, the POS particles were incubated with RPE cells in medium supplemented with 10% fetal bovine serum (Sigma-Aldrich) with or without blockers. The incubation was carried out at RT or +37 °C in 5% CO<sub>2</sub> for desired times. After the incubation, the monolayers were fixed with paraformaldehyde (PFA, Electron Microscopy Sciences, PA, USA) according to the protocol described in section 4.6.1.

Phagocytosis was studied with mouse RPE by dissecting the eyes under dim red light at different points of the diurnal cycle and then incubating the eyecups with blockers (**Study I**) and/or fixing the tissue with PFA (**Study I, III**). Phagocytosis was imaged live by placing the insert in the Aireka imaging chamber (AirekaCells, China) after a 20 min POS incubation (as described in 4.6.3). To quantify the POS particles, samples in each condition from at least three experiments were imaged with either Zeiss laser scanning confocal microscope (LSM780, Zeiss, Jena, Germany) or Nikon A1R (Nikon Instruments Europe BV, Netherlands) confocal microscope. After filtering the images with a Gaussian function, the obtained Z-maximum intensity projections were binarized with a global threshold. The number of POS particles was quantified by the particle analysis of ImageJ. When only internalized particles were analyzed, the image analysis was performed as previously described (Viheriälä et al. 2021). Further details on the phagocytosis assay analysis can be found in **Study I, III**.

## 4.6 Sample preparation for microscopy imaging

### 4.6.1 Immunocytochemistry (I, II, III)

Immunofluorescence stainings were used to investigate the localization of Nav channels and gap junctions in stem cell-derived and mouse RPE and their

involvement in the phagocytosis process. All samples were washed with PBS before fixation with 4% PFA (15 min) or 1% PFA (10 min). The permeabilization was performed with 0.1% Triton X-100 diluted in PBS (15 min) and blocking with 3% BSA (BSA, 1 h) (All from Sigma-Aldrich). The primary and secondary antibodies (listed in table 3) were diluted in the blocking buffer and incubated with the samples for 1 h. All incubations were carried out at room temperature (RT).

#### 4.6.2 Pre-embedding and cryosections

EM studies were conducted to assess the localization of NaV channels and Cx43 with higher resolution and investigate their possible co-localization with POS. In **Study I**, hESC-RPE were investigated in phagocytosis also with and without TTX. The sample preparation protocol for electron microscopy (EM) is described in detail in **Study I–III** and summarized in table 4. With hESC-RPE, the pre-embedded samples were sectioned perpendicular to the monolayer at 200 nm intervals with a Leica ultracut UCT ultramicrotome (Leica Mikrosysteme GmbH, Austria). For mouse RPE, the cryo-EM method was chosen to preserve the tissue's integrity and morphology, particularly its apical microvilli. However, it is worth noting that this EM method often yields less robust signals at the expense of sample preservation (Jones 2016). Once the samples were frozen, the cryosections were prepared with a Leica EM UC7 cryoultramicrotome (Leica Microsystems, Vienna, Austria) and immunolabeled.

#### 4.6.3 Fixed samples and live imaging

Confocal microscopy was performed by acquiring pixel stacks using either Nikon A1R or Zeiss LSM780 confocal microscopes. The description for excitation laser lines and emission filters can be found in **Studies I–III**. The data was saved in either .czi or .nd formats, and the images were further processed with ImageJ (Schneider, Rasband, and Eliceiri 2012). Final figures were assembled using Adobe Photoshop CC (2015.5.1 release) and Illustrator CC (2015.3.1 release) (Adobe Systems, San Jose, USA). The live imaging of AICS-mGJA1 RPE was performed by securing the insert under a slice anchor in the Aireka coverslip cell chamber with the apical side facing the LSM780 objective. The chamber was filled with cell culture medium with or without blockers (listed in table 6) and kept at 37°C. A Z-stack was obtained every 30 min with LSM780 confocal for a total duration of 90 – 150min

**Table 3.** List of antibodies and actin or DNA binding agents used in studies I, II, and III

<b>Antibody</b>	<b>Manufacturer</b>	<b>Cat. no</b>	<b>Dilution</b>	<b>Study</b>
<b>CRALBP</b>	Abcam	ab15051	1:400	I
<b>Nav1.1</b>	Alomone labs	ASC-001	1:200	I
<b>Nav1.2</b>	Abcam	ab99044	1:200	I
<b>Nav1.3</b>	Alomone labs	ASC-004	1:200	I
<b>Nav1.4</b>	Alomone labs	ASC-020	1:200	I, II
<b>Nav1.5</b>	Alomone labs	AGP-008	1:200	I
<b>Nav1.6</b>	Alomone labs	ASC-009	1:200	I
<b>Nav1.7</b>	Alomone labs	ASC-008	1:200	I
<b>Nav1.8</b>	Alomone labs	AGP-029	1:200	I
<b>Nav1.9</b>	Alomone labs	AGP-030	1:200	I
<b>Pan Nav</b>	Alomone labs	ASC-003	1:200	I
<b>Rab7</b>	Abcam	ab50533	1:50	n/a
<b>ZO-1</b>	Life Technologies	33-9100	1:50	I, II, III
<b>Opsin</b>	Sigma-Aldrich	O4886	1:200	I, III
<b>Cx43</b>	Sigma-Aldrich	C6219	1:200	II, III
<b>Cx36</b>	Thermo Fisher	37-4600	1:50	II
<b>Cx46</b>	Santa Cruz Biotechnology	sc-365394	1:50	II
<b>Rac1</b>	BD Biosciences	610650	1:100	III
<b>Cx43-S373</b>	Thermo Fisher	PA5-64670	1:200	III
<b>Cx43-S279</b>	Thermo Fisher	PA564640	1:200	III
<b>Anti-rabbit AlexaFluor 488</b>	Thermo Fisher	A-21206	1:200	I, III
<b>Anti-rabbit AlexaFluor 488</b>	Thermo Fisher	A-11029	1:200	I, II, III
<b>Anti-rabbit AlexaFluor 568</b>	Thermo Fisher	A-11011	1:200	I, II, III
<b>Anti-rabbit Alexa 647</b>	Thermo Fisher	A-31573	1:200	I
<b>Anti-mouse Alexa Fluor 405</b>	Thermo Fisher	A-31553	1:200	I
<b>Anti-mouse AlexaFluor 488</b>	Thermo Fisher	A-21202	1:200	I, II, III
<b>Anti-mouse AlexaFluor 568</b>	Thermo Fisher	A10037	1:200	I, III
<b>Anti-mouse Alexa 647</b>	Thermo Fisher	A-21236	1:200	I
<b>Anti-guinea pig AlexaFluor 568</b>	Thermo Fisher	A-11075	1:200	I
<b>Anti-guinea pig AlexaFluor 568</b>	Thermo Fisher	A-21450	1:200	I
<b>Ph AlexaFluor 647</b>	Thermo Fisher	A22287	1:50; 1:100	I, II,
<b>Ph Atto 633</b>	Sigma-Aldrich	68825	1:50	I
<b>Ph tetramethylrhodamine B</b>	Sigma-Aldrich	P1951	1:400	I
<b>Ph Atto 488</b>	Sigma-Aldrich	49409	1:100	III
<b>Ph Atto 643</b>	ATTO-TECH	AD643-81	1:100	II, III
<b>ProLong Gold</b>	Thermo Fisher	P36935		I
<b>ProLong Diamond</b>	Thermo Fisher	P36961		I, II, III

Abbreviations: Ph: Phalloidin, ZO-1: Zonula occludens-1, Rab: Ras-related protein, Rac1: Ras-related C3 botulinum toxin substrate 1

#### 4.6.4 Electron microscopy

hESC-RPE slices were imaged with JEOL JEM-1400 transmission electron microscope (JEOL Ltd., Tokyo, Japan) equipped with Quemesa CCD camera (Olympus Soft Imaging Solutions GMBH, Münster, Germany). Mouse cryosections were examined with a Tecnai G2 Spirit 120 kV transmission electron microscope (FEI, Eindhoven, The Netherlands), and images were captured by a Quemesa CCD camera using RADIUS software (EMSYS GmbH, Münster, Germany).

**Table 4.** Summary of EM sample preparation used in Studies I, II, and III

Method	hESC-RPE	mouse RPE
	Epon pre-embedding EM	Cryo-EM
<b>Fixation</b>	Periodate-lysine-paraformaldehyde, 2 h at RT	4% PFA and 2.5% sucrose in 0.1 M PB, overnight at +4 °C
<b>Freezing and sectioning</b>	n/a	Immersed for 2.3 M sucrose in PB and rotated for 4 h at +4°C, liquid nitrogen and then sectioned
<b>Post-sectioning</b>	n/a	Placed on nickel grids, 2% gelatine in PBS, 20 min; 0.1% glycyl-PB, 10 min
<b>Blocking</b>	0.01% saponin and 0.1% BSA in 0.1 M PB (Buffer A), 1 h at RT	Protein A/G Gold conjugates, 15 min
<b>Primary antibodies (ab)</b>	Diluted in Buffer A, 1 h at RT (2x concentration for all ab)	Diluted in 0.1% BSAc, 45 min (4x concentration for all ab)
<b>Secondary ab</b>	1.4 nm gold-conjugated, 1 h at RT	Protein A conjugated 10 nm gold, 30 min
<b>Washes</b>	Buffer A and H <sub>2</sub> O	0.1% BSAc in PBS
<b>Post-fixation</b>	1% glutaraldehyde in phosphate buffer, 10 min at RT	n/a
<b>Quenching</b>	50 mM NH <sub>4</sub> Cl in PB, 5 min at RT	n/a
<b>Enhancement and gold toning</b>	HQ-silver, 5 min, 2% sodium acetate 3 x 5 min at RT, 0.05% gold chloride, 10 min +4 °C, 0.3% sodium thiosulphate, 2 x 10 min at +4 °C	n/a
<b>Reduction, dehydration, and staining</b>	1% osmium tetroxide in 0.1 M PB, 1 h at +4 °C Ethanol (70%, 96%, 100%) 2% uranyl acetate	Stained with neutral UA Coated with 2% methyl cellulose containing 0.4 % UA
<b>Embedding and sectioning</b>	Epon, polymerization, and then sectioning	n/a

Abbreviations: EM: electron microscopy, PFA: periodate-lysine-paraformaldehyde, PB: phosphate buffer, RT: room temperature, UA: uranyl acetate.

## 4.7 Western blot (I, II)

Western blot analysis was used to investigate further the Nav channel and Cx isoform compositions in RPE. The hESC- and mouse RPE protein lysates were obtained by incubating cell pellets in a Halt protease inhibitor cocktail (Thermo Fisher Scientific, MA, USA) supplemented RIPA buffer and centrifugation. When lysates were prepared from monolayers, the cells were triturated and incubated in 50mM HEPES, 150mM NaCl supplemented with 1% Triton-X-100, Halt protease, and phosphatase Inhibitor Cocktail (Thermo Fisher Scientific), and pelleted by centrifugation.

The lysates were fractionated by SDS-PAGE, and the transfer to the membrane was carried out with a Trans Blot Turbo Transfer system (Bio-Rad, Ca, USA). The blots were then blocked with 3% BSA in PBS + 0.1% Tween-20 at RT and labeled with primary antibodies overnight at +4 °C and 1 h with the secondary antibodies (Table 5). The blots were developed with the WesternBright ECL system (Advansta, CA, USA) and imaged with ChemiDoc XRS+ (Bio-Rad). The stripping step was performed with Restore™ Western Blot Stripping Buffer (Thermo Fisher Scientific) for subsequent control protein investigation. The blocking and antibody labeling steps were carried out as described for the target proteins. Detailed protocol for Western blot can be found in **Study I, II**.

**Table 5.** List of antibodies used in Western blot during **Study I and II**

Antibody	Manufacturer	Cat. no	Dilution	Study
<b>Nav1.4</b>	Thermo Fisher	PA5-36989	1:500	I
<b>Nav1.5</b>	Alomone labs	AGP-008	1:500	I
<b>Nav1.6</b>	Alomone labs	ASC-009	1:1000	I
<b>Nav1.8</b>	Alomone labs	ASC-016	1:5000	I
<b>β-actin</b>	Abcam	ab6276	1:2000	I
<b>Cx43</b>	Sigma-Aldrich	C6219	1:2000	II
<b>Cx36</b>	Thermo Fisher	37-4600	1:500	II
<b>Cx46</b>	Santa Cruz Biotechnology	sc-365394	1:500	II
<b>GAPDH</b>	Santa Cruz Biotechnology	Sc-47724	1:500	II
<b>RPE65</b>	GeneTex	GTX103472	1:1000	II
<b>Anti-rabbit HRP</b>	Abcam	ab6721	1:20,000: 1:3000	I I, II
<b>Anti-mouse HRP</b>	Abcam	A-21236	1:20,000: 1:3000	I II
<b>Anti-guinea pig HRP</b>	Abcam	ab6908	1:3000	I

Abbreviations: GAPDH: glyceraldehyde 3-phosphate dehydrogenase, RPE65: Retinoid isomerohydrolase, HRP: horseradish peroxidase.

## 4.8 Pharmacology

This thesis investigated the Nav channels and gap junctions in stem cell-derived and mouse RPE using various pharmacological agents enlisted in table 6. In each experiment, control cells were treated with equal amounts of vehicle used to dissolve the pharmacological agent. The incubation times and further details on each blocker experiment are described in **Study I–III**.

zebrafish

**Table 6.** List of blockers used during **Study I–III**

Blocker (Target)	Manufacturer	Cat. no	Concentration	Study
QX-314-Cl (Nav)	Sigma-Aldrich	552233	2 mM	I
TTX (Nav)	Tocris	1069	10 nM–10 $\mu$ M	I
4,9-AnhydroTTX (Nav1.6)	Tocris	6159	30 nM	I
A-803467 (Nav1.8)	Sigma-Aldrich	A3109	1 $\mu$ M	I
$\mu$ -Conotoxin GIIIB (Nav1.4)	Alomone Labs	C-270	600 nM	I
MFA (Cx)	Sigma-Aldrich	M4531	100 $\mu$ M	II
TAT-Gap19 (Cx43 Hemichannel)	Sigma-Aldrich	SML2319	90 $\mu$ M	II
Rho/Rac/Cdc42 Activator I	Cytoskeleton Inc	CN04	1 $\mu$ g/ml	III
PD 98059 (MEK)	Sigma-Aldrich	513001	50 $\mu$ M	III
PMA (PKC)	Tocris	1201	165 nmol	III
Roscovitine (Cdk5)	R&D Systems	1332/10	100 $\mu$ M	III

Abbreviations: TTX: tetrodotoxin, MFA: meclofenamic acid, Rho: Ras homologous, Rac1: Ras-related C3 botulinum toxin substrate 1, Cdc42: Cell division control protein 42 homolog, MEK: Mitogen-activated protein kinase, PMA: Phorbol 12-myristate 13-acetate, PKC: Protein kinase C, Cdk5: Cyclin-dependent kinase 5.

## 4.9 Statistical analysis

To assess the effect of blockers and analyze the efficiency of the phagocytosis process, the cells treated with pharmacological modulators or short hairpin RNA (shRNA) were compared against controls. All statistical tests were carried out with the IBM SPSS Statistics for Windows, version 26 (IBM Corp., N.Y., USA). In the patch clamp recordings, the normality was assessed either by Kurtosis or Shapiro-Wilk test. The differences between control and blocker recordings were then analyzed by the Mann-Whitney U test or 2-tailed unpaired Student's t-test. In the

POS quantification analyses, the data's normality was tested using Shapiro–Wilk test. The differences between control and blocker groups were first analyzed using ANOVA and then by pairwise comparisons using Kruskal–Wallis or the Mann Whitney U test.

## 5 SUMMARY OF THE RESULTS

### 5.1 Discovery of Nav channels and characterization of gap junctions in RPE (Study I and II)

In this thesis, we discovered the cellular machinery that provides RPE the capacity for fast electrical signaling. Moreover, our results reveal how the electrical signals in RPE are spread in the monolayer. This work required setting up the experimental methodology to enable the direct measurements of cell-cell coupling from intact mouse RPE monolayers by dual patch clamp technique. Interestingly, these experiments uncovered links between cellular electrical communication in RPE and phagocytosis of photoreceptor outer segments. Lastly, we identified a regulator of gap junctions which to date had not, to my knowledge, been investigated in RPE tissue.

#### 5.1.1 Several subtypes of Nav channels function in RPE

A striking result of this thesis work was the discovery of Nav channels in mature RPE tissue. As outlined in chapter 2.3.4, these channels had previously been dismissed as cell culture artifacts. Our initial discovery of Nav channels in RPE was obtained by patch clamp recordings from intact hESC-RPE monolayers. Further identification of the family of Nav channels in both hESC- and mouse RPE was performed with immunocytochemistry (Figure 9A), confocal microscopy, western blotting, and mass spectrometry. Patch clamp recordings revealed typical characteristics of a Nav channel (Figure 9B), such as fast activation and inactivation and their voltage-dependence (Table 7). The current amplitude could be reduced by applying classical blockers for this channel family, such as TTX. The immunolabeling with an antibody recognizing universally all Nav subtypes (Pan Nav) showed that the channels localized in cell-cell junctions and apical membrane. Surprisingly, when the recordings were performed from dissociated RPE cells, the conventional recording configuration in the epithelial field, the currents were substantially more infrequent and had considerably lower amplitudes (**Study I: page 3, Figure 1D**). In the



dissociated cells, the Nav<sub>v</sub> labeling was found in the sequestered ZO-I positive belt, situated between the apical and basal halves of the cell (**Study I: page 4, Figure 2E**).

**Table 7.** Characteristics of Nav<sub>v</sub> current identified in patch clamp recordings in **Study I**

Summary of results* (unit, n = recorded cells)	Value
Resting membrane potential (mV, n = 15)	-47 ± 1
Maximum current amplitude (pA, n = 21)	370 ± 60
Membrane capacitance (pF, n = 21)	28 ± 2
Current density (pA/pF, n = 21)	14 ± 3
Activation voltage (mV)	ca. -50
Peak voltage (mV)	ca. -13
Half-inactivation voltage (V <sub>1/2</sub> , mV, n = 7)	-94 ± 1
Recovery from inactivation (τ, ms, n = 5)	54 ± 3

\*Values are mean ± SEM or obtained from curve fitting

Out of the nine known Nav<sub>v</sub> channel subtypes, all were identified with at least one of the used methods except subtype Nav<sub>v</sub>1.2 (Table 8). The Na<sub>x</sub> channel was also identified. However, channel subtypes Nav<sub>v</sub>1.4–Nav<sub>v</sub>1.6 and Nav<sub>v</sub>1.8 were found to be most prominent in RPE. Most of these channel subtypes were found to localize in the cell-cell junctions explaining the robust junctional localization we had observed with Pan Nav<sub>v</sub>. Of the subunits, Nav<sub>v</sub>1.4 had a distinctive labeling pattern as it localized into specific junctional foci. Other Nav<sub>v</sub> subtypes, such as Nav<sub>v</sub>1.6 and Nav<sub>v</sub>1.8, were also found to localize in the apical membrane (**Study I: page 6, Figure 3A and 3B**). We then wanted to confirm the presence and functionality of the major Nav<sub>v</sub> subtypes we identified using other methods. Thus, selective blockers for Nav<sub>v</sub>1.4, Nav<sub>v</sub>1.6, and Nav<sub>v</sub>1.8 were used in patch clamp recordings (Table 6 and table 8) with or without the addition of TTX that significantly reduced the current amplitude (**Study I: page 6, Figure 3C and 3D**). At the time of **Study I**, a selective blocker for Nav<sub>v</sub>1.5 was not commercially available.

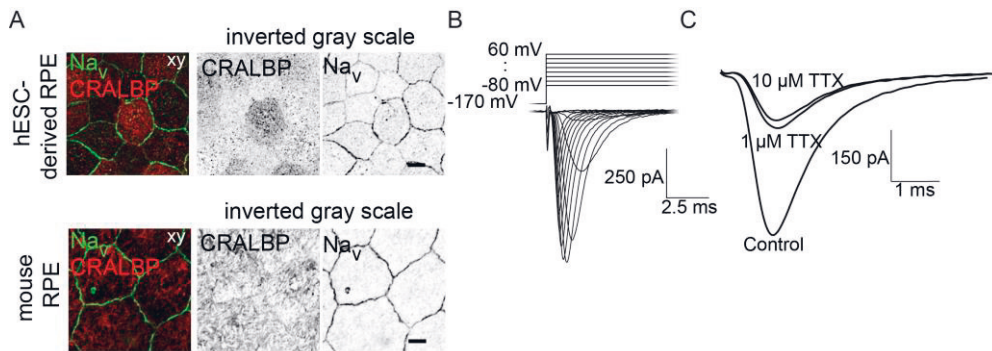


**Figure 9.** A) Laser scanning confocal microscopy (LSCM) images on Nav distribution in hESC-RPE (top) and mouse RPE (bottom) stained against Nav channels (green) and RPE marker CRALBP (red) as well as their corresponding inverted greyscale Z-maximum intensity projections. Scale bars 10  $\mu$ m. B) Whole-cell patch clamp recordings from mature hESC-RPE either in control conditions or C) after applying 1–10  $\mu$ M TTX. The images are reproduced and modified under the terms of the Creative Commons license from **Study I**. Abbreviations: CRALBP: retinaldehyde binding protein 1, TTX: tetrodotoxin.

**Table 8.** Identified Nav subtypes in RPE and the methods used in **Study I**, resistance to TTX, and selective blockers used in the recordings are listed below.

Nav channel subtype	Method	TTX-R	Selective blocker
Nav1.1	IF (1% PFA), MS	no	-
Nav1.2	n/a	no	-
Nav1.3	IF (1% PFA), MS	no	-
Nav1.4	IF (4% PFA), MS, shRNA	no	$\mu$ -Conotoxin GIIIB
Nav1.5	IF (4% PFA), MS	yes	-
Nav1.6	IF (4% PFA), MS	no	4,9-AnhydroTTX
Nav1.7	IF (1% PFA), MS	no	-
Nav1.8	IF (4% PFA), MS	yes	A-803467
Nav1.9	IF (1% PFA), MS	yes	-
Na <sub>x</sub>	MS	-	-

Abbreviations: TTX: tetrodotoxin, TTX-R: resistant to TTX, IF: immunofluorescence, MS: mass spectrometry, shRNA: small hairpin RNA, PFA: paraformaldehyde.

## 5.1.2 Cx43 is the major isoform in RPE, and electrical connectivity is low at baseline (Study II)

The Cx isoform distribution was investigated in hESC- and mouse RPE using Western blots that showed that Cx43 was the major isoform of this tissue. Cx36 was also identified but at much lower levels. Isoform Cx46 was not detected in either hESC- or mouse RPE (Figure 10A). Immunocytochemistry stainings showed that Cx43 localized at specific junctional foci at the cell-cell junctions, but some labeling was also found on the apical membrane (Figure 10B). The electrical connectivity of RPE was investigated by analyzing input resistance and the coupling coefficients (See chapter 4 and **Study II** for details) obtained from simultaneously recorded cell pairs. These recordings demonstrated that RPE cells generally exhibit low input resistance. Yet, it was significantly increased after gap junctions were blocked with meclofenamic acid (MFA) (Figure 10C).

Interestingly, the electrical coupling was found to be relatively low in hESC- and mouse RPE preparations and decreased dramatically with increasing inter-pair distance (Table 9). As RPE cells had previously been suggested to be connected via gap junctions in developing chicks (Pearson et al. 2005, 2004) and neonate rats (Himpens et al. 1999), I had initially hypothesized (see section 3) that the coupling coefficients would be higher. The strong effect of MFA also suggested extensive electrical coupling. This discrepancy was investigated further by building a computational model indicating that the blockade of gap junctional conductance was insufficient to achieve the observed change in the cell's input resistance (**Study II: page 14, Figure 6A**). The apical labeling of Cx43 indicated that RPE cells could also have hemichannels. Their functionality was verified by a dye uptake study and a selective blocker for Cx43 hemichannels TAT-Gap19 that increased the input resistance of both hESC- and mouse RPE cells (**Study II: page 14, Figure 6C and 6D**). Thus, the strong effect of MFA can, at least partially, be explained with apical hemichannels, which contribute to the input resistance, but do not affect the intercellular coupling coefficient.

**Table 9.** Coupling coefficients obtained from simultaneously recorded pairs of RPE cells

Inter-pair distance	hESC-RPE (n=recorded pairs)	Mouse RPE (n=recorded pairs)
Adjacent	0.12 +/- 0.024 (n=5)	0.09 +/- 0.015 (n = 21)
1 cell between	0.04 +/- 0.007 (n = 7)	0.068 +/- 0.014 (n = 3)
2 cells between	0.01 +/- 0.003 (n= 4)	0.039 +/- 0.008 (n = 3)
3 cells between	0.01+/- 0.005 (n=3)	0.036 +/- 0.008 (n=4)

\*Values are mean  $\pm$  SEM

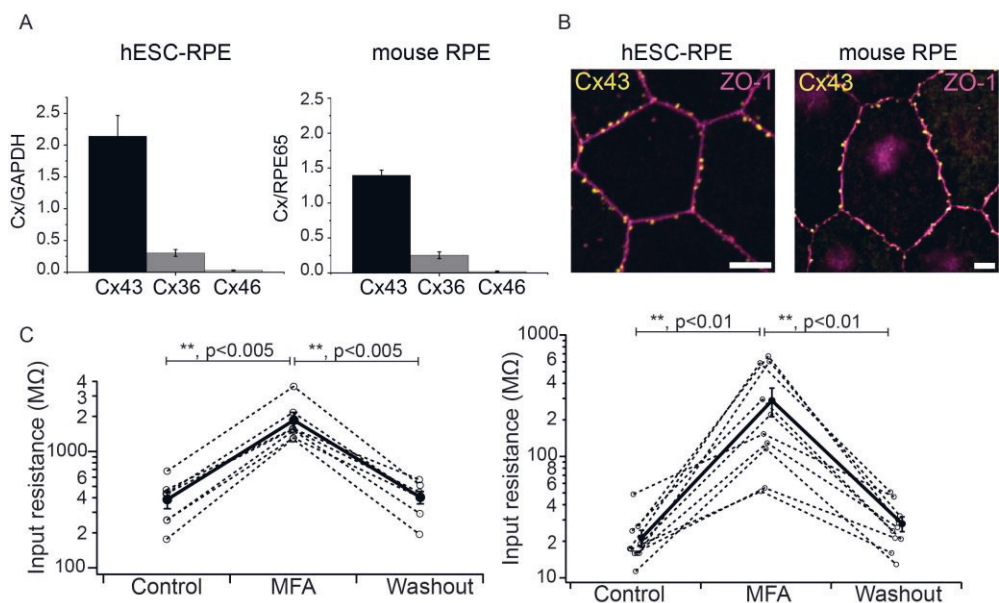


**Figure 10.** A) Western blot analysis of Cx43, Cx36, and Cx46 isoforms. Whole cell lysates were analyzed by electroblotting, and the band intensities for the Cx isoforms were analyzed against either GAPDH (hESC-RPE) or RPE65 (mouse RPE). B) Laser scanning confocal microscopy (LSCM) images on Cx43 distribution in hESC-RPE (left) and mouse RPE (right) stained against Cx43 channels (yellow) and tight junction marker ZO-1 (magenta). Scale bars 5 μm. C) Whole-cell patch clamp recordings from mature hESC-RPE (left) or mouse RPE (right) either in control conditions or after the application of MFA. The images are reproduced and modified under the terms of the Creative Commons license from **Study II**. Abbreviations: GAPDH: Glyceraldehyde 3-phosphate dehydrogenase, RPE65: retinoid isomerohydrolase MFA: meclofenamic acid, ZO-1: zonula occludens-1.

*The level of electrical coupling is regulated by Cdk5 (Study III)*

Our electrophysiological recordings suggested that the input resistance can be dynamically regulated in RPE, and the measurements conducted during phagocytosis (**Study III: page 52, Supplementary Figure 2**) implicate that the circadian rhythm might regulate the connectivity. Therefore, we wanted to investigate the possible mechanisms by which the connectivity is diurnally modulated. We focused on kinase Cdk5 as it has previously been linked to the regulation of the circadian cycle (Kwak et al. 2013; Brenna et al. 2019). Cdk5 kinase had not, to my knowledge, been previously investigated in RPE tissue. The presence of Cdk5 was investigated by immunolabeling mouse RPE at various circadian time points. The results showed that the kinase was present in the tissue and changed its localization pattern

according to the diurnal rhythm. At the light onset, Cdk5 was found at specific clusters, while its labeling was much more diffuse during the day (**Study III: page 48, Figure 5D**). The presence of Cdk5 and the effect of its inhibitor roscovitine were then investigated in hESC-RPE by analyzing mRNA levels. This quantification showed that the level of Cdk5 was significantly lower after roscovitine treatment. Moreover, roscovitine also significantly reduced the GJA1 (Cx43) level, while the control protein GAPDH was unaffected (**Study III: page 47, Figure 4A**).

The effect of roscovitine on gap junctional localization and electrical coupling was investigated in mEGFP-tagged Cx43 hiPSC-RPE cells (**Study III: page 47, Figure 4B**). These experiments showed that blocking Cdk5 increased the junctional labeling of Cx43. In addition, our paired patch clamp recordings with hESC-RPE showed that after roscovitine incubation, the cells had significantly higher coupling coefficients than vehicle-treated RPE cells (**Study III: page 48, Figure 5A**).

## 5.2 The role of Nav channels and gap junctions in phagocytosis

To unravel the contribution of Nav channels and gap junctions to RPE physiology, we focused on one particularly essential function of RPE, the renewal of photoreceptor outer segments. This task is one of the most time-restricted functions of RPE, requiring rapid coordination on a monolayer level and dramatic reorganization of the actin cytoskeleton. Cdk5 kinase had not, to my knowledge, been previously investigated in RPE tissue.

### 5.2.1 Nav channels and gap junctions translocate during POS phagocytosis (Study I, III)

We first wanted to analyze what happens to Nav channels and gap junctions during POS phagocytosis in hESC- and mouse RPE by investigating them with immunolabeling. We focused on two of the main Nav subtypes we had found, Nav1.4 and Nav1.8, and the major Cx isoform, Cx43. Strikingly, our results showed that Nav channels and Cx43 change their localization from the cell-cell junctions and localized adjacent to the POS particles. In mouse RPE, this change in labeling pattern was evident both at light onset and two hours after the light onset (**Study I: page 7, Figure 4 and Study III: page 44, Figure 1**). In hESC-RPE, the number of Cx43 foci was significantly higher after 30 min of POS challenge, and much of

the label was found on the apical membrane or in the cytosol. After 2 hours of POS, very minimal junctional labeling was detected. Overall, these experiments indicated that Nav channels and gap junctions are dynamically regulated during the phagocytosis process.

This change in Nav channel and gap junction localization was studied in more detail by EM by labeling the target proteins with gold nanoparticles either in epon-embedded slices (hESC) or cryosections (mouse) (Figure 11 and **Study III: page 45, Figure 2C**). The results showed that in control conditions (no phagocytosis for hESC, afternoon for mouse RPE), the labeling of Nav1.4, Nav1.8, and Cx43 was found mostly junctional or in the apical membrane. Yet, during peak phagocytosis (2 h POS for hESC or 1.5 h from the light onset for mouse), the labeling was much more diffuse, while junctional foci were decreased. Labeling for Nav1.4 and Cx43 was also identified adjacent to internalized phagosomes. In mouse RPE, the Cx43 label was found in structures resembling annular gap junctions. After 4 h of POS incubation, junctional labeling had partly or fully restored for Cx43, while Nav1.8 was still located adjacent to internalized POS. The opsin-adjacent localization pattern was also found with confocal microscopy in immunostainings for Nav1.4, Nav1.8, and Cx43 (**Study I: page 7, Figure 4A, Study III: page 46, Figure 1**).

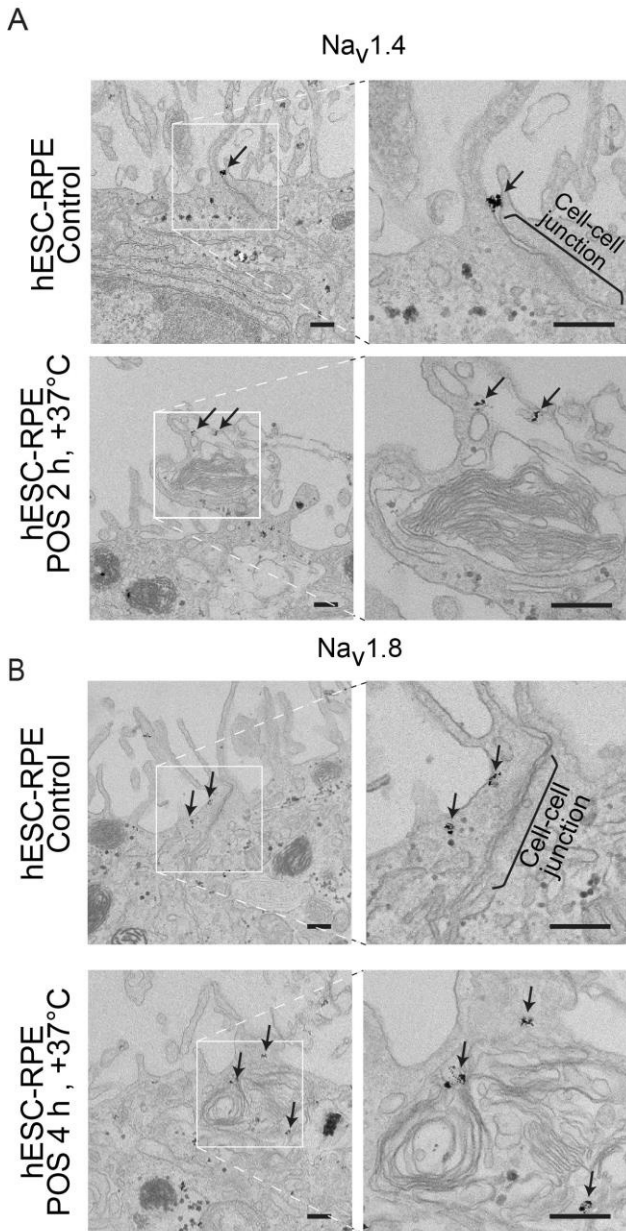


**Figure 11.** A) Nav1.4 and B) Nav1.8 in control conditions (top) and during phagocytosis of purified photoreceptor outer segments (bottom). In control samples, both channels localized adjacent to the cell-cell junctions (black arrows). However, after incubating the monolayers with outer segment particles for either 2 h or 4 h, the Nav localization (black arrows) was also identified around the phagocytic cups and recently ingested phagosomes. Scale bars 250 nm. The images are modified under the terms of the Creative Commons license from **Study I**.

## 5.2.2 Nav1.4 translocation is inhibited by Nav blockers, Cx43 translocation is regulated by PKC and Cdk5 (Study I, III)

Nav1.4 and Cx43 translocation regulation was investigated by immunolabeling hESC- and mouse RPE. Interestingly, Nav translocation was drastically inhibited after the monolayers had been treated with TTX and/or specific blockers for Nav1.4. This phenomenon occurred in both RPE preparations (**Study I: page 8, Figure 5**). Moreover, Nav1.8 was found to correlate with Rab7, and they both also localized with opsin during the 2 h follow-up of phagocytosis (Figures 12A and 12B). The overall labeling patterns for Nav1.8 and Rab7 were much more homogenous 10 h after light onset when the peak phagocytosis was over (Figure 12C).

The regulation of Cx43 turnover was investigated using phospho-specific Cx43 antibodies, of which S279 was found to be most significant for POS phagocytosis (**Study III: page 46 Figure 3**). This modification was found to appear after 15–30 min of POS incubation and disappear by 2 h. S279 was not detected in hESC-RPE without the addition of POS particles, but in mice, some level of staining was identified at all times of the circadian cycle (**Study III: page 48, Figure 5E**). However, at light onset, S279 localized together with opsin and was much more diffuse than during the day.

The Cx43 phosphorylation was analyzed further by investigating the activities of various kinases such as MAPK, PKC, and Cdk5 (**Study III: page 46, Figure 3, page 48, Figure 5**). The data showed that PKC activation was sufficient to induce Cx43 internalization even without the addition of POS. On the other hand, inhibiting MAPK had no apparent effect on Cx43, nor did it affect S279 emergence (**Study III: page 46, Figure 3C**). Interestingly, Cdk5 inhibition was found to inhibit Cx43 translocation but not prevent S279 emergence (**Study III: page 48, Figure 5B**). Therefore, the reversibility of roscovitine treatment was investigated in mEGFP-tagged Cx43 hiPSC-RPE by switching it to either vehicle or phorbol 12-myristate 13-acetate (PMA)-supplemented medium. The results showed that roscovitine was not fully reversible by 90 min in vehicle-treated cells. However, when roscovitine was replaced with PMA, the Cx43 foci were rapidly internalized. Furthermore, immunolabeling showed that in the PMA-treated cells, Cx43 was phosphorylated at S279 before the internalization of gap junctions (**Study III: page 47, Figure 4**). The translocation of Cx43 might be involved in the Rac1 pathway as these proteins were found to localize to the same clusters at a specific phagocytosis timepoint (**Study III: page 48, Figure 6**).



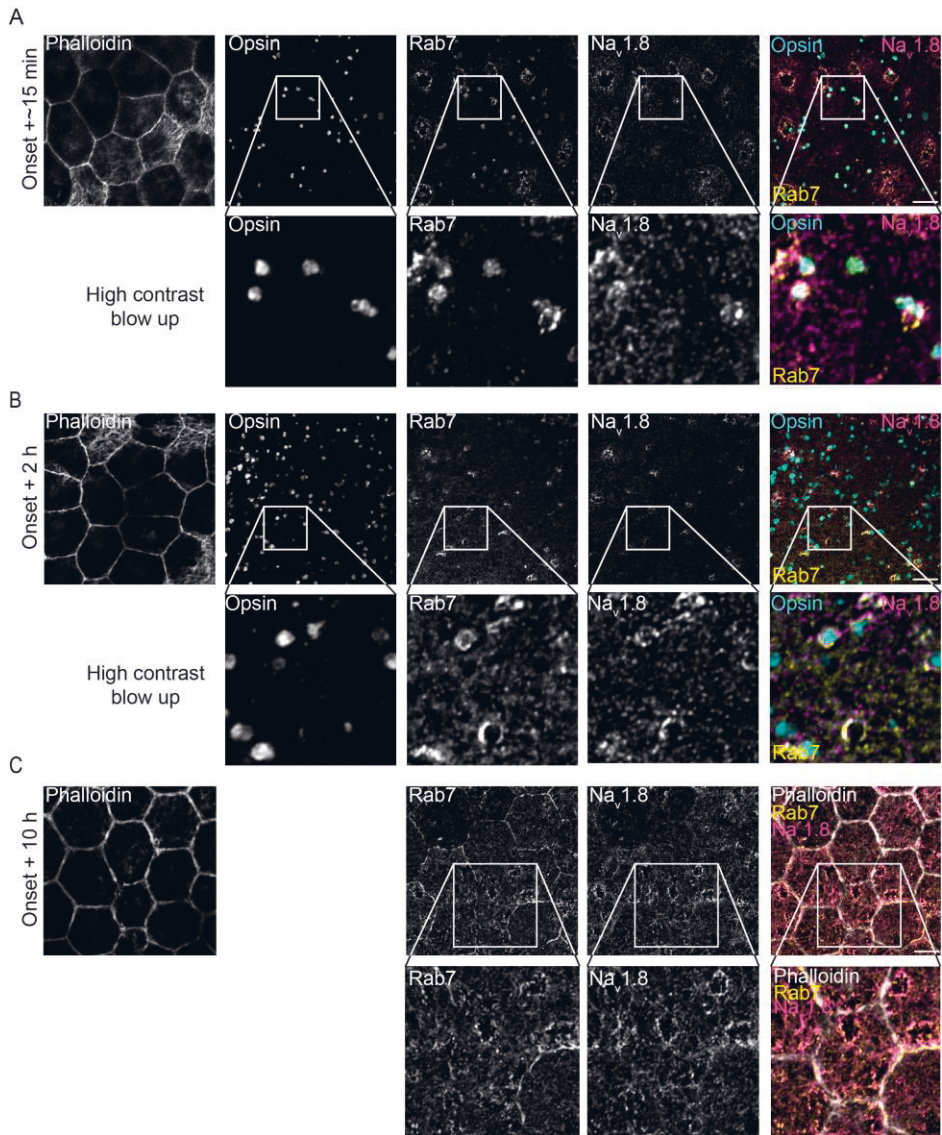


**Figure 12.** The role of Nav1.8 and the interaction of Nav1.8 and endosomal marker Rab7 was studied in mouse RPE by dissecting the eyes at various time points of the diurnal cycle. Filamentous actin was labeled with phalloidin (grey) to highlight the cellular morphology and cell-cell junctions. A high contrast blow-up of selected regions is shown with white boxes. Laser scanning confocal microscopy Z-maximum intensity projections of mouse RPE prepared (A) at 15 min after the light onset showed clustering of Rab7 (yellow) and Nav1.8 (magenta) together with POS particles (opsin, blue). (B) 2 h after the light onset, Nav1.8 (magenta) and Rab7 (yellow) co-localized with POS (blue) but started to show more homogeneous localization patterns. (C) 10 h after light onset, diffuse labeling was demonstrated for Rab7 (yellow) and Nav1.8 (magenta). Scale bars 10  $\mu$ m. Image modified from our bioRxiv manuscript (Johansson et al. 2019) that was not included in **Study I-III**.

### 5.2.3 Inhibition of Nav channel activity and gap junction translocation decreases the efficiency of phagocytosis (Study I, III)

The importance of Nav channel activity and Cx43 translocation on phagocytosis was investigated by quantifying the number of POS particles in hESC-RPE with or without the presence of Nav blockers and roscovitine (**Study I: page 10, Figure 7, Study III: page 48, Figure 5C**). An example of POS assays can be found in Figure 13. The results showed no difference in POS binding between control and Nav blocker-treated samples. However, in control samples, the ingestion and processing of the POS particles were more efficient as their number first increased significantly and then decreased. The observed change suggests that the POS particles are cleaved into smaller fragments and then degraded. However, in the Nav blocker-treated samples, the number of POS particles did not change between the internalization and further processing steps, suggesting delayed processing. The decrease in phagocytosis was also observed in opsin labeling in EM images (**Study I: page 10, Figure 7B**) and in hESC-RPE, where Nav1.4 activity had been silenced with shRNA (**Study I: page 9, Figure 6**). Taken together, these findings showed that the activity of Nav channels and their translocation are important for POS phagocytosis. Interestingly, inhibiting gap junction translocation by roscovitine was also found to decrease the total number of POS particles (**Study III: page 48, Figure 5C**). The binding and internalization steps were not studied separately, but the timing of S279 suggests that Cx43 is involved in the early stages of the phagocytosis pathway. Moreover, the number of internalized particles was reduced with pharmacologically activated Rac1, which also inhibited the translocation of Cx43 and decreased its mRNA level (**Study III: page 49, Figure 6, page 51, Supplementary Figure 1C**). Our investigation with roscovitine (**Study III: page 49, Figure 6A**) and previous literature (Posada-Duque, Palacio-Castañeda, and Cardona-Gómez 2015; Alexander, Yang, and Hinds 2004; Ito et al. 2014) indicate that Rac1 is regulated by Cdk5.

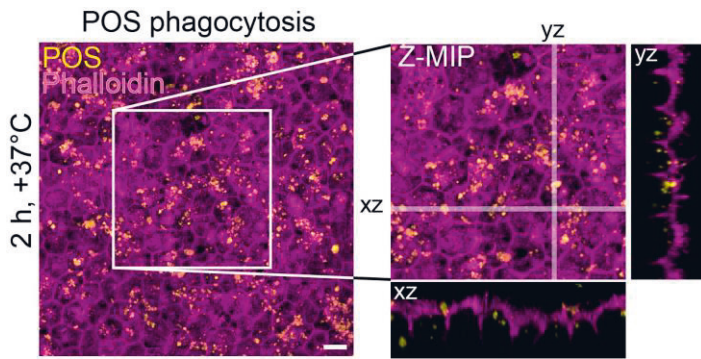


**Figure 13.** POS phagocytosis assay of hESC-derived RPE. Laser scanning confocal microscopy example of purified outer segments labeled with opsin (yellow) that were quantified to analyze the efficiency of the phagocytosis process *in vitro* by counting total numbers of POS or internalized particles (shown in yz and yz cross-sections). Phalloidin (magenta) was used as a counterstain to assess the engulfment of POS. Scale bar 10  $\mu\text{m}$ . The images are reproduced and modified under the terms of the Creative Commons license from **Study I**.

## 6 DISCUSSION

### 6.1 RPE cells are capable of fast electrical signaling

Prior to this study, the presence of  $\text{Na}_v$  channels in RPE had remained elusive. The currents had only been recorded in sub-confluent cultures and not in freshly isolated single cells from intact RPE tissue, and the recordings from RPE monolayers had been missing. Our data show that the lack of  $\text{Na}_v$  currents in isolated cells results from the fact that these channels become sequestered during enzymatic treatments. We believe that the single-cell morphology, squeezing the channel-rich area to a tight space between apical and basolateral sides, makes the channels electrically less accessible. In **Study I**, we determined that mature intact RPE expresses several functional  $\text{Na}_v$  channels that largely localize to the cell-cell junctions or apical membrane. This work adds to the growing body of evidence that the purpose of these channels extends beyond action potential generation in cell types such as neurons and cardiac myocytes. Our findings raise questions about the mechanisms that enable  $\text{Na}_v$  channels to fulfill their noncanonical physiological roles in RPE. While to date,  $\text{Na}_v$  currents have already been identified in various other non-excitable cell types, detailed models justifying their activation range in these cell types are lacking.

It is probable that the activation of  $\text{Na}_v$  channels in non-excitable cells requires the concerted activity of multiple ion channel types to enable rapid switching between inactivated, closed, and open conducting states. While we do not have data showing that, in physiological conditions, RPE cells would generate action potentials, new work from our group (Ignatova et al., 2022, in revision) and the initial reports of  $\text{Na}_v$  currents in cultured RPE (Botchkin and Matthews 1994) demonstrate that RPE cells can support action potential-like membrane voltage changes in laboratory conditions. Membrane potential hyperpolarization relieves the inactivation of  $\text{Ca}_v$  and  $\text{Na}_v$  channels which is a prerequisite to their subsequent transition to the open state (Chiu 1977; W. A. Catterall 2000a). It has been speculated that in other non-excitable cells, such as red blood cells, this hyperpolarization could be accomplished by stochastic activation of a  $\text{Ca}^{2+}$ -dependent potassium channel (Gardos channel) (Kaestner et al. 2018). In RPE, this change in membrane potential

could be attributed to its BK-type  $K^+$  channels, which have been thought to be highly activated by L-type  $Ca^{2+}$  channels (Wimmers, Halsband, et al. 2008). When BK channels are activated in this manner, their voltage dependence has been shown to shift to the physiological range of RPE resting potentials (Tao and Kelly 1996; Wimmers, Coepicus, et al. 2008).

Interestingly, studies with smooth muscle cells have demonstrated that  $Ca^{2+}$  sparks can initiate hyperpolarization up to  $\sim 20$  mV (Sancho and Kyle 2021). It is worth noting that in **Study I**, the half-maximal inactivation of  $Na_V$  channels was determined to be  $-94$  mV. This inactivation value would mean that the membrane potential of RPE cells (typically  $\sim -50$  mV for cultured RPE and  $\sim -70$  mV for mouse RPE cells, **Study II**) had to change significantly to relieve enough of the channels from the inactivated state. Thus, in these conditions, the resulting window current, which can be seen in the region where inactivation and activation curves overlap, would be very small (Figure 14). However, it is worth noting that this window was only estimated based on the total population of  $Na_V$  channels averaging the activity of all channel subtypes. Notably, the voltage dependence of inactivation and activation varies between  $Na_V$  channel types. For instance, the activation of the  $Na_V1.8$  subtype is known to occur at more depolarized membrane potentials compared to other  $Na_V$  channels and shows slower inactivation with persistent current (X. Huang et al. 2022). It is also possible that certain  $Na_V$  channel subtypes affect the window current more than others (Frenz et al. 2014). More importantly, the recordings in **Study I** were performed with a cesium-based internal solution that typically eliminates  $K^+$  currents and were carried out at RT. Notably, more recent work from our group, where the recordings were carried out in more physiological conditions, indicates that the half-maximal inactivation was closer to  $\sim -60$  mV (Ignatova et al., 2022, *in revision*). Therefore, the hyperpolarization induced by BK channels would be sufficient to activate a portion of the  $Na_V$  channels.

It is possible that the opening of BK channels could act in a stochastic manner, and their subsequent closure would then, in part, help to depolarize the membrane to open  $Na_V$  channels. Previous studies with vascular myocytes have suggested that KCNQ channels, since they have very negative thresholds, could serve as subthreshold brakes to prevent the activation of  $Ca_V$  channels. Thus, reducing the activity of KCNQ channels would also lower the threshold for  $Ca_V$  channel activation (Mani and Byron 2011). Reducing the activity of the KCNQ channels found in apical and basolateral membranes in RPE (Korkka, Skottman, and Nymark 2022; Pattnaik and Hughes 2012) could also help to activate  $Na_V$  channels. These channels have also been speculated to reduce their activity on the basolateral side to

help combat the  $K^+$  changes caused by light exposure (Reichhart and Strauß 2020). Alternatively, various modifications have been shown to alter  $Na_v$  channels' gating and voltage dependence. For instance, the threshold for activation has been shown to shift to the hyperpolarizing direction by changing the type or structure of the membrane phospholipids, particularly sphingomyelins, to enable the channel voltage sensors to enter the active state with less energy (Combs et al. 2013). Alternatively, the threshold can be modified by the auxiliary  $\beta$  subunits of the  $Na_v$  channels (E. J. Yu et al. 2005). As the current density in non-excitable cells is typically lower when compared to neurons (Black and Waxman 2013), smaller proportions of active channels could still have meaningful consequences on physiology.  $Na^+$  transients have been observed in hippocampal astrocytes after Schaffer collateral stimulation, suggesting that this signaling occurs in response to excitatory synaptic activity (Langer et al. 2012). If a small population of  $Na_v$  channels is opened, their depolarization could help activate additional  $Ca_v$  channels. The fast kinetics of the channels enables this regulation to be very dynamic.

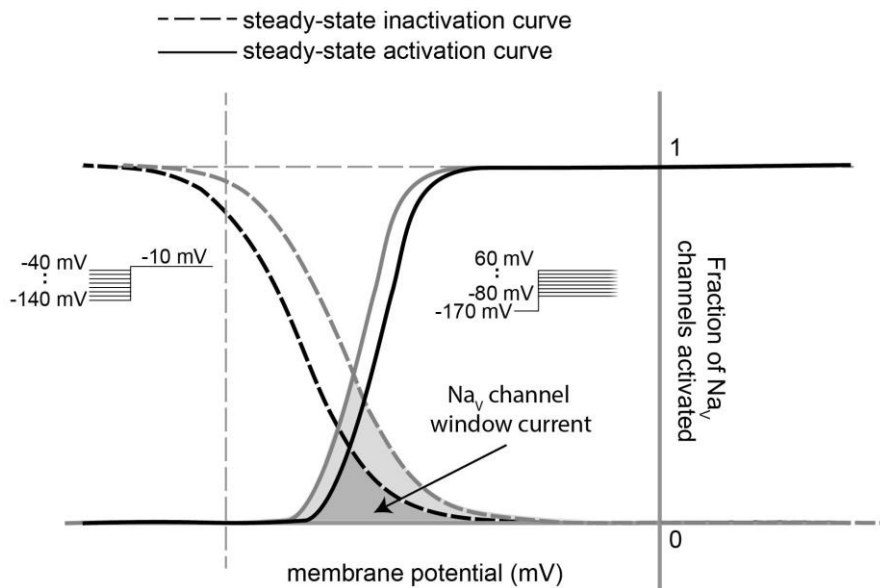


**Figure 14.** Schematic illustration of the steady-state inactivation (dashed line) and activation (solid line) curves of  $Na_v$  channels and the resulting window current (grey area). The inactivation (left) is obtained by plotting a test pulse against the hyperpolarizing prepulse, while the activation (right) is analyzed from a series of depolarizing voltage steps, as shown in **Study 1**. Within this range of membrane voltages, a population of  $Na_v$  channels is activated and their inactivation is submaximal. This window current is increased (light grey area) when either the inactivation or activation of  $Na_v$  channels is shifted. This change can be caused by multiple mechanisms, including the auxiliary  $\beta$  subunits or membrane stretch.

## 6.2 The electrical connectivity of RPE cells can be dynamically modified

Gap junctions in RPE have shown to be unusual as they predominantly localize within the tight junctions. Thus, the interaction of gap and tight junctions has been speculated to be particularly important to RPE (Lawrence J. Rizzolo et al. 2011; Hudspeth and Yee 1973). It has been well established that gap junctions provide various functional properties to the retinal circuitry and that these channels are important regulators for retinal organogenesis. Yet, the electrophysiological characteristics and the extent of physiological coupling had not been investigated in detail in mature RPE. This study demonstrated that the input resistance, similar to what had been obtained in astrocytes, was low in RPE cells, indicating that the cells display considerable overall permeability to ions at rest (McNeill et al. 2021).

Despite the extensive network of Cx43 plaques, the resulting coupling coefficients, like the cells' input resistance, were found to be relatively low. The values reported in **Study II** are compared to retinal neurons and other cell types in table 10. This comparison showed that the values obtained in RPE are lower than previously reported for retinal neurons or other epithelia but higher than the original values reported for astrocytes. The differences between RPE and other epithelial cells could reflect species-dependent variation or, alternatively, reflect the uniqueness of RPE's structure and functional demands mentioned in the literature review. Yet, the recordings obtained in **Study II** also show that the electrophysiological properties, including input resistance, are not homogenous in RPE. Moreover, in these recordings, the connectome was not investigated concerning their localization in the eye. Previous studies have shown that RPE cells can display different morphological features such as shape, size, and level of pigmentation depending on their retinal localization (Kim et al. 2021; Boulton and Dayhaw-Barker 2001). The expression levels of various proteins, including Na<sup>+</sup>K<sup>+</sup>-ATPase, also exhibit regional variation. This heterogeneity has partly been explained by the fact that different areas of RPE develop at different timeframes (Burke and Hjelmeland 2005). Interestingly, recent work in human RPE identified several distinct cell populations which differ, for instance, in terms of their susceptibility to retinal diseases (Ortolan et al. 2022). Thus, it is reasonable to speculate that RPE cells might also display functional mosaicism. In fact, individual RPE cells show variation in their K<sup>+</sup> channel functionality (Korkka, Skottman, and Nymark 2022).

**Table 10.** Reported coupling coefficients (CC) for retinal neurons and other cell types.

Retinal neuron	CC	Species	Reference
<b>Cones</b>	~0.15	macaque	(Hornstein, Verweij, and Schnapf 2004; Trenholm and Awatramani 2019)
<b>Rods</b>	0.07–0.15	tiger salamander	(J. Zhang and Wu 2005; Werblin 1978; Trenholm and Awatramani 2019)
<b>Cone-rod pairs</b>	~0.15	tiger salamander	(Attwell, Wilson, and Wu 1984; Trenholm and Awatramani 2019)
<b>Horizontal cells</b>	0.5 (values >0.9 have also been reported)	white perch <sup>1</sup> , catfish <sup>2</sup> , zebrafish <sup>3</sup> giant danio <sup>4</sup>	<sup>1</sup> (Lasater and Dowling 1985), <sup>2</sup> (DeVries and Schwartz 1989), <sup>3</sup> (D. G. McMahon 1994), <sup>4</sup> (D. G. McMahon and Mattson 1996)
<b>Bipolar cells</b>	~0.3	carp <sup>1</sup> , teleost fish <sup>2</sup> , rabbit <sup>3</sup> , primate <sup>4</sup> , goldfish <sup>5</sup>	<sup>1</sup> (Kujiraoka and Saito 1986), <sup>2</sup> (Umino et al. 1994), <sup>3</sup> (Mills 1999), <sup>4</sup> (Dacey et al. 2000), <sup>5</sup> (Arai, Tanaka, and Tachibana 2010)
<b>Amacrine cells</b>	~0.3	rat	(Veruki and Hartveit 2002)
<b>Ganglion cells</b>	~0.15-0.32	rat <sup>1</sup> , mouse <sup>2</sup>	<sup>1</sup> (Hidaka, Akahori, and Kurosawa 2004), <sup>2</sup> (Trenholm et al. 2013)
Other cell types	CC	Species	Reference
<b>RPE</b>	~0.045 – ~0.13	mice, human	<b>Study II</b>
<b>Proximal tubule-derived epithelial cells (HK2 cell line)</b>	0.48	human	(Hills et al. 2013)
<b>Epithelial cells of the body column</b>	0.2–0.7	hydra	(Fraser et al. 1987)
<b>Sustentacular cells of the olfactory epithelium</b>	0.39	mouse	(Vogalis, Hegg, and Lucero 2005)
<b>Osteoblast-like cells (derived from calvarial fragments)</b>	0.1 and 0.8	guinea pig	(Schirmmacher et al. 1993)
<b>Salivary gland acinar cells</b>	0.33-1	mouse <sup>1</sup> , rat <sup>2</sup>	<sup>1</sup> (Kater and Galvin 1978), <sup>2</sup> (Hammer and Sheridan 1978)
<b>Pancreatic acinar tissue</b>	0–1	mouse	(Iwatsuki and Petersen 1978)
<b>Cardiac Purkinje strand (heart fibers)</b>	0.66	canine	(De Mello 1986)
<b>Astrocytes</b>	0.018–0.039	rat	(Xu et al. 2010)

Abbreviations: HK2: immortalized proximal tubule epithelial cell line



In addition to the cell-to-cell variance, **Study II** and **III** demonstrate that either gap junction blockers or phosphorylation can dynamically modify the coupling in RPE. Interestingly, in other epithelial cells, such as hepatoma cells, gap junctions have been shown to synchronize responses to the hormone vasopressin. A subset of the cells exhibit increased hormone receptor expression and can thus serve as pacemakers for the reaction (Leite et al. 2002). Similar coordinated cellular behavior has also been observed in fibroblasts during chemosensing (Sun et al. 2012). We observed functional hemichannels on the apical membrane of RPE cells, and during development, these channels have been linked to ATP signaling between the retina and RPE (Pearson et al. 2005). Therefore, it is intriguing to speculate whether Cx43 and possibly Cx36 proteins could help synchronize the signaling of molecules including Ca<sup>2+</sup> and ATP between the two tissues in the mature eye. Interestingly, changes in adenosine levels in the subretinal space have been implicated in light sensitivity (Stella et al. 2003). Moreover, purinergic signaling has been speculated to serve as the light peak retinal signal in phagocytosis (Reichhart and Strauß 2020), and studies in ARPE-19 cells have shown that glutamate triggers ATP release via NMDA receptors from RPE cells (Reigada, Lu, and Mitchell 2006).

### 6.3 Voltage-gated sodium channels and gap junctions are involved in the phagocytosis pathway

Novel roles for Nav channels, Cx43, and Cdk5 in POS phagocytosis were identified in this thesis. Our phagocytosis assays with blockers and shRNA-treated cells highlight their importance in phagocytosis, but the molecular mechanisms detailing how these proteins relate to the molecular pathway are not entirely understood. Our findings indicate that the roles of Nav and Cx43 might require spatiotemporal regulation (A summary of the results is illustrated in Figure 15 and **Study III: page 50, Figure 7**). This speculation is particularly interesting for Cx43, as it was shown to be phosphorylated and localized adjacent to Rac1 after 30 min of POS challenge. These findings suggest that its involvement occurs early in the phagocytosis pathway. Nav channels were not found to regulate the binding of POS but rather the further processing of the phagocytosed particles. However, in **Study I**, the POS binding was investigated by keeping the samples at room temperature. While this is a common practice in phagocytosis studies (Mazzoni, Safa, and Finnemann 2014), it is not a physiological way to investigate voltage-gated ion channels. Thus, it might not

accurately reveal their role, especially related to their kinetics. Furthermore, immunostainings alone do not provide the required temporal resolution to study the dynamics of the phagocytosis process. Therefore, as the activation of Nav channels during the phagocytosis process is speculated, the initial steps of the pathway cannot be excluded.

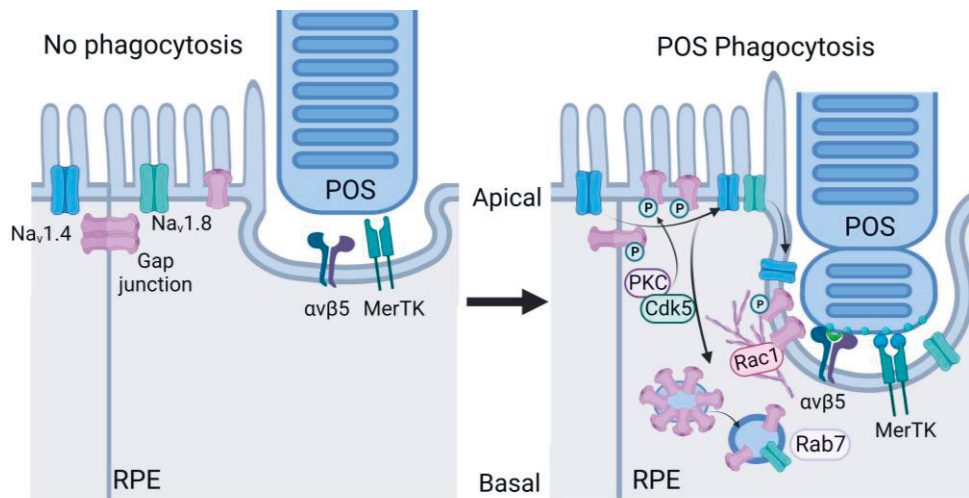


**Figure 15.** Summary of the discovered roles of Nav channels and gap junctions in photoreceptor outer segment (POS) phagocytosis. Without phagocytosis, Nav channels and gap junctions were found to localize at the cell-cell junctions or in the apical membrane. With the addition of POS, gap junctions become phosphorylated and translocated away from the junctions and internalized. This turnover is regulated by kinases such as PKC and Cdk5. Once translocated, Cx43 localizes adjacent to Rac1 and might thus play a role in the formation of phagocytic cups. Nav1.4 and Nav1.8 are also found in the forming phagosomes or adjacent to internalized POS. Inhibiting their activity reduced the phagocytosis efficiency. Nav1.8 was found to localize adjacent to the endosomal marker Rab7.

The Nav channel release from inactivation could be caused by the light exposure-induced apical hyperpolarization combined with the activity of BK channels. Interestingly, membrane stretch can also induce BK channel activity independently from  $Ca^{2+}$  (Sheu, Wu, and Hu 2005). In addition, membrane stretch has been shown to reversibly accelerate both the activation and inactivation of Nav channels and increase their peak current amplitude (Morris and Juranka 2007; Ou et al. 2003; Morris 2011). As the RPE cell membrane and the plasma membrane of the outer segments are separated by an extracellular space of only 10–20 nm (Steinberg and Wood 1974), the changes in outer segment lipids and the initial stages of their

removal could be sufficient to induce BK channel activity. Yet, as these channels have been linked to POS phagocytosis rhythmicity (Müller et al. 2014), it is likely that a circadian component is required in their activation as well. Alternatively, as MerTK activation leads to the generation of inositol trisphosphate (IP<sub>3</sub>), this could facilitate the increase in cytosolic Ca<sup>2+</sup> required for BK activation. In POS phagocytosis, activation of L-type Ca<sub>v</sub> channels is thought to occur after the ligation of integrin receptors (Karl et al. 2008). Their initial depolarization could be sufficient to activate Na<sub>v</sub> channels. Rapid changes in gap junctional gating initiated by altered levels of Cdk5, PKC, and other kinases, would mean that less input is required to cause changes in the membrane potential. The rapid activation of Na<sub>v</sub> channels could stimulate further activation of Ca<sub>v</sub> and be necessary for the plausible voltage-dependent activation of Rac1 (Yang et al. 2020).

As Ca<sub>v</sub> channels have also been found to localize adjacent to POS particles, translocation of Na<sub>v</sub> and Cx43 proteins could provide local signaling microdomains at the forming phagosomal cups. The previously observed circadian differences in Ca<sub>v</sub> mRNA level (Müller et al. 2014) suggest that these channels could be internalized together with Na<sub>v</sub> and Cx43. The close vicinity of these channels would lead to more remarkable local changes in ion concentrations, as has been speculated for BK and L-type Ca<sub>v</sub> channel interaction (Wimmers, Halsband, et al. 2008). Translocation of Cx43, or its C-terminus, to the phagocytic cups could, in addition to enabling stochastic changes in the input resistance, serve as a signaling scaffold to keep its associated kinases more active and thus influence other proteins in the phagocytosis pathway (Kameritsch, Pogoda, and Pohl 2012; Leithe, Mesnil, and Aasen 2018; Solan and Lampe 2018). Yet, as the EM results of **Study I** and **Study III** showed that Na<sub>v</sub> and Cx43 were found around internalized POS particles, it is likely that the roles of these proteins are complex and that their regulation requires integration from multiple pathways. The intricacy is demonstrated by the fact that we found Na<sub>v</sub>1.8 to localize near Rab7. One possibility for this interaction is the regulation of endosomal acidification, as shown for Na<sub>v</sub>1.5 in macrophages (Carrithers et al. 2007). While Rab7 is associated with late endosomes, some studies have shown that it can also be involved in earlier maturation steps and cargo sorting (Girard et al. 2014). In primary mouse RPE cultures, both Rab5 and Rab7 have been shown to enter the phagocytic cups before their closure (Umapathy et al. 2021). These findings demonstrate that Na<sub>v</sub> channels could be involved in the early and later stages of POS phagocytosis.

As the activity of all ion channels depends on their abundance and correct surface location, it is possible that the internalization of some of its ion channels helps RPE

to regulate its physiology during phagocytosis. Overexpression of Rab7 can reduce the current mediated by  $K_v1.5$  channels in human embryonic kidney cells (HEK279) and cardiac myoblast cells (Zadeh et al. 2008). Moreover, increasing evidence suggests that recycling Cx43 may be crucial in modulating gap junction levels under basal conditions and in response to numerous types of cellular stress (Leithe, Mesnil, and Aasen 2018). Once internalized, these channels could be degraded or targeted back to the membrane, demonstrating that all ion channels would not have to be synthesized de novo after completing POS removal (Estadella et al. 2020). As POS digestion represents an enormous metabolic load for RPE cells, the channel translocation and subsequent recycling could help the epithelium generate sufficient local membrane potential changes and conserve energy while restoring it to basal conditions.

## 6.4 Are voltage-gated sodium channels and gap junctions in the RPE regulated by the circadian rhythm?

While our data demonstrate that Nav channels and Cx43 are required for efficient phagocytosis, at this stage, it remains unclear whether phosphorylation-induced translocation of Cx43 regulates the reorganization of Nav channels or whether the Nav channel translocation also drives the turnover of gap junctions. As we did not use genetically modified mouse lines to investigate whether the lack of either of these channels would result in shifts or removal of the phagocytosis peak, their definitive effect on the rhythm is not conclusive. However, circadian regulation of gating properties and their impacts on physiological functions have thus far been recognized in various ion channels of photoreceptors. The most studied example is the so-called dark current mediated by CNGC channels that relies on rhythmic affinity for the channel ligand. These gating properties can be modulated by phosphorylation, and many of the regulatory kinases are thought to be under circadian control. Dopamine, somatostatin, and  $Ca^{2+}$ /calmodulin binding have also been indicated in the rhythmic modulation of CNGC channels (Ko 2020; Douglas G. McMahon, Iuvone, and Tosini 2014; Chae, Ko, and Dryer 2007).

In addition to CNGC, various ion channels and ion transport mechanisms in RPE are thought to have rhythmic mRNA expression (Milićević et al. 2019; Müller et al. 2014). However, the underlying mechanisms, particularly in vertebrate species,

are not entirely understood (Ko, Shi, and Ko 2009). As many other ion channels have already been shown to regulate the circadian rhythm of phagocytosis (Müller et al. 2014), Nav channels and Cx43 may also be involved in controlling the timing of the phagocytosis peak. This circadian regulation could also occur through Cdk5 as it has been shown to regulate the circadian clock (Kwak et al. 2013; Brenna et al. 2019) and dopaminergic transmission in the striatum (Chergui, Svenningsson, and Greengard 2004).

Our results in **Study III** with hESC-RPE demonstrated that gap junctions become phosphorylated at S279 during phagocytosis. Moreover, previous studies have shown circadian changes in the phosphorylation of Cx36 in photoreceptors. While our data indicate that Cx43 phosphorylation may change according to the circadian rhythm, the effect was not as binary as observed for photoreceptors (Hongyan Li et al. 2013). In **Study III**, some level of S279 was found at all timepoints, albeit the labeling pattern was much more diffuse during phagocytosis. This difference could be attributed to dissimilarities between Cx36 and Cx43, or perhaps more likely, different needs to finetune the connectivity in response to changing light levels. As the level of input resistance is low in RPE in basal conditions, more nuanced and temporary changes in input resistance could generate sufficient effects in the downstream pathway. Interestingly, pulldown studies with myoblasts have shown that the C-terminus of Cx43 interacts with  $\alpha 5$  integrins and this interaction increases during shear stress. Moreover, this interaction is considered critical for Cx43 hemichannel opening induced by mechanical stress, and integrin activation is thought to be regulated by PI3K kinase (Batra et al. 2012). PI3K kinase inhibition, on the other hand, has been shown to cause phagocytic cups to contain less F-actin and block their subsequent engulfment (Bullock, Duan, and Finnemann 2013). As integrin  $\alpha v \beta 5$  is one of the core circadian regulators of POS phagocytosis, it could mediate the translocation of Cx43. Dynamic changes in gap junctional gating caused by phosphorylation combined with the opening of hemichannels caused by integrin activation could explain why these changes in input resistance are difficult to detect experimentally. This notion could also explain why we only sporadically recorded individual cells with much higher input resistance in Study III.

The difference between cultured and mouse RPE baseline, non-phagocytosis level of S279, indicates that gap junctions are more dynamically regulated *in vivo*. Alternatively, a continuous residual level of S279 could be necessary to keep the connectivity low in mouse RPE we observed in **Study II**. Importantly, this thesis did not investigate S368, the typical target residue for PKC (P. D. Lampe et al. 2000). At the time of Study III, we had not found a commercially available antibody that

would work reliably in immunofluorescence experiments. However, some studies have suggested that PKC could serve as a master regulatory kinase and, therefore, indirectly cause the phosphorylation of S279 (Nimlamool, Andrews, and Falk 2015; Sorgen et al. 2018). A cascade of kinases might also regulate gap junctions during phagocytosis, as shown for other pathways, including epidermal wound repair (Lastwika et al. 2019; Solan and Lampe 2014). Therefore, it is plausible that PKC and Cdk5 regulate the Cx43 turnover in phagocytosis. In **Study III**, gap junction internalization was induced after the PMA treatment, even without the addition of POS. However, p25, the activator target of Cdk5, has been suggested to be regulated by PKC during myogenesis (de Thonel et al. 2010). Thus, pharmacological over-activation of PKC with PMA might also result in the activation of Cdk5. This theory is strengthened by the fact that physiological levels of PKC activation during phagocytosis were insufficient to induce gap junction internalization if Cdk5 had been inhibited. The results from **Study III** indicate that S279 phosphorylation by PKC-mediated pathway serves as a mechanism to ‘prime’ the epithelium for phagocytosis, but Cdk5 activity is required to onset the translocation of Cx43. Ultimately, the changes observed in gap junctions could help to prepare the epithelium for its onerous yet essential daily task.

## 6.5 Future perspectives

The extensive array of Nav channel subtypes in RPE suggests that these channels may play additional roles that have not been studied in this Thesis. In addition to healthy tissue, the channels may be altered in pathological states. In astrocytes, Nav channel expression has been shown to increase in response to seizures or various central nervous system perturbations, although the underlying mechanisms are not entirely understood (de Lanerolle and Lee 2005; McNeill et al. 2021). On the other hand, gap junctions have been indicated in various ocular pathologies, including diabetic retinopathy (Roy et al. 2017). Still, the consequences of impaired cellular communication have not been thoroughly investigated concerning phagocytosis. Future studies will hopefully elaborate on the roles of Nav channels and gap junctions in healthy and diseased RPE.

In addition to studying the involvement of Nav channels in POS phagocytosis using a knockdown mouse line, the activation of these channels could be investigated

with a computational model designed for non-excitabile cells. Here, we have offered speculations and justifications for how such a channel family could serve its physiological role. However, most current hypotheses rely on conclusions made for excitable tissues. Thus, a more comprehensive model could provide answers for the phagocytosis pathway and the roles of Nav and Cx43 in the epithelium. Furthermore, it could benefit studies with other Nav channels expressing non-excitabile cells.

The modifications of gap junctions should be studied with mass spectrometry to investigate the role of Cx phosphorylation more definitively in RPE. Such analysis would enable the investigation of all possible phosphorylations instead of relying on those against which we have high-quality antibodies. A pulldown assay could be conducted to study the scaffold properties of Cx43 and analyze what proteins are associated with it. Ultimately, the knockdown of Cx43 would offer a better tool to learn how the lack of gap junctions affects phagocytosis efficiency. If such knockdown would affect cellular viability, only the specific phosphorylation sites could be disrupted, or the entire C-terminal end of Cx43 could be removed. The potential electrical communication and hemichannels between RPE and the retina would be exciting to study with a preparation where we could simultaneously record from RPE cells and their associated photoreceptors. Future studies will hopefully provide a platform for such investigations to enable us to discover how active partner RPE truly is in vision.

## 7 SUMMARY AND CONCLUSIONS

This dissertation addressed how ionic mechanisms regulate the phagocytosis of photoreceptor outer segments. The results provide new insight into the physiology of RPE and how it can be studied in RPE *ex vivo* tissue. Moreover, the results add to the growing body of evidence that non-excitabile cells can dynamically finetune their electrical properties to meet environmental and circadian changes. Overall, the results obtained in this thesis demonstrate that RPE, in its interactions with the neural retina, is much more active than previously thought. The following list details the conclusions drawn from the results of the studies.

1. An extensive family of Nav channels is expressed in mature RPE cells *in vitro* and *in vivo*. These channels mediate a current sensitive to specific blockers of Nav channels and localize primarily to the vicinity of cell-cell junctions and apical membrane.
2. Cx43 is the major Cx isoform present in RPE, and it can be found forming both gap junctions between neighboring cells and functional hemichannels on the apical membrane. Despite the extensive junctional labeling, the electrical connectivity of RPE cells is relatively low but readily modifiable by phosphorylation.
3. Nav currents are important for phagosome processing, and their role is possibly related to Rab7. Nav channel localization changes during the phagocytosis process.
4. Cx43 gap junctions dramatically change their localization during phagocytosis and can be found to localize in the forming phagocytic cups or ingested POS particles. The phagocytosis efficiency is affected when the translocation is prevented.
5. Cx43 translocation is regulated by phosphorylation by kinases such as Cdk5 and PKC, and Cx43 is implicated in the Rac1 pathway. Cdk5 could be related to the circadian regulation of POS phagocytosis.



## 8 REFERENCES

- Aasen, Trond, and David P. Kelsell. 2009. "Connexins in Skin Biology." In *Connexins: A Guide*, edited by Andrew L. Harris and Darren Locke, 307–21. Totowa, NJ: Humana Press.
- Adachi, A., T. Nogi, and S. Ebihara. 1998. "Phase-Relationship and Mutual Effects between Circadian Rhythms of Ocular Melatonin and Dopamine in the Pigeon." *Brain Research* 792 (2): 361–69.
- Akanuma, Shin-Ichi, Hideyuki Higashi, Souhei Maruyama, Koji Murakami, Masanori Tachikawa, Yoshiyuki Kubo, and Ken-Ichi Hosoya. 2018. "Expression and Function of Connexin 43 Protein in Mouse and Human Retinal Pigment Epithelial Cells as Hemichannels and Gap Junction Proteins." *Experimental Eye Research* 168 (March): 128–37.
- Alexander, Kamilah, Hai-Su Yang, and Philip W. Hinds. 2004. "Cellular Senescence Requires CDK5 Repression of Rac1 Activity." *Molecular and Cellular Biology* 24 (7): 2808–19.
- Almedawar, Seba, Katerina Vafia, Sven Schreiter, Katrin Neumann, Shahryar Khattak, Thomas Kurth, Marius Ader, Mike O. Karl, Stephen H. Tsang, and Elly M. Tanaka. 2020. "MERTK-Dependent Ensheatment of Photoreceptor Outer Segments by Human Pluripotent Stem Cell-Derived Retinal Pigment Epithelium." *Stem Cell Reports* 14 (3): 374–89.
- Anand, Rahul J., Shipan Dai, Steven C. Gribar, Ward Richardson, Jeff W. Kohler, Rosemary A. Hoffman, Maria F. Branca, et al. 2008. "A Role for Connexin43 in Macrophage Phagocytosis and Host Survival after Bacterial Peritoneal Infection." *Journal of Immunology* 181 (12): 8534–43.
- Anderson, D. H., S. K. Fisher, and R. H. Steinberg. 1978. "Mammalian Cones: Disc Shedding, Phagocytosis, and Renewal." *Investigative Ophthalmology & Visual Science* 17 (2): 117–33.
- Arai, Itaru, Masashi Tanaka, and Masao Tachibana. 2010. "Active Roles of Electrically Coupled Bipolar Cell Network in the Adult Retina." *The Journal of Neuroscience: The Official Journal of the Society for Neuroscience* 30 (27): 9260–70.
- Armstrong, C. M. 1981. "Sodium Channels and Gating Currents." *Physiological Reviews* 61 (3): 644–83.

- Aschoff, J., and H. Pohl. 1978. "Phase Relations between a Circadian Rhythm and Its Zeitgeber within the Range of Entrainment." *Die Naturwissenschaften* 65 (2): 80–84.
- Attwell, D., M. Wilson, and S. M. Wu. 1984. "A Quantitative Analysis of Interactions between Photoreceptors in the Salamander (*Ambystoma*) Retina." *The Journal of Physiology* 352 (July): 703–37.
- Axelsen, Lene N., Martin Stahlhut, Shabaz Mohammed, Bjarne Due Larsen, Morten S. Nielsen, Niels-Henrik Holstein-Rathlou, Søren Andersen, Ole N. Jensen, James K. Hennan, and Anne Louise Kjølbye. 2006. "Identification of Ischemia-Regulated Phosphorylation Sites in Connexin43: A Possible Target for the Antiarrhythmic Peptide Analogue Rotigaptide (ZP123)." *Journal of Molecular and Cellular Cardiology* 40 (6): 790–98.
- Baba, Kenkichi, Jason P. DeBruyne, and Gianluca Tosini. 2017. "Dopamine 2 Receptor Activation Entrain Circadian Clocks in Mouse Retinal Pigment Epithelium." *Scientific Reports* 7 (1): 5103.
- Baba, Kenkichi, Varunika Goyal, and Gianluca Tosini. 2022. "Circadian Regulation of Retinal Pigment Epithelium Function." *International Journal of Molecular Sciences* 23 (5). <https://doi.org/10.3390/ijms23052699>.
- Baba, Kenkichi, Ilaria Piano, Polina Lyuboslavsky, Micah A. Chrenek, Jana T. Sellers, Shuo Zhang, Claudia Gargini, Li He, Gianluca Tosini, and P. Michael Iuvone. 2018. "Removal of Clock Gene *Bmal1* from the Retina Affects Retinal Development and Accelerates Cone Photoreceptor Degeneration during Aging." *Proceedings of the National Academy of Sciences of the United States of America* 115 (51): 13099–104.
- Baba, Kenkichi, Anamika Sengupta, Manfredi Tosini, Susana Contreras-Alcantara, and Gianluca Tosini. 2010. "Circadian Regulation of the PERIOD 2::LUCIFERASE Bioluminescence Rhythm in the Mouse Retinal Pigment Epithelium-Choroid." *Molecular Vision* 16 (December): 2605–11.
- Baden, Tom, Philipp Berens, Katrin Franke, Miroslav Román Rosón, Matthias Bethge, and Thomas Euler. 2016. "The Functional Diversity of Retinal Ganglion Cells in the Mouse." *Nature* 529 (7586): 345–50.
- Bae, J. Alexander, Shang Mu, Jinseop S. Kim, Nicholas L. Turner, Ignacio Tartavull, Nico Kemnitz, Chris S. Jordan, et al. 2018. "Digital Museum of Retinal Ganglion Cells with Dense Anatomy and Physiology." *Cell* 173 (5): 1293-1306.e19.
- Batra, Nidhi, Sirisha Burra, Arlene J. Siller-Jackson, Sumin Gu, Xuechun Xia, Gregory F. Weber, Douglas DeSimone, et al. 2012. "Mechanical Stress-Activated Integrin A5β1 Induces Opening of Connexin 43 Hemichannels." *Proceedings of the National Academy of Sciences of the United States of America* 109 (9): 3359–64.
- Beneski, D. A., and W. A. Catterall. 1980. "Covalent Labeling of Protein Components of the Sodium Channel with a Photoactivable Derivative of

- Scorpion Toxin." *Proceedings of the National Academy of Sciences of the United States of America* 77 (1): 639–43.
- Berendt, Frank J., Kang-Sik Park, and James S. Trimmer. 2010. "Multisite Phosphorylation of Voltage-Gated Sodium Channel Alpha Subunits from Rat Brain." *Journal of Proteome Research* 9 (4): 1976–84.
- Berson, David M., Felice A. Dunn, and Motoharu Takao. 2002. "Phototransduction by Retinal Ganglion Cells That Set the Circadian Clock." *Science* 295 (5557): 1070–73.
- Berthoud, V. M., M. B. Rook, O. Traub, E. L. Hertzberg, and J. C. Sáez. 1993. "On the Mechanisms of Cell Uncoupling Induced by a Tumor Promoter Phorbol Ester in Clone 9 Cells, a Rat Liver Epithelial Cell Line." *European Journal of Cell Biology* 62 (2): 384–96.
- Besharse, J. C., and J. G. Hollyfield. 1979. "Turnover of Mouse Photoreceptor Outer Segments in Constant Light and Darkness." *Investigative Ophthalmology & Visual Science* 18 (10): 1019–24.
- Bialek, S., D. P. Joseph, and S. S. Miller. 1995. "The Delayed Basolateral Membrane Hyperpolarization of the Bovine Retinal Pigment Epithelium: Mechanism of Generation." *The Journal of Physiology* 484 ( Pt 1) (April): 53–67.
- Black, Joel A., and Stephen G. Waxman. 2013. "Noncanonical Roles of Voltage-Gated Sodium Channels." *Neuron* 80 (2): 280–91.
- Bloomfield, Stewart A., and Béla Völgyi. 2009. "The Diverse Functional Roles and Regulation of Neuronal Gap Junctions in the Retina." *Nature Reviews. Neuroscience* 10 (7): 495–506.
- Bok, D. 1990. "Processing and Transport of Retinoids by the Retinal Pigment Epithelium." *Eye* 4 ( Pt 2): 326–32.
- . 1993. "The Retinal Pigment Epithelium: A Versatile Partner in Vision." *Journal of Cell Science. Supplement* 17: 189–95.
- Bok, D., and M. O. Hall. 1971. "The Role of the Pigment Epithelium in the Etiology of Inherited Retinal Dystrophy in the Rat." *The Journal of Cell Biology* 49 (3): 664–82.
- Bosch, E., J. Horwitz, and D. Bok. 1993. "Phagocytosis of Outer Segments by Retinal Pigment Epithelium: Phagosome-Lysosome Interaction." *The Journal of Histochemistry and Cytochemistry: Official Journal of the Histochemistry Society* 41 (2): 253–63.
- Botchkina, L. M., and G. Matthews. 1994. "Voltage-Dependent Sodium Channels Develop in Rat Retinal Pigment Epithelium Cells in Culture." *Proceedings of the National Academy of Sciences of the United States of America* 91 (10): 4564–68.
- Boulton, M., and P. Dayhaw-Barker. 2001. "The Role of the Retinal Pigment Epithelium: Topographical Variation and Ageing Changes." *Eye* 15 (Pt 3): 384–89.
- Bowmaker, J. K., and H. J. Dartnall. 1980. "Visual Pigments of Rods and Cones in a Human Retina." *The Journal of Physiology* 298 (January): 501–11.

- Brenna, Andrea, Iwona Olejniczak, Rohit Chavan, Jürgen A. Ripperger, Sonja Langmesser, Elisabetta Camerini, Zehan Hu, Claudio De Virgilio, Jörn Dengjel, and Urs Albrecht. 2019. “Cyclin-Dependent Kinase 5 (CDK5) Regulates the Circadian Clock.” *ELife* 8 (November). <https://doi.org/10.7554/eLife.50925>.
- Bulloj, Ayelen, Wei Duan, and Silvia C. Finnemann. 2013. “PI 3-Kinase Independent Role for AKT in F-Actin Regulation during Outer Segment Phagocytosis by RPE Cells.” *Experimental Eye Research* 113 (August): 9–18.
- Burke, Janice M., and Leonard M. Hjelmeland. 2005. “Mosaicism of the Retinal Pigment Epithelium: Seeing the Small Picture.” *Molecular Interventions* 5 (4): 241–49.
- Burstyn-Cohen, Tal, Erin D. Lew, Paqui G. Través, Patrick G. Burrola, Joseph C. Hash, and Greg Lemke. 2012. “Genetic Dissection of TAM Receptor-Ligand Interaction in Retinal Pigment Epithelial Cell Phagocytosis.” *Neuron* 76 (6): 1123–32.
- Caceres, Paulo S., and Enrique Rodriguez-Boulan. 2020. “Retinal Pigment Epithelium Polarity in Health and Blinding Diseases.” *Current Opinion in Cell Biology* 62 (February): 37–45.
- Cao, Lin, Jie Liu, Jin Pu, Gillian Milne, Mei Chen, Heping Xu, Alan Shipley, John V. Forrester, Colin D. McCaig, and Noemi Lois. 2018. “Polarized Retinal Pigment Epithelium Generates Electrical Signals That Diminish with Age and Regulate Retinal Pathology.” *Journal of Cellular and Molecular Medicine* 22 (11): 5552–64.
- Carrithers, Michael D., Gouri Chatterjee, Lisette M. Carrithers, Roosevelt Offoha, Uzoma Iheagwara, Christoph Rahner, Morven Graham, and Stephen G. Waxman. 2009. “Regulation of Podosome Formation in Macrophages by a Splice Variant of the Sodium Channel SCN8A.” *The Journal of Biological Chemistry* 284 (12): 8114–26.
- Carrithers, Michael D., Sulayman Dib-Hajj, Lisette M. Carrithers, Gouzel Tokmoulina, Marc Pypaert, Elizabeth A. Jonas, and Stephen G. Waxman. 2007. “Expression of the Voltage-Gated Sodium Channel NaV1.5 in the Macrophage Late Endosome Regulates Endosomal Acidification.” *Journal of Immunology* 178 (12): 7822–32.
- Carter, Stephen P., Ailís L. Moran, David Matallanas, Gavin J. McManus, Oliver E. Blacque, and Breandán N. Kennedy. 2020. “Genetic Deletion of Zebrafish Rab28 Causes Defective Outer Segment Shedding, but Not Retinal Degeneration.” *Frontiers in Cell and Developmental Biology* 8 (March): 136.
- Catterall, W. A. 1995. “Structure and Function of Voltage-Gated Ion Channels.” *Annual Review of Biochemistry* 64: 493–531.
- . 2000a. “Structure and Regulation of Voltage-Gated Ca<sup>2+</sup> Channels.” *Annual Review of Cell and Developmental Biology* 16: 521–55.
- . 2000b. “From Ionic Currents to Molecular Mechanisms: The Structure and Function of Voltage-Gated Sodium Channels.” *Neuron* 26 (1): 13–25.

- Catterall, William A. 2010. "Ion Channel Voltage Sensors: Structure, Function, and Pathophysiology." *Neuron* 67 (6): 915–28.
- . 2011. "Voltage-Gated Calcium Channels." *Cold Spring Harbor Perspectives in Biology* 3 (8): a003947.
- . 2014. "Structure and Function of Voltage-Gated Sodium Channels at Atomic Resolution." *Experimental Physiology* 99 (1): 35–51.
- Chae, Kwon-Seok, Gladys Y-P Ko, and Stuart E. Dryer. 2007. "Tyrosine Phosphorylation of cGMP-Gated Ion Channels Is under Circadian Control in Chick Retina Photoreceptors." *Investigative Ophthalmology & Visual Science* 48 (2): 901–6.
- Chaitin, M. H., and M. O. Hall. 1983. "Defective Ingestion of Rod Outer Segments by Cultured Dystrophic Rat Pigment Epithelial Cells." *Investigative Ophthalmology & Visual Science* 24 (7): 812–20.
- Chatelier, Aurélien, Aurélie Mercier, Boris Tremblier, Olivier Thériault, Majed Moubarak, Najate Benamer, Pierre Corbi, Patrick Bois, Mohamed Chahine, and Jean François Faivre. 2012. "A Distinct de Novo Expression of Nav1.5 Sodium Channels in Human Atrial Fibroblasts Differentiated into Myofibroblasts." *The Journal of Physiology* 590 (17): 4307–19.
- Chen, Jia, Lifeng Pan, Zhiyi Wei, Yanxiang Zhao, and Mingjie Zhang. 2008. "Domain-Swapped Dimerization of ZO-1 PDZ2 Generates Specific and Regulatory Connexin43-Binding Sites." *The EMBO Journal* 27 (15): 2113–23.
- Chergui, Karima, Per Svenningsson, and Paul Greengard. 2004. "Cyclin-Dependent Kinase 5 Regulates Dopaminergic and Glutamatergic Transmission in the Striatum." *Proceedings of the National Academy of Sciences of the United States of America* 101 (7): 2191–96.
- Chiu, S. Y. 1977. "Inactivation of Sodium Channels: Second Order Kinetics in Myelinated Nerve." *The Journal of Physiology* 273 (3): 573–96.
- Clapham, David E. 2007. "Calcium Signaling." *Cell* 131 (6): 1047–58.
- Combs, David J., Hyeon-Gyu Shin, Yanping Xu, Yajamana Ramu, and Zhe Lu. 2013. "Tuning Voltage-Gated Channel Activity and Cellular Excitability with a Sphingomyelinase." *The Journal of General Physiology* 142 (4): 367–80.
- Contreras-Vallejos, Erick, Elias Utreras, and Christian Gonzalez-Billault. 2012. "Going out of the Brain: Non-Nervous System Physiological and Pathological Functions of Cdk5." *Cellular Signalling* 24 (1): 44–52.
- Cooper, Cynthia D., and Paul D. Lampe. 2002. "Casein Kinase 1 Regulates Connexin-43 Gap Junction Assembly\*." *The Journal of Biological Chemistry* 277 (47): 44962–68.
- Cour, M. la, H. Lund-Andersen, and T. Zeuthen. 1986. "Potassium Transport of the Frog Retinal Pigment Epithelium: Autoregulation of Potassium Activity in the Subretinal Space." *The Journal of Physiology* 375 (June): 461–79.
- Cox, Kimberly H., and Joseph S. Takahashi. 2019. "Circadian Clock Genes and the Transcriptional Architecture of the Clock Mechanism." *Journal of Molecular Endocrinology* 63 (4): R93–102.

- Dacey, D., O. S. Packer, L. Diller, D. Brainard, B. Peterson, and B. Lee. 2000. "Center Surround Receptive Field Structure of Cone Bipolar Cells in Primate Retina." *Vision Research* 40 (14): 1801–11.
- De Mello, W. C. 1986. "Interaction of Cyclic AMP and Ca<sup>2+</sup> in the Control of Electrical Coupling in Heart Fibers." *Biochimica et Biophysica Acta* 888 (1): 91–99.
- Deguchi, J., A. Yamamoto, T. Yoshimori, K. Sugawara, Y. Moriyama, M. Futai, T. Suzuki, K. Kato, M. Uyama, and Y. Tashiro. 1994. "Acidification of Phagosomes and Degradation of Rod Outer Segments in Rat Retinal Pigment Epithelium." *Investigative Ophthalmology & Visual Science* 35 (2): 568–79.
- DeVera, Christopher, Jendayi Dixon, Micah A. Chrenek, Kenkichi Baba, Yun Z. Le, P. Michael Iuvone, and Gianluca Tosini. 2022. "The Circadian Clock in the Retinal Pigment Epithelium Controls the Diurnal Rhythm of Phagocytic Activity." *International Journal of Molecular Sciences* 23 (10). <https://doi.org/10.3390/ijms23105302>.
- DeVries, S. H., and D. A. Baylor. 1995. "An Alternative Pathway for Signal Flow from Rod Photoreceptors to Ganglion Cells in Mammalian Retina." *Proceedings of the National Academy of Sciences of the United States of America* 92 (23): 10658–62.
- DeVries, S. H., and E. A. Schwartz. 1989. "Modulation of an Electrical Synapse between Solitary Pairs of Catfish Horizontal Cells by Dopamine and Second Messengers." *The Journal of Physiology* 414 (July): 351–75.
- D'hondt, Catheluyne, Jegan Iyyathurai, Bernard Himpens, Luc Leybaert, and Geert Bultynck. 2014. "Cx43-Hemichannel Function and Regulation in Physiology and Pathophysiology: Insights from the Bovine Corneal Endothelial Cell System and Beyond." *Frontiers in Physiology* 5 (September): 348.
- Dosch, Michel, Joël Zindel, Fadi Jebbawi, Nicolas Melin, Daniel Sanchez-Taltavull, Deborah Stroka, Daniel Candinas, and Guido Beldi. 2019. "Connexin-43-Dependent ATP Release Mediates Macrophage Activation during Sepsis." *eLife* 8 (February). <https://doi.org/10.7554/eLife.42670>.
- Duncan, Jacque L., Matthew M. LaVail, Douglas Yasumura, Michael T. Matthes, Haidong Yang, Nikolaus Trautmann, Aimee V. Chappelow, et al. 2003. "An RCS-like Retinal Dystrophy Phenotype in Mer Knockout Mice." *Investigative Ophthalmology & Visual Science* 44 (2): 826–38.
- Dunn, Clarence A., and Paul D. Lampe. 2014. "Injury-Triggered Akt Phosphorylation of Cx43: A ZO-1-Driven Molecular Switch That Regulates Gap Junction Size." *Journal of Cell Science* 127 (Pt 2): 455–64.
- Dvoriashyna, Mariia, Alexander J. E. Foss, Eamonn A. Gaffney, and Rodolfo Repetto. 2020. "Fluid and Solute Transport across the Retinal Pigment Epithelium: A Theoretical Model." *Journal of the Royal Society, Interface / the Royal Society* 17 (163): 20190735.

- Estadella, Irene, Oriol Pedrós-Gámez, Magalí Colomer-Molera, Manel Bosch, Alexander Sorokin, and Antonio Felipe. 2020. "Endocytosis: A Turnover Mechanism Controlling Ion Channel Function." *Cells* 9 (8). <https://doi.org/10.3390/cells9081833>.
- Esteve-Rudd, Julian, Roni A. Hazim, Tanja Diemer, Antonio E. Paniagua, Stefanie Volland, Ankita Umapathy, and David S. Williams. 2018. "Defective Phagosome Motility and Degradation in Cell Nonautonomous RPE Pathogenesis of a Dominant Macular Degeneration." *Proceedings of the National Academy of Sciences of the United States of America* 115 (21): 5468–73.
- Ey, Birgit, Annette Eyking, Guido Gerken, Daniel K. Podolsky, and Elke Cario. 2009. "TLR2 Mediates Gap Junctional Intercellular Communication through Connexin-43 in Intestinal Epithelial Barrier Injury\*." *The Journal of Biological Chemistry* 284 (33): 22332–43.
- Falk, Matthias M., Rachael M. Kells, and Viviana M. Berthoud. 2014. "Degradation of Connexins and Gap Junctions." *FEBS Letters* 588 (8): 1221–29.
- Farahbakhsh, Z. T., K. Hideg, and W. L. Hubbell. 1993. "Photoactivated Conformational Changes in Rhodopsin: A Time-Resolved Spin Label Study." *Science* 262 (5138): 1416–19.
- Fernandez-Godino, Rosario, Donita L. Garland, and Eric A. Pierce. 2016. "Isolation, Culture and Characterization of Primary Mouse RPE Cells." *Nature Protocols* 11 (7): 1206–18.
- Fijisawa, K., J. Ye, and J. A. Zadunaisky. 1993. "A Na<sup>+</sup>/Ca<sup>2+</sup> Exchange Mechanism in Apical Membrane Vesicles of the Retinal Pigment Epithelium." *Current Eye Research* 12 (3): 261–70.
- Finnemann, S. C., V. L. Bonilha, A. D. Marmorstein, and E. Rodriguez-Boulan. 1997. "Phagocytosis of Rod Outer Segments by Retinal Pigment Epithelial Cells Requires Alpha(v)Beta5 Integrin for Binding but Not for Internalization." *Proceedings of the National Academy of Sciences of the United States of America* 94 (24): 12932–37.
- Finnemann, S. C., and E. Rodriguez-Boulan. 1999. "Macrophage and Retinal Pigment Epithelium Phagocytosis: Apoptotic Cells and Photoreceptors Compete for Alphavbeta3 and Alphavbeta5 Integrins, and Protein Kinase C Regulates Alphavbeta5 Binding and Cytoskeletal Linkage." *The Journal of Experimental Medicine* 190 (6): 861–74.
- Finnemann, S. C., and R. L. Silverstein. 2001. "Differential Roles of CD36 and Alphavbeta5 Integrin in Photoreceptor Phagocytosis by the Retinal Pigment Epithelium." *The Journal of Experimental Medicine* 194 (9): 1289–98.
- Finnemann, Silvia C. 2003. "Focal Adhesion Kinase Signaling Promotes Phagocytosis of Integrin-Bound Photoreceptors." *The EMBO Journal* 22 (16): 4143–54.
- Fox, J. A., B. A. Pfeffer, and G. L. Fain. 1988. "Single-Channel Recordings from Cultured Human Retinal Pigment Epithelial Cells." *The Journal of General Physiology* 91 (2): 193–222.

- Fraser, Scott E., Colin R. Green, Hans R. Bode, and Norton B. Gilula. 1987. "Selective Disruption of Gap Junctional Communication Interferes with a Patterning Process in Hydra." *Science* 237 (4810): 49–55.
- Frenz, Christopher T., Anne Hansen, Nicholas D. Dupuis, Nicole Shultz, Simon R. Levinson, Thomas E. Finger, and Vincent E. Dionne. 2014. "NaV1.5 Sodium Channel Window Currents Contribute to Spontaneous Firing in Olfactory Sensory Neurons." *Journal of Neurophysiology* 112 (5): 1091–1104.
- Fu, Yingbin, and King-Wai Yau. 2007. "Phototransduction in Mouse Rods and Cones." *Pflügers Archiv: European Journal of Physiology* 454 (5): 805–19.
- Gaietta, Guido, Thomas J. Deerinck, Stephen R. Adams, James Bouwer, Oded Tour, Dale W. Laird, Gina E. Sosinsky, Roger Y. Tsien, and Mark H. Ellisman. 2002. "Multicolor and Electron Microscopic Imaging of Connexin Trafficking." *Science* 296 (5567): 503–7.
- Genovese, Federica, Johannes Reisert, and Vladimir J. Kefalov. 2021. "Sensory Transduction in Photoreceptors and Olfactory Sensory Neurons: Common Features and Distinct Characteristics." *Frontiers in Cellular Neuroscience* 15 (October): 761416.
- Girard, Emmanuelle, Daniela Chmiest, Natalie Fournier, Ludger Johannes, Jean-Louis Paul, Benoît Védie, and Christophe Lamaze. 2014. "Rab7 Is Functionally Required for Selective Cargo Sorting at the Early Endosome." *Traffic* 15 (3): 309–26.
- Glass, Aaron M., Benjamin J. Wolf, Karin M. Schneider, Michael F. Princiotta, and Steven M. Taffet. 2013. "Connexin43 Is Dispensable for Phagocytosis." *Journal of Immunology* 190 (9): 4830–35.
- Goetz, Jillian, Zachary F. Jessen, Anne Jacobi, Adam Mani, Sam Cooler, Devon Greer, Sabah Kadri, et al. 2022. "Unified Classification of Mouse Retinal Ganglion Cells Using Function, Morphology, and Gene Expression." *Cell Reports* 40 (2): 111040.
- Goodenough, D. A., J. A. Goliger, and D. L. Paul. 1996. "Connexins, Connexons, and Intercellular Communication." *Annual Review of Biochemistry* 65: 475–502.
- Goodenough, Daniel A., and David L. Paul. 2003. "Beyond the Gap: Functions of Unpaired Connexon Channels." *Nature Reviews. Molecular Cell Biology* 4 (4): 285–94.
- . 2009. "Gap Junctions." *Cold Spring Harbor Perspectives in Biology* 1 (1): a002576.
- Goyal, Varunika, Christopher DeVera, Virginie Laurent, Jana Sellers, Micah A. Chrenek, David Hicks, Kenkichi Baba, P. Michael Iuvone, and Gianluca Tosini. 2020. "Dopamine 2 Receptor Signaling Controls the Daily Burst in Phagocytic Activity in the Mouse Retinal Pigment Epithelium." *Investigative Ophthalmology & Visual Science* 61 (5): 10.
- Grace, M. S., A. Chiba, and M. Menaker. 1999. "Circadian Control of Photoreceptor Outer Segment Membrane Turnover in Mice Genetically Incapable of Melatonin Synthesis." *Visual Neuroscience* 16 (5): 909–18.



- Gregory, C. Y., T. A. Abrams, and M. O. Hall. 1994. "Stimulation of A2 Adenosine Receptors Inhibits the Ingestion of Photoreceptor Outer Segments by Retinal Pigment Epithelium." *Investigative Ophthalmology & Visual Science* 35 (3): 819–25.
- Griff, E. R., Y. Shirao, and R. H. Steinberg. 1985. "Ba<sup>2+</sup> Unmasks K<sup>+</sup> Modulation of the Na<sup>+</sup>-K<sup>+</sup> Pump in the Frog Retinal Pigment Epithelium." *The Journal of General Physiology* 86 (6): 853–76.
- Griff, E. R., and R. H. Steinberg. 1984. "Changes in Apical [K<sup>+</sup>] Produce Delayed Basal Membrane Responses of the Retinal Pigment Epithelium in the Gecko." *The Journal of General Physiology* 83 (2): 193–211.
- Grunnet, Morten, Thomas Jespersen, Nanna MacAulay, Nanna K. Jørgensen, Nicole Schmitt, Olaf Pongs, Søren-Peter Olesen, and Dan A. Klaerke. 2003. "KCNQ1 Channels Sense Small Changes in Cell Volume." *The Journal of Physiology* 549 (Pt 2): 419–27.
- Gundersen, D., J. Orłowski, and E. Rodriguez-Boulan. 1991. "Apical Polarity of Na,K-ATPase in Retinal Pigment Epithelium Is Linked to a Reversal of the Ankyrin-Fodrin Submembrane Cytoskeleton." *The Journal of Cell Biology* 112 (5): 863–72.
- Guy, H. R., and P. Seetharamulu. 1986. "Molecular Model of the Action Potential Sodium Channel." *Proceedings of the National Academy of Sciences of the United States of America* 83 (2): 508–12.
- Hall, M. O., T. A. Abrams, and T. W. Mittag. 1991. "ROS Ingestion by RPE Cells Is Turned off by Increased Protein Kinase C Activity and by Increased Calcium." *Experimental Eye Research* 52 (5): 591–98.
- . 1993. "The Phagocytosis of Rod Outer Segments Is Inhibited by Drugs Linked to Cyclic Adenosine Monophosphate Production." *Investigative Ophthalmology & Visual Science* 34 (8): 2392–2401.
- Hall, M. O., D. Bok, and A. D. Bacharach. 1969. "Biosynthesis and Assembly of the Rod Outer Segment Membrane System. Formation and Fate of Visual Pigment in the Frog Retina." *Journal of Molecular Biology* 45 (2): 397–406.
- Hall, Michael O., Martin S. Obin, Mary J. Heeb, Barry L. Burgess, and Toshka A. Abrams. 2005. "Both Protein S and Gas6 Stimulate Outer Segment Phagocytosis by Cultured Rat Retinal Pigment Epithelial Cells." *Experimental Eye Research* 81 (5): 581–91.
- Hamann, Steffen, Jens F. Kiilgaard, Morten la Cour, Jan U. Prause, and Thomas Zeuthen. 2003. "Cotransport of H<sup>+</sup>, Lactate, and H<sub>2</sub>O in Porcine Retinal Pigment Epithelial Cells." *Experimental Eye Research* 76 (4): 493–504.
- Hamm, H. E., and M. Menaker. 1980. "Retinal Rhythms in Chicks: Circadian Variation in Melatonin and Serotonin N-Acetyltransferase Activity." *Proceedings of the National Academy of Sciences of the United States of America* 77 (8): 4998–5002.

- Hammer, M. G., and J. D. Sheridan. 1978. "Electrical Coupling and Dye Transfer between Acinar Cells in Rat Salivary Glands." *The Journal of Physiology* 275 (February): 495–505.
- Hanayama, Rikinari, Masato Tanaka, Keiko Miwa, Azusa Shinohara, Akihiro Iwamatsu, and Shigekazu Nagata. 2002. "Identification of a Factor That Links Apoptotic Cells to Phagocytes." *Nature* 417 (6885): 182–87.
- Hanke-Gogokhia, Christin, Guillermo L. Lehmann, Ignacio Benedicto, Erwin de la Fuente-Ortega, Vadim Y. Arshavsky, Ryan Schreiner, and Enrique Rodriguez-Boulan. 2021. "Apical CLC-2 in Retinal Pigment Epithelium Is Crucial for Survival of the Outer Retina." *FASEB Journal: Official Publication of the Federation of American Societies for Experimental Biology* 35 (7): e21689.
- Hartsock, Andrea, and W. James Nelson. 2008. "Adherens and Tight Junctions: Structure, Function and Connections to the Actin Cytoskeleton." *Biochimica et Biophysica Acta* 1778 (3): 660–69.
- Hattar, S., H. W. Liao, M. Takao, D. M. Berson, and K. W. Yau. 2002. "Melanopsin-Containing Retinal Ganglion Cells: Architecture, Projections, and Intrinsic Photosensitivity." *Science* 295 (5557): 1065–70.
- Hervé, Jean-Claude, and Mickaël Derangeon. 2013. "Gap-Junction-Mediated Cell-to-Cell Communication." *Cell and Tissue Research* 352 (1): 21–31.
- Hess, H. H. 1975. "The High Calcium Content of Retinal Pigmented Epithelium." *Experimental Eye Research* 21 (5): 471–79.
- Hidaka, Soh, Yasushi Akahori, and Yoshikazu Kurosawa. 2004. "Dendrodendritic Electrical Synapses between Mammalian Retinal Ganglion Cells." *The Journal of Neuroscience: The Official Journal of the Society for Neuroscience* 24 (46): 10553–67.
- Hills, Claire E., Michael I. Kerr, Mark J. Wall, and Paul E. Squires. 2013. "Visfatin Reduces Gap Junction Mediated Cell-to-Cell Communication in Proximal Tubule-Derived Epithelial Cells." *Cellular Physiology and Biochemistry: International Journal of Experimental Cellular Physiology, Biochemistry, and Pharmacology* 32 (5): 1200–1212.
- Himpens, B., P. Stalmans, P. Gomez, M. Malfait, and J. Vereecke. 1999. "Intra- and Intercellular Ca<sup>2+</sup> Signaling in Retinal Pigment Epithelial Cells during Mechanical Stimulation." *FASEB Journal: Official Publication of the Federation of American Societies for Experimental Biology* 13 Suppl: S63-8.
- Hodgkin, A. L., and A. F. Huxley. 1952. "The Dual Effect of Membrane Potential on Sodium Conductance in the Giant Axon of *Loligo*." *The Journal of Physiology* 116 (4): 497–506.
- Hoon, Mrinalini, Haruhisa Okawa, Luca Della Santina, and Rachel O. L. Wong. 2014. "Functional Architecture of the Retina: Development and Disease." *Progress in Retinal and Eye Research* 42 (September): 44–84.
- Hornstein, Eric P., Jan Verweij, and Julie L. Schnapf. 2004. "Electrical Coupling between Red and Green Cones in Primate Retina." *Nature Neuroscience* 7 (7): 745–50.

- Huang, Richard Y-C, James G. Laing, Evelyn M. Kanter, Viviana M. Berthoud, Mingwei Bao, Henry W. Rohrs, R. Reid Townsend, and Kathryn A. Yamada. 2011. "Identification of CaMKII Phosphorylation Sites in Connexin43 by High-Resolution Mass Spectrometry." *Journal of Proteome Research* 10 (3): 1098–1109.
- Huang, Xiaoshuang, Xueqin Jin, Gaoxingyu Huang, Jian Huang, Tong Wu, Zhangqiang Li, Jiaofeng Chen, Fang Kong, Xiaojing Pan, and Nieng Yan. 2022. "Structural Basis for High-Voltage Activation and Subtype-Specific Inhibition of Human Nav1.8." *Proceedings of the National Academy of Sciences of the United States of America* 119 (30): e2208211119.
- Hubbell, W. L., and M. D. Bownds. 1979. "Visual Transduction in Vertebrate Photoreceptors." *Annual Review of Neuroscience* 2: 17–34.
- Hudspeth, A. J., and A. G. Yee. 1973. "The Intercellular Junctional Complexes of Retinal Pigment Epithelia." *Investigative Ophthalmology* 12 (5): 354–65.
- Hutnik, Cindy M. L., Cady E. Pocrnich, Hong Liu, Dale W. Laird, and Qing Shao. 2008. "The Protective Effect of Functional Connexin43 Channels on a Human Epithelial Cell Line Exposed to Oxidative Stress." *Investigative Ophthalmology & Visual Science* 49 (2): 800–806.
- Ikarashi, Rina, Honami Akechi, Yuzuki Kanda, Alsawaf Ahmad, Kouhei Takeuchi, Eri Morioka, Takashi Sugiyama, Takashi Ebisawa, Masaaki Ikeda, and Masayuki Ikeda. 2017. "Regulation of Molecular Clock Oscillations and Phagocytic Activity via Muscarinic Ca<sup>2+</sup> Signaling in Human Retinal Pigment Epithelial Cells." *Scientific Reports* 7 (March): 44175.
- Immel, J., and R. H. Steinberg. 1986. "Spatial Buffering of K<sup>+</sup> by the Retinal Pigment Epithelium in Frog." *The Journal of Neuroscience: The Official Journal of the Society for Neuroscience* 6 (11): 3197–3204.
- Ingram, Norianne T., Alapakkam P. Sampath, and Gordon L. Fain. 2016. "Why Are Rods More Sensitive than Cones?" *The Journal of Physiology* 594 (19): 5415–26.
- Ishikawa, Makoto, Yu Sawada, and Takeshi Yoshitomi. 2015. "Structure and Function of the Interphotoreceptor Matrix Surrounding Retinal Photoreceptor Cells." *Experimental Eye Research* 133 (April): 3–18.
- Isom, L. L., K. S. De Jongh, D. E. Patton, B. F. Reber, J. Offord, H. Charbonneau, K. Walsh, A. L. Goldin, and W. A. Catterall. 1992. "Primary Structure and Functional Expression of the Beta 1 Subunit of the Rat Brain Sodium Channel." *Science* 256 (5058): 839–42.
- Ito, Yuki, Akiko Asada, Hiroyuki Kobayashi, Tetsuya Takano, Govinda Sharma, Taro Saito, Yasutaka Ohta, Mutsuki Amano, Kozo Kaibuchi, and Shin-Ichi Hisanaga. 2014. "Preferential Targeting of P39-Activated Cdk5 to Rac1-Induced Lamellipodia." *Molecular and Cellular Neurosciences* 61 (July): 34–45.
- Iuvone, P. M., C. L. Galli, C. K. Garrison-Gund, and N. H. Neff. 1978. "Light Stimulates Tyrosine Hydroxylase Activity and Dopamine Synthesis in Retinal Amacrine Neurons." *Science* 202 (4370): 901–2.

- Iwatsuki, N., and O. H. Petersen. 1978. "Electrical Coupling and Uncoupling of Exocrine Acinar Cells." *The Journal of Cell Biology* 79 (2 Pt 1): 533–45.
- Jaeger, Catherine, Cristina Sandu, André Malan, Katell Mellac, David Hicks, and Marie-Paule Felder-Schmittbuhl. 2015. "Circadian Organization of the Rodent Retina Involves Strongly Coupled, Layer-Specific Oscillators." *FASEB Journal: Official Publication of the Federation of American Societies for Experimental Biology* 29 (4): 1493–1504.
- Janssen-Bienhold, U., R. Dermietzel, and R. Weiler. 1998. "Distribution of Connexin43 Immunoreactivity in the Retinas of Different Vertebrates." *The Journal of Comparative Neurology* 396 (3): 310–21.
- Jiang, Mei, Julian Esteve-Rudd, Vanda S. Lopes, Tanja Diemer, Concepción Lillo, Agrani Rump, and David S. Williams. 2015. "Microtubule Motors Transport Phagosomes in the RPE, and Lack of KLC1 Leads to AMD-like Pathogenesis." *The Journal of Cell Biology* 210 (4): 595–611.
- Johansson, Julia K., Viivi I. Karema-Jokinen, Satu Hakanen, Antti Jylhä, Hannu Uusitalo, Maija Vihinen-Ranta, Heli Skottman, Teemu O. Ihalainen, and Soile Nymark. 2019. "Sodium Channels Enable Fast Electrical Signaling and Regulate Phagocytosis in the Retinal Pigment Epithelium." *BMC Biology* 17 (1): 63.
- Johnson, Ross G., Rita A. Meyer, Xin-Ren Li, Doris M. Preus, Lana Tan, Haiying Grunenwald, Alicia F. Paulson, Dale W. Laird, and Judson D. Sheridan. 2002. "Gap Junctions Assemble in the Presence of Cytoskeletal Inhibitors, but Enhanced Assembly Requires Microtubules." *Experimental Cell Research* 275 (1): 67–80.
- Jones, Jonathan C. R. 2016. "Pre- and Post-Embedding Immunogold Labeling of Tissue Sections." *Methods in Molecular Biology* 1474: 291–307.
- Jonnal, Ravi S., Jason R. Besecker, Jack C. Derby, Omer P. Kocaoglu, Barry Cense, Weihua Gao, Qiang Wang, and Donald T. Miller. 2010. "Imaging Outer Segment Renewal in Living Human Cone Photoreceptors." *Optics Express* 18 (5): 5257–70.
- Joseph, D. P., and S. S. Miller. 1991. "Apical and Basal Membrane Ion Transport Mechanisms in Bovine Retinal Pigment Epithelium." *The Journal of Physiology* 435 (April): 439–63.
- Kaestner, Lars, Xijia Wang, Laura Hertz, and Ingolf Bernhardt. 2018. "Voltage-Activated Ion Channels in Non-Excitable Cells-A Viewpoint Regarding Their Physiological Justification." *Frontiers in Physiology* 9 (April): 450.
- Kameritsch, Petra, Kristin Pogoda, and Ulrich Pohl. 2012. "Channel-Independent Influence of Connexin 43 on Cell Migration." *Biochimica et Biophysica Acta* 1818 (8): 1993–2001.
- Karl, Mike O., Wolfram Kroeger, Soenke Wimmers, Vladimir M. Milenkovic, Monika Valtink, Katrin Engelmann, and Olaf Strauss. 2008. "Endogenous Gas6 and Ca<sup>2+</sup> -Channel Activation Modulate Phagocytosis by Retinal Pigment Epithelium." *Cellular Signalling* 20 (6): 1159–68.

- Kater, S. B., and N. J. Galvin. 1978. "Physiological and Morphological Evidence for Coupling in Mouse Salivary Gland Acinar Cells." *The Journal of Cell Biology* 79 (1): 20–26.
- Kennedy, B. G., and N. J. Mangini. 1996. "Plasma Membrane Calcium-ATPase in Cultured Human Retinal Pigment Epithelium." *Experimental Eye Research* 63 (5): 547–56.
- Kerschensteiner, Daniel. 2022. "Feature Detection by Retinal Ganglion Cells." *Annual Review of Vision Science* 8 (September): 135–69.
- Kevany, Brian M., and Krzysztof Palczewski. 2010. "Phagocytosis of Retinal Rod and Cone Photoreceptors." *Physiology* 25 (1): 8–15.
- Kim, Yong-Kyu, Hanyi Yu, Vivian R. Summers, Kevin J. Donaldson, Salma Ferdous, Debresha Shelton, Nan Zhang, et al. 2021. "Morphometric Analysis of Retinal Pigment Epithelial Cells From C57BL/6J Mice During Aging." *Investigative Ophthalmology & Visual Science* 62 (2): 32.
- Kindzelskii, A. L., V. M. Elner, S. G. Elner, D. Yang, B. A. Hughes, and H. R. Petty. 2004. "Toll-like Receptor 4 (TLR4) of Retinal Pigment Epithelial Cells Participates in Transmembrane Signaling in Response to Photoreceptor Outer Segments." *The Journal of General Physiology* 124 (2): 139–49.
- Kirichenko, E. Yu, S. N. Skatchkov, and A. M. Ermakov. 2021. "Structure and Functions of Gap Junctions and Their Constituent Connexins in the Mammalian CNS." *Biochemistry (Moscow) Supplement. Series A, Membrane and Cell Biology* 15 (2): 107–19.
- Kirischuk, S., H. Kettenmann, and A. Verkhratsky. 1997. "Na<sup>+</sup>/Ca<sup>2+</sup> Exchanger Modulates Kainate-Triggered Ca<sup>2+</sup> Signaling in Bergmann Glial Cells in Situ." *FASEB Journal: Official Publication of the Federation of American Societies for Experimental Biology* 11 (7): 566–72.
- Ko, Gladys Y-P. 2020. "Circadian Regulation in the Retina: From Molecules to Network." *The European Journal of Neuroscience* 51 (1): 194–216.
- Ko, Gladys Y-P, Liheng Shi, and Michael L. Ko. 2009. "Circadian Regulation of Ion Channels and Their Functions." *Journal of Neurochemistry* 110 (4): 1150–69.
- Koerdt, Sophia Nina, and Volker Gerke. 2017. "Annexin A2 Is Involved in Ca<sup>2+</sup>-Dependent Plasma Membrane Repair in Primary Human Endothelial Cells." *Biochimica et Biophysica Acta, Molecular Cell Research* 1864 (6): 1046–53.
- Kojima, Ariko, Ken-Ichi Nakahama, Kyoko Ohno-Matsui, Noriaki Shimada, Keisuke Mori, Sachiko Iseki, Tetsuji Sato, Manabu Mochizuki, and Ikuo Morita. 2008. "Connexin 43 Contributes to Differentiation of Retinal Pigment Epithelial Cells via Cyclic AMP Signaling." *Biochemical and Biophysical Research Communications* 366 (2): 532–38.
- Kokkinaki, Maria, Niaz Sahibzada, and Nady Golestaneh. 2011. "Human Induced Pluripotent Stem-Derived Retinal Pigment Epithelium (RPE) Cells Exhibit Ion Transport, Membrane Potential, Polarized Vascular Endothelial Growth Factor Secretion, and Gene Expression Pattern Similar to Native RPE." *Stem Cells* 29 (5): 825–35.

- Korkka, Iina, Julia K. Johansson, Heli Skottman, Jari Hyttinen, and Soile Nymark. 2018. "Characterization of Chloride Channels in Human Embryonic Stem Cell Derived Retinal Pigment Epithelium." In *EMBEC & NBC 2017*, 454–57. Springer Singapore.
- Korkka, Iina, Heli Skottman, and Soile Nymark. 2022. "Heterogeneity of Potassium Channels in Human Embryonic Stem Cell-Derived Retinal Pigment Epithelium." *Stem Cells Translational Medicine* 11 (7): 753–66.
- Korkka, Iina, Taina Viheriälä, Kati Juuti-Uusitalo, Hannele Uusitalo-Järvinen, Heli Skottman, Jari Hyttinen, and Soile Nymark. 2019. "Functional Voltage-Gated Calcium Channels Are Present in Human Embryonic Stem Cell-Derived Retinal Pigment Epithelium." *Stem Cells Translational Medicine* 8 (2): 179–93.
- Kretz, Markus, Karen Maass, and Klaus Willecke. 2004. "Expression and Function of Connexins in the Epidermis, Analyzed with Transgenic Mouse Mutants." *European Journal of Cell Biology* 83 (11–12): 647–54.
- Kuffler, S. W. 1953. "Discharge Patterns and Functional Organization of Mammalian Retina." *Journal of Neurophysiology* 16 (1): 37–68.
- Kujiraoka, T., and T. Saito. 1986. "Electrical Coupling between Bipolar Cells in Carp Retina." *Proceedings of the National Academy of Sciences of the United States of America* 83 (11): 4063–66.
- Kumar, Mohit, and Bikash R. Pattnaik. 2014. "Focus on Kir7.1: Physiology and Channelopathy." *Channels* 8 (6): 488–95.
- Kwak, Yongdo, Jaehoon Jeong, Saebom Lee, Young-Un Park, Seol-Ae Lee, Dong-Hee Han, Joung-Hun Kim, et al. 2013. "Cyclin-Dependent Kinase 5 (Cdk5) Regulates the Function of CLOCK Protein by Direct Phosphorylation." *The Journal of Biological Chemistry* 288 (52): 36878–89.
- Kwon, Whijin, and Spencer A. Freeman. 2020. "Phagocytosis by the Retinal Pigment Epithelium: Recognition, Resolution, Recycling." *Frontiers in Immunology* 11 (November): 604205.
- Laing, J. G., and E. C. Beyer. 1995. "The Gap Junction Protein Connexin43 Is Degraded via the Ubiquitin Proteasome Pathway." *The Journal of Biological Chemistry* 270 (44): 26399–403.
- Laing, James G., and Eric C. Beyer. 1995. "The Gap Junction Protein Connexin43 Is Degraded via the Ubiquitin Proteasome Pathway (\*)." *The Journal of Biological Chemistry* 270 (44): 26399–403.
- Laird, D. W., K. L. Puranam, and J. P. Revel. 1991. "Turnover and Phosphorylation Dynamics of Connexin43 Gap Junction Protein in Cultured Cardiac Myocytes." *Biochemical Journal* 273(Pt 1) (January): 67–72.
- Lakkaraju, Aparna, Ankita Umapathy, Li Xuan Tan, Lauren Daniele, Nancy J. Philp, Kathleen Boesze-Battaglia, and David S. Williams. 2020. "The Cell Biology of the Retinal Pigment Epithelium." *Progress in Retinal and Eye Research*, February, 100846.

- Lampe, P. D. 1994. "Analyzing Phorbol Ester Effects on Gap Junctional Communication: A Dramatic Inhibition of Assembly." *The Journal of Cell Biology* 127 (6 Pt 2): 1895–1905.
- Lampe, P. D., W. E. Kurata, B. J. Warn-Cramer, and A. F. Lau. 1998. "Formation of a Distinct Connexin43 Phosphoisoform in Mitotic Cells Is Dependent upon P34cdc2 Kinase." *Journal of Cell Science* 111 ( Pt 6) (March): 833–41.
- Lampe, P. D., E. M. TenBroek, J. M. Burt, W. E. Kurata, R. G. Johnson, and A. F. Lau. 2000. "Phosphorylation of Connexin43 on Serine368 by Protein Kinase C Regulates Gap Junctional Communication." *The Journal of Cell Biology* 149 (7): 1503–12.
- Lampe, Paul D., and Alan F. Lau. 2004. "The Effects of Connexin Phosphorylation on Gap Junctional Communication." *The International Journal of Biochemistry & Cell Biology* 36 (7): 1171–86.
- Lanerolle, Nihal C. de, and Tih-Shih Lee. 2005. "New Facets of the Neuropathology and Molecular Profile of Human Temporal Lobe Epilepsy." *Epilepsy & Behavior: E&B* 7 (2): 190–203.
- Langer, Julia, Jonathan Stephan, Martin Theis, and Christine R. Rose. 2012. "Gap Junctions Mediate Intercellular Spread of Sodium between Hippocampal Astrocytes in Situ." *Glia* 60 (2): 239–52.
- Lasater, E. M., and J. E. Dowling. 1985. "Dopamine Decreases Conductance of the Electrical Junctions between Cultured Retinal Horizontal Cells." *Proceedings of the National Academy of Sciences of the United States of America* 82 (9): 3025–29.
- Lastwika, Kristin J., Clarence A. Dunn, Joell L. Solan, and Paul D. Lampe. 2019. "Phosphorylation of Connexin 43 at MAPK, PKC or CK1 Sites Each Distinctly Alter the Kinetics of Epidermal Wound Repair." *Journal of Cell Science* 132 (18). <https://doi.org/10.1242/jcs.234633>.
- Lauf, Undine, Ben N. G. Giepmans, Patricia Lopez, Sebastien Braconnot, Shu-Chih Chen, and Matthias M. Falk. 2002. "Dynamic Trafficking and Delivery of Connexons to the Plasma Membrane and Accretion to Gap Junctions in Living Cells." *Proceedings of the National Academy of Sciences of the United States of America* 99 (16): 10446–51.
- Laurent, Virgine, Anamika Sengupta, Aída Sánchez-Bretaña, David Hicks, and Gianluca Tosini. 2017. "Melatonin Signaling Affects the Timing in the Daily Rhythm of Phagocytic Activity by the Retinal Pigment Epithelium." *Experimental Eye Research* 165 (December): 90–95.
- LaVail, M. M. 1976. "Rod Outer Segment Disk Shedding in Rat Retina: Relationship to Cyclic Lighting." *Science* 194 (4269): 1071–74.
- . 1980. "Circadian Nature of Rod Outer Segment Disc Shedding in the Rat." *Investigative Ophthalmology & Visual Science* 19 (4): 407–11.
- Law, Ah-Lai, Célia Parinot, Jonathan Chatagnon, Basile Gravez, José-Alain Sahel, Shomi S. Bhattacharya, and Emeline F. Nandrot. 2015. "Cleavage of Mer Tyrosine Kinase (MerTK) from the Cell Surface Contributes to the

- Regulation of Retinal Phagocytosis.” *The Journal of Biological Chemistry* 290 (8): 4941–52.
- Lee, Yool. 2021. “Roles of Circadian Clocks in Cancer Pathogenesis and Treatment.” *Experimental & Molecular Medicine* 53 (10): 1529–38.
- Leite, M. Fatima, Keiji Hirata, Thomas Pusl, Angela D. Burgstahler, Keisuke Okazaki, J. Miguel Ortega, Alfredo M. Goes, Marco A. M. Prado, David C. Spray, and Michael H. Nathanson. 2002. “Molecular Basis for Pacemaker Cells in Epithelia.” *The Journal of Biological Chemistry* 277 (18): 16313–23.
- Leithe, Edward, Marc Mesnil, and Trond Aasen. 2018. “The Connexin 43 C-Terminus: A Tail of Many Tales.” *Biochimica et Biophysica Acta, Biomembranes* 1860 (1): 48–64.
- Lera Ruiz, Manuel de, and Richard L. Kraus. 2015. “Voltage-Gated Sodium Channels: Structure, Function, Pharmacology, and Clinical Indications.” *Journal of Medicinal Chemistry* 58 (18): 7093–7118.
- Lewis, Tylor R., Sean R. Kundinger, Brian A. Link, Christine Insinna, and Joseph C. Besharse. 2018. “Kif17 Phosphorylation Regulates Photoreceptor Outer Segment Turnover.” *BMC Cell Biology* 19 (1): 25.
- Li, Hanjun, Gaelle Spagnol, Li Zheng, Kelly L. Stauch, and Paul L. Sorgen. 2016. “Regulation of Connexin43 Function and Expression by Tyrosine Kinase 2.” *The Journal of Biological Chemistry* 291 (30): 15867–80.
- Li, Hongyan, Alice Z. Chuang, and John O’Brien. 2009. “Photoreceptor Coupling Is Controlled by Connexin 35 Phosphorylation in Zebrafish Retina.” *The Journal of Neuroscience: The Official Journal of the Society for Neuroscience* 29 (48): 15178–86.
- Li, Hongyan, Zhijing Zhang, Michael R. Blackburn, Steven W. Wang, Christophe P. Ribelayga, and John O’Brien. 2013. “Adenosine and Dopamine Receptors Coregulate Photoreceptor Coupling via Gap Junction Phosphorylation in Mouse Retina.” *The Journal of Neuroscience: The Official Journal of the Society for Neuroscience* 33 (7): 3135–50.
- Lin, R., B. J. Warn-Cramer, W. E. Kurata, and A. F. Lau. 2001. “V-Src Phosphorylation of Connexin 43 on Tyr247 and Tyr265 Disrupts Gap Junctional Communication.” *The Journal of Cell Biology* 154 (4): 815–27.
- Linnertz, R., A. Wurm, T. Pannicke, K. Krügel, M. Hollborn, W. Härtig, I. Iandiev, P. Wiedemann, A. Reichenbach, and A. Bringmann. 2011. “Activation of Voltage-Gated Na<sup>+</sup> and Ca<sup>2+</sup> Channels Is Required for Glutamate Release from Retinal Glial Cells Implicated in Cell Volume Regulation.” *Neuroscience* 188 (August): 23–34.
- Liu, Ren, Bo Tian, Marla Gearing, Stephen Hunter, Keqiang Ye, and Zixu Mao. 2008. “Cdk5-Mediated Regulation of the PIKE-A-Akt Pathway and Glioblastoma Cell Invasion.” *Proceedings of the National Academy of Sciences of the United States of America* 105 (21): 7570–75.
- Lobato-Álvarez, Jorge A., María L. Roldán, Teresa Del Carmen López-Murillo, Ricardo González-Ramírez, José Bonilla-Delgado, and Liora Shoshani.



2016. "The Apical Localization of Na<sup>+</sup>, K<sup>+</sup>-ATPase in Cultured Human Retinal Pigment Epithelial Cells Depends on Expression of the B2 Subunit." *Frontiers in Physiology* 7 (October): 450.
- Loeffler, K. U., and N. J. Mangini. 1998. "Immunohistochemical Localization of Na<sup>+</sup>/Ca<sup>2+</sup> Exchanger in Human Retina and Retinal Pigment Epithelium." *Graefe's Archive for Clinical and Experimental Ophthalmology = Albrecht von Graefes Archiv Fur Klinische Und Experimentelle Ophthalmologie* 236 (12): 929–33.
- Losso, Jack N., Robert E. Truax, and Gerald Richard. 2010. "Trans-Resveratrol Inhibits Hyperglycemia-Induced Inflammation and Connexin Downregulation in Retinal Pigment Epithelial Cells." *Journal of Agricultural and Food Chemistry* 58 (14): 8246–52.
- Macfarlane, S. N., and H. Sontheimer. 1998. "Spinal Cord Astrocytes Display a Switch from TTX-Sensitive to TTX-Resistant Sodium Currents after Injury-Induced Gliosis in Vitro." *Journal of Neurophysiology* 79 (4): 2222–26.
- Malfait, M., P. Gomez, T. A. van Veen, J. B. Parys, H. De Smedt, J. Vereecke, and B. Himpens. 2001. "Effects of Hyperglycemia and Protein Kinase C on Connexin43 Expression in Cultured Rat Retinal Pigment Epithelial Cells." *The Journal of Membrane Biology* 181 (1): 31–40.
- Malhotra, J. D., K. Kazen-Gillespie, M. Hortsch, and L. L. Isom. 2000. "Sodium Channel Beta Subunits Mediate Homophilic Cell Adhesion and Recruit Ankyrin to Points of Cell-Cell Contact." *The Journal of Biological Chemistry* 275 (15): 11383–88.
- Mamaeva, Daria, Zhour Jazouli, Mattia L. DiFrancesco, Nejla Erkilic, Gregor Dubois, Cecile Hilaire, Isabelle Meunier, Hassan Boukhaddaoui, and Vasiliki Kalatzis. 2021. "Novel Roles for Voltage-Gated T-Type Ca<sup>2+</sup> and ClC-2 Channels in Phagocytosis and Angiogenic Factor Balance Identified in Human iPSC-Derived RPE." *FASEB Journal: Official Publication of the Federation of American Societies for Experimental Biology* 35 (4): e21406.
- Mangel, S. C., W. H. Baldrige, R. Weiler, and J. E. Dowling. 1994. "Threshold and Chromatic Sensitivity Changes in Fish Cone Horizontal Cells Following Prolonged Darkness." *Brain Research* 659 (1–2): 55–61.
- Mani, Bharath K., and Kenneth L. Byron. 2011. "Vascular KCNQ Channels in Humans: The Sub-Threshold Brake That Regulates Vascular Tone?" *British Journal of Pharmacology*.
- Mao, Yingyu, and Silvia C. Finnemann. 2012. "Essential Diurnal Rac1 Activation during Retinal Phagocytosis Requires Avβ5 Integrin but Not Tyrosine Kinases Focal Adhesion Kinase or Mer Tyrosine Kinase." *Molecular Biology of the Cell* 23 (6): 1104–14.
- . 2013. "Analysis of Photoreceptor Outer Segment Phagocytosis by RPE Cells in Culture." *Methods in Molecular Biology* 935: 285–95.
- Mazzoni, Francesca, Hussein Safa, and Silvia C. Finnemann. 2014. "Understanding Photoreceptor Outer Segment Phagocytosis: Use and Utility of RPE Cells in Culture." *Experimental Eye Research* 126 (September): 51–60.

- McMahon, D. G. 1994. "Modulation of Electrical Synaptic Transmission in Zebrafish Retinal Horizontal Cells." *The Journal of Neuroscience: The Official Journal of the Society for Neuroscience* 14 (3 Pt 2): 1722–34.
- McMahon, D. G., and M. P. Mattson. 1996. "Horizontal Cell Electrical Coupling in the Giant Danio: Synaptic Modulation by Dopamine and Synaptic Maintenance by Calcium." *Brain Research* 718 (1–2): 89–96.
- McMahon, Douglas G., P. Michael Iuvone, and Gianluca Tosini. 2014. "Circadian Organization of the Mammalian Retina: From Gene Regulation to Physiology and Diseases." *Progress in Retinal and Eye Research* 39 (March): 58–76.
- McNeill, Jessica, Christopher Rudyk, Michael E. Hildebrand, and Natalina Salmaso. 2021. "Ion Channels and Electrophysiological Properties of Astrocytes: Implications for Emergent Stimulation Technologies." *Frontiers in Cellular Neuroscience* 15 (May): 644126.
- Mellman, Ira, and W. James Nelson. 2008. "Coordinated Protein Sorting, Targeting and Distribution in Polarized Cells." *Nature Reviews. Molecular Cell Biology* 9 (11): 833–45.
- Meşe, Gülistan, Gabriele Richard, and Thomas W. White. 2007. "Gap Junctions: Basic Structure and Function." *The Journal of Investigative Dermatology* 127 (11): 2516–24.
- Milićević, Nemanja, Ouafa Ait-Hmyed Hakkari, Udit Bagchi, Cristina Sandu, Aldo Jongejan, Perry D. Moerland, Jacqueline B. Ten Brink, David Hicks, Arthur A. Bergen, and Marie-Paule Felder-Schmittbuhl. 2021. "Core Circadian Clock Genes *Per1* and *Per2* Regulate the Rhythm in Photoreceptor Outer Segment Phagocytosis." *FASEB Journal: Official Publication of the Federation of American Societies for Experimental Biology* 35 (7): e21722.
- Milićević, Nemanja, Angelica Duursma, Anneloor L. M. A. Ten Asbroek, Marie-Paule Felder-Schmittbuhl, and Arthur A. Bergen. 2019. "Does the Circadian Clock Make RPE-Mediated Ion Transport 'Tick' via SLC12A2 (NKCC1)?" *Chronobiology International* 36 (11): 1592–98.
- Miller, S. S., and R. H. Steinberg. 1977. "Passive Ionic Properties of Frog Retinal Pigment Epithelium." *The Journal of Membrane Biology* 36 (4): 337–72.
- . 1982. "Potassium Transport across the Frog Retinal Pigment Epithelium." *The Journal of Membrane Biology* 67 (3): 199–209.
- Mills, S. L. 1999. "Unusual Coupling Patterns of a Cone Bipolar Cell in the Rabbit Retina." *Visual Neuroscience* 16 (6): 1029–35.
- Miyagishima, Kiyoharu J., Qin Wan, Barbara Corneo, Ruchi Sharma, Mostafa R. Lotfi, Nathan C. Boles, Fang Hua, et al. 2016. "In Pursuit of Authenticity: Induced Pluripotent Stem Cell-Derived Retinal Pigment Epithelium for Clinical Applications." *Stem Cells Translational Medicine* 5 (11): 1562–74.
- Moran, Ailís L., Stephen P. Carter, Joanna J. Kaylor, Zhichun Jiang, Sanne Broekman, Eugene T. Dillon, Alicia Gómez Sánchez, et al. 2022. "Dawn and Dusk Peaks of Outer Segment Phagocytosis, and Visual Cycle Function

- Require Rab28.” *FASEB Journal: Official Publication of the Federation of American Societies for Experimental Biology* 36 (5): e22309.
- Moran, Ailis L., John D. Fehilly, Daniel Floss Jones, Ross Collery, and Breandán N. Kennedy. 2022. “Regulation of the Rhythmic Diversity of Daily Photoreceptor Outer Segment Phagocytosis in Vivo.” *FASEB Journal: Official Publication of the Federation of American Societies for Experimental Biology* 36 (10): e22556.
- Morioka, Eri, Yuzuki Kanda, Hayato Koizumi, Tsubasa Miyamoto, and Masayuki Ikeda. 2018. “Histamine Regulates Molecular Clock Oscillations in Human Retinal Pigment Epithelial Cells via H1 Receptors.” *Frontiers in Endocrinology* 9 (March): 108.
- Morris, Catherine E. 2011. “Voltage-Gated Channel Mechanosensitivity: Fact or Friction?” *Frontiers in Physiology* 2 (May): 25.
- Morris, Catherine E., and Peter F. Juranka. 2007. “Nav Channel Mechanosensitivity: Activation and Inactivation Accelerate Reversibly with Stretch.” *Biophysical Journal* 93 (3): 822–33.
- Müller, Claudia, and Silvia C. Finnemann. 2020. “RPE Phagocytosis.” In *Retinal Pigment Epithelium in Health and Disease*, edited by Alexa Karina Klettner and Stefan Dithmar, 47–63. Cham: Springer International Publishing.
- Müller, Claudia, Néstor Más Gómez, Peter Ruth, and Olaf Strauss. 2014. “CaV1.3 L-Type Channels, MaxiK Ca(2+)-Dependent K(+) Channels and Bestrophin-1 Regulate Rhythmic Photoreceptor Outer Segment Phagocytosis by Retinal Pigment Epithelial Cells.” *Cellular Signalling* 26 (5): 968–78.
- Murali, Aishwarya, Subramanian Krishnakumar, Anuradha Subramanian, and Sowmya Parameswaran. 2020. “Bruch’s Membrane Pathology: A Mechanistic Perspective.” *European Journal of Ophthalmology* 30 (6): 1195–1206.
- Musil, L. S., E. C. Beyer, and D. A. Goodenough. 1990. “Expression of the Gap Junction Protein Connexin43 in Embryonic Chick Lens: Molecular Cloning, Ultrastructural Localization, and Post-Translational Phosphorylation.” *The Journal of Membrane Biology* 116 (2): 163–75.
- Mustafi, Debarshi, Andreas H. Engel, and Krzysztof Palczewski. 2009. “Structure of Cone Photoreceptors.” *Progress in Retinal and Eye Research* 28 (4): 289–302.
- Nag, Tapas Chandra, and Shashi Wadhwa. 2012. “Ultrastructure of the Human Retina in Aging and Various Pathological States.” *Micron* 43 (7): 759–81.
- Nandrot, Emeline F., and Silvia C. Finnemann. 2006. “Altered Rhythm of Photoreceptor Outer Segment Phagocytosis in Beta5 Integrin Knockout Mice.” *Advances in Experimental Medicine and Biology* 572: 119–23.
- . 2008. “Lack of Alpha5beta5 Integrin Receptor or Its Ligand MFG-E8: Distinct Effects on Retinal Function.” *Ophthalmic Research* 40 (3–4): 120–23.
- Nandrot, Emeline F., Yoonhee Kim, Scott E. Brodie, Xiaozhu Huang, Dean Sheppard, and Silvia C. Finnemann. 2004. “Loss of Synchronized Retinal

- Phagocytosis and Age-Related Blindness in Mice Lacking Alfvbeta5 Integrin.” *The Journal of Experimental Medicine* 200 (12): 1539–45.
- Neverisky, Daniel L., and Geoffrey W. Abbott. 2015. “Ion Channel-Transporter Interactions.” *Critical Reviews in Biochemistry and Molecular Biology* 51 (4): 257–67.
- Nguyen-Legros, J., and D. Hicks. 2000. “Renewal of Photoreceptor Outer Segments and Their Phagocytosis by the Retinal Pigment Epithelium.” *International Review of Cytology* 196: 245–313.
- Nimlamool, Wutigri, Rachael M. Kells Andrews, and Matthias M. Falk. 2015. “Connexin43 Phosphorylation by PKC and MAPK Signals VEGF-Mediated Gap Junction Internalization.” *Molecular Biology of the Cell* 26 (15): 2755–68.
- Noda, Masaharu, and Takeshi Y. Hiyama. 2015. “The Na(x) Channel: What It Is and What It Does.” *The Neuroscientist: A Review Journal Bringing Neurobiology, Neurology and Psychiatry* 21 (4): 399–412.
- Norris, Rachael P., Marina Freudzon, Lisa M. Mehlmann, Ann E. Cowan, Alexander M. Simon, David L. Paul, Paul D. Lampe, and Laurinda A. Jaffe. 2008. “Luteinizing Hormone Causes MAP Kinase-Dependent Phosphorylation and Closure of Connexin 43 Gap Junctions in Mouse Ovarian Follicles: One of Two Paths to Meiotic Resumption.” *Development* 135 (19): 3229–38.
- Nunes, Paula, and Nicolas Demaurex. 2010. “The Role of Calcium Signaling in Phagocytosis.” *Journal of Leukocyte Biology* 88 (1): 57–68.
- Oakley, B., 2nd. 1987. “Measurement of Potassium Turnover in Rod Photoreceptors in Toad Isolated Retina Using Ion-Selective Microelectrodes.” *Canadian Journal of Physiology and Pharmacology* 65 (5): 1018–27.
- Oakley, B., 2nd, D. G. Flaming, and K. T. Brown. 1979. “Effects of the Rod Receptor Potential upon Retinal Extracellular Potassium Concentration.” *The Journal of General Physiology* 74 (6): 713–37.
- Oh, Y., and S. G. Waxman. 1994. “The Beta 1 Subunit MRNA of the Rat Brain Na+ Channel Is Expressed in Glial Cells.” *Proceedings of the National Academy of Sciences of the United States of America* 91 (21): 9985–89.
- Okada, Yasunobu. n.d. *Patch Clamp Techniques*. Springer Japan. Accessed November 7, 2022.
- Okami, T., A. Yamamoto, K. Omori, T. Takada, M. Uyama, and Y. Tashiro. 1990. “Immunocytochemical Localization of Na+,K(+)-ATPase in Rat Retinal Pigment Epithelial Cells.” *The Journal of Histochemistry and Cytochemistry: Official Journal of the Histochemistry Society* 38 (9): 1267–75.
- Okano, Kiichiro, Akiko Maeda, Yu Chen, Vishal Chauhan, Johnny Tang, Grazyna Palczewska, Tsutomu Sakai, Hiroshi Tsuneoka, Krzysztof Palczewski, and Tadao Maeda. 2012. “Retinal Cone and Rod Photoreceptor Cells Exhibit Differential Susceptibility to Light-Induced Damage.” *Journal of Neurochemistry* 121 (1): 146–56.

- Orellana, Juan A. 2016. "Physiological Functions of Glial Cell Hemichannels." *Advances in Experimental Medicine and Biology* 949: 93–108.
- Ortolan, Davide, Ruchi Sharma, Andrei Volkov, Arvydas Maminishkis, Nathan A. Hotaling, Laryssa A. Hury, Catherine Cukras, Stefano Di Marco, Silvia Bisti, and Kapil Bharti. 2022. "Single-Cell-Resolution Map of Human Retinal Pigment Epithelium Helps Discover Subpopulations with Differential Disease Sensitivity." *Proceedings of the National Academy of Sciences of the United States of America* 119 (19): e2117553119.
- Ou, Yijun, Peter Strege, Steven M. Miller, Jonathan Makielski, Michael Ackerman, Simon J. Gibbons, and Gianrico Farrugia. 2003. "Syntrophin Gamma 2 Regulates SCN5A Gating by a PDZ Domain-Mediated Interaction." *The Journal of Biological Chemistry* 278 (3): 1915–23.
- Paez, P. M., D. Fulton, C. S. Colwell, and A. T. Campagnoni. 2009. "Voltage-Operated Ca(2+) and Na(+) Channels in the Oligodendrocyte Lineage." *Journal of Neuroscience Research* 87 (15): 3259–66.
- Palczewski, Krzysztof. 2006. "G Protein-Coupled Receptor Rhodopsin." *Annual Review of Biochemistry* 75: 743–67.
- Park, Darren J., Tracey A. Freitas, Christopher J. Wallick, Carrie V. Guyette, and Bonnie J. Warn-Cramer. 2006. "Molecular Dynamics and in Vitro Analysis of Connexin43: A New 14-3-3 Mode-1 Interacting Protein." *Protein Science: A Publication of the Protein Society* 15 (10): 2344–55.
- Park, Darren J., Christopher J. Wallick, Kendra D. Martyn, Alan F. Lau, Chengshi Jin, and Bonnie J. Warn-Cramer. 2007. "Akt Phosphorylates Connexin43 on Ser373, a 'Mode-1' Binding Site for 14-3-3." *Cell Communication & Adhesion* 14 (5): 211–26.
- Pattnaik, Bikash R., and Bret A. Hughes. 2012. "Effects of KCNQ Channel Modulators on the M-Type Potassium Current in Primate Retinal Pigment Epithelium." *American Journal of Physiology. Cell Physiology* 302 (5): C821–33.
- Paulson, A. F., P. D. Lampe, R. A. Meyer, E. TenBroek, M. M. Atkinson, T. F. Walseth, and R. G. Johnson. 2000. "Cyclic AMP and LDL Trigger a Rapid Enhancement in Gap Junction Assembly through a Stimulation of Connexin Trafficking." *Journal of Cell Science* 113 ( Pt 17) (September): 3037–49.
- Pearson, Rachael A., Marina Catsicas, David L. Becker, Philippa Bayley, Nanna L. Lüneborg, and Peter Mobbs. 2004. "Ca(2+) Signalling and Gap Junction Coupling within and between Pigment Epithelium and Neural Retina in the Developing Chick." *The European Journal of Neuroscience* 19 (9): 2435–45.
- Pearson, Rachael A., Nicholas Dale, Enrique Llaudet, and Peter Mobbs. 2005. "ATP Released via Gap Junction Hemichannels from the Pigment Epithelium Regulates Neural Retinal Progenitor Proliferation." *Neuron* 46 (5): 731–44.
- Peichl, Leo. 2005. "Diversity of Mammalian Photoreceptor Properties: Adaptations to Habitat and Lifestyle?" *The Anatomical Record. Part A, Discoveries in Molecular, Cellular, and Evolutionary Biology* 287 (1): 1001–12.

- Peirson, Stuart N., Petra H. M. Bovee-Geurts, Daniela Lupi, Glen Jeffery, Willem J. DeGrip, and Russell G. Foster. 2004. "Expression of the Candidate Circadian Photopigment Melanopsin (Opn4) in the Mouse Retinal Pigment Epithelium." *Brain Research. Molecular Brain Research* 123 (1–2): 132–35.
- Pinto, L. H., and D. J. Klumpp. 1998. "Localization of Potassium Channels in the Retina." *Progress in Retinal and Eye Research* 17 (2): 207–30.
- Pogoda, Kristin, Petra Kameritsch, Mauricio A. Retamal, and José L. Vega. 2016. "Regulation of Gap Junction Channels and Hemichannels by Phosphorylation and Redox Changes: A Revision." *BMC Cell Biology* 17 Suppl 1 (May): 11.
- Posada-Duque, Rafael Andrés, Valentina Palacio-Castañeda, and Gloria Patricia Cardona-Gómez. 2015. "CDK5 Knockdown in Astrocytes Provide Neuroprotection as a Trophic Source via Rac1." *Molecular and Cellular Neurosciences* 68 (September): 151–66.
- Procida, Kristina, Lone Jørgensen, Nicole Schmitt, Mario Delmar, Steven M. Taffet, Niels-Henrik Holstein-Rathlou, Morten Schak Nielsen, and Thomas Hartig Braunstein. 2009. "Phosphorylation of Connexin43 on Serine 306 Regulates Electrical Coupling." *Heart Rhythm: The Official Journal of the Heart Rhythm Society* 6 (11): 1632–38.
- Qi, Guang-Jian, Qiang Chen, Li-Jun Chen, Yang Shu, Lu-Lu Bu, Xiao-Yun Shao, Pei Zhang, Feng-Juan Jiao, Jin Shi, and Bo Tian. 2016. "Phosphorylation of Connexin 43 by Cdk5 Modulates Neuronal Migration During Embryonic Brain Development." *Molecular Neurobiology* 53 (5): 2969–82.
- Quinn, R. H., and S. S. Miller. 1992. "Ion Transport Mechanisms in Native Human Retinal Pigment Epithelium." *Investigative Ophthalmology & Visual Science* 33 (13): 3513–27.
- Rabin, Jeff C. 2013. "The Retina: An Approachable Part of the Brain." *Optometry and Vision Science: Official Publication of the American Academy of Optometry* 90 (1): e36.
- Raviola, E., and N. B. Gilula. 1973. "Gap Junctions between Photoreceptor Cells in the Vertebrate Retina." *Proceedings of the National Academy of Sciences of the United States of America* 70 (6): 1677–81.
- Reaume, A. G., P. A. de Sousa, S. Kulkarni, B. L. Langille, D. Zhu, T. C. Davies, S. C. Juneja, G. M. Kidder, and J. Rossant. 1995. "Cardiac Malformation in Neonatal Mice Lacking Connexin43." *Science* 267 (5205): 1831–34.
- Reese, K. A., and J. H. Caldwell. 1999. "Immunocytochemical Localization of NaCh6 in Cultured Spinal Cord Astrocytes." *Glia* 26 (1): 92–96.
- Reichhart, Nadine, and Olaf Strauss. 2014. "Ion Channels and Transporters of the Retinal Pigment Epithelium." *Experimental Eye Research* 126 (September): 27–37.
- Reichhart, Nadine, and Olaf Strauß. 2020. "Regulation of Ion Transport Through Retinal Pigment Epithelium: Impact in Retinal Degeneration." In *Ion Transport Across Epithelial Tissues and Disease: Ion Channels and Transporters of*

- Epithelia in Health and Disease - Vol. 2*, edited by Kirk L. Hamilton and Daniel C. Devor, 307–31. Cham: Springer International Publishing.
- Reigada, David, Wennan Lu, and Claire H. Mitchell. 2006. “Glutamate Acts at NMDA Receptors on Fresh Bovine and on Cultured Human Retinal Pigment Epithelial Cells to Trigger Release of ATP.” *The Journal of Physiology* 575 (Pt 3): 707–20.
- Ribelayga, Christophe, Yu Cao, and Stuart C. Mangel. 2008. “The Circadian Clock in the Retina Controls Rod-Cone Coupling.” *Neuron* 59 (5): 790–801.
- Ribelayga, Christophe, and Stuart C. Mangel. 2005. “A Circadian Clock and Light/Dark Adaptation Differentially Regulate Adenosine in the Mammalian Retina.” *The Journal of Neuroscience: The Official Journal of the Society for Neuroscience* 25 (1): 215–22.
- . 2010. “Identification of a Circadian Clock-Controlled Neural Pathway in the Rabbit Retina.” *PloS One* 5 (6): e11020.
- Rivedal, E., H. Yamasaki, and T. Sanner. 1994. “Inhibition of Gap Junctional Intercellular Communication in Syrian Hamster Embryo Cells by TPA, Retinoic Acid and DDT.” *Carcinogenesis* 15 (4): 689–94.
- Rizzolo, L. J. 1990. “The Distribution of Na<sup>+</sup>,K<sup>(+)</sup>-ATPase in the Retinal Pigmented Epithelium from Chicken Embryo Is Polarized in Vivo but Not in Primary Cell Culture.” *Experimental Eye Research* 51 (4): 435–46.
- Rizzolo, Lawrence J. 2007. “Development and Role of Tight Junctions in the Retinal Pigment Epithelium.” In *International Review of Cytology*, 258:195–234. Academic Press.
- Rizzolo, Lawrence J., Shaomin Peng, Yan Luo, and Wei Xiao. 2011. “Integration of Tight Junctions and Claudins with the Barrier Functions of the Retinal Pigment Epithelium.” *Progress in Retinal and Eye Research* 30 (5): 296–323.
- Roy, Sayon, Jean X. Jiang, An-Fei Li, and Dongjoon Kim. 2017. “Connexin Channel and Its Role in Diabetic Retinopathy.” *Progress in Retinal and Eye Research* 61 (November): 35–59.
- Ruggiero, Linda, Mark P. Connor, Jeannie Chen, Ralf Langen, and Silvia C. Finnemann. 2012. “Diurnal, Localized Exposure of Phosphatidylserine by Rod Outer Segment Tips in Wild-Type but Not Itgb5<sup>-/-</sup> or Mfge8<sup>-/-</sup> Mouse Retina.” *Proceedings of the National Academy of Sciences of the United States of America* 109 (21): 8145–48.
- Russell, J. M. 2000. “Sodium-Potassium-Chloride Cotransport.” *Physiological Reviews* 80 (1): 211–76.
- Sáez, J. C., A. C. Nairn, A. J. Czernik, G. I. Fishman, D. C. Spray, and E. L. Hertzberg. 1997. “Phosphorylation of Connexin43 and the Regulation of Neonatal Rat Cardiac Myocyte Gap Junctions.” *Journal of Molecular and Cellular Cardiology* 29 (8): 2131–45.
- Sakai, H., and T. Saito. 1997. “Na<sup>+</sup> and Ca<sup>2+</sup> Channel Expression in Cultured Newt Retinal Pigment Epithelial Cells: Comparison with Neuronal Types of Ion Channels.” *Journal of Neurobiology* 32 (4): 377–90.

- Sancho, Maria, and Barry D. Kyle. 2021. "The Large-Conductance, Calcium-Activated Potassium Channel: A Big Key Regulator of Cell Physiology." *Frontiers in Physiology* 12 (October): 750615.
- Sanes, Joshua R., and Richard H. Masland. 2015. "The Types of Retinal Ganglion Cells: Current Status and Implications for Neuronal Classification." *Annual Review of Neuroscience* 38 (July): 221–46.
- Saw, Thuan Beng, Xumei Gao, Muchun Li, Jianan He, Anh Phuong Le, Supatra Marsh, Keng-Hui Lin, Alexander Ludwig, Jacques Prost, and Chwee Teck Lim. 2022. "Transepithelial Potential Difference Governs Epithelial Homeostasis by Electromechanics." *Nature Physics* 18 (9): 1122–28.
- Scheuer, Todd. 2011. "Regulation of Sodium Channel Activity by Phosphorylation." *Seminars in Cell & Developmental Biology* 22 (2): 160–65.
- Schirrmacher, K., F. Brümmer, R. Düsing, and D. Bingmann. 1993. "Dye and Electric Coupling between Osteoblast-like Cells in Culture." *Calcified Tissue International* 53 (1): 53–60.
- Schneider, Caroline A., Wayne S. Rasband, and Kevin W. Eliceiri. 2012. "NIH Image to ImageJ: 25 Years of Image Analysis." *Nature Methods* 9 (7): 671–75.
- Segawa, Katsumori, Sachiko Kurata, Yuichi Yanagihashi, Thijn R. Brummelkamp, Fumihiko Matsuda, and Shigekazu Nagata. 2014. "Caspase-Mediated Cleavage of Phospholipid Flippase for Apoptotic Phosphatidylserine Exposure." *Science* 344 (6188): 1164–68.
- Segawa, Y., and B. A. Hughes. 1994. "Properties of the Inwardly Rectifying K<sup>+</sup> Conductance in the Toad Retinal Pigment Epithelium." *The Journal of Physiology* 476 (1): 41–53.
- Segretain, Dominique, and Matthias M. Falk. 2004. "Regulation of Connexin Biosynthesis, Assembly, Gap Junction Formation, and Removal." *Biochimica et Biophysica Acta* 1662 (1–2): 3–21.
- Sethna, Saamil, Tess Chamakkala, Xiaowu Gu, Timothy C. Thompson, Guangwen Cao, Michael H. Elliott, and Silvia C. Finnemann. 2016. "Regulation of Phagolysosomal Digestion by Caveolin-1 of the Retinal Pigment Epithelium Is Essential for Vision." *The Journal of Biological Chemistry* 291 (12): 6494–6506.
- Shah, Maithili M., Anna-Marie Martinez, and William H. Fletcher. 2002. "The Connexin43 Gap Junction Protein Is Phosphorylated by Protein Kinase A and Protein Kinase C: In Vivo and in Vitro Studies." *Molecular and Cellular Biochemistry* 238 (1–2): 57–68.
- Shahi, Pawan K., Xinling Liu, Bryce Aul, Andrea Moyer, Akshita Pattnaik, Jerod Denton, De-Ann M. Pillers, and Bikash R. Pattnaik. 2017. "Abnormal Electroretinogram after Kir7.1 Channel Suppression Suggests Role in Retinal Electrophysiology." *Scientific Reports* 7 (1): 10651.
- Shaw, Robin M., Alex J. Fay, Manojkumar A. Puthenveedu, Mark von Zastrow, Yuh-Nung Jan, and Lily Y. Jan. 2007. "Microtubule Plus-End-Tracking Proteins Target Gap Junctions Directly from the Cell Interior to Adherens Junctions." *Cell* 128 (3): 547–60.



- Shelby, Shameka J., Karen Colwill, Sirano Dhe-Paganon, Tony Pawson, and Debra A. Thompson. 2013. "MERTK Interactions with SH2-Domain Proteins in the Retinal Pigment Epithelium." *PLoS One* 8 (2): e53964.
- Sheu, Shwu-Jiuan, Sheng-Nan Wu, and Dan-Ning Hu. 2005. "Stretch-Stimulated Activity of Large Conductance Calcium-Activated Potassium Channels in Human Retinal Pigment Epithelial Cells." *Journal of Ocular Pharmacology and Therapeutics: The Official Journal of the Association for Ocular Pharmacology and Therapeutics* 21 (6): 429–35.
- Skottman, Heli. 2010. "Derivation and Characterization of Three New Human Embryonic Stem Cell Lines in Finland." *In Vitro Cellular & Developmental Biology. Animal* 46 (3–4): 206–9.
- Söhl, Goran, Stephan Maxeiner, and Klaus Willecke. 2005. "Expression and Functions of Neuronal Gap Junctions." *Nature Reviews. Neuroscience* 6 (3): 191–200.
- Söhl, Goran, and Klaus Willecke. 2003. "An Update on Connexin Genes and Their Nomenclature in Mouse and Man." *Cell Communication & Adhesion* 10 (4–6): 173–80.
- Solan, Joell L., and Paul D. Lampe. 2008. "Connexin 43 in LA-25 Cells with Active v-Src Is Phosphorylated on Y247, Y265, S262, S279/282, and S368 via Multiple Signaling Pathways." *Cell Communication & Adhesion* 15 (1): 75–84.
- . 2014. "Specific Cx43 Phosphorylation Events Regulate Gap Junction Turnover in Vivo." *FEBS Letters* 588 (8): 1423–29.
- . 2016. "Kinase Programs Spatiotemporally Regulate Gap Junction Assembly and Disassembly: Effects on Wound Repair." *Seminars in Cell & Developmental Biology* 50 (February): 40–48.
- . 2018. "Spatio-Temporal Regulation of Connexin43 Phosphorylation and Gap Junction Dynamics." *Biochimica et Biophysica Acta, Biomembranes* 1860 (1): 83–90.
- . 2020. "Src Regulation of Cx43 Phosphorylation and Gap Junction Turnover." *Biomolecules* 10 (12). <https://doi.org/10.3390/biom10121596>.
- Solan, Joell L., Lucrecia Marquez-Rosado, Paul L. Sorgen, Perry J. Thornton, Philip R. Gafken, and Paul D. Lampe. 2007. "Phosphorylation at S365 Is a Gatekeeper Event That Changes the Structure of Cx43 and Prevents Down-Regulation by PKC." *The Journal of Cell Biology* 179 (6): 1301–9.
- Somasundaran, Shreya, Ian J. Constable, Carla B. Mellough, and Livia S. Carvalho. 2020. "Retinal Pigment Epithelium and Age-Related Macular Degeneration: A Review of Major Disease Mechanisms." *Clinical & Experimental Ophthalmology* 48 (8): 1043–56.
- Sontheimer, H., E. Fernandez-Marques, N. Ullrich, C. A. Pappas, and S. G. Waxman. 1994. "Astrocyte Na<sup>+</sup> Channels Are Required for Maintenance of Na<sup>+</sup>/K<sup>+</sup>-ATPase Activity." *The Journal of Neuroscience: The Official Journal of the Society for Neuroscience* 14 (5 Pt 1): 2464–75.

- Sontheimer, H., and S. G. Waxman. 1992. "Ion Channels in Spinal Cord Astrocytes in Vitro. II. Biophysical and Pharmacological Analysis of Two Na<sup>+</sup> Current Types." *Journal of Neurophysiology* 68 (4): 1001–11.
- Sorgen, Paul L., Andrew J. Trease, Gaelle Spagnol, Mario Delmar, and Morten S. Nielsen. 2018. "Protein-Protein Interactions with Connexin 43: Regulation and Function." *International Journal of Molecular Sciences* 19 (5). <https://doi.org/10.3390/ijms19051428>.
- Sparrow, J. R., D. Hicks, and C. P. Hamel. 2010. "The Retinal Pigment Epithelium in Health and Disease." *Current Molecular Medicine* 10 (9): 802–23.
- Spencer, William J., Tylor R. Lewis, Jillian N. Pearring, and Vadim Y. Arshavsky. 2020. "Photoreceptor Discs: Built Like Ectosomes." *Trends in Cell Biology* 30 (11): 904–15.
- Srisakuldee, Wattamon, Maya M. Jeyaraman, Barbara E. Nickel, Stéphane Tanguy, Zhi-Sheng Jiang, and Elissavet Kardami. 2009. "Phosphorylation of Connexin-43 at Serine 262 Promotes a Cardiac Injury-Resistant State." *Cardiovascular Research* 83 (4): 672–81.
- Steinberg, R. H. 1974. "Phagocytosis by Pigment Epithelium of Human Retinal Cones." *Nature* 252 (5481): 305–7.
- . 1985. "Interactions between the Retinal Pigment Epithelium and the Neural Retina." *Documenta Ophthalmologica. Advances in Ophthalmology* 60 (4): 327–46.
- Steinberg, R. H., and S. Miller. 1973. "Aspects of Electrolyte Transport in Frog Pigment Epithelium." *Experimental Eye Research* 16 (5): 365–72.
- Steinberg, R. H., and I. Wood. 1974. "Pigment Epithelial Cell Ensheathment of Cone Outer Segments in the Retina of the Domestic Cat." *Proceedings of the Royal Society of London. Series B, Containing Papers of a Biological Character. Royal Society* 187 (1089): 461–78.
- Stella, Salvatore L., Jr, Eric J. Bryson, Lucia Cadetti, and Wallace B. Thoreson. 2003. "Endogenous Adenosine Reduces Glutamatergic Output from Rods through Activation of A2-like Adenosine Receptors." *Journal of Neurophysiology* 90 (1): 165–74.
- Strauss, Olaf. 2005. "The Retinal Pigment Epithelium in Visual Function." *Physiological Reviews* 85 (3): 845–81.
- Strick, David J., Wei Feng, and Douglas Vollrath. 2009. "Mertk Drives Myosin II Redistribution during Retinal Pigment Epithelial Phagocytosis." *Investigative Ophthalmology & Visual Science* 50 (5): 2427–35.
- Sun, Bo, Josephine Lembong, Valery Normand, Matthew Rogers, and Howard A. Stone. 2012. "Spatial-Temporal Dynamics of Collective Chemosensing." *Proceedings of the National Academy of Sciences of the United States of America* 109 (20): 7753–58.
- Swarup, Aditi, Ivy S. Samuels, Brent A. Bell, John Y. S. Han, Jianhai Du, Erik Massenzio, E. Dale Abel, Kathleen Boesze-Battaglia, Neal S. Peachey, and Nancy J. Philp. 2019. "Modulating GLUT1 Expression in Retinal Pigment Epithelium Decreases Glucose Levels in the Retina: Impact on

- Photoreceptors and Müller Glial Cells.” *American Journal of Physiology. Cell Physiology* 316 (1): C121–33.
- Takahashi, Joseph S. 2017. “Transcriptional Architecture of the Mammalian Circadian Clock.” *Nature Reviews. Genetics* 18 (3): 164–79.
- Takahashi, Joseph S., Hee-Kyung Hong, Caroline H. Ko, and Erin L. McDearmon. 2008. “The Genetics of Mammalian Circadian Order and Disorder: Implications for Physiology and Disease.” *Nature Reviews. Genetics* 9 (10): 764–75.
- Tao, Q., and M. E. Kelly. 1996. “Calcium-Activated Potassium Current in Cultured Rabbit Retinal Pigment Epithelial Cells.” *Current Eye Research* 15 (3): 237–46.
- Teirstein, P. S., A. I. Goldman, and P. J. O’Brien. 1980. “Evidence for Both Local and Central Regulation of Rat Rod Outer Segment Disc Shedding.” *Investigative Ophthalmology & Visual Science* 19 (11): 1268–73.
- TenBroek, E. M., P. D. Lampe, J. L. Solan, J. K. Reynhout, and R. G. Johnson. 2001. “Ser364 of Connexin43 and the Upregulation of Gap Junction Assembly by CAMP.” *The Journal of Cell Biology* 155 (7): 1307–18.
- Terman, J. S., C. E. Remé, and M. Terman. 1993. “Rod Outer Segment Disk Shedding in Rats with Lesions of the Suprachiasmatic Nucleus.” *Brain Research* 605 (2): 256–64.
- Thio, C. L., and H. Sontheimer. 1993. “Differential Modulation of TTX-Sensitive and TTX-Resistant Na<sup>+</sup> Channels in Spinal Cord Astrocytes Following Activation of Protein Kinase C.” *The Journal of Neuroscience: The Official Journal of the Society for Neuroscience* 13 (11): 4889–97.
- Thio, C. L., S. G. Waxman, and H. Sontheimer. 1993. “Ion Channels in Spinal Cord Astrocytes in Vitro. III. Modulation of Channel Expression by Coculture with Neurons and Neuron-Conditioned Medium.” *Journal of Neurophysiology* 69 (3): 819–31.
- Thonel, Aurélie de, Saima E. Ferraris, Hanna-Mari Pallari, Susumu Y. Imanishi, Vitaly Kochin, Tomohisa Hosokawa, Shin-Ichi Hisanaga, Cecilia Sahlgren, and John E. Eriksson. 2010. “Protein Kinase Czeta Regulates Cdk5/P25 Signaling during Myogenesis.” *Molecular Biology of the Cell* 21 (8): 1423–34.
- Tibber, Marc S., David Becker, and Glen Jeffery. 2007. “Levels of Transient Gap Junctions between the Retinal Pigment Epithelium and the Neuroblastic Retina Are Influenced by Catecholamines and Correlate with Patterns of Cell Production.” *The Journal of Comparative Neurology* 503 (1): 128–34.
- Tikidji-Hamburyan, Alexandra, Katja Reinhard, Riccardo Storchi, Johannes Dietter, Hartwig Seitter, Katherine E. Davis, Saad Idrees, et al. 2017. “Rods Progressively Escape Saturation to Drive Visual Responses in Daylight Conditions.” *Nature Communications* 8 (1): 1813.
- To, C. H., and S. A. Hodson. 1998. “The Glucose Transport in Retinal Pigment Epithelium Is via Passive Facilitated Diffusion.” *Comparative Biochemistry and Physiology. Part A, Molecular & Integrative Physiology* 121 (4): 441–44.

- Tong, Xiao-Ping, Xiang-Yao Li, Bing Zhou, Wanhua Shen, Zhi-Jun Zhang, Tian-Le Xu, and Shumin Duan. 2009. "Ca(2+) Signaling Evoked by Activation of Na(+) Channels and Na(+)/Ca(2+) Exchangers Is Required for GABA-Induced NG2 Cell Migration." *The Journal of Cell Biology* 186 (1): 113–28.
- Tosini, G., and M. Menaker. 1996. "Circadian Rhythms in Cultured Mammalian Retina." *Science* 272 (5260): 419–21.
- Tosini, Gianluca, Nikita Pozdeyev, Katsuhiko Sakamoto, and P. Michael Iuvone. 2008. "The Circadian Clock System in the Mammalian Retina." *BioEssays: News and Reviews in Molecular, Cellular and Developmental Biology* 30 (7): 624–33.
- Toyofuku, T., Y. Akamatsu, H. Zhang, T. Kuzuya, M. Tada, and M. Hori. 2001. "C-Src Regulates the Interaction between Connexin-43 and ZO-1 in Cardiac Myocytes." *The Journal of Biological Chemistry* 276 (3): 1780–88.
- Tran, Vu, Xiaodong Zhang, Lin Cao, Hanqing Li, Benjamin Lee, Michelle So, Yaohui Sun, Wei Chen, and Min Zhao. 2013. "Synchronization Modulation Increases Transepithelial Potentials in MDCK Monolayers through Na/K Pumps." *PLoS One* 8 (4): e61509.
- Trenholm, Stuart, and Gautam B. Awatramani. 2019. "Myriad Roles for Gap Junctions in Retinal Circuits." In *Webvision: The Organization of the Retina and Visual System*, edited by Helga Kolb, Eduardo Fernandez, and Ralph Nelson. Salt Lake City (UT): University of Utah Health Sciences Center.
- Trenholm, Stuart, Amanda J. McLaughlin, David J. Schwab, and Gautam B. Awatramani. 2013. "Dynamic Tuning of Electrical and Chemical Synaptic Transmission in a Network of Motion Coding Retinal Neurons." *The Journal of Neuroscience: The Official Journal of the Society for Neuroscience* 33 (37): 14927–38.
- Umaphathy, Ankita, Julie Chung, Madeline Tomlinson, Caleb Lim, and David S. Williams. 2021. "Spatiotemporal Dynamics of Photoreceptor Outer Segment Phagosome Ingestion by the Retinal Pigment Epithelium." *Investigative Ophthalmology & Visual Science* 62 (8): 2952–2952.
- Umino, O., M. Maehara, S. Hidaka, S. Kita, and Y. Hashimoto. 1994. "The Network Properties of Bipolar-Bipolar Cell Coupling in the Retina of Teleost Fishes." *Visual Neuroscience* 11 (3): 533–48.
- Vaajasaari, Hanna, Tanja Ilmarinen, Kati Juuti-Uusitalo, Kristiina Rajala, Niina Onnela, Susanna Narkilahti, Riitta Suuronen, Jari Hyttinen, Hannu Uusitalo, and Heli Skottman. 2011. "Toward the Defined and Xeno-Free Differentiation of Functional Human Pluripotent Stem Cell-Derived Retinal Pigment Epithelial Cells." *Molecular Vision* 17 (February): 558–75.
- Van Campenhout, Raf, Axelle Cooreman, Kaat Leroy, Olga M. Rusiecka, Pieter Van Brantegem, Pieter Annaert, Serge Muyldermans, et al. 2020. "Non-Canonical Roles of Connexins." *Progress in Biophysics and Molecular Biology* 153 (July): 35–41.

- Veruki, Margaret Lin, and Espen Hartveit. 2002. "AII (Rod) Amacrine Cells Form a Network of Electrically Coupled Interneurons in the Mammalian Retina." *Neuron* 33 (6): 935–46.
- Viheriälä, Taina, Juhana Sorvari, Teemu O. Ihalainen, Anni Mörö, Pyry Grönroos, Sabrina Schlie-Wolter, Boris Chichkov, Heli Skottman, Soile Nymark, and Tanja Ilmarinen. 2021. "Culture Surface Protein Coatings Affect the Barrier Properties and Calcium Signalling of HESC-RPE." *Scientific Reports* 11 (1): 1–14.
- Vogalis, Fivos, Colleen C. Hegg, and Mary T. Lucero. 2005. "Electrical Coupling in Sustentacular Cells of the Mouse Olfactory Epithelium." *Journal of Neurophysiology* 94 (2): 1001–12.
- Wang, Y., and S. C. Mangel. 1996. "A Circadian Clock Regulates Rod and Cone Input to Fish Retinal Cone Horizontal Cells." *Proceedings of the National Academy of Sciences of the United States of America* 93 (10): 4655–60.
- Warn-Cramer, B. J., G. T. Cottrell, J. M. Burt, and A. F. Lau. 1998. "Regulation of Connexin-43 Gap Junctional Intercellular Communication by Mitogen-Activated Protein Kinase." *The Journal of Biological Chemistry* 273 (15): 9188–96.
- Warn-Cramer, B. J., P. D. Lampe, W. E. Kurata, M. Y. Kanemitsu, L. W. Loo, W. Eckhart, and A. F. Lau. 1996. "Characterization of the Mitogen-Activated Protein Kinase Phosphorylation Sites on the Connexin-43 Gap Junction Protein." *The Journal of Biological Chemistry* 271 (7): 3779–86.
- Weingeist, Thomas A. 1982. "The Retinal Pigment Epithelium." *Archives of Ophthalmology* 100 (4): 666–666.
- Wen, R., G. M. Lui, and R. H. Steinberg. 1994. "Expression of a Tetrodotoxin-Sensitive Na<sup>+</sup> Current in Cultured Human Retinal Pigment Epithelial Cells." *The Journal of Physiology* 476 (2): 187–96.
- Weng, T. X., B. F. Godley, G. F. Jin, N. J. Mangini, B. G. Kennedy, A. S. L. Yu, and N. K. Wills. 2002. "Oxidant and Antioxidant Modulation of Chloride Channels Expressed in Human Retinal Pigment Epithelium." *American Journal of Physiology. Cell Physiology* 283 (3): C839–49.
- Werblin, F. S. 1978. "Transmission along and between Rods in the Tiger Salamander Retina." *The Journal of Physiology* 280 (July): 449–70.
- White, T. W., and D. L. Paul. 1999. "Genetic Diseases and Gene Knockouts Reveal Diverse Connexin Functions." *Annual Review of Physiology* 61: 283–310.
- Willecke, Klaus, Jürgen Eiberger, Joachim Degen, Dominik Eckardt, Alessandro Romualdi, Martin Guldenagel, Urban Deutsch, and Goran Söhl. 2002. "Structural and Functional Diversity of Connexin Genes in the Mouse and Human Genome." *Biological Chemistry* 383 (5): 725–37.
- Willoughby, Colin E., Diego Ponzin, Stefano Ferrari, Aires Lobo, Klara Landau, and Yadollah Omid. 2010. "Anatomy and Physiology of the Human Eye: Effects of Mucopolysaccharidoses Disease on Structure and Function - a Review." *Clinical & Experimental Ophthalmology* 38 (August): 2–11.

- Wimmers, Sönke, Linn Coepicus, Rita Rosenthal, and Olaf Strauss. 2008. "Expression Profile of Voltage-Dependent Ca<sup>2+</sup> Channel Subunits in the Human Retinal Pigment Epithelium." *Graefe's Archive for Clinical and Experimental Ophthalmology = Albrecht von Graefes Archiv Fur Klinische Und Experimentelle Ophthalmologie* 246 (5): 685–92.
- Wimmers, Sönke, Claire Halsband, Sebastian Seyler, Vladimir Milenkovic, and Olaf Strauss. 2008. "Voltage-Dependent Ca<sup>2+</sup> Channels, Not Ryanodine Receptors, Activate Ca<sup>2+</sup>-Dependent BK Potassium Channels in Human Retinal Pigment Epithelial Cells." *Molecular Vision* 14 (December): 2340–48.
- Wimmers, Sönke, Mike O. Karl, and Olaf Strauss. 2007. "Ion Channels in the RPE." *Progress in Retinal and Eye Research* 26 (3): 263–301.
- Wollmann, Guido, Steffen Lenzner, Wolfgang Berger, Rita Rosenthal, Mike O. Karl, and Olaf Strauss. 2006. "Voltage-Dependent Ion Channels in the Mouse RPE: Comparison with Norrie Disease Mice." *Vision Research* 46 (5): 688–98.
- Wu, Samuel M. 2010. "Synaptic Organization of the Vertebrate Retina: General Principles and Species-Specific Variations: The Friedenwald Lecture." *Investigative Ophthalmology & Visual Science* 51 (3): 1263–74.
- Xie, H., D. W. Laird, T. H. Chang, and V. W. Hu. 1997. "A Mitosis-Specific Phosphorylation of the Gap Junction Protein Connexin43 in Human Vascular Cells: Biochemical Characterization and Localization." *The Journal of Cell Biology* 137 (1): 203–10.
- Xu, Guangjin, Wei Wang, Harold K. Kimelberg, and Min Zhou. 2010. "Electrical Coupling of Astrocytes in Rat Hippocampal Slices under Physiological and Simulated Ischemic Conditions." *Glia* 58 (4): 481–93.
- Yang, Ming, Andrew D. James, Rakesh Suman, Richard Kasprovicz, Michaela Nelson, Peter J. O'Toole, and William J. Brackenbury. 2020. "Voltage-Dependent Activation of Rac1 by Nav 1.5 Channels Promotes Cell Migration." *Journal of Cellular Physiology* 235 (4): 3950–72.
- Yarov-Yarovoy, Vladimir, David Baker, and William A. Catterall. 2006. "Voltage Sensor Conformations in the Open and Closed States in ROSETTA Structural Models of K(+) Channels." *Proceedings of the National Academy of Sciences of the United States of America* 103 (19): 7292–97.
- Yogo, Keiichiro, Takuya Ogawa, Motofusa Akiyama, Norihiro Ishida, and Tatsuo Takeya. 2002. "Identification and Functional Analysis of Novel Phosphorylation Sites in Cx43 in Rat Primary Granulosa Cells." *FEBS Letters* 531 (2): 132–36.
- Young, R. W. 1978. "The Daily Rhythm of Shedding and Degradation of Rod and Cone Outer Segment Membranes in the Chick Retina." *Investigative Ophthalmology & Visual Science* 17 (2): 105–16.
- Young, R. W., and D. Bok. 1969. "Participation of the Retinal Pigment Epithelium in the Rod Outer Segment Renewal Process." *The Journal of Cell Biology* 42 (2): 392–403.

- Yu, Esther J., Seong-Hoon Ko, Paul W. Lenkowski, Alena Pance, Manoj K. Patel, and Antony P. Jackson. 2005. "Distinct Domains of the Sodium Channel Beta3-Subunit Modulate Channel-Gating Kinetics and Subcellular Location." *Biochemical Journal* 392 (Pt 3): 519–26.
- Yu, Frank H., and William A. Catterall. 2003. "Overview of the Voltage-Gated Sodium Channel Family." *Genome Biology* 4 (3): 207.
- Zadeh, Alireza Dehghani, Hongjian Xu, Matthew E. Loewen, Geoffrey P. Noble, David F. Steele, and David Fedida. 2008. "Internalized Kv1.5 Traffics via Rab-Dependent Pathways." *The Journal of Physiology* 586 (20): 4793–4813.
- Zhang, Jian, and Samuel M. Wu. 2005. "Physiological Properties of Rod Photoreceptor Electrical Coupling in the Tiger Salamander Retina." *The Journal of Physiology* 564 (Pt 3): 849–62.
- Zhang, Y. W., I. Morita, M. Ikeda, K. W. Ma, and S. Murota. 2001. "Connexin43 Suppresses Proliferation of Osteosarcoma U2OS Cells through Post-Transcriptional Regulation of P27." *Oncogene* 20 (31): 4138–49.
- Zhang, Zhijing, Hongyan Li, Xiaoqin Liu, John O'Brien, and Christophe P. Ribelayga. 2015. "Circadian Clock Control of Connexin36 Phosphorylation in Retinal Photoreceptors of the CBA/Caj Mouse Strain." *Visual Neuroscience* 32 (January): E009.
- Zhao, Jing, Wei Zhong, Lixia Sun, Yuan Yin, and Yajuan Zheng. 2017. "Effect of Chloride Channel Activity on Retinal Pigment Cell Proliferation and Migration." *Molecular Medicine Reports* 15 (4): 1771–76.
- Zheng, Li, Hanjun Li, Andrew Cannon, Andrew J. Trease, Gaelle Spagnol, Hong Zheng, Stanley Radio, Kaushik Patel, Surinder Batra, and Paul L. Sorgen. 2019. "Phosphorylation of Cx43 Residue Y313 by Src Contributes to Blocking the Interaction with Drebrin and Disassembling Gap Junctions." *Journal of Molecular and Cellular Cardiology* 126 (January): 36–49.
- Zielicka, Zofia, Jennifer A. E. Williams, and Stephen E. Moss. 2015. "Gap Junctions Modulate the Phagocytic Activity of Retinal Pigment Epithelial Cells." *Investigative Ophthalmology & Visual Science* 56 (7): 2322–2322.
- Zsiros, Emese, Katalin Kis-Toth, Peter Hajdu, Rezso Gaspar, Joanna Bielanska, Antonio Felipe, Eva Rajnavolgyi, and Gyorgy Panyi. 2009. "Developmental Switch of the Expression of Ion Channels in Human Dendritic Cells." *Journal of Immunology* 183 (7): 4483–92.





# PUBLICATIONS



# PUBLICATION

I

## **Sodium channels enable fast electrical signaling and regulate phagocytosis in the retinal pigment epithelium**

Johansson J.K, Karema-Jokinen V.I, Hakanen S., Jylhä A., Uusitalo H., Vihinen-Ranta M., Skottman H., Ihalainen T.O. & Nymark S.

BMC biology (2019), 17(1): 1-19.

<https://doi.org/10.1186/s12915-019-0681-1>

**Publication reprinted with the permission of the copyright holders**




RESEARCH ARTICLE

Open Access



# Sodium channels enable fast electrical signaling and regulate phagocytosis in the retinal pigment epithelium

Julia K. Johansson<sup>1</sup>, Viivi I. Karema-Jokinen<sup>1</sup>, Satu Hakanen<sup>2</sup>, Antti Jylhä<sup>1</sup>, Hannu Uusitalo<sup>1,3</sup>, Maija Vihinen-Ranta<sup>2</sup>, Heli Skottman<sup>1</sup>, Teemu O. Ihalainen<sup>1</sup> and Soile Nymark<sup>1\*</sup> 

## Abstract

**Background:** Voltage-gated sodium ( $\text{Na}_v$ ) channels have traditionally been considered a trademark of excitable cells. However, recent studies have shown the presence of  $\text{Na}_v$  channels in several non-excitable cells, such as astrocytes and macrophages, demonstrating that the roles of these channels are more diverse than was previously thought. Despite the earlier discoveries, the presence of  $\text{Na}_v$  channel-mediated currents in the cells of retinal pigment epithelium (RPE) has been dismissed as a cell culture artifact. We challenge this notion by investigating the presence and possible role of  $\text{Na}_v$  channels in RPE both *ex vivo* and *in vitro*.

**Results:** Our work demonstrates that several subtypes of  $\text{Na}_v$  channels are found in human embryonic stem cell (hESC)-derived and mouse RPE, most prominently subtypes  $\text{Na}_v1.4$ ,  $\text{Na}_v1.6$ , and  $\text{Na}_v1.8$ . Whole cell patch clamp recordings from the hESC-derived RPE monolayers showed that the current was inhibited by TTX and QX-314 and was sensitive to the selective blockers of the main  $\text{Na}_v$  subtypes. Importantly, we show that the  $\text{Na}_v$  channels are involved in photoreceptor outer segment phagocytosis since blocking their activity significantly reduces the efficiency of particle internalization. Consistent with this role, our electron microscopy results and immunocytochemical analysis show that  $\text{Na}_v1.4$  and  $\text{Na}_v1.8$  accumulate on phagosomes and that pharmacological inhibition of  $\text{Na}_v$  channels as well as silencing the expression of  $\text{Na}_v1.4$  with shRNA impairs the phagocytosis process.

**Conclusions:** Taken together, our study shows that  $\text{Na}_v$  channels are present in RPE, giving this tissue the capacity of fast electrical signaling. The channels are critical for the physiology of RPE with an important role in photoreceptor outer segment phagocytosis.

**Keywords:** RPE, Ion channels,  $\text{Na}_v$ , Patch clamp, Phagocytosis, Retina, Photoreceptors

## Introduction

In the vertebrate eye, the retinal pigment epithelium (RPE) forms a barrier between the retina and the choroid [1–3]. Its cells are associated closely with photoreceptors: their apical sides surround the outer segments with long microvilli, and the basolateral sides are attached to Bruch's membrane, an extracellular matrix separating the RPE from the choroid [3, 4]. The RPE has many functions that are vital to retinal maintenance and vision, such as maintaining the visual cycle, secreting

important growth factors, delivering nutrients to the photoreceptors from the bloodstream while removing metabolic end products, and absorbing scattered light [1, 3]. Additionally, RPE maintains ionic homeostasis in the subretinal space [5] and sustains photoreceptor renewal by phagocytosing their shed outer segments [1, 6]. Phagocytosis is highly essential for vision, and it is under strict diurnal control, initiated at light onset for rods and typically at light offset for cones [7, 8]. This evolutionarily conserved molecular pathway is receptor mediated and precisely regulated; however, the exact signaling cascades are still not completely understood [9]. Recent studies imply the importance of specific ion channels in this process including the L-type calcium channels as

\* Correspondence: soilenymark@tuni.fi

<sup>1</sup>BioMediTech, Faculty of Medicine and Health Technology, Tampere University, Tampere, Finland

Full list of author information is available at the end of the article



well as calcium-dependent potassium and chloride channels [10–12].

Since the first single-cell recordings from RPE in 1988 [13], a large variety of different ion channels have been identified in them [5]. Among these are several voltage-gated calcium, potassium, and chloride channels. However, the identity of sodium conductive ion channels in RPE has remained elusive [5], even though the importance of sodium homeostasis to normal RPE function is acknowledged. Of the two main families of sodium channels, there is evidence of both epithelial  $\text{Na}^+$  channels and voltage-gated  $\text{Na}^+$  ( $\text{Na}_v$ ) channels in RPE [5, 14, 15, 18, 19]. However, electrophysiological data demonstrating their functionality is missing in mature RPE. More importantly,  $\text{Na}_v$  channels that are characteristic of excitable cells have to date only been detected from cultured RPE. This has resulted in the interpretation that their expression is due to neuroepithelial differentiation that can occur in culture [5, 20, 21].

Here, we shed light on this crucial issue by demonstrating the presence of  $\text{Na}_v$  channels both in cultured human embryonic stem cell (hESC)-derived RPE and freshly isolated mouse RPE. We show that  $\text{Na}_v$  channels co-regulate photoreceptor outer segment (POS) phagocytosis. Our hypothesis is supported by a recent demonstration of the involvement of  $\text{Na}_v$  channels in phagocytosis of mycobacteria by macrophages [22]. Our work provides evidence that  $\text{Na}_v1.8$  accumulates with the phagosomal particles.  $\text{Na}_v1.4$  also accumulates to phagosomes but displays localization to cell–cell junctions outside phagocytosis. Interestingly, selective  $\text{Na}_v$  channel blockers significantly reduced this phagosomal translocation. Moreover, the selective blockers combined with the universal  $\text{Na}_v$  blocker tetrodotoxin (TTX) reduced the total number of ingested POS particles by up to 41% while not affecting their binding. Reduction was also observed when the expression of  $\text{Na}_v1.4$  was silenced with short hairpin RNA (shRNA). More generally, our observations add to the growing body of evidence that  $\text{Na}_v$  channels play diverse roles in a variety of classically non-excitabile cell types ranging from astrocytes and microglia to macrophages and cancer cells (for review, see [23]). Collectively, our results show that this epithelium is electrically more complex than was previously thought.

## Results

### Functional voltage-gated sodium channels are present in RPE derived from human embryonic stem cells

We used whole-cell recordings from mature hESC-derived RPE in  $\text{K}^+$  free intracellular solution to observe transient inward currents elicited by a series of depolarizing voltage pulses after strong hyperpolarization to  $-170$  mV (Fig. 1c,  $n = 19$ ). These recordings were performed from an intact monolayer (Fig. 1a, results summarized in Fig. 1j) in the presence and absence of a gap-

junction antagonist (18 $\alpha$ -glycyrrhetic acid). Resembling currents, but with only a fraction of the amplitude, were occasionally identified in cells from freshly dissociated mature hESC-derived RPE (Fig. 1b, d,  $n = 6$ ), that is the conventional configuration for RPE patch clamp recordings. The current resembled the  $\text{Na}_v$  current characteristic of excitable cells: it had the typical current–voltage relationship (Fig. 1e) and showed fast activation and inactivation (Fig. 1i). The current was activated at about  $-50$  mV and peaked at about  $-13$  mV with a maximum amplitude of  $330 \pm 50$  pA (mean  $\pm$  SEM,  $n = 19$ ). The average membrane capacitance was  $28 \pm 2$  pF ( $n = 19$ ), and the average current density was  $13 \pm 3$  pA/pF ( $n = 19$ ). The average resting membrane potential, measured in the presence of  $\text{K}^+$ -based intracellular solution was  $-47 \pm 1$  mV (mean  $\pm$  SEM,  $n = 15$ ). The inactivation time constant decayed exponentially with increasing command voltages, while the decay of the activation time constant was more shallow (Fig. 1i). The steady-state inactivation curve was determined by measuring the amplitude of a response to  $-10$  mV test pulse following a series of prepulses (from  $-140$  mV to  $-40$  mV at 10 mV intervals). The normalized current amplitude was plotted against the prepulse voltage and fitted with the Boltzmann equation

$$I/I_{\max}(V) = 1/\{1 + \exp[(V - V_{1/2})/k]\} \quad (1)$$

resulting in the half-inactivation voltage  $V_{1/2} = -94 \pm 1$  mV ( $n = 7$ ) (Fig. 1f). To investigate the time dependency of recovery from inactivation, we used a paired-pulse protocol (Fig. 1g). The current was recorded after a second depolarizing pulse given at increasing time intervals until it finally recovered to its full size. The second peak currents were subsequently normalized to the prepulse peak current and plotted against the time between the two voltage pulses (Fig. 1h). Our data was fitted with an exponential function, and the best fit yielded to  $\tau = 54 \pm 3$  ms ( $n = 5$ ).

The presence of  $\text{Na}_v$  currents was confirmed using the universal extracellular  $\text{Na}_v$  channel blocker TTX. By comparing the responses elicited with a voltage step from  $-170$  to  $-10$  mV, it was evident that addition of  $1 \mu\text{M}$  TTX to the bath reduced the amplitude of the current to roughly one half of that recorded in the control extracellular solution (Fig. 2a, left). Thus, the recorded current was sensitive to TTX but required reasonably high concentrations. Furthermore, the sensitivity to TTX varied between the cells and in some cases even  $10 \mu\text{M}$  TTX was not enough to block the current (Fig. 2a, left). The current was also sensitive to  $2 \text{ mM}$  QX-314, an intracellular  $\text{Na}_v$  channel blocker added to the internal solution of the patch pipette that typically removed the current rapidly after breaking into the whole-cell configuration (Fig. 2a, right).

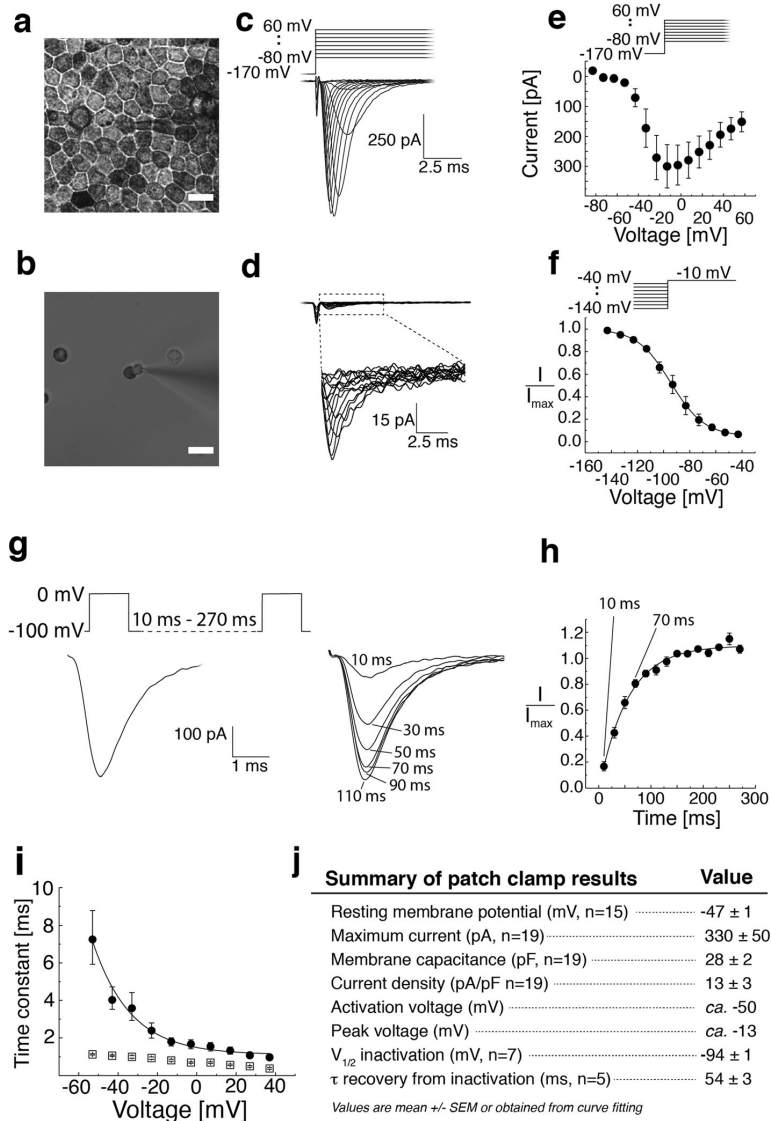


**Fig. 1** Patch clamp recordings of Na<sup>+</sup> currents from hESC-derived RPE. **a, b** Brightfield light microscopy images of hESC-derived RPE cells. **a** Mature hESC-derived RPE grown on insert for 2 months showing strongly pigmented cells and characteristic epithelial morphology. **b** Mature hESC-derived RPE was dissociated yielding single cells with typical morphology showing pigmented apical and non-pigmented basal sides. Scale bars 10 μm. Whole-cell patch clamp recordings as responses to a series of depolarizing voltage pulses (-80 to +60 mV, 10 mV steps) after strong hyperpolarization (-170 mV) either **c** from mature monolayer of hESC-derived RPE or **d** from single hESC-derived RPE cells. Patch clamp pipette is visible in the center of the **a** and **b** images. **e-i** Analysis of the monolayer recordings. **e** The average current-voltage relationship (*I* vs *V<sub>m</sub>*, mean ± SEM, *n* = 12). **f** Steady-state inactivation curve was analyzed by plotting the normalized peak current at -10 mV test pulse against the prepulse voltage (-140 to -40 mV, 10 mV steps) and fitting the data with the Boltzmann equation. The best fit was obtained with *V*<sub>1/2</sub> = -94 ± 1 mV and *k* = 10 (*n* = 7). Data points indicate mean ± SEM. **g, h** The time dependency of recovery from inactivation. The second peak currents were normalized and plotted against the voltage pulse interval (10–270 ms). The best fit to an exponential function was obtained with τ = 54 ± 3 ms (*n* = 5) (individual datapoints for **h** available in Additional file 7: Table S2). **i** The activation (squares) and inactivation (circles) time constants were obtained from single exponential fits to the rising and decaying phases of the current responses shown in **c** and plotted against the command voltage (*n* = 7). **j** Summary of the patch clamp results

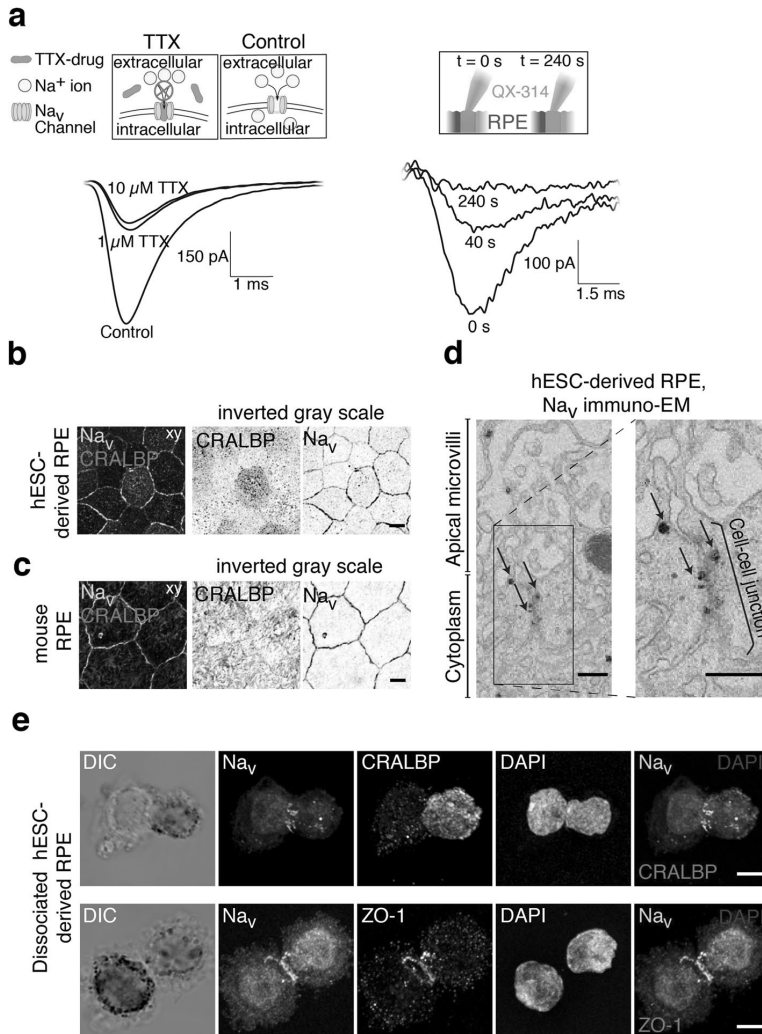


**Fig. 2** Blocker sensitivity and distribution of Na<sub>v</sub> channels. Patch clamp recordings were performed on mature hESC-derived RPE monolayers. **a** Applying TTX extracellularly (either 1 μM or 10 μM) did not entirely block the current (left). The current was completely removed by intracellular QX-314 (2 mM) (right). Laser scanning confocal microscopy (LSCM) images on Na<sub>v</sub> distribution in RPE cells. LSCM data inverted greyscale Z-maximum intensity projections of **b** hESC-derived and **c** mouse RPE stained against Na<sub>v</sub> channels (green) and RPE marker CRALBP (red). Scale bars 10 μm. **d** Immunogold labeling and transmission electron microscopy images showing Na<sub>v</sub> distribution at the apical membrane in the vicinity of the cell-cell junctions (black arrows). Scale bars 250 nm. **e** Dissociated hESC-derived RPE cells were let to adhere to poly-L-lysine coated coverslips for 30 min, fixed and immunolabeled against Na<sub>v</sub> together with CRALBP (up) or tight junction marker ZO-1 (down). The Na<sub>v</sub> label concentrated on the belt-like region in the middle of the cell, between the basal and apical sides. Scale bars 5 μm

**Voltage-gated sodium channels localize near cell-cell junctions in RPE**

Our patch clamp data indicated that functional Na<sub>v</sub> channels are present in the hESC-derived RPE. The cellular localization of the channels was investigated by

performing immunofluorescence studies where the cellular retinaldehyde-binding protein (CRALBP), a marker for RPE cells [16, 17], was labeled together with the universal Na<sub>v</sub> channel marker. These hESC-derived RPE samples were then imaged with a laser scanning confocal



microscope (LSCM) by acquiring 3D image stacks (Fig. 2b), and the data were denoised by deconvolution. This showed that Na<sub>v</sub> channels were present in fully differentiated RPE. Furthermore, the Na<sub>v</sub> label concentrated primarily on the cellular borders with low expression elsewhere on the cell membrane while the CRALBP label was more uniformly localized to the apical side of the hESC-derived RPE (Fig. 2b).

Since the expression of Na<sub>v</sub> channels in RPE has previously been thought to be induced *in vitro* by the cell culturing [18, 19] and since cells derived from ESCs might not fully replicate the pattern of ion channel expression *in vivo* [11, 20, 24–28], we wanted to confirm their presence by using freshly isolated and non-cultured mouse RPE (Fig. 2c). The same labeling showed highly similar distributions in mouse RPE as in hESC-derived RPE: the CRALBP label was cytoplasmic on the apical side of the cells while Na<sub>v</sub> concentrated more on the cellular borders. Furthermore, the immunogold labeling for electron microscopy (immuno-EM) demonstrated the presence of Na<sub>v</sub> channels in the cell–cell junctions (Fig. 2d) and our immunolabeling with the tight junction marker ZO-1 showed highly overlapping distributions, strongly suggesting the primary Na<sub>v</sub> localization near the tight junctions (Additional file 1: Figure S1).

We investigated the mechanism underlying the previously reported lack of Na<sub>v</sub> currents from acutely isolated RPE cells (Fig. 1d). The hESC-derived RPE cells were seeded on glass coverslips for 30 min and immunolabeled with the universal Na<sub>v</sub> marker, CRALBP and ZO-1. Surprisingly, the Na<sub>v</sub> label was primarily concentrated in the narrow region separating the apical and basolateral sides of the cell. Together with ZO-1, Na<sub>v</sub> channels formed a clear ring-like structure between the apical and basal membranes following relaxation of junctional tension (Fig. 2e). Due to this junctional disruption, Na<sub>v</sub> channels might not be accessible to pass ionic currents in acutely dissociated RPE cells.

#### RPE cells express various voltage-gated sodium channel subtypes

Since ten different Na<sub>v</sub> channel subtypes, Na<sub>v</sub>1.1–Na<sub>v</sub>1.9 and Na<sub>x</sub>, have been identified with drastically different expression profiles in diverse cell types, we wanted to investigate which specific channel subtypes are functionally expressed in the RPE cells. At the mRNA level, previous work has detected all of the Na<sub>v</sub> channels in donated human RPE-choroid preparations, specifically Na<sub>v</sub> subtypes 1.2–1.6 and Na<sub>v</sub>1.9 [29, 30]. We performed immunolabeling experiments with mouse and hESC-derived RPE using specific antibodies against channel subtypes Na<sub>v</sub>1.1–Na<sub>v</sub>1.9 (Fig. 3a, b, Additional file 2: Figure S2). Confocal microscopy showed that Na<sub>v</sub>1.4 localizes as beads-on-a-string to the cell–cell junctions

(Fig. 3a, b). Na<sub>v</sub>1.8, on the other hand, localized overall to the apical side of the RPE cells (Fig. 3a, b). These data suggested that especially the Na<sub>v</sub>1.4 and Na<sub>v</sub>1.8 channels, which are usually expressed in skeletal muscle and dorsal root ganglia [31, 32], respectively, are also present in RPE cells. Na<sub>v</sub>1.6 the predominant channel of the adult central nervous system [33] showed a more homogenous labeling pattern in hESC-derived RPE and foci-like pattern in mouse RPE (Fig. 3a, b).

Subtypes Na<sub>v</sub>1.1, Na<sub>v</sub>1.3, Na<sub>v</sub>1.5, Na<sub>v</sub>1.7, and Na<sub>v</sub>1.9 were detected in cell–cell junctions and apical membrane but their labeling was more prominent after fixation with lower concentration of paraformaldehyde (Additional file 2: Figure S2). The subtype Na<sub>v</sub>1.2 was only weakly detected in both hESC-derived and mouse RPE. Additionally, we investigated the changes in channel subtype localization patterns during maturation of hESC-derived RPE (Additional file 3: Figure S3). The immunolabeling experiments indicated that the subtypes Na<sub>v</sub>1.4, Na<sub>v</sub>1.5, and Na<sub>v</sub>1.8 changed from homogeneous cellular distribution to more specific localization either to cell–cell junctions (Na<sub>v</sub>1.4) or to the apical side of the epithelium (Na<sub>v</sub>1.5 and Na<sub>v</sub>1.8) during the first 9 days of maturation.

To further verify the functional expression of the most prominent channel subtypes by electrophysiology, we repeated our patch clamp recordings using highly selective blockers for the channels Na<sub>v</sub>1.4, Na<sub>v</sub>1.6, and Na<sub>v</sub>1.8. The average current–voltage relationship (*I*–*V* curve) was determined from all these recordings (*n* = 7) (Fig. 3c). The current was sensitive to the combination of 30 nM 4,9-anhydro-TTX (Na<sub>v</sub>1.6 blocker), 1 μM A-803467 (Na<sub>v</sub>1.8 blocker), and 600 nM μ-conotoxin GIIB (Na<sub>v</sub>1.4 blocker), and the effect of inhibition was more potent with each added blocker thus confirming the expression and functionality of these channel subtypes in the hESC-derived RPE. However, the effect of inhibition was more significant when the blockers were combined with 10 μM TTX indicating the presence of Na<sub>v</sub> subtypes additional to 1.4, 1.6, and 1.8 (*n* = 11) (Fig. 3d).

Finally, the channel subtype composition was verified by carrying out mass spectrometry (MS) analysis of gel bands obtained from hESC-derived RPE protein lysates that had been tested to show the main Na<sub>v</sub> subtypes by Western blot (Additional file 4: Figure S4). Here, we followed the “two-peptide rule” [34], considering a hit positive if two or more specific peptides were identified. Intriguingly, all of the nine types, except subtype Na<sub>v</sub>1.2, were identified. This analysis thus further confirmed the expression of the three major subtypes (Na<sub>v</sub>1.4, Na<sub>v</sub>1.6, Na<sub>v</sub>1.8) in RPE and was also positive for the Na<sub>x</sub> channel expression (Fig. 3e).

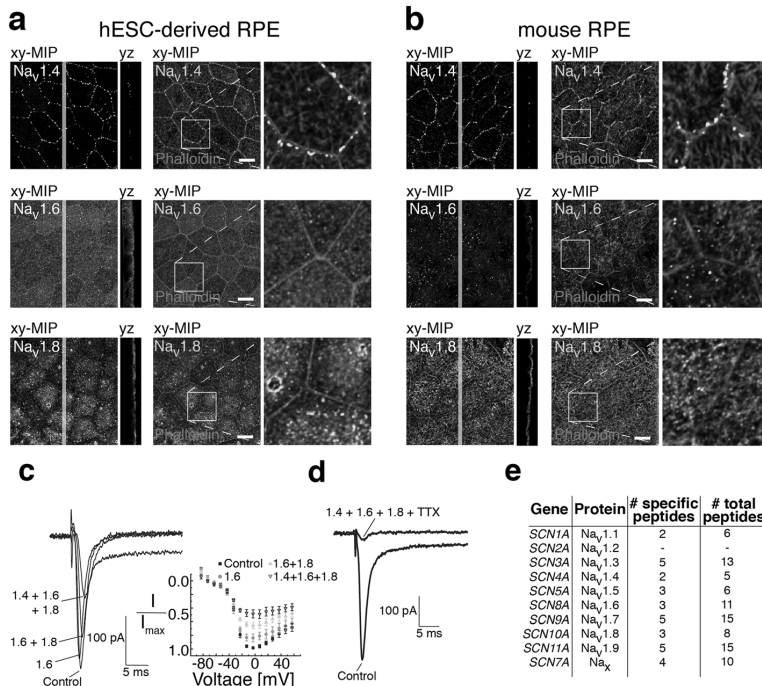


**Fig. 3** Immunolabeling of different Na<sub>v</sub> subtypes in hESC-derived and mouse RPE, mass-spectrometry studies of Na<sub>v</sub> expression, and patch clamp recordings with selective Na<sub>v</sub> blockers. **a, b** The specific pattern of Na<sub>v</sub> subtypes was studied by immunolabeling. Laser scanning confocal microscopy Z-maximum intensity projections (xy-MIP) and yz cross-sections of **a** mature hESC-derived or **b** mouse RPE. Na<sub>v</sub> subtypes 1.4, 1.6, and 1.8 (green) were immunolabeled together with filamentous actin (phalloidin stain, red). Scale bars 10 μm. Right side panels show a higher magnification of the highlighted regions. Patch clamp recordings were performed on mature hESC-derived RPE using selective blockers for channel subtypes. **c** Na<sub>v</sub> subtypes were sequentially blocked by extracellularly applied 4,9-AnhydroTTX (30 nM, Na<sub>v</sub>1.6 blocker), A-803467 (1 μM, Na<sub>v</sub>1.8 blocker) and μ-Conotoxin GIB (600 nM, Na<sub>v</sub>1.4 blocker). The average normalized peak current–voltage relationship ( $I/I_{max}$  vs  $V_m$ ) was determined from all recordings (mean ± SEM, n = 7). **d** Applying the selective blockers in combination with TTX (10 μM) removed most of the Na<sub>v</sub> currents (n = 11). **e** Mass spectrometry analysis of Na<sub>v</sub> channel expression in hESC-derived RPE. Specific peptides were identified for all Na<sub>v</sub> subtypes, excluding Na<sub>v</sub>1.2

**Voltage-gated sodium channels Na<sub>v</sub>1.4 and Na<sub>v</sub>1.8 are involved in POS phagocytosis in RPE**

Our previous experiments showed that several Na<sub>v</sub> subtypes are present in both mouse and mature hESC-derived RPE. However, their physiological relevance remained unknown. Phagocytosis of POS is one of the major roles of RPE [3], and a plausible candidate function for the Na<sub>v</sub> channels, as it requires rapid activation and high synchronization [35]. We therefore next investigated the potential importance of Na<sub>v</sub> channels for POS phagocytosis.

To study their role in the phagocytosis process, we performed immunolabeling experiments with mouse eyes that had been prepared at light onset near the diurnal peak of phagocytosis. The role of the channels in POS uptake was studied by comparing the immunolabeling of the three major subtypes (Na<sub>v</sub>1.4, Na<sub>v</sub>1.6 and Na<sub>v</sub>1.8) and opsins. Interestingly, at light onset, Na<sub>v</sub>1.4 and Na<sub>v</sub>1.8 localized to the bound POS

particles (Fig. 4a). To confirm this redistribution of Na<sub>v</sub> channels, we next performed immuno-EM experiments (Fig. 4b, c), where we labeled the subtypes with gold nanoparticles in hESC-derived RPE. When the cells had not been exposed to POS particles, the localization of both channel subtypes was junction adjacent. This labeling pattern was particularly evident for Na<sub>v</sub>1.4 (Fig. 4b) that formed clusters at the apical part of the cell–cell junctions. After 2 h or 4 h of phagocytosis, however, we could again observe the change in labeling distribution as the channels interacted directly with the phagocytic cups or recently ingested phagosomes (Fig. 4b, c).

The redistribution of Na<sub>v</sub> channels occurring during phagocytosis (Fig. 5a) was studied ex vivo with the channel blockers (Fig. 5b). For this purpose, we developed an assay where freshly opened mouse eyecups were incubated in physiological conditions with blocker solutions for 1 h starting at 15 min prior to light onset. The blocker for

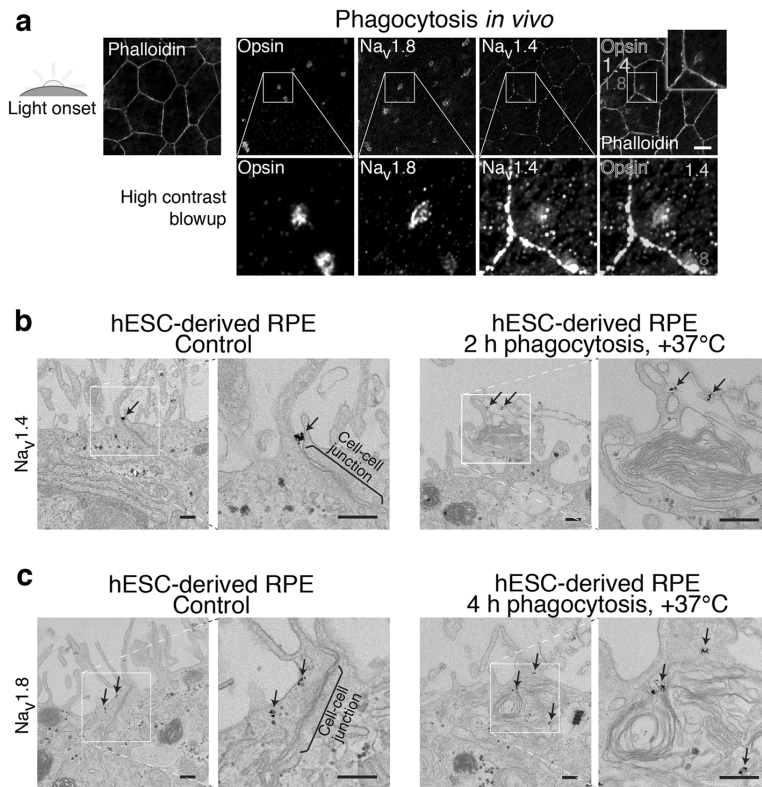


**Fig. 4** POS phagocytosis and the role of Na<sub>v</sub>1.4 and Na<sub>v</sub>1.8. **a** Phagocytosis was studied by dissecting mouse eyes at various time points during the circadian cycle. Filamentous actin was stained with phalloidin (gray in the merged image) to highlight epithelial cell–cell junctions. Laser scanning confocal microscopy Z-maximum intensity projections of mouse RPE prepared at light onset showed localization of opsin labeled POS particles (blue) and Na<sub>v</sub>1.4 (green) together with Na<sub>v</sub>1.8 (red). Lower panels show a high contrast blowup of highlighted regions. Scale bars 10 μm. To study phagocytosis in vitro, mature hESC-derived RPE were labeled with 1.4 nm nanogold-conjugated antibodies against **b** Na<sub>v</sub>1.4 and **c** Na<sub>v</sub>1.8 during phagocytosis of purified porcine POS particles and in control conditions. Without POS exposure, both channels showed localization near the cell-cell junctions (black arrows) but by incubating the monolayers with POS particles for **b** 2 h or **c** 4 h, the localization (black arrows) was also evident around the phagocytic cups and recently ingested phagosomes. Scale bars 250 nm

Na<sub>v</sub>1.4 as well as the combination of all Na<sub>v</sub> blockers significantly prevented the disappearance of Na<sub>v</sub>1.4 from cell–cell junctions when compared to the control (Fig. 5b). The inhibition effect was similarly observed in hESC-derived RPE in vitro when the cells were incubated for 2 h with POS mixed with blocker solutions (Fig. 5c). We did not observe significant differences in the overall labeling pattern of Na<sub>v</sub>1.8 after the blocker incubation. Taken together, these experiments indicate the participation of Na<sub>v</sub> channels in the phagocytic processes of RPE cells in vitro and in vivo.

**Na<sub>v</sub>1.4 knockdown and the inhibition of Na<sub>v</sub> channels significantly reduces the number of ingested POS particles in hESC-derived RPE**

Our LSCM and immuno-EM imaging of POS phagocytosis in RPE indicated a close interaction between Na<sub>v</sub>

channels and phagocytosed POS particles. Therefore, we hypothesized that reducing the Na<sub>v</sub> channel activity could affect the rate of phagocytosis. After observing the dramatic change in the localization of Na<sub>v</sub>1.4, we decided to study its effect further by silencing the channel subtype expression by shRNAs (Fig. 6). Due to the challenges associated with passaging of hESC-derived RPE cells, such as loss of the cobblestone morphology and poor cell proliferation, we opted for the lentivirus shRNA constructs. The transduction of the RPE cells had to be conducted several days after the cell seeding yielding a monolayer with sparse distribution of single GFP-positive cells (Fig. 6e). Since it was not possible to confirm the knockdown efficiency in hESC-derived RPE, the constructs were first validated with ARPE-19 cells (Additional file 5: Figure S5). The cells were transduced

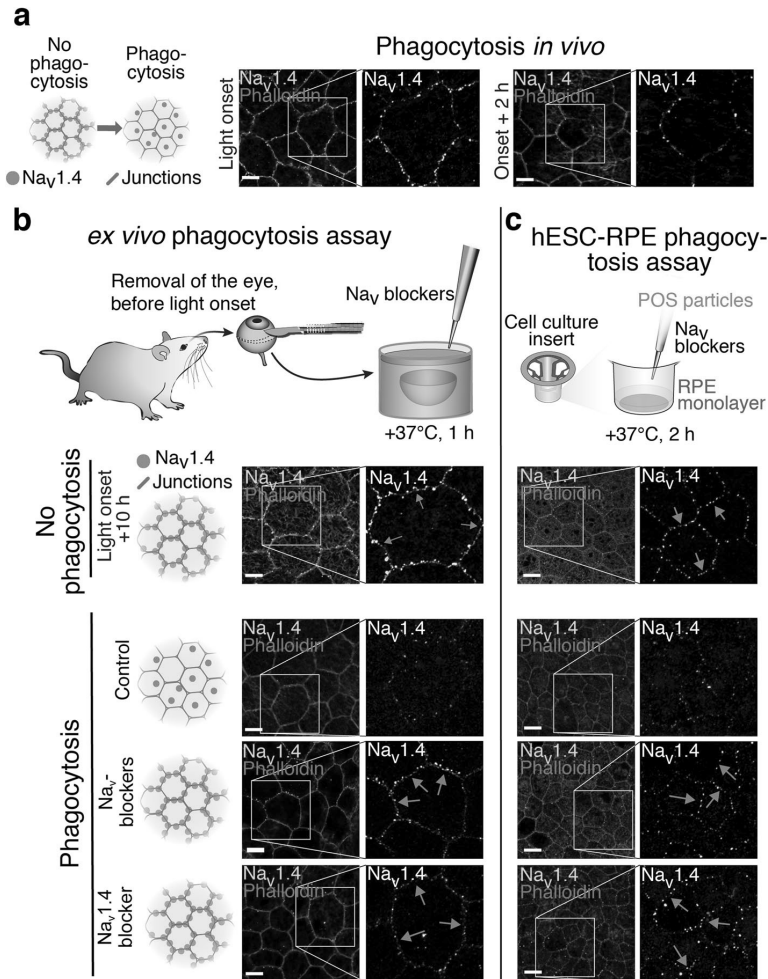


**Fig. 5** Redistribution of Na<sub>v</sub>1.4 during POS phagocytosis. The redistribution of Na<sub>v</sub>1.4 during phagocytosis and the effect of Na<sub>v</sub> blockers to the process was studied in mouse and hESC-derived RPE. Filamentous actin was stained with phalloidin (red) to highlight epithelial cell-cell junctions. Laser scanning confocal microscopy Z-maximum intensity projections of **a** Na<sub>v</sub>1.4 localization in mouse RPE at light onset and 2 h after it showed strong reduction of the beads-on-a-string type labeling from cell-cell junctions. Different assays were used to investigate Na<sub>v</sub>1.4 distribution during phagocytosis and the effect of selective blockers for Na<sub>v</sub>1.4 (600 nM μ-Conotoxin GIIIB) and Na<sub>v</sub>1.8 (1 μM A-803467) in combination with 10 μM TTX, or only of the selective blocker for Na<sub>v</sub>1.4. **b** The redistribution of Na<sub>v</sub>1.4 was studied *ex vivo* by incubating opened mouse eyecups in control solution or with the selective blockers. In both of the blocker samples, the redistribution was inhibited and the beads-on-a-string type labeling remained visible (white arrows) in the cell-cell junctions. **c** The hESC-derived RPE phagocytosis assay *in vitro* showed a highly similar redistribution of Na<sub>v</sub>1.4 and the blockers had the same effect as in the *ex vivo* mouse eyecup assay. Scale bars 10 μm

with the shRNA constructs and collected for Western blot. Next, the knockdown effect of the verified construct was confirmed in hESC-derived RPE by conducting single cell patch clamp recordings and applying μ-conotoxin GIIIB extracellularly (Fig. 6a-d). The cells expressing the target shRNA had both highly reduced Na<sub>v</sub> currents and minimal reactivity to

the blocker (Fig. 6d) when compared to EGFP-expressing (Fig. 6c) or wildtype hESC-derived RPE cells (Fig. 6b). Intriguingly, when the cells were used in the phagocytosis assay (Fig. 6e), the silencing of Na<sub>v</sub>1.4 caused a drastic reduction in the total number of POS particles found in individual GFP-positive cells on the monolayer (Fig. 6f, g).

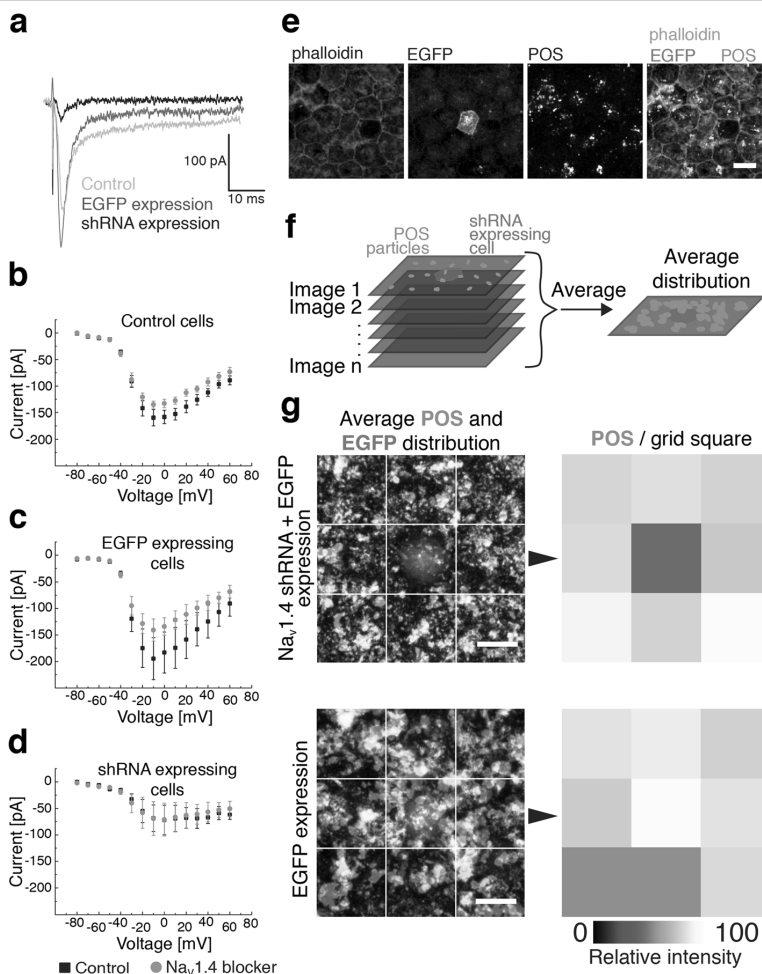


**Fig. 6** POS phagocytosis assay of shRNA Na<sub>v</sub>1.4 silenced hESC-derived RPE. Whole-cell patch clamp recordings were performed on mature hESC-derived RPE monolayers as responses to a series of depolarizing voltage pulses (-80 to +60 mV) after strong hyperpolarization **a** from control RPE cells, control vector cells (EGFP) and cells where Na<sub>v</sub>1.4 had been silenced with lentiviral vectors encoding shRNAs. The average current-voltage relationship (mean ± SEM) was plotted for **b** Control hESC-derived RPE (n = 4), **c** EGFP expressing cells (n = 3), and **d** shRNA expressing cells (n = 3) (individual datapoints for **b-cd** available in Additional file 8: Table S3). **e** The level of POS phagocytosis was analyzed with the EGFP expressing hESC-derived RPE cells. Filamentous actin was stained with phalloidin (blue) to highlight epithelial cell-cell junctions, EGFP (red) was used to identify the transduced cells and POS were labeled with opsin (green). **f** The average distribution of POS particles was analyzed from several images that had a single shRNA expressing cell placed in the middle. **g** The relative intensity of POS labeling in each square of the 3 × 3 grid was analyzed from Na<sub>v</sub>1.4 shRNA cells (n = 22 images) and control EGFP cells (n = 18 images). Scale bars 10 μm

To then study the effect of all Na<sub>v</sub> channels on a larger population of cells, we performed the in vitro phagocytosis assay (Fig. 7a) in the presence of Na<sub>v</sub>1.4 and 1.8 blockers and TTX. The effect was first quantified by counting the number of particles from the immuno-EM images that had been tagged with gold nanoparticle labeled opsin (Fig. 7b). This revealed a drastic reduction in the total number of bound and

internalized POS particles. To better analyze the effect, the assay was carried out by imaging large fields of immunolabeled opsin and ZO-1 and by comparing the number of POS particles in Na<sub>v</sub> blocker and control conditions after 2 h at +37 °C (Fig. 7c). The results showed that the blocker combination caused a 34% (n = 18) reduction in the total number of POS particles labeled with opsin (Fig. 7d).

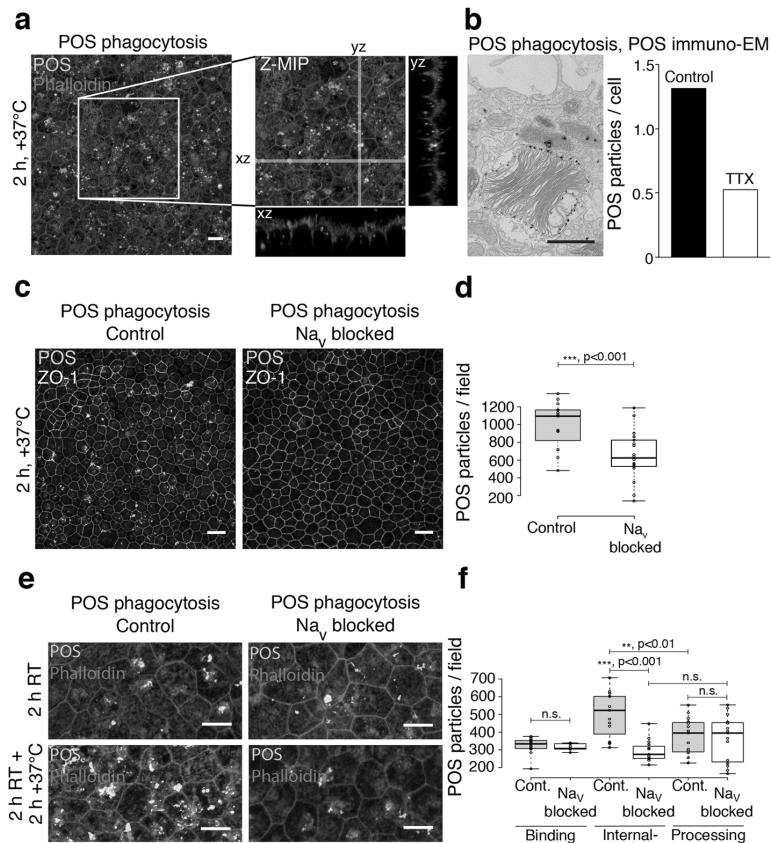


**Fig. 7** POS phagocytosis assay of hESC-derived RPE with selective Na<sub>v</sub> blockers. POS phagocytosis assays were performed on mature hESC-derived RPE by incubating the monolayers with purified porcine POS particles with or without Na<sub>v</sub> blockers (600 nM μ-Conotoxin GIIIB, 1 μM A-803467 and 10 μM TTX). **a** Laser scanning confocal microscopy (LSCM) Z-maximum intensity projections (Z-MIP) and yz and xz cross-sections of the RPE and POS particles (green) with filamentous actin staining (red) after 2 h of phagocytic challenge. Scale bar 10 μm. **b** Quantification of POS particles from TEM images with immunogold labeled opsin showed a 60% decrease of POS particles/cell in the presence of the blockers. Scale bar 250 nm. **c** LSCM Z-MIP images of ZO-1 (gray) together with opsin (green). Scale bars 20 μm. **d** Quantification of control (n = 15) and Na<sub>v</sub> blocker samples (n = 18) during phagocytosis (2 h +37°C) showed a 34% reduction in the total number of POS particles in the presence of Na<sub>v</sub> blockers. **e, f** Na<sub>v</sub> channel role in POS binding, internalization and further processing. **e** LSCM Z-MIP images of phalloidin (red) together with opsin (green) during POS binding and internalization. Scale bars 10 μm. **f** Quantification of the binding phase (2 h RT, Control n = 15, Na<sub>v</sub> blockers n = 10) showed no significant reduction in POS numbers due to Na<sub>v</sub> channel blockers, but a 41% decrease in the internalization phase (2 h RT + 2 h at +37°C, Control n = 15, Na<sub>v</sub> blocker n = 15). In control cells, the POS numbers decreased in the processing phase, but not in the presence of Na<sub>v</sub> channel inhibitors (2 h RT + 5 h at +37°C, 25% decrease, Control n = 15, Na<sub>v</sub> blocker n = 15). Center lines show the medians; box limits indicate the 25th and 75th percentiles as determined by R software and whiskers extend to minimum and maximum values

Next, we wanted to independently quantify the binding and internalization stages of the phagocytosis pathway. The binding was investigated by incubating the POS-supplemented hESC-derived RPE cells at room temperature (RT) [35, 36] with 5% CO<sub>2</sub>. Most of the unbound POS were then removed by gentle washing, and the monolayers were placed in the incubator for either 2 h or 5 h to investigate the internalization stage of

phagocytosis. This was carried out also with the combination of Na<sub>v</sub> blockers and the total number of POS particles was compared to control cells at each timepoint (Fig. 7e, f). The results showed no statistically significant changes (p = 0.1) in the number of POS particles due to the Na<sub>v</sub> inhibition in the particle binding phase (2 h RT, Control n = 15, Na<sub>v</sub> blockers n = 10). However, Na<sub>v</sub> blocking caused a 41% reduction of POS particle

numbers in the internalization phase (2 h RT + 2 h at +37 °C, Control  $n = 15$ , Na<sub>v</sub> blocker  $n = 15$ ) ( $p < 0.001$ ). In control cells, the internalized particles were degraded, which was detected as a 25% reduction in particle numbers in the processing phase (2 h RT + 5 h at +37 °C,  $n = 15$ ,  $p < 0.01$ ) (Fig. 7f). Na<sub>v</sub> blocking substantially reduced further processing of POS particles in RPE cells as there were no significant changes in particle numbers between internalization and processing phases ( $n = 15$ ,  $p = 0.16$ ). Together, our data indicate that functional Na<sub>v</sub> channels directly interact with phagosomes (Fig. 4) and that they are involved in the POS particle internalization and further processing (Fig. 7e, f).

## Discussion

Recent studies show revolution in our understanding of the roles that Na<sub>v</sub> channels have in cellular functions; no longer are these proteins considered important only in “classically” electrically excitable tissues. Here, we provide the first evidence, to our knowledge, that Na<sub>v</sub> channels are expressed in the epithelial cells (Figs. 1, 2, and 3, Additional file 1: Figure S1, Additional file 2: Figure S2) and that their activity co-regulates phagocytosis in RPE. Our observations of Na<sub>v</sub> channels and Na<sub>v</sub>-mediated currents in intact RPE preparations (mature hESC-derived RPE monolayers and freshly isolated mouse RPE) demonstrate that previous observations of Na<sub>v</sub>-mediated currents in cultured RPE cells are not preparation-dependent artifacts [18, 19]. Rather, the absence of Na<sub>v</sub>-mediated currents in acutely isolated RPE cells (Fig. 1d) likely results from the destruction of tight junction complexes during dissociation (Fig. 2e). Internalization of Na<sub>v</sub> channels, of course, would result in diminution or absence of membrane currents mediated by these channels as observed by us (Fig. 1d) and others [18, 19]. Reductions in Na<sub>v</sub> currents have also been reported in dorsal root ganglion neurons following peripheral axotomy [37, 38] but this effect was found to be reversible by exposure to growth factors [37, 38]. The observation of Na<sub>v</sub> currents in recordings from hESC-derived RPE monolayers, we believe, is strong evidence that cells in RPE with intact tight junctions usually express functional Na<sub>v</sub> channels in their plasma membranes.

The properties of Na<sub>v</sub>-mediated currents in hESC-derived RPE cells are consistent with the earlier recordings from other non-neuronal cells [23]. Furthermore, non-excitabile cells have been shown to display varying sensitivity to TTX based on their Na<sub>v</sub> subtype composition [23], and our recordings from RPE align with this observation. The high TTX concentration needed for a full inhibition of the current is supported by the finding that RPE cells were labeled strongly by an anti-Na<sub>v</sub>1.8 antibody; Na<sub>v</sub>1.8 is the least sensitive of Na<sub>v</sub> channels to

TTX [39]. Our pharmacological analysis of Na<sub>v</sub>-mediated currents using Na<sub>v</sub> subtype-specific blockers, immunofluorescence microscopy and MS-based analysis (Fig. 3, Additional file 2: Figure S2) indicated that Na<sub>v</sub>1.1 as well as Na<sub>v</sub>1.3–Na<sub>v</sub>1.9 subtypes are present in the RPE together with the sodium concentration sensitive Na<sub>x</sub> channel [40]. This data was further supported by the Na<sub>v</sub> current characteristics: the relatively slow recovery from inactivation [41, 42] (Fig. 1h) and the large variation visible in the early phase of the recovery, indicate the presence of several different Na<sub>v</sub> subtypes in the RPE. Compared to neurons, other non-excitabile cells, such as non-process bearing astrocytes and supporting cells of the porcine vomeronasal organ [43–45], have been shown to exhibit more negative steady-state half-inactivation voltages, and similar  $V_{1/2}$  values were found for hESC-derived RPE (Fig. 1f). Accordingly, and similarly to astrocytes [46], we never observed spontaneous action potentials in these cells. Earlier recordings from RPE have shown  $V_{1/2}$  values much closer to neurons; however, these results were obtained after only a short period in culture [15, 19]. As our data demonstrates that the Na<sub>v</sub> channel localization and subtype composition is dynamically regulated during development (Additional file 3: Figure S3), we believe that RPE maturation stage including the junctional localization of the channels could greatly influence their electrophysiological properties. This is supported by the previous recordings that identified Na<sub>v</sub> channels in astrocytes in hippocampal slices [46].

For the MS-based identification of Na<sub>v</sub> proteins, we chose to perform the analysis from gel bands [47–49] due to the high sensitivity and possibility for absolute protein identification [48] provided by this approach. However, it was challenging to purify the Na<sub>v</sub> channel proteins from the RPE cells, most probably due to their several transmembrane domains and high hydrophobicity [50]. Therefore, the number of detected Na<sub>v</sub> channel-specific peptides does not necessarily directly correlate to their relative abundance. Na<sub>v</sub>1.4 and Na<sub>v</sub>1.8 of the identified Na<sub>v</sub> subtypes showed the strongest staining in the immunohistochemical analysis and carried over one third of the total current in patch clamp recordings. Therefore, we focused on these two channel subtypes while investigating the physiological roles of Na<sub>v</sub> channels. It is noteworthy, however, that the subtypes Na<sub>v</sub>1.1, Na<sub>v</sub>1.3, Na<sub>v</sub>1.5, and Na<sub>v</sub>1.7 only showed strong junctional labeling after fixation with 1% PFA. Our antibodies labeling these subtypes are directed against different residues of the same intracellular loop between the domains III and IV. Importantly, this region might be sequestered in the dense cell–cell junctions thus hampering their detection through conventional immunocytochemistry [51]. On the other hand, cells

derived from ESCs can bear differences compared to native cells regarding subtype composition. Earlier studies have demonstrated high similarity but also certain deviations in terms of ion channel distribution and biophysical characteristics as well as channel pharmacology and transcriptional profile [11, 20, 24–28].

Previous studies have shown that in macrophages,  $\text{Na}_v$  channels have important roles in phagocytosis [22, 52–54]. We observed an accumulation of  $\text{Na}_v1.4$  and  $\text{Na}_v1.8$  towards POS particles during phagocytosis. The translocation of  $\text{Na}_v1.4$  from tight junctions was still evident 2 h after light onset (Fig. 5a), near the peak expression level of a phagocyte cell surface tyrosine kinase receptor MerTK [55]. The involvement of  $\text{Na}_v1.4$  in phagocytosis was supported by the fact that its silencing decreased the amount of POS particles (Fig. 6). Furthermore, following  $\text{Na}_v$  blocker incubation, we observed a decrease in its translocation (Fig. 5) with a concurrent reduction in the number of POS particles (Fig. 7).  $\text{Na}_v$  channel redistribution has been observed in demyelinated axonal membrane [56] suggesting that these ion channels can display dynamic regulation of distribution and have important implications in various pathologies.

Participation of  $\text{Na}_v$  channel activity to POS phagocytosis was further indicated by their direct association with both the forming phagocytic cups and ingested phagosomes (Fig. 4). Although inhibition of  $\text{Na}_v$  channels did not abolish phagocytosis, the observed 41% attenuation (Fig. 7) was similar to the previously reported effect of TTX in microglia [57]. Our assays suggest that the  $\text{Na}_v$  channels are involved in the engulfment and further processing of the phagosomes, since inhibiting  $\text{Na}_v$  activity did not impair the binding of POS particles (Fig. 7). Interestingly, changes in intracellular free calcium concentration regulate phagocytosis in RPE [58] and, more specifically, particle engulfment in other phagocytes [59].  $\text{Na}_v$  mediated sodium influx could result in increased calcium concentration via reversed functioning of sodium-calcium exchangers expressed in the RPE apical membrane [60, 61] thus affecting phagocytosis. Alternatively,  $\text{Na}_v$  channels could regulate endosomal acidification by providing a sodium efflux pathway to enhance the entry of protons, similarly to macrophages [22, 53]. In these cells, phagocytosis has been associated with membrane potential hyperpolarization due to the activation of a  $\text{Ca}^{2+}$ -dependent  $\text{K}^+$  conductance [62, 63]. Such change in potential could relieve the  $\text{Na}_v$  channel inactivation in the early phase of phagocytosis, and the channels could subsequently be activated in the phagosomes and endosomes with membrane potential in the  $\text{Na}_v$  activation range [64–66]. Furthermore, the channels could be involved directly in the circadian control of the pathway, as has been recently shown for other ion channels [10].

The fact that RPE expresses such a versatile array of  $\text{Na}_v$  channels suggests that besides phagocytosis, these channels also have other roles in the physiology of the RPE. Overall, sodium homeostasis is critical to epithelial transport mechanisms, and our observation of  $\text{Na}_v$  channels, including the non-voltage-gated  $\text{Na}_x$  channel, brings a new piece in the ongoing identification of the sodium conducting proteins in RPE. In excitable cells,  $\text{Na}_v$  and  $\text{Ca}^{2+}$  channels form local signaling complexes that are essential for various intracellular processes [67]. Similar roles for these channels could be possible in RPE as well. Moreover, epithelial cells, including RPE, show strong calcium waves in response to mechanical stimulation [68–70], and it is likely that  $\text{Na}_v$  channels are involved in the process. It is well established that the  $\text{Ca}^{2+}$  binding protein calmodulin (Cam) interacts directly with the C-terminal domain of  $\text{Na}_v$  [71], and it was recently shown that the  $\text{Ca}^{2+}$ -free form of Cam, ApoCam, enhances the  $\text{Na}_v$  channel opening by several-fold [72]. Thus,  $\text{Na}^+$ - and  $\text{Ca}^{2+}$ -dependent signaling pathways can interact in epithelia as has been reported in the case of astrocytes [73]. Lastly, it has been suggested that retinal Müller cells that display similar low  $\text{Na}_v$  channel densities could be activated by the adjacent neurons and it is possible that RPE cells could also serve as voltage sensors reacting to signals arising from photoreceptors [44, 74].

## Conclusion

The results of this study demonstrate that functional  $\text{Na}_v$  channels are present in mouse and hESC-derived RPE cells with intact tight junctions. Specifically, we confirm the presence of  $\text{Na}_v1.1$  as well as  $\text{Na}_v1.3$ – $\text{Na}_v1.9$  subtypes and the sodium concentration sensitive  $\text{Na}_x$  channel, showing that their expression is not due to specific culturing conditions. Our data shows that the most prominent subtypes  $\text{Na}_v1.4$  and  $\text{Na}_v1.8$  are involved in photoreceptor outer segment renewal by directly interacting with phagosomes. Inhibiting the activity of these channels by either pharmacological blockers or shRNA-mediated silencing impairs the phagocytosis process, particularly at the engulfment or further processing stages. Collectively, we demonstrate that  $\text{Na}_v$  channels yield RPE cells the capacity for fast voltage sensitivity and that the channels are a vital part of its physiology.

## Methods

### Antibodies and reagents

Catalog and batch numbers as well as other information for the chemicals and antibodies used in this study can be found from the Additional file 6: Table S1.

### Cell culturing

Human ESC lines Regea08/023 and Regea08/017 were cultured as previously described [11, 75]. Briefly, the



hESC-derived RPE were spontaneously differentiated in floating cell clusters. The pigmented areas were isolated manually and the cells were dissociated with Tryple Select (1X, Thermo Fisher Scientific) and filtered through cell strainer (BD Biosciences, NJ, USA). The isolated cells were then seeded on collagen IV-coated (human placenta, 5 µg/cm<sup>2</sup>; Sigma-Aldrich, MO, USA) 24-well plates (NUNC, Thermo Fisher Scientific, Tokyo, Japan) for enrichment. Subsequently, the pigmented cells were replated for maturation on culture inserts (Millicell Hanging Cell Culture Insert, polyethylene terephthalate, 1.0 µm pore size, EMD Millipore, MA, USA) coated either with Collagen IV (10 µg/cm<sup>2</sup>) or with collagen IV and laminin (1.8 µg/cm<sup>2</sup>, LN521, Biolamina, Sweden). The cells were cultured at +37 °C in 5% CO<sub>2</sub> in culture medium consisting of Knock-Out Dulbecco's modified Eagle's medium (KO-DMEM), 15% Knock-Out serum replacement (KO-SR), 2 mM GlutaMax, 0.1 mM 2-mercaptoethanol (all from Life Technologies, Carlsbad, CA), 1% Minimum Essential Medium nonessential amino acids, and 50 U/mL penicillin/streptomycin (from Cambrex BioScience, Walkersville, MD, USA). The culture medium was replenished three times a week. Mature monolayers typically showed transepithelial resistance values (TER) of over 200 Ω cm<sup>2</sup>.

**Generation of Na<sub>v</sub>1.4 shRNA cultures**

ARPE-19 cells (ATCC, USA) were maintained in DMEM/F12 medium containing 10% FBS, 1% GlutaMAX and 1% penicillin/streptomycin at 37 °C with 5% CO<sub>2</sub>. The medium was changed 3 times a week. The confluent cells were dissociated with trypsin-EDTA (25200-056, Thermo Fisher Scientific) and transfected the following day with shRNA expression vectors containing the reporter vector pLKO.1-CMV-tGFP or pLKO.1-puro-CMV-TurboGFP (Sigma-Aldrich). The expression of shRNA was then investigated by Western blot analysis for Na<sub>v</sub>1.4 for clones TRCN0000416043, TRCN0000425151, and TRCN000044419. This was carried out by comparing the labeling intensity against β-actin that was used as the loading control (*n* = 3). The normalization was carried out by subtracting the background intensity ( $I_{Nav}^{Bgrnd}, I_{Actin}^{Bgrnd}$ ) from the intensity of Na<sub>v</sub> and β-actin bands ( $I_{Nav}^{Band}, I_{Actin}^{Band}$ ). The bands were then normalized to the maximum intensity ( $I_{Nav}^{Max}, I_{Actin}^{Max}$ ), yielding normalized Western blot band intensities between values 0 and 1 as follows:

$$I_{Nav}^{Norm} = \frac{I_{Nav}^{Band} - I_{Nav}^{Bgrnd}}{I_{Nav}^{Max} - I_{Nav}^{Bgrnd}} \text{ and } I_{Actin}^{Norm} = \frac{I_{Actin}^{Band} - I_{Actin}^{Bgrnd}}{I_{Actin}^{Max} - I_{Actin}^{Bgrnd}} \quad (2)$$

These normalized intensities were then used to calculate the relative knockdown as

$$I_{knockdown} = \frac{I_{Nav}^{Norm}}{I_{Actin}^{Norm}} \quad (3)$$

After Western blot analysis, 2 µl of the verified clone TRCN000044419 (8.1 × 10<sup>6</sup> TU/ml) and 8 mg/ml polybrene were added on hESC-derived RPE cells grown on insert. Transduction was made 5–23 days after the cell seeding and virus particles were incubated for 1 day before changing medium. The silencing of Na<sub>v</sub>1.4 current was verified by patch clamp from matured, 8–10 weeks old, hESC-derived RPE cells.

**Sample preparation**

For monolayer patch clamp recordings and immunolabeling, the membrane of the culture insert was removed from the insert holder and cut into smaller pieces. The cells were rinsed three times either with PBS (for immunolabeling) or with Ames' solution (for patch clamp recordings). For the experiments on dissociated cells, the hESC-derived RPE monolayers were treated with TrypLE Select for 10 min in +37 °C, gently mechanically triturated with a pipette and centrifuged for 5 min at 1000 rpm. Dissociated cells were resuspended in culture medium, seeded on glass coverslips coated with poly-L-lysine (Sigma-Aldrich) and allowed to settle down for 10 min for patch clamp recordings and 30 min for immunolabeling.

Mouse RPE was prepared for immunolabeling as follows. C57BL/6 mice were euthanized by CO<sub>2</sub> inhalation and cervical dislocation. The eyes were enucleated and bisected along the equator, and the eyecups were sectioned in Ames' solution buffered with 10 mM HEPES and supplemented with 10 mM NaCl, pH was adjusted to 7.4 with NaOH (Sigma-Aldrich). The retina was gently removed from the eyecup leaving the RPE firmly attached to the eyecup preparation.

**Patch clamp recordings**

Ionic currents were recorded from mature hESC-derived RPE monolayers or freshly dissociated cells using the standard patch clamp technique in whole-cell configuration. Patch pipettes (resistance 5–6 MΩ) were filled with an internal solution containing (in mM) 83 CsCH<sub>3</sub>SO<sub>3</sub>, 25 CsCl, 10 TEA-Cl, 5.5 EGTA, 0.5 CaCl<sub>2</sub>, 4 ATP-Mg, 0.1 GTP-Na, 10 HEPES, and 5 NaCl; pH was adjusted to ~7.2 with CsOH and osmolarity was ~290 mOsm (Gonotec, Osmomat 030, Labo Line Oy, Helsinki, Finland). For the recordings with K<sup>+</sup>-based internal solution, CsCl was replaced with KCl and CsCH<sub>3</sub>SO<sub>3</sub> was replaced with K-gluconate. In some experiments, the internal solution also contained 2 mM QX-314-Cl (from Sigma-Aldrich). During all recordings, the tissue was perfused at 2.5 ml min<sup>-1</sup> with Ames' solution (Sigma-Aldrich) buffered with 10 mM HEPES and supplemented

with 10 mM NaCl and 5 mM TEA-Cl. The pH was adjusted to 7.4 with NaOH and the osmolarity set to ~305 mOsm. The bath solution contained 10 nM–10  $\mu$ M TTX citrate (from Tocris Bioscience) when the effect of TTX on the recorded currents was investigated, and 30  $\mu$ M 18 $\alpha$ -glycyrrhetic acid (from Sigma-Aldrich) when the effect of gap junctional coupling was tested. For the channel subtype recordings, the bath solution was supplemented with 30 nM 4,9-AnhydroTTX, 1  $\mu$ M A-803467, or 600 nM  $\mu$ -Conotoxin GIIB. All recordings were made in voltage clamp mode with pClamp 10.2 software using the Axopatch 200B patch clamp amplifier connected to an acquisition computer via AD/DA Digi-data 1440 (Molecular Devices, USA). The access resistance was below 30 M $\Omega$  and the membrane resistance above 150 M $\Omega$ . Series resistance was 15–30 M $\Omega$  and was not compensated. Holding potentials were corrected for a 3 mV liquid junction potential during the data analysis. All recordings were performed at room temperature.

### Immunolabeling

Prior to immunolabeling, samples were washed three times with PBS and fixed for 15 min with 4% paraformaldehyde or 10 min with 1% paraformaldehyde (pH 7.4; Sigma-Aldrich). After repeated washes with PBS, samples were permeabilized by incubating in 0.1% Triton X-100 in PBS (Sigma-Aldrich) for 15 min and subsequently blocked with 3% BSA (BSA; Sigma-Aldrich) for 1 h. All immunolabeling incubations were done at room temperature.

Primary antibodies against the following proteins were used in this study: cellular retinaldehyde-binding protein (CRALBP) 1:400 (ab15051, Abcam), Na<sub>v</sub>1.1 1:200 (ASC-001, Alomone labs), Na<sub>v</sub>1.2 1:200 (ab99044, Abcam), Na<sub>v</sub>1.3 1:200 (ASC-004, Alomone labs), Na<sub>v</sub>1.4 1:200 (ASC-020, Alomone labs), Na<sub>v</sub>1.5 1:200 (AGP-008, Alomone labs), Na<sub>v</sub>1.6 1:200 (ASC-009, Alomone labs), Na<sub>v</sub>1.7 1:200 (ASC-008, Alomone labs), Na<sub>v</sub>1.8 1:200 (AGP-029, Alomone labs), Na<sub>v</sub>1.9 1:200 (AGP-030, Alomone labs), Pan Na<sub>v</sub> (Na<sub>v</sub>) 1:200 (ASC-003, Alomone labs), and Zonula occludens-1 (ZO-1) 1:50 (33-9100, Life Technologies). All primary antibodies were diluted in 3% BSA in PBS and incubated for 1 h.

The incubation with primary antibodies was followed by three PBS washes and 1 h incubation with secondary antibodies; goat anti-rabbit Alexa Fluor 568 (A-11011), donkey anti-rabbit Alexa Fluor 488 (A-21206), donkey anti-mouse Alexa Fluor 568 (A10037), donkey anti-mouse Alexa Fluor 488 (A-21202), goat anti-guinea pig Alexa Fluor 568 (A-11075), goat anti-mouse Alexa Fluor 488 (A-11029), donkey anti-rabbit Alexa 647 (A-31573), donkey anti-mouse Alexa 647 (A-21236), goat anti-guinea pig Alexa Fluor 647 (A-21450) and goat anti-

mouse Alexa Fluor 405 (A-31553) (all from Molecular Probes, Thermo Fisher Scientific) diluted 1:200 in 3% BSA in PBS. Actin was visualized using either a direct phalloidin Alexa Fluor 647 conjugate 1:50 (A22287, Thermo Fisher Scientific), Atto-633 1:50 (68825, Sigma-Aldrich) or tetramethylrhodamine B conjugate 1:400 (P1951, Sigma-Aldrich) and the nuclei were stained with 4', 6'-diamidino-2-phenylidole (DAPI) included in the ProLong Gold antifade mounting medium (P36935, Thermo Fisher Scientific).

### Pre-embedding immunogold labeling

The hESC-derived RPE monolayers were washed three times with phosphate-buffered saline (PBS) and then fixed for 2 h at RT in periodate-lysine-paraformaldehyde (PLP) fixative. Fixed cells were prepared for pre-embedding EM as described previously [76, 77]. Cells were treated with 0.01% saponin and 0.1% BSA in 0.1 M phosphate buffer, pH 7.4 (Buffer A) before adding the primary antibodies diluted in Buffer A. The concentration of all primary antibodies was doubled for the experiment compared to immunolabeling. After 1 h incubation at RT and washes with Buffer A, 1.4 nm nanogold-conjugated polyclonal Fab' fragment of goat anti-rabbit IgG or of goat anti-mouse IgG (Nanoprobes.com, Yaphank, NY, USA) diluted to 1:50 in Buffer A was applied for 1 h, followed by washes with Buffer A and 0.1 M phosphate buffer (pH 7.4). Cells were post-fixed with 1% glutaraldehyde in phosphate buffer for 10 min at RT, quenched with 50 mM NH<sub>4</sub>Cl in phosphate buffer for 5 min at RT, and then washed with phosphate buffer and water.

The samples were treated in dark with HQ-silver (Nanoprobes.com) for 5 min followed by washes with water and gold toning (2% sodium acetate 3  $\times$  5 min at RT, 0.05% gold chloride 10 min at +4  $^{\circ}$ C, 0.3% sodium thiosulphate 2  $\times$  10 min at +4  $^{\circ}$ C). After washes with water, the cells were reduced in 1% osmium tetroxide in 0.1 M phosphate buffer for 1 h at +4  $^{\circ}$ C and dehydrated with graded series of ethanol (70%, 96%, 100%), then stained with 2% uranyl acetate. Finally, the monolayers were embedded in Epon (TAAB Embedding resin, medium, TAAB Laboratories Equipment Ltd., Berks, UK) and after polymerization, sections perpendicular to the membrane were cut with an ultramicrotome (Leica ultracut UCT ultramicrotome, Leica Mikrosysteme GmbH, Austria). The thin sections (200 nm) were placed on carbon-coated single-slot grids and were imaged with JEOL JEM-1400 transmission electron microscope (JEOL Ltd., Tokyo, Japan) equipped with bottom-mounted Quemesa CCD camera (4008  $\times$  2664 pixels). High voltage of 80 kV was used for imaging.

### Western blotting

The hESC-derived RPE and ARPE-19 protein lysates were obtained by incubating  $1 \times 10^6$  cell pellets in RIPA buffer supplemented with Halt protease inhibitor cocktail (87786, Thermo Fisher Scientific) for 30 min at +4 °C on constant agitation. The lysate was then centrifuged at +4 °C for 20 min at 12,000×g, mixed with Novex sample buffer (NP0007, Thermo Fisher Scientific) and heated at +70 °C for 10 min. The protein lysates were then loaded onto 3–8% NuPage gel (EA0375, Thermo Fisher Scientific) or Bolt™ 4–12% Bis-Tris Plus Gels (NW04120, Thermo Fisher Scientific), fractionated by SDS-PAGE and then either processed for MS analysis or transferred to nitrocellulose membrane via Trans Blot Turbo Transfer system according to the manufacturer's protocols (BioRad).

The resulting blot was blocked with 3% BSA in PBS + 0.1% Tween-20 5 h at RT and then labeled overnight at +4 °C with the primary antibodies against various Na<sub>v</sub> subtypes diluted in blocking solution. The following antibodies were labeled with this protocol: Na<sub>v</sub>1.4 1:500 (PA5-36989, Thermo Fisher Scientific), Na<sub>v</sub>1.5 1:500 (AGP-008, Alomone labs), Na<sub>v</sub>1.6 1:1000 (ASC-009, Alomone labs), and β-actin 1:2000 (ab6276, Abcam). The membranes were subsequently washed three times for 15 min with PBS + 0.1% Tween-20 and incubated with a 1:20,000 dilution of horseradish peroxidase-conjugated goat anti-rabbit IgG (ab6721, Abcam), goat anti-guinea pig IgG (ab6908, Abcam), or anti-mouse IgG (A-21236, Thermo Fisher Scientific) antibodies for 1 h at RT. For Na<sub>v</sub>1.8 1:5000 (ASC-016, Alomone labs), the protocol was modified as follows: blocking was overnight at +4 °C, primary antibody labeling was for 1 h at RT, washing was three times for 10 min with PBS + 0.01% Tween-20 and the secondary antibody was incubated with a 1:3000 dilution for 1 h at RT. After subsequent washes, the membranes were developed with the WesternBright ECL system (K-12045-D20, Advansta) and imaged with ChemiDoc XRS+.

### Sample preparation of mass spectrometry

The SDS-page gels were labeled overnight at RT with coomassie blue dye to identify the bands. Protein bands ranging from 200 to 260 kDa were excised from the gel and destained by submerging the samples in acetonitrile (ACN) and 50 mM triethyl ammonium bicarbonate (TEAB) (1:1) solution for 30 min. Samples were subsequently alkylated and reduced by adding 25 mM tris (2-carboxyethyl) phosphine hydrochloride (TCEP) and 50 mM TEAB (1:1) and set in thermos mixer at +60 °C with interval mixing for 1 h. After supernatant removal, the samples were submerged with 10× Iodine acetamide in 50 mM TEAB for 30 min in dark. Samples were then washed with 50 mM TEAB:ACN 1:1 solution three times

and dried with vacuum concentrator prior to trypsinization (1 μg of trypsin in 50 mM ammonium bicarbonate solution) for 16 h at +37 °C. Obtained peptides were eluted from the gel fragments using 50% ACN, 5% formic acid (FA) solution. Supernatants were again dried using vacuum concentrator, eluted to the analysis buffer (2% Acetonitrile, 0.1% Formic acid), and injected to the NanoLC-MSTOF instrument. All solvents and other materials were purchased from Thermo Fisher Scientific (San Jose, CA, USA) except Trypsin (TPKC treated, Sciex).

### Identification of proteins

Identification of the proteins was done using Protein Pilot® 4.5 (Sciex, Redwood City, USA) and all data dependent analysis (DDA) runs MS/MS spectra were identified against respective Na<sub>v</sub> channel protein data retrieved from UniprotKB/SwissProt library. FDR 1% and 99% peptide confidence level was used in the library creation and only distinctive peptides were used in the identification. Mass accuracy was set to 5 ppm for each peptide.

### NanoLC-MSTOF parameters

Proteins were analyzed by Nano-RPLC-MSTOF instrumentation using Eksigent 425 NanoLC coupled to high-speed TripleTOF™ 5600+ mass spectrometer (Ab Sciex, Concord, Canada). A microcapillary RP-LC column (cHiPLC® ChromXP C18-CL, 3 μm particle size, 120 Å, 75 μm i.d × 15 cm, Eksigent Concord, Canada) was used for LC separation of peptides. Samples were first loaded into trap column (cHiPLC® ChromXP C18-CL, 3 μm particle size, 120 Å, 75 μm i.d × 5 mm) from autosampler and flushed for 10 min at 2 μl/min (2% ACN, 0.1% FA). The flush system was then switched to line with analytical column. The peptide samples were analyzed with 120 min 6 step gradient using eluent A: 0.1% FA in 1% ACN and eluent B: 0.1% FA in ACN (eluent B from 5 to 7% over 2 min; 7 to 24% over 55 min; 24 to 40% over 29 min; 40 to 60% over 6 min; 60 to 90% over 2 min and kept at 90% for 15 min; 90 to 5% over 0.1 min and kept at 5% for 13 min) at 300 nl/min.

The following key parameters were applied for TripleTOF mass spectrometer in shotgun identification analysis: ion spray voltage floating (ISVF) 2300 V, curtain gas (CUR) 30, interface heater temperature (IHT) +125 °C, ion source gas 1 13, declustering potential (DP) 100 V. Methods were run by Analyst TF 1.5 software (Ab Sciex, USA). For IDA parameters, 0.25 s MS survey scan in the mass range 350–1250 m/z was followed by 60 MS/MS scans in the mass range of 100–1500 Da (total cycle time 3.302 s). Switching criteria were set to ions greater than mass to charge ratio (m/z) 350 and smaller than 1250 (m/z) with charge state 2–5 and an

abundance threshold of more than 120 counts. Former target ions were excluded for 12 S. *IDA* rolling collision energy (CE) parameters script was used for automatically controlling CE.

#### Phagocytosis assay for hESC-derived and mouse RPE

The porcine POS particles were isolated and purified as previously described [75, 78]. Briefly, the eyecups obtained from a slaughterhouse were opened and retinas were removed using forceps under dim red light. The retinas were shaken gently in 0.73 M sucrose phosphate buffer and separated after filtering in sucrose gradient using an ultracentrifuge (Optima ultracentrifuge, Beckman Coulter, Inc., Brea, CA) at 112,400 × g for 1 h at +4 °C. The collected POS layer was centrifuged 3000×g for 10 min at +4 °C and stored in 73 mM sucrose phosphate buffer at −80 °C.

The purified POS particles were fed to the hESC-derived RPE cells in a KO-DMEM medium supplemented with 10% fetal bovine serum (FBS) and incubated for either 2 h at RT or 2 h, 4 h or 5 h at +37 °C in 5% CO<sub>2</sub>. In the blocker experiments, selective blockers for Na<sub>v</sub>1.4, Na<sub>v</sub>1.8 and TTX were also added to the medium for the incubation. Then the monolayers were washed twice briefly with PBS and fixed with PFA according to the immunostaining protocol. Phagocytosis was studied *in vivo* by preparing the mouse eyes under dim red light either at light onset or 2 h and 10 h after it. The mice were reared in normal 12-h light/dark cycle. When blockers were used, the eyecup was opened and then incubated in blocker solutions diluted in Ames' as described above, for 1 h at +37 °C with the retina left intact.

#### Quantification of POS particles in hESC-derived RPE

To detect and quantify POS particles, large random fields were imaged from 3 different samples in each condition with Zeiss LSM780 LSCM (the total number of images in each case is included in the figure legends as “n”). The images were first blurred with a Gaussian function after which a Z-maximum intensity projection was binarized using a global threshold. The number of POS particles was then analyzed from the images converted to mask. In the hESC-derived RPE where subtype Na<sub>v</sub>1.4 had been silenced with lentiviral vectors encoding shRNAs, phagocytosis was analyzed by capturing several fields with a GFP-positive cell in the center of the image. The MIP images were then combined and the average distribution of POS particle labeling was compared between control-GFP (EGFP) construct and the clone TRCN000044419. The image was split into a 3 × 3 grid and the relative intensity of POS labeling was analyzed for each individual square of the grid.

#### Statistical analysis of the POS phagocytosis quantification

Each phagocytosis experiment was repeated three times and the images were pooled together. The normality of the data was tested by using Shapiro–Wilk normality test and the differences were first analyzed using ANOVA. Finally, pairwise comparison was conducted by using Kruskal–Wallis test to confirm the possible statistical significance between the experimental conditions.

#### Confocal microscopy and image processing

Confocal microscopy was performed with Zeiss LSM780 LSCM on inverted Zeiss Cell Observer microscope (Zeiss, Jena, Germany) by using Plan-Apochromat 63x/1.4 oil immersion objective. Voxel size was set to  $x = y = 66$  nm and  $z = 200$  nm and 1024 × 1024 pixel stacks of 70–120 slices were acquired with line average of 2. The Alexa Fluor 405 was excited with 405 nm diode laser; Alexa Fluor 488 with 488 nm laserline from Argon laser; Alexa Fluor 568 and TRITC with 561 nm DPSS or 562 nm *InTune* laser; Atto 633 and Alexa Fluor 647 with 633 nm HeNe and with 628 nm *InTune* laser. Emission was detected with windows of (in nm) 410–495 (DAPI, Alexa Fluor 405), 499–579 (Alexa Fluor 488), 579–642 (Alexa Fluor 568), and 642–755 (Alexa Fluor 647). Laser powers were minimized to avoid bleaching and photomultiplier tube sensitivities were adjusted to obtain optimal signal-to-noise ratio of the signal. The data was saved in .czi format and deconvolved using Huygens Essential (SVI, Hilversum, Netherlands) software. The deconvolution was performed with theoretical PSF, signal-to-noise ratio of 5 and quality threshold of 0.01. Information regarding the refractive index of the sample was provided by the manufacturer of the ProLong Gold antifade mounting media. Images were further processed with ImageJ [79] and only linear brightness and contrast adjustments were performed for the pixel intensities. Final figures were assembled using Adobe Photoshop CC (2015.5.1 release) and Illustrator CC (2015.3.1 release) (Adobe Systems, San Jose, USA).

#### Additional files

**Additional file 1: Figure S1.** Immunolabeling of Na<sub>v</sub> in hESC-derived and mouse RPE. Z-maximum intensity projections (Z-MIP) of (a) hESC-derived and (b) mouse RPE stained against Na<sub>v</sub> channels (green) and tight junction marker ZO-1 (red), together with cross-sectional X-MIPs from the highlighted regions. (PNG 729 kb)

**Additional file 2: Figure S2.** Immunolabeling of different Na<sub>v</sub> subtypes in hESC-derived and mouse RPE. Different Na<sub>v</sub> channel subtypes were immunolabeled in (a) mature hESC-derived and (b) mouse RPE that had been fixed with 1% PFA. Laser scanning confocal microscopy Z-maximum intensity projections of Na<sub>v</sub> subtypes (green) labeled together with filamentous actin (phalloidin, red). In both samples, the subtypes Na<sub>v</sub>1.1, Na<sub>v</sub>1.3, Na<sub>v</sub>1.5, Na<sub>v</sub>1.7 and Na<sub>v</sub>1.9 showed labeling in cell-cell junctions and apical membrane. The subtype Na<sub>v</sub>1.2 gave extremely weak signals in both samples. Scale bars 10 μm. (PNG 4721 kb)

**Additional file 3: Figure S3.** Immunolabeling of different Na<sub>v</sub> subtypes during development of hESC-derived RPE. hESC-derived RPE cells were seeded on cell culture inserts and fixed at various timepoints during development. Laser scanning confocal microscopy Z-maximum intensity projections showed that during maturation from 1 d to 9 d after cell seeding, the cellular distribution of subtype Na<sub>v</sub>1.1 stayed homogenous. Contrarily, cellular distribution of subtypes Na<sub>v</sub>1.4 and Na<sub>v</sub>1.5 changed from homogeneous (1 d) to more organized beads (9 d) at the cell-cell junctions (Na<sub>v</sub>1.4) or to bright spots in the cell (Na<sub>v</sub>1.5). The cellular distribution of Na<sub>v</sub>1.8 was initially homogenous but at 9 d, the subtype also showed localization to one or few bright spots in the cells. Scale bars 10 μm. (PNG 1453 kb)

**Additional file 4: Figure S4.** Western blot analysis of different subtypes in hESC-derived RPE. Whole cell lysates of hESC-derived RPE cells were analyzed by electroblotting and the resulting nitrocellulose membranes were stained against the subunits Na<sub>v</sub>1.4-Na<sub>v</sub>1.6 and Na<sub>v</sub>1.8. All subunits showed positive bands between 130 and 250 kDa. The Western blots were used as guides for the gel excision for mass spectrometry analysis. (PNG 83 kb)

**Additional file 5: Figure S5.** Western blot analysis of shRNA knock-down of Na<sub>v</sub>1.4 in ARPE-19 cells. Whole cell lysates of ARPE-19 cells transfected with shRNA expressing EGFP or the lentivirus constructs were analyzed by Western blot. The nitrocellulose membranes were stained against the subunit Na<sub>v</sub>1.4. The staining showed positive bands between 130 and 250 kDa for lysates obtained from EGFP expressing cells as well as cells transfected with shRNA clone 1 (TRCN0000416043) but the labeling intensity was decreased for lysates obtained from cells transfected with the clone 2 (TRCN0000425151) and especially with clone 3 (TRCN0000044419). The labeling band intensity was compared against the β-actin band (between 35 and 55 kDa) that was used as the loading control. Based on the Western blot, the expression of Na<sub>v</sub>1.4 was normalized for EGFP and all shRNA constructs, and we therefore selected clone 3 (TRCN0000044419) for further experiments (Individual datapoints available in Additional file 9: Table S4). (PNG 328 kb)

**Additional file 6: Table S1.** List of chemical and antibody details. (DOCX 46 kb)

**Additional file 7: Table S2.** Individual datapoints for Fig. 1h. (DOCX 55 kb)

**Additional file 8: Table S3.** Individual datapoints for Fig. 6b-d. (DOCX 69 kb)

**Additional file 9: Table S4.** Individual datapoints for Figure S5. (DOCX 37 kb)

#### Acknowledgements

We would like to acknowledge the following contributors. We are grateful to Dr. Jari Hyttinen (Tampere University) for resources and support. We thank Drs. Kristian Donner (University of Helsinki) and Joshua Singer (University of Maryland) for valuable comments on the manuscript. We acknowledge Outi Heikkilä, Outi Melin, Hanna Pekkanen (all from Tampere University), Elina Hurskainen and Salla Mattola (both from University of Jyväskylä) for technical assistance and Dr. Hannele Uusitalo-Järvinen (Tampere University) as well as Dr. Petri Ala-Laurila's Lab (University of Helsinki) for providing the animal tissue. Tampere Facility of Electrophysiological Measurements, Tampere Imaging Facility, Tampere Mass Spectrometry Facility (Tampere University), and Electron Microscopy Unit (University of Helsinki, Institute of Biotechnology) are gratefully acknowledged for their services.

#### Authors' contributions

Conception and design of the study as well as data acquisition, analysis, and interpretation were performed by KJK, VJJ, SH, AJ, TOI, and SN. The expertise on human embryonic stem cells and RPE differentiation was provided by HS, and the expertise on electron microscopy by SH and MV-R. The mass spectrometry expertise was provided by AJ and HU. All authors contributed to the writing of the manuscript with KJK, TOI, and SN who are mainly responsible. All authors read and approved the final manuscript.

#### Funding

This work was supported by the Academy of Finland Grants 287287 (SN), 294054 (SN), 319257 (SN), 267471 (TOI), by Emil Aaltonen Foundation (SN), by

Päivikki and Sakari Sohlberg Foundation (HS), and by Jane and Aatos Erkkö Foundation (MV-R).

#### Availability of data and materials

All data generated or analyzed during this study are included in this published article and its supplementary information files. Patch clamp, confocal imaging, and mass spectrometry datasets are available in the Zenodo repository [80]. Where  $n < 6$ , the individual data values are provided in additional files and cited in the figure legends (Additional file 7: Table S2, Additional file 8: Table S3, Additional file 9: Table S4).

#### Ethics approval and consent to participate

The National Authority for Medicolegal Affairs Finland has approved the study with human embryos (Dnro 1426/32/300/05). The supportive statement from the ethics committee of the Pirkanmaa hospital district Finland allows us to derive and expand hESC-lines from surplus embryos excluded from infertility treatments, and to use the lines for research purposes (R05116). New cell lines were not derived in this study. In mouse studies, all animals were treated in accordance with the ARVO Statement for the Use of Animals in Ophthalmic and Vision Research using protocols approved and monitored by the Animal Experiment Board of Finland.

#### Consent for publication

Not applicable.

#### Competing interests

The authors declare that they have no competing interests.

#### Author details

<sup>1</sup>BioMediTech, Faculty of Medicine and Health Technology, Tampere University, Tampere, Finland. <sup>2</sup>Department of Biological and Environmental Science and Nanoscience Center, University of Jyväskylä, Jyväskylä, Finland. <sup>3</sup>Tays Eye Centre, Tampere University Hospital, Tampere, Finland.

Received: 25 March 2019 Accepted: 11 July 2019

Published online: 15 August 2019

#### References

- Bok D. The retinal pigment epithelium: a versatile partner in vision. *J Cell Sci Suppl.* 1993;17:189–95 <http://www.ncbi.nlm.nih.gov/pubmed/8144697>. Accessed 29 Aug 2016.
- Steinberg RH. Interactions between the retinal pigment epithelium and the neural retina. *Doc Ophthalmol.* 1985;60:327–46 <http://www.ncbi.nlm.nih.gov/pubmed/3905312>. Accessed 29 Aug 2016.
- Strauss O. The retinal pigment epithelium in visual function. *Physiol Rev.* 2005;85:845–81. <https://doi.org/10.1152/physrev.00021.2004>.
- Takei Y, Ozanics V. Origin and development of Bruch's membrane in monkey fetuses: an electron microscopic study. *Investig Ophthalmol.* 1975; 14:903–16 <http://www.ncbi.nlm.nih.gov/pubmed/811582>. Accessed 1 Sep 2016.
- Wimmers S, Karl MO, Strauss O. Ion channels in the RPE. *Prog Retin Eye Res.* 2007;26:263–301. <https://doi.org/10.1016/j.preteyeres.2006.12.002>.
- Young RW, Bok D. Participation of the retinal pigment epithelium in the rod outer segment renewal process. *J Cell Biol.* 1969;42:392–403.
- Young RW. The daily rhythm of shedding and degradation of rod and cone outer segment membranes in the chick retina. *Invest Ophthalmol Vis Sci.* 1978;17:1105–16 <http://www.ncbi.nlm.nih.gov/pubmed/624604>. Accessed 19 Feb 2017.
- LaVail MM. Circadian nature of rod outer segment disc shedding in the rat. *Invest Ophthalmol Vis Sci.* 1980;19:407–11. <http://www.ncbi.nlm.nih.gov/pubmed/7358492>. Accessed 19 Feb 2017.
- Kevany BM, Palczewski K. Phagocytosis of retinal rod and cone photoreceptors. *Physiology (Bethesda).* 2010;25(1):8–15. <https://doi.org/10.1152/physiol.00038.2009>.
- Müller C, Gómez NM, Ruth P, Strauß O. Ca<sub>v</sub>1.3 L-type channels, maxiK Ca (2+)-dependent K(+) channels and bestrophin-1 regulate rhythmic photoreceptor outer segment phagocytosis by retinal pigment epithelial cells. *Cell Signal.* 2014;26:968–78.
- Korkka I, Viheriälä T, Juuti-Uusitalo K, Uusitalo-Järvinen H, Skottman H, Hyttinen J, et al. Functional voltage-gated calcium channels are present in

- human embryonic stem cell-derived retinal pigment epithelium. *Stem Cells Transl Med.* 2019;8(2):179–93. <https://doi.org/10.1002/sctm.18-0026>.
12. Karl MQ, Kroeger W, Wimmers S, Milenkovic VM, Valtink M, Engelmann K, et al. Endogenous Gas6 and Ca<sup>2+</sup>-channel activation modulate phagocytosis by retinal pigment epithelium. *Cell Signal.* 2008;20:1159–68. <https://doi.org/10.1016/j.cellsig.2008.02.005>.
  13. Fox JA, Pfeffer BA, Fain GL. Single-channel recordings from cultured human retinal pigment epithelial cells. *J Gen Physiol.* 1988;91:193–222 <https://www.ncbi.nlm.nih.gov/pmc/articles/PMC2216133/>. Accessed 23 Jan 2016.
  14. Kokkinaki M, Sahibzada N, Golestaneh N. Human induced pluripotent stem-derived retinal pigment epithelium (RPE) cells exhibition transport, membrane potential, polarized vascular endothelial growth factor secretion, and gene expression pattern similar to native RPE. *Stem Cells.* 2011;29:825–35. <https://doi.org/10.1002/stem.635>.
  15. Sakai H, Saito T. Na<sup>+</sup> and Ca<sup>2+</sup> channel expression in cultured newt retinal pigment epithelial cells: comparison with neuronal types of ion channels. *J Neurobiol.* 1997;32:377–90 <http://www.ncbi.nlm.nih.gov/pubmed/9087890>. Accessed 19 Feb 2017.
  16. Bunt-Milam AH, Saari JC. Immunocytochemical localization of two retinoid-binding proteins in vertebrate retina. *J Cell Biol.* 1983;97:703–12 <http://www.ncbi.nlm.nih.gov/pubmed/6350319>. Accessed 26 Aug 2016.
  17. Crabb JW, Carlson A, Chen Y, Goldflam S, Intres R, West KA, et al. Structural and functional characterization of recombinant human cellular retinaldehyde-binding protein. *Protein Sci.* 1998;7(3):746–57. <https://www.ncbi.nlm.nih.gov/pmc/articles/PMC2143945/>.
  18. Botchkin LM, Matthews G. Voltage-dependent sodium channels develop in rat retinal pigment epithelium cells in culture. *Proc Natl Acad Sci U S A.* 1994;91:4564–8 <https://www.ncbi.nlm.nih.gov/pmc/articles/PMC43826/>. Accessed 23 Jan 2016.
  19. Wen R, Lui GM, Steinberg RH. Expression of a tetrodotoxin-sensitive Na<sup>+</sup> current in cultured human retinal pigment epithelial cells. *J Physiol.* 1994; 476:187–96. <https://doi.org/10.1113/jphysiol.1994.sp020122>.
  20. Reichhart N, Strauß O. Ion channels and transporters of the retinal pigment epithelium. *Exp Eye Res.* 2014;126:27–37.
  21. Miyagishima KJ, Wan Q, Corneo B, Sharma R, Lotfi MR, Boles NC, et al. In pursuit of authenticity: induced pluripotent stem cell-derived retinal pigment epithelium for clinical applications. *Stem Cells Transl Med.* 2016;5: 1562–74. <https://doi.org/10.5966/sctm.2016-0037>.
  22. Carrithers LM, Hulseberg P, Sandor M, Carrithers MD. The human macrophage sodium channel NaV1.5 regulates mycobacteria processing through organelle polarization and localized calcium oscillations. *FEMS Immunol Med Microbiol.* 2011;63:319–27. <https://doi.org/10.1111/j.1574-695X.2011.00853.x>.
  23. Black JA, Waxman SG. Noncanonical roles of voltage-gated sodium channels. *Neuron.* 2013;80:280–91. <https://doi.org/10.1016/j.neuron.2013.09.012>.
  24. Sachinidis A, Fleischmann BK, Kolossov E, Wartenberg M, Sauer H, Hescheler J. Cardiac specific differentiation of mouse embryonic stem cells. *Cardiovasc Res.* 2003;58:278–91. [https://doi.org/10.1016/S0008-6363\(03\)00248-7](https://doi.org/10.1016/S0008-6363(03)00248-7). Accessed 5 Mar 2019.
  25. Wang K, Terrenoire C, Sampson KJ, Iyer V, Osteen JD, Lu J, et al. Biophysical properties of slow potassium channels in human embryonic stem cell derived cardiomyocytes implicate subunit stoichiometry. *J Physiol.* 2011; 589(Pt 24):6093–104. <https://doi.org/10.1113/jphysiol.2011.220863>.
  26. Synnergren J, Améen C, Jansson A, Sartipy P. Global transcriptional profiling reveals similarities and differences between human stem cell-derived cardiomyocyte clusters and heart tissue. *Physiol Genomics.* 2012;44:245–58. <https://doi.org/10.1152/physiolgenomics.00118.2011>.
  27. Kang J, Chen X-L, Ji J, Lei Q, Rampe D. Ca<sup>2+</sup> channel activators reveal differential L-type Ca<sup>2+</sup> channel pharmacology between native and stem cell-derived cardiomyocytes. *J Pharmacol Exp Ther.* 2012;341:510–7. <https://doi.org/10.1124/jpet.112.192609>.
  28. Hescheler J, Fleischmann BK, Lentini S, Maltsev VA, Rohwedel J, Wobus AM, et al. Embryonic stem cells: a model to study structural and functional properties in cardiomyogenesis. *Cardiovasc Res.* 1997;36:149–62. [https://doi.org/10.1016/S0008-6363\(97\)00193-4](https://doi.org/10.1016/S0008-6363(97)00193-4). Accessed 5 Mar 2019.
  29. Boojij JC, ten Brink JB, Swagemakers SMA, Verkerk AJMH, Essing AHW, van der Spek PJ, et al. A new strategy to identify and annotate human RPE-specific gene expression. *PLoS One.* 2010;5:e9341. <https://doi.org/10.1371/journal.pone.0009341>.
  30. Whitmore SS, Wagner AH, DeLuca AP, Drack AV, Stone EM, Tucker BA, et al. Transcriptomic analysis across nasal, temporal, and macular regions of human neural retina and RPE/choroid by RNA-Seq. *Exp Eye Res.* 2014;129: 93–106. <https://doi.org/10.1016/j.exer.2014.11.001>.
  31. Bao L. Trafficking regulates the subcellular distribution of voltage-gated sodium channels in primary sensory neurons. *Mol Pain.* 2015;11:61. <https://www.ncbi.nlm.nih.gov/pmc/articles/PMC4590712/>.
  32. Ptáček LJ, George AL, Griggs RC, Tawil R, Kallen RG, Barchi RL, et al. Identification of a mutation in the gene causing hyperkalemic periodic paralysis. *Cell.* 1991;67:1021–7. [https://doi.org/10.1016/0092-8674\(91\)90374-8](https://doi.org/10.1016/0092-8674(91)90374-8).
  33. Goldin AL. Diversity of mammalian voltage-gated sodium channels. *Ann N Y Acad Sci.* 1999;868(1):38–50. <https://doi.org/10.1111/j.1749-6632.1999.tb11272.x>.
  34. Carr S, Aebersold R, Baldwin M, Burlingame A, Clauser K, Nesvizhskii A, et al. The need for guidelines in publication of peptide and protein identification data. *Mol Cell Proteomics.* 2004;3:531–3. <https://doi.org/10.1074/mcp.T400006-MCP200>.
  35. Mazzoni F, Safa H, Finnemann SC. Understanding photoreceptor outer segment phagocytosis: use and utility of RPE cells in culture. *Exp Eye Res.* 2014;126:51–60. <https://doi.org/10.1016/j.exer.2014.01.010>.
  36. Mayerson PL, Hall MO. Rat retinal pigment epithelial cells show specificity of phagocytosis in vitro. *J Cell Biol.* 1986;103:299–308 <http://www.ncbi.nlm.nih.gov/pubmed/3522605>. Accessed 15 Jun 2018.
  37. Cummins TR, Black JA, Dib-Hajj SD, Waxman SG. Glial-derived neurotrophic factor upregulates expression of functional SNS and Na<sup>v</sup> sodium channels and their currents in axotomized dorsal root ganglion neurons. *J Neurosci.* 2000;20:8754–61 <http://www.ncbi.nlm.nih.gov/pubmed/11102483>. Accessed 26 Feb 2019.
  38. Black JA, Langworthy K, Hinson AW, Dib-Hajj SD, Waxman SG. NGF has opposing effects on Na<sup>+</sup> channel III and SNS gene expression in spinal sensory neurons. *Neuroreport.* 1997;8:2331–5 <http://www.ncbi.nlm.nih.gov/pubmed/9243635>. Accessed 26 Feb 2019.
  39. Catterall WA, Goldin AL, Waxman SG. International Union of Pharmacology. International Union of Pharmacology. XXXIX. Compendium of voltage-gated ion channels: sodium channels. *Pharmacol Rev.* 2003;55:575–8. <https://doi.org/10.1124/pr.55.4.7>.
  40. Noda M, Hiyama TY. The Na<sup>+</sup> channel. *Neurosci.* 2015;21:399–412. <https://doi.org/10.1177/1073858414541009>.
  41. Herzog RI, Cummins TR, Ghassemi F, Dib-Hajj SD, Waxman SG. Distinct repriming and closed-state inactivation kinetics of Nav1.6 and Nav1.7 sodium channels in mouse spinal sensory neurons. *J Physiol.* 2003;551:741–50. <https://doi.org/10.1113/jphysiol.2003.047357>.
  42. Cummins TR, Aglieco F, Renganathan M, Herzog RI, Dib-Hajj SD, Waxman SG. Nav1.3 sodium channels: rapid repriming and slow closed-state inactivation display quantitative differences after expression in a mammalian cell line and in spinal sensory neurons. *J Neurosci.* 2001;21: 5952–61. <https://doi.org/10.1523/JNEUROSCI.121-16-05952.2001>.
  43. Ishida T, Takei R, Gautam SH, Otsuguro K, Ohta T, Ito S, et al. Voltage-gated channel properties of epithelial cells in porcine vomeronasal organ. *Neurosci Lett.* 2008;441:277–81. <https://doi.org/10.1016/j.neulet.2008.06.045>.
  44. Sontheimer H, Black JA, Waxman SG. Voltage-gated Na<sup>+</sup> channels in glia: properties and possible functions. *Trends Neurosci.* 1996;19:325–31 <http://www.ncbi.nlm.nih.gov/pubmed/8843601>. Accessed 14 Mar 2019.
  45. Sontheimer H, Waxman SG. Ion channels in spinal cord astrocytes in vitro. II. Biophysical and pharmacological analysis of two Na<sup>+</sup> current types. *J Neurophysiol.* 1992;68:1001–11. <https://doi.org/10.1152/jn.1992.68.4.1001>.
  46. Sontheimer H, Waxman SG. Expression of voltage-activated ion channels by astrocytes and oligodendrocytes in the hippocampal slice. 1993. <https://doi.org/10.1152/jn.1993.70.5.1863>.
  47. Aebersold R, Mann M. Mass spectrometry-based proteomics. *Nature.* 2003; 422:198–207. <https://doi.org/10.1038/nature01511>.
  48. Shevchenko A, Loboda A, Ens W, Schraven B, Standing KG, Shevchenko A. Archived polyacrylamide gels as a resource for proteome characterization by mass spectrometry. *Electrophoresis.* 2001;22:1194–203. [https://doi.org/10.1002/1522-2683\(02\)6<1194::AID-ELPS1194>3.0.CO;2-A](https://doi.org/10.1002/1522-2683(02)6<1194::AID-ELPS1194>3.0.CO;2-A).
  49. Havlis J, Shevchenko A. Absolute quantification of proteins in solutions and in polyacrylamide gels by mass spectrometry. *Anal Chem.* 2004;76:3029–36. <https://doi.org/10.1021/ac035286f>.
  50. Wilkinson TC, Gardener MJ, Williams WA. Discovery of functional antibodies targeting ion channels. *J Biomol Screen.* 2015;20:454–67. <https://doi.org/10.1177/1087057114560698>.
  51. Konno K, Watanabe M. Immunohistochemistry for Ion Channels and Their Interacting Molecules: Tips for Improving Antibody Accessibility.

- New York: Humana Press; 2016. p. 171–8. [https://doi.org/10.1007/978-1-4939-3064-7\\_13](https://doi.org/10.1007/978-1-4939-3064-7_13).
52. Craner MJ, Damarjian TG, Liu S, Hains BC, Lo AC, Black JA, et al. Sodium channels contribute to microglia/macrophage activation and function in EAE and MS. *Glia*. 2005;49:220–9. <https://doi.org/10.1002/glia.20112>.
  53. Carrithers MD, Dib-Hajj S, Carrithers LM, Tokmoulina G, Pypaert M, Jonas EA, et al. Expression of the voltage-gated sodium channel NaV1.5 in the macrophage late endosome regulates endosomal acidification. *J Immunol*. 2007;178:7822–32. <http://www.ncbi.nlm.nih.gov/pubmed/17548620>. Accessed 11 Mar 2019.
  54. Carrithers MD, Chatterjee G, Carrithers LM, Offoha R, Iheagwara U, Rahner C, et al. Regulation of podosome formation in macrophages by a splice variant of the sodium channel SCN8A. *J Biol Chem*. 2009;284:8114–26. <https://doi.org/10.1074/jbc.M801892200>.
  55. Nandrot EF, Kim Y, Brodie SE, Huang X, Sheppard D, Finnemann SC. Loss of synchronized retinal phagocytosis and age-related blindness in mice lacking alphavbeta5 integrin. *J Exp Med*. 2004;200:1539–45. <https://doi.org/10.1084/jem.20041447>.
  56. Craner MJ, Lo AC, Black JA, Waxman SG. Abnormal sodium channel distribution in optic nerve axons in a model of inflammatory demyelination. *Brain*. 2003;126:1552–61. <https://doi.org/10.1093/brain/awg153>.
  57. Black JA, Liu S, Waxman SG. Sodium channel activity modulates multiple functions in microglia. *Glia*. 2009;57:1072–81. <https://doi.org/10.1002/glia.20830>.
  58. Karl M, Kroeger W, Wimmers S, Milenkovic V, Valtink M, Engelmann K, Strauss O. Endogenous Gas6 and Ca2+-channel activation modulate phagocytosis by retinal pigment epithelium. *Cellular Signalling*. 2008;20(6):1159–68. <https://doi.org/10.1016/j.cellsig.2008.02.005>.
  59. Gronski MA, Kinchen JM, Juncadella JJ, Franc NC, Ravichandran KS. An essential role for calcium flux in phagocytes for apoptotic cell engulfment and the anti-inflammatory response. *Cell Death Differ*. 2009;16:1323–31. <https://doi.org/10.1038/cdd.2009.55>.
  60. Mangini NJ, Haugh-Scheidt L, Valle JE, Cragoe EJ, Ripps H, Kennedy BG. Sodium-calcium exchanger in cultured human retinal pigment epithelium. *Exp Eye Res*. 1997;65:821–34. <http://www.ncbi.nlm.nih.gov/pubmed/9441706>. Accessed 20 Jun 2018.
  61. Fijisawa K, Ye J, Zadunaisky JA. A Na<sup>+</sup>/Ca<sup>2+</sup> exchange mechanism in apical membrane vesicles of the retinal pigment epithelium. *Curr Eye Res*. 1993;12:261–70. <http://www.ncbi.nlm.nih.gov/pubmed/8482115>. Accessed 20 Jun 2018.
  62. Araujo EG, Persechini PM, Oliveira-Castro GM. Electrophysiology of phagocytic membranes. Role of divalent cations in membrane hyperpolarizations of macrophage polykaryons. *Biochim Biophys Acta Biomembr*. 1986;856:362–72. [https://doi.org/10.1016/0005-2736\(86\)90047-7](https://doi.org/10.1016/0005-2736(86)90047-7).
  63. Ince C, Coremans JM, Ypey DL, Leijh PC, Verveen AA, van Furth R. Phagocytosis by human macrophages is accompanied by changes in ionic channel currents. *J Cell Biol*. 1988;106:1873–8. <https://doi.org/10.1083/JCB.106.6.1873>.
  64. Marshansky V, Futai M. The V-type H<sup>+</sup>-ATPase in vesicular trafficking: targeting, regulation and function. *Curr Opin Cell Biol*. 2008;20:415–26. <https://doi.org/10.1016/j.cceb.2008.03.015>.
  65. Steinberg BE, Touret N, Vargas-Caballero M, Grinstein S. In situ measurement of the electrical potential across the phagosomal membrane using FRET and its contribution to the proton-motive force. *Proc Natl Acad Sci*. 2007;104:9523–8. <https://doi.org/10.1073/pnas.0700783104>.
  66. Xu H, Ren D. Lysosomal physiology. *Annu Rev Physiol*. 2015;77:57–80. <https://doi.org/10.1146/annurev-physiol-021014-071649>.
  67. Catterall WA. Signaling complexes of voltage-gated sodium and calcium channels. *Neurosci Lett*. 2010;486:107–16. <https://doi.org/10.1016/j.neulet.2010.08.085>.
  68. Abu Khamidakh AE, Juuti-Uusitalo K, Larsson K, Skottman H, Hyytinen J. Intercellular Ca<sup>2+</sup> wave propagation in human retinal pigment epithelium cells induced by mechanical stimulation. *Exp Eye Res*. 2013;108:129–39. <https://doi.org/10.1016/j.exer.2013.01.009>.
  69. Churchill GC, Atkinson MM, Louis CF. Mechanical stimulation initiates cell-to-cell calcium signaling in ovine lens epithelial cells. *J Cell Sci*. 1996;355–65. <http://www.ncbi.nlm.nih.gov/pubmed/8838659>. Accessed 19 Feb 2017.
  70. Stalmans P, Himpens B. A decreased Ca<sup>2+</sup>-wave propagation is found among cultured RPE cells from dystrophic RCS rats. *Invest Ophthalmol Vis Sci*. 1998;39:1493–502. <http://www.ncbi.nlm.nih.gov/pubmed/9660499>. Accessed 19 Feb 2017.
  71. Wang C, Chung BC, Yan H, Wang H-G, Lee S-Y, Pitt GS. Structural analyses of Ca<sup>2+</sup>/CaM interaction with NaV channel C-termini reveal mechanisms of calcium-dependent regulation. *Nat Commun*. 2014;5:4896. <https://doi.org/10.1038/ncomms5896>.
  72. Adams PJ, Ben-Johny M, Dick IE, Inoue T, Yue DT. Apocalmodulin itself promotes ion channel opening and Ca<sup>2+</sup> regulation. *Cell*. 2014;159:608–22. <https://doi.org/10.1016/j.cell.2014.09.047>.
  73. Langer J, Stephan J, Theis M, Rose CR. Gap junctions mediate intercellular spread of sodium between hippocampal astrocytes in situ. *Glia*. 2012;60:239–52. <https://doi.org/10.1002/glia.21259>.
  74. Chao TI, Skachkov SN, Eberhardt W, Reichenbach A. Na<sup>+</sup> channels of Müller (glial) cells isolated from retinae of various mammalian species including man. *Glia*. 1994;10:173–85. <https://doi.org/10.1002/glia.440100304>.
  75. Vaajasaari H, Ilmarinen T, Juuti-Uusitalo K, Rajala K, Onnela N, Narkkilahti S, et al. Toward the defined and xeno-free differentiation of functional human pluripotent stem cell-derived retinal pigment epithelial cells. *Mol Vis*. 2011;17:558–75. <http://www.ncbi.nlm.nih.gov/pubmed/21364903>. Accessed 29 Aug 2016.
  76. Pohl K, Stierhof Y-D. Action of gold chloride (“gold toning”) on silver-enhanced 1 nm gold markers. *Microsc Res Tech*. 1998;42:59–65. [https://doi.org/10.1002/\(SICI\)1097-0029\(19980701\)42:1<59::AID-JEMT7>3.0.CO;2-M](https://doi.org/10.1002/(SICI)1097-0029(19980701)42:1<59::AID-JEMT7>3.0.CO;2-M).
  77. Sawada H, Esaki M. A practical technique to postfix nanogold-immunolabeled specimens with osmium and to embed them in Epon for electron microscopy. *J Histochem Cytochem*. 2000;48:493–8. <https://doi.org/10.1177/002215540004800407>.
  78. Mao Y, Finnemann SC. Analysis of photoreceptor outer segment phagocytosis by RPE cells in culture. *Methods Mol Biol*. 2013;935:285–95. [https://doi.org/10.1007/978-1-62703-080-9\\_20](https://doi.org/10.1007/978-1-62703-080-9_20).
  79. Schneider CA, Rasband WS, Eliceiri KW. NIH image to ImageJ: 25 years of image analysis. *Nat Methods*. 2012;9:671–5. <https://doi.org/10.1038/nmeth.2089>.
  80. Johansson JK, Karema-Jokinen V, Hakanen S, Jylha A, Uusitalo H, Vihinen-Ranta M, et al. Sodium channels enable fast electrical signaling and regulate phagocytosis in the retinal pigment epithelium. 2019. <https://doi.org/10.5281/ZENODO.3270652>. Accessed 09 July 2019.

## Publisher's Note

Springer Nature remains neutral with regard to jurisdictional claims in published maps and institutional affiliations.

Ready to submit your research? Choose BMC and benefit from:

- fast, convenient online submission
- thorough peer review by experienced researchers in your field
- rapid publication on acceptance
- support for research data, including large and complex data types
- gold Open Access which fosters wider collaboration and increased citations
- maximum visibility for your research: over 100M website views per year

At BMC, research is always in progress.

Learn more [biomedcentral.com/submissions](https://biomedcentral.com/submissions)







# PUBLICATION

## II

### **Gap junctions and connexin hemichannels both contribute to the electrical properties of retinal pigment epithelium**

Fadjukov J., Wienbar S., Hakanen S., Aho V., Vihinen-Ranta M., Ihalainen T.O., Schwartz G.W. & Nymark S.

Journal of General Physiology (2022), 154(4): e202112916.

<https://doi.org/10.1085/jgp.202112916>

**Publication reprinted with the permission of the copyright holders**



ARTICLE

# Gap junctions and connexin hemichannels both contribute to the electrical properties of retinal pigment epithelium

Julia Fadjukov<sup>1</sup>, Sophia Wienbar<sup>2,3,4</sup>, Satu Hakanen<sup>5</sup>, Vesa Aho<sup>5</sup>, Maija Vihinen-Ranta<sup>5</sup>, Teemu O. Ihalainen<sup>1</sup>, Gregory W. Schwartz<sup>2,3,4</sup>, and Soile Nymark<sup>1</sup>

Gap junctions are intercellular channels that permit the transfer of ions and small molecules between adjacent cells. These cellular junctions are particularly dense in the retinal pigment epithelium (RPE), and their contribution to many retinal diseases has been recognized. While gap junctions have been implicated in several aspects of RPE physiology, their role in shaping the electrical properties of these cells has not been characterized in mammals. The role of gap junctions in the electrical properties of the RPE is particularly important considering the growing appreciation of RPE as excitable cells containing various voltage-gated channels. We used a whole-cell patch clamp to measure the electrical characteristics and connectivity between RPE cells, both in cultures derived from human embryonic stem cells and in the intact RPE monolayers from mouse eyes. We found that the pharmacological blockade of gap junctions eliminated electrical coupling between RPE cells, and that the blockade of gap junctions or Cx43 hemichannels significantly increased their input resistance. These results demonstrate that gap junctions function in the RPE not only as a means of molecular transport but also as a regulator of electrical excitability.

## Introduction

Gap junctions are intercellular channels formed from two juxtaposed connexin (Cx) protein assemblies called hemichannels. Hemichannels have a hexameric structure and are formed from six Cx proteins, and they have physiological roles independent from gap junctions (Goodenough et al., 1996; Goodenough and Paul, 2009, 2003; Akanuma et al., 2018). On the apical membrane of various cell types, hemichannels may promote cell survival by enabling sustained Ca<sup>2+</sup> oscillations, control membrane permeability (D'hondt et al., 2014; Decrock et al., 2009) or volume (Quist et al., 2000). In astrocytes, hemichannels have been shown to transmit autocrine and paracrine signaling molecules, such as ATP and glutamate (Orellana, 2016). The human Cx protein family comprises at least 20 closely related members that vary in their expression pattern, with many cells expressing multiple types (Beyer and Berthoud, 2018; Goldberg et al., 2004; Akanuma et al., 2018). Gap junctions mediate cell-to-cell communication and homeostasis in most tissues by permitting the rapid transfer of small molecules (1–1.5 kD) and ions between adjacent cells (van Campenhout et al., 2020; Goodenough et al., 1996).

Gap junctions have been recognized as vital components of the retinal circuitry for nearly 50 yr (Bloomfield and Völgyi, 2009; Raviola and Gilula, 1973). In addition to serving a wide variety of functions in the healthy visual system, gap junctions have been implicated in various ophthalmological pathologies, such as retinal edema and age-related macular degeneration (Bao, 2015). In many of these disorders, the impairments, such as defective responses to oxidative stress, have been found to originate not in the retina itself but in the tissue underlying the retina called the retinal pigment epithelium (RPE; Sparrow et al., 2010). This monolayer of densely pigmented cells forms a part of the blood–retinal barrier that transports nutrients, regenerates visual pigment, absorbs excess light, and helps photoreceptors renew their membrane (Bok, 1993; Strauss, 2005). All these tasks are crucial for maintaining vision, and they require physiological homeostasis of the RPE, including intact cell–cell contacts. Various *in vitro* models have suggested that gap junctions are implicated in RPE malfunctions (Hutnik et al., 2008; Chen et al., 2015). Furthermore, Cx43 protein, the major gap-junction constituent of RPE in vertebrates (Janssen-Bienhold

<sup>1</sup>Faculty of Medicine and Health Technology, Tampere University, Tampere, Finland; <sup>2</sup>Department of Ophthalmology, Northwestern University, Chicago, IL; <sup>3</sup>Department of Physiology, Feinberg School of Medicine, Northwestern University, Chicago, IL; <sup>4</sup>Department of Neurobiology, Weinberg College of Arts and Sciences, Northwestern University, Evanston, IL; <sup>5</sup>Department of Biological and Environmental Science and Nanoscience Center, University of Jyväskylä, Jyväskylä, Finland.

Correspondence to Soile Nymark: soile.nymark@tuni.fi.

© 2022 Fadjukov et al. This article is distributed under the terms of an Attribution–Noncommercial–Share Alike–No Mirror Sites license for the first six months after the publication date (see <http://www.rupress.org/terms/>). After six months it is available under a Creative Commons License (Attribution–Noncommercial–Share Alike 4.0 International license, as described at <https://creativecommons.org/licenses/by-nc-sa/4.0/>).



et al., 1998), has been shown to have numerous roles in processes such as cell differentiation, proliferation, and cellular viability (Zhang et al., 2001; Pearson et al., 2004; Hutnik et al., 2008).

In addition to gap junctions, several other ion transport mechanisms co-regulate the physiology of RPE. These include a large array of ion channels (Wimmers et al., 2007), of which voltage-gated ion channels are particularly relevant because membrane voltage changes have been shown to be the fastest way of regulating cellular connectivity (Goodenough and Paul, 2009). Gap junctions in turn may influence the activity of ion channels since they modulate the overall electrical properties of RPE (Coulon and Landisman, 2017). This is important as ion channels regulate various functions of RPE, including phagocytosis and growth factor secretion (Wimmers et al., 2007; Müller et al., 2014; Johansson et al., 2019; Korkka et al., 2019).

Despite the significance of ionic mechanisms for visual health and disease, the level of RPE gap junction-mediated electrical coupling has not been thoroughly characterized. Hudspeth and Yee (1973) reported that RPE cells are electrically connected in mudpuppies (*Necturus maculosus*) and frogs (*Rana pipiens*) but, to date, the physiological characteristics of RPE cell coupling and the role of gap junctions in this process have not been described in mammals. The conventional approach to study the electrical properties of the RPE is to record them from single, enzymatically isolated cells (Johansson et al., 2019; Wollmann et al., 2006; Cao et al., 2018). However, recent work by our group shows that recordings can also be performed from a cultured RPE monolayer (Johansson et al., 2019), and here we extend our recordings into the intact mouse RPE.

In this study, we measured the electrical connectivity of RPE cells in cultured human embryonic stem cell (hESC)-derived RPE and mouse RPE. Our results reveal Cx43-mediated electrical coupling in mammalian RPE that can be inhibited using the universal gap junction blocker, meflofenamic acid (MFA). Our data also demonstrate that Cx43 and potentially Cx36 play a large role in determining the input resistance of RPE cells, a key determinant of electrical excitability. Surprisingly, Cx43 provided a major conductance in RPE cells not only through gap junctions between cells but also via hemichannels on the apical surface.

## Materials and methods

### Cell culturing

Human ESC lines Regea08/017 and Regea11/013 were cultured and differentiated as previously described (Vaajasaari et al., 2011; Viheriala et al., 2021). Cells were plated with a density of  $2.5 \times 10^5$  cells/cm<sup>2</sup> onto collagen IV- (C5533; Sigma-Aldrich, 10 µg/cm<sup>2</sup>) and Laminin 521 (LN521; Biolamina; 1.8 µg/cm<sup>2</sup>)-coated culture inserts (Millicell Hanging Cell Culture Insert, polyethylene terephthalate, 1.0 µm pore size; EMD Millipore) and maintained at 37°C in 5% CO<sub>2</sub> in the knock-out Dulbecco's modified Eagle's medium (10829-018; Gibco) supplemented with 15% knock-out serum replacement (10828-028; Gibco), 2 mM GlutaMax (35050-038; Gibco), 0.1 mM 2-mercaptoethanol (81350-010; Gibco), 1% minimum essential medium nonessential amino

acids (1140050; Thermo Fisher Scientific), and 50 U/ml penicillin/streptomycin (from Cambrex BioScience). The medium was changed three times per week and the samples were allowed to mature for 8–12 wk prior to experiments. The maturity of the hESC-RPE was evaluated by immunostainings, TER measurements, and functional assays, similar to Korkka et al. (2019).

The hESC lines of this study were obtained through collaboration with Dr. Heli Skottman's group. The National Authority for Medicolegal Affairs Finland approved their study with human embryos (Dnro 1426/32/300/05). The supportive statement from the local ethics committee of the Pirkanmaa hospital district Finland allowed the derivation and expansion of hESC lines from surplus embryos excluded from infertility treatments and the use of these lines for research purposes (R05116). Novel cell lines were not derived in this study.

### Immunolabeling

All the following immunolabeling steps were done at room temperature. Samples were fixed for 15 min with 4% paraformaldehyde (pH 7.4; 15713; Electron Microscopy Sciences). After three washes with PBS, permeabilization was carried out by incubating the samples for 15 min in 0.1% Triton X-100 in PBS (Sigma-Aldrich). Next, the samples were blocked with 3% BSA/PBS (Sigma-Aldrich) for 1 h.

All the primary antibodies were diluted in the blocking solution and incubated for 1 h: Connexin 43 (Cx43) 1:200 (C6219; Sigma-Aldrich, RRID:AB\_476857), Connexin 36 1:50 (37-4600; Thermo Fisher Scientific, RRID:AB\_2533320), Connexin 46 1:50 (sc-365394; Santa Cruz Biotechnology, RRID:AB\_10850181), and ZO-1 1:50 (33-9100; Thermo Fisher Scientific, RRID:AB\_2533147). This was followed by three PBS washes and 1 h incubation with the secondary antibodies that were all diluted at 1:200 in 3% BSA in PBS: goat anti-rabbit Alexa Fluor 568 and donkey anti-mouse Alexa Fluor 488 (Thermo Fisher Scientific). The nuclei were stained with 4',6'-diamidino-2-phenylidole (DAPI) included in the mounting medium (P36935; Thermo Fisher Scientific).

### Western blotting

The hESC- and mouse RPE lysates were prepared by triturating the cells in a solution containing 50 mM HEPES, 150 mM NaCl, pH 7.4, supplemented with 1% Triton-X-100, and Halt protease and phosphatase inhibitor cocktail (78440; Thermo Fisher Scientific), and then incubating them for 30 min at +4°C. The lysate was then centrifuged at +4°C for 5 min at 16,900 ×g, mixed with Bolt LDS sample buffer (B0007; Thermo Fisher Scientific), and heated to +96°C for 5 min. The lysates were then loaded onto Bolt 4–12% Bis-Tris Plus Gel (NW04120BOX; Thermo Fisher Scientific), fractionated by SDS-PAGE with the protein standard (SeeBlue Plus2 Pre-Stained Protein standard, LC5925; Thermo Fisher Scientific), and then transferred onto polyvinylidene difluoride membrane via Trans Blot Turbo Transfer system according to the manufacturer's protocols (Bio-Rad).

The blocking was carried out with 3% BSA in PBS + 0.1% Tween-20 for 1 h at RT, and then the blot was labeled overnight at +4°C with the Cx antibodies included in the immunolabeling protocol: Cx43 (1:2,000), Cx36 (1:500), and Cx46 (1:500). The membranes were subsequently washed 3 × 10 min with PBS +

0.01% Tween-20 and incubated with a 1:3,000 dilution of horseradish peroxidase-conjugated goat anti-rabbit IgG (ab6721; Abcam) or anti-mouse IgG (A-21236; Thermo Fisher Scientific) antibodies for 1 h at RT. After subsequent washes, the membranes were developed with the WesternBright ECL system (K-12045-D20; Advansta) and imaged with ChemiDoc XRS+. Next, the blots were stripped by incubating them with Restore Western Blot Stripping Buffer for 15 min at room temperature and by washing the blots three times with PBS before and after the stripping. The blots were then reblocked and labeled with the loading control GAPDH (1:500; Sc-47724; Santa Cruz Biotechnology, RRID:AB\_627678) or RPE65 (1:1,000; GTX103472; GeneTex, RRID:AB\_2037911) that was detected as described for the other antibodies.

#### Dye coupling and carboxyfluorescein dye uptake

For the dye coupling experiments, a single RPE cell was patched in whole-cell configuration with intracellular solution containing either 0.5% w/v neurobiotin (mol wt 358 D, SP-1120; Vector Laboratories) or 0.01% Alexa Fluor 488 (mol wt 570.48 D, A10436; Thermo Fisher Scientific). These recordings were carried out with a Nikon FN1 Upright Fluorescence Microscope. After 15 min to allow for the neurobiotin to fully dialyze and pass through gap junctions to the neighboring cells, the sample was fixed, permeabilized, and blocked as described for the immunostaining experiments, and the neurobiotin was labeled for 1 h at room temperature with 1:500 streptavidin Alexa Fluor 568 conjugate (SI1226; Invitrogen) that was diluted in the blocking buffer. The samples were washed and mounted according to the provided immunostaining protocol, and the labeling was detected with the 561-nm excitation laserline from Nikon A1R confocal microscope. For Alexa Fluor 488, the dye was allowed to diffuse for 45 min after which it was detected with the 488-nm laserline from Argon laser of LSM780 laser scanning confocal microscope in inverted Zeiss Cell Observer microscope body (Zeiss).

The carboxyfluorescein dye uptake was analyzed as previously described (Potter et al., 2021). Briefly, the hESC- and mouse RPE cells were incubated in calcium-free balanced salt solution containing 200  $\mu$ M 5(6)-carboxyfluorescein diacetate (21879; Sigma-Aldrich) for 10 min at 37°C and 5% CO<sub>2</sub>. Next, the solution was replaced with a calcium-containing balanced salt solution with 200  $\mu$ M 5(6)-carboxyfluorescein diacetate that was incubated at 37°C and 5% CO<sub>2</sub> for 5 min. The samples were washed with calcium-containing balanced salt solution without 5(6)-carboxyfluorescein diacetate and kept in the same solution for the entire duration of the imaging. The images were captured using Nikon FN1 Upright Fluorescence Microscope with a 488-nm laserline.

#### Pre-embedding immunogold labeling and cryo-electron microscopy

The RPE cells were fixed and prepared for immunogold labeling as previously described (Johansson et al., 2019). First, the samples were washed three times with PBS and fixed with periodate-lysine-paraformaldehyde (PLP) for 2 h at RT. Prior to primary antibody incubation, the cells were treated with 0.01%

saponin and 0.1% BSA in 0.1 M phosphate buffer, pH 7.4 (Buffer A). All primary antibody concentrations were doubled from immunolabeling for this assay. Next, 1.4 nm nanogold-conjugated polyclonal Fab' fragment of goat anti-rabbit IgG (<https://nanoprobes.com/>) diluted to 1:50 in Buffer A was applied for 1 h, followed by washes with Buffer A and 0.1 M phosphate buffer (pH 7.4). Cells were postfixed for 10 min at RT with 1% glutaraldehyde in phosphate buffer, quenched for 5 min with 50 mM NH<sub>4</sub>Cl in phosphate buffer, and then washed with phosphate buffer and water. Samples were treated with HQ-silver (<https://nanoprobes.com/>) for 5 min in the dark and washed with water. This was followed by gold toning with 2% sodium acetate 3 × 5 min at room temperature, 0.05% gold chloride 10 min at +4°C, 0.3% sodium thiosulphate 2 × 10 min at +4°C, and washes with water. Next, the samples were reduced for 1 h at +4°C with 1% osmium tetroxide in 0.1 M phosphate buffer, dehydrated with graded series of ethanol (70, 96, 100%), and stained with 2% uranyl acetate. Finally, the labeled samples were embedded in Epon (TAAB Embedding resin, medium, TAAB Laboratories Equipment Ltd) and polymerized. Next, the monolayers were sectioned at 200-nm intervals perpendicular to the membrane with an ultramicrotome (Leica ultracut UCT ultramicrotome; Leica Mikrosysteme GmbH). These slices were placed on carbon-coated single-slot grids and imaged at 80 kV voltage with JEOL JEM-1400 transmission electron microscope (JEOL Ltd.) equipped with bottom-mounted Quemesa charge-coupled device camera (4,008 × 2,664 pixels).

For immunoelectron microscopy analysis, mouse eyes on a mixed C57/BL6 background were removed and fixed in 4% paraformaldehyde in 0.1 M phosphate buffer (pH 7.4) with 2.5% sucrose overnight. Small coronal sections of the retina were immersed in 2.3 M sucrose in PBS and rotated at +4°C for 4 h. Specimens were frozen in liquid nitrogen, and thin cryosections were cut with a Leica EM UC7 cryoultramicrotome (Leica Mikrosysteme GmbH). The sections were picked on Butvar-coated nickel grids. The grids were first incubated in 2% gelatine in PBS for 20 min and then in 0.1% glycine-PBS for 10 min followed by incubation in a blocking solution for Protein A/G Gold conjugates (Aurion) for 15 min. Then 0.1% BSAc (Aurion) in PBS was used in the washing steps and in the dilutions of antibodies and gold conjugates. Sections were exposed to the primary antibody against Cx43 (1:50) for 45 min. This was followed by incubation with protein A-conjugated 10 nm gold (Cell Microscopy Core, University Medical Center Utrecht) for 30 min. The controls were prepared by replacing the primary antibody with PBS. The grids were stained with neutral uranyl acetate (UA) and coated with 2% methyl cellulose containing 0.4% UA. Sections were examined with a Tecnai G2 Spirit 120 kV transmission electron microscope (FEI), and the images were captured by a Quemesa charge-coupled device camera (Olympus Soft Imaging Solutions GMBH) using RADIUS software (EMSYS GmbH).

#### Confocal microscopy and image processing

LSM780 confocal microscope and Plan-Apochromat 63×/1.4 oil immersion objective were used for confocal microscopy by setting the voxel size to  $x = y = 66$  nm and  $z = 200$  nm, and 1,024 × 1,024 pixel stacks of 70–120 slices were acquired with a line

average of 2. The following lasers were used for the fluorophores: DAPI was excited with 405 nm diode laser; Alexa Fluor 488 with 488 nm laserline from Argon laser; and Alexa Fluor 568 with 561 nm diode-pumped solid-state laser or 561 nm *InTune* laser. Emission was detected with windows of (in nm): 410–495 (DAPI; Alexa Fluor 405), 499–579 (Alexa Fluor 488), and 579–642 (Alexa Fluor 568). Laser powers and photomultiplier tube sensitivities were optimized for minimal bleaching and an optimal signal-to-noise ratio. The images were saved in CZI format and deconvolved using Huygens Essential (SVI) software with theoretical PSF, signal-to-noise ratio of 5, and a quality threshold of 0.01. The refractive index of the mounting media was provided by the manufacturer (Thermo Fisher Scientific). The images were finalized with ImageJ (Schneider et al., 2012) by only performing linear brightness and contrast adjustments for the pixel intensities.

For the Cx43 quantification, the cell perimeters were analyzed using a custom macro for automated multicellular tissue analysis for maximum intensity projections (ImageJ/Fiji-Advanced Digital Microscopy Core Facility–IRB Barcelona). The Cx43 plaques were quantified in ImageJ by analyzing particles from the segmented cell junctions provided by the analysis macro. Only particles localized to the epithelial cell borders were considered for the analysis. The normality was analyzed with the Shapiro-Wilk test, and the statistical significance was assessed by Mann-Whitney *U* Test that was performed with the IBM SPSS Statistics for Windows, version 26 (IBM Corp.). For the dye-coupling experiments, the images were aligned by placing the original patched cell to the center of the field. These aligned images were converted into an image stack, and the data were combined into an averaged projection with ImageJ. Final figure panels were assembled using Adobe Illustrator (Adobe Systems).

Cx43 labeling was also quantified from immunoelectron microscopy images. Here, the cells were separated from the background by manually selecting an intensity threshold for each cell (Fig. 1 E). Some cells had regions within them that had similar intensities as the cell exterior. These were taken into account by assigning background regions that were smaller than one-tenth of the image size of the cells. The labeled Cx43 was segmented automatically by using the maximum entropy threshold (Kapur et al., 1985). This also segmented the mitochondria, which were excluded from the segmentation by excluding all the contiguous objects that were over 500 pixels ( $\approx 6,000 \text{ nm}^2$ ) in size (Fig. 1 E). The Euclidean distance transform of the cell border was calculated for each cell, and the label density within  $1 \mu\text{m}$  from the cell border was calculated. The label density, as a function of increasing distance from the cell border, was also calculated by grouping the pixels into bins of increasing distance from the border and calculating the label fraction of each bin. The bin size was 15 pixels (52 nm).

#### Patch-clamp recordings

All mice were between 4 and 10 wk old and on a mixed C57/BL6 background. Both male and female mice were used in this study. All procedures were approved by the Animal Care and Use Committee at Northwestern University and in accordance with

the ARVO Statement for the Use of Animals in Ophthalmic and Vision Research and Finland Animal Welfare Act 1986. For electrophysiological experiments, the RPE dissections were conducted under IR light (940 nm) with assistance from IR visible light converter (night vision) goggles and separate IR dissection scope attachments (B.E. Meyers Owl Night Vision Scopes, Model #7200I). The retina was gently removed, and a piece of the eyecup with RPE attached to the choroid was then mounted with RPE side up on a 12-mm poly-D-lysine-coated glass coverslip (354086, BioCoat Cellware; Corning), which was secured to a recording dish via grease under a slice anchor (Warner Instruments). For hESC-RPE recordings, the culture insert was removed from the holder and cut into four pieces that were mounted under the slice anchor on the recording chamber using grease. For both the RPE preparations, the dish was then placed on the electrophysiology rig (SliceScope Pro 6000; Scientifica; or Eclipse FNI upright microscope-based system; Nikon; with pE-4000; CoolLed) and superfused with carbogenated Ames medium (A-1372-25; US Biological Life Sciences; 9 ml per min), and then warmed to 32°C. RPE cells were illuminated at 950 nm for visualization.

The currents were recorded from mature hESC-derived RPE monolayers or mouse RPE cells using the standard patch-clamp technique in whole-cell configuration. In paired recordings, two adjacent RPE cells or pairs at a varying intercellular distance were patched and recorded simultaneously. Patch pipettes (5–7 M $\Omega$ , BF120-69-10; Sutter Instruments) were filled with an intracellular solution composed of (in mM) 125 K-aspartate, 10 KCl, 1 MgCl<sub>2</sub>, 10 HEPES, 1 CaCl<sub>2</sub>, 2 EGTA, 4 Mg-ATP, and 0.5 Tris-GTP (277 mOsm; pH  $\sim$ 7.15 with KOH). For blocking the gap junctions, the bath solution was supplemented with 100  $\mu\text{M}$  MFA (M4531; Sigma-Aldrich). When Cx43 hemichannels were investigated, the intracellular solution was supplemented with 90  $\mu\text{M}$  TAT-Gap19 trifluoroacetate salt (SML2319-IMG; Sigma-Aldrich), and the recording time was kept under 15 min. All recordings were made in current-clamp mode with a two-channel patch-clamp amplifier (MultiClamp 700B; Molecular Devices). To analyze the input resistance, we applied a series of injected current pulses (from  $-25$  to  $50 \text{ pA}$  for hESC-RPE and from  $-500$  to  $+1,500 \text{ pA}$  for mouse RPE) and measured the changes in the membrane potential. Series resistance was not compensated.

#### Patch-clamp data analysis

The offline analysis was performed with a custom open-source MATLAB analysis package (GitHub - SchwartzNU/Symphony-Analysis: Symphony analysis code for SchwartzLab at Northwestern University) and Clampfit software (Molecular Devices). The coupling coefficient was calculated as a change in voltage in the recorded cell over a change in voltage in the stimulated cell. The effect of the MFA blocker was analyzed with two-tailed unpaired Student's *t* test. The normality of hemichannel blocker data was assessed by a Kurtosis test, and the statistical significance of the blocker effect was assessed by the Mann-Whitney *U* test. All statistical tests were performed with the IBM SPSS Statistics for Windows, version 26 (IBM Corp.). Final figures were assembled in Igor Pro and Adobe Illustrator.

### RPE connectivity modeling

The model was largely based on the work by Fortier and Bagna (2006) who investigated how gap junction resistance values contribute to the input resistance of a cell in a hexagonal grid (Fig. 6 A). We had two key assumptions: (1) all cells have the same total input resistance ( $R_i$ ) and all cells have the same single cell input resistance in the absence of gap junctions ( $R$ ), and (2) each cell has exactly  $f = 6$  coupled cells. This differential equation model is quite simple, and thus the addition of variability in the input resistances of the cells (Assumption 1) did not substantially add to our understanding of the role of gap junctions. Assumption 2 was determined to be valid due to the breadth of the literature that described epithelial cells, and specifically RPE, to have six neighbors in a majority of cases (Liu et al., 2016; Ishii and Rohrer, 2017). Therefore, given two paired cells we get that the voltage change in the injected cell is equal to:

$$V_{11} = I_1 \frac{R(R_j + R)}{2R + R_j}, \quad (1)$$

where  $V_{11}$  is the voltage change in cell 1 with current  $I_1$  injected into cell 1, and  $R_j$  is the resistance of the gap junctions.

We then get the voltage change in the paired cell as:

$$V_{12} = I_1 \frac{R^2}{2R + R_j}. \quad (2)$$

Therefore, the coupling coefficient between the two cells is given as:

$$CC = \frac{V_{12}}{V_{11}} = \frac{R^2}{R \times R_j + R^2}. \quad (3)$$

The input resistance of the cell can be calculated as follows:

$$R = \frac{R_i(R_j + R)}{(R_j + R) - fR_i}. \quad (4)$$

We then solved for  $R$  for a variety of  $R_i$  and  $R_j$  values to determine the contribution of gap junctions to the input resistance of RPE cells. The coupling coefficients and input resistances were then related to the measured values from cultured and mouse RPE recordings. The differential equations were solved numerically in MATLAB and all the code can be found at <https://github.com/SchwartzNU/SymphonyAnalysis/tree/master/RPE>.

## Results

### RPE cells display an extensive network of Cx43-based gap junctions

The localization of Cx43 proteins was analyzed by immunolabeling both hESC-derived and mouse RPE monolayers. Confocal microscopy demonstrated that both the RPE preparations showed an extensive network of gap junction plaques adjacent to the cell-cell junctions marked with Zonula occludens-1 (ZO-1) protein labeling (Fig. 1). Furthermore, the labeling demonstrates that the hESC-RPE cells (Fig. 1 A) resemble the mouse RPE cells found in vivo (Fig. 1 B), with respect to Cx43 expression and localization.

We next wanted to analyze in more detail the variation in the distribution of Cx43 plaques between cells in the monolayer and

between the two RPE preparations (Fig. 1 C). The quantification of Cx43 plaques showed moderate variation in the number of foci per cell junctions within the monolayer, but significant differences between the two RPE preparations ( $P < 0.00001$ , Mann-Whitney  $U$  Test). For mouse RPE cells, the average number of puncta per micrometer was  $0.53 \pm 0.01$  (average perimeter of cells was  $85 \pm 1.19 \mu\text{m}$ ,  $n$  of cells = 160) while for hESC-RPE the value was  $0.39 \pm 0.01$  (average perimeter of cells was  $37 \pm 0.14 \mu\text{m}$ ,  $n$  of cells = 1,042; Fig. 1 C).

Detailed localization of the gap junctions was investigated by immunogold labeling and electron microscopy of hESC-RPE. The imaging showed that the gap junctions were localized toward the apical membrane of the cells and that Cx43 labeling was also present outside the cell junctional area in the apical membrane (Fig. 1 D). To analyze the localization, the cell border and Cx43 labels were segmented from the microscopy images. The mean label density within  $1 \mu\text{m}$  from the cell border was  $0.008 \pm 0.003$  (mean  $\pm$  standard deviation) on the apical side and  $0.0021 \pm 0.0013$  on the basal side (Fig. 1 E;  $n = 12$  cells). This was analyzed as a function of the distance from the cell border showing that the label density at the basal side was very low near the cellular border, which started to increase toward the central regions of the cell. At the apical side, the label density was at its highest near the border and decreased toward the central parts (Fig. 1 E). The localization of the Cx43 was found to be similar in cryo-sectioned mouse eyecups (Fig. 1 F). Therefore, both hESC-RPE and mouse RPE monolayers express Cx43 and form gap junctions between cells as well as hemichannels on the apical side of the cells.

### RPE cells show weak expression of Cx36 but not

#### Cx46 isoforms

Previous work has suggested that Cx43 is the primary Cx expressed in RPE (Akanuma et al., 2018; Pearson et al., 2005); however, other Cx isoforms have also been found in mice (Milićević et al., 2021) and rats (Malfait et al., 2001). To investigate the isoform distribution, hESC-RPE and mouse RPE whole mounts were labeled with antibodies against Cx36 and Cx46 proteins (Fig. 2 A). Our immunostaining showed that Cx36 was weakly positive and mostly localized as spots on the apical membrane. This labeling pattern was observed for both hESC (Fig. 2 A) and mouse RPE monolayers (Fig. 2 B). Cx46, on the other hand, was found to be negative in both preparations. To confirm our findings, we analyzed the isoform distribution in RPE by immunoblotting against Cx43, Cx36, and Cx46; GAPDH and RPE65 were used as loading controls in hESC-RPE and mouse RPE, respectively (Fig. 2 C). This showed that the highest fraction of Cx proteins in RPE is accounted for by Cx43, Cx36 is weakly detected at the protein level, and Cx46 band was not identified.

### RPE cell input resistance is reversibly increased by MFA

Input resistance is a core property affecting the electrical excitability of cells; the higher the input resistance, the more the membrane will resist the movement of charges (ions) and the more the membrane voltage will change with a given ionic current. Both Cx43 gap junctions and hemichannels are potential sources of electrical conductance that would be expected to lower the

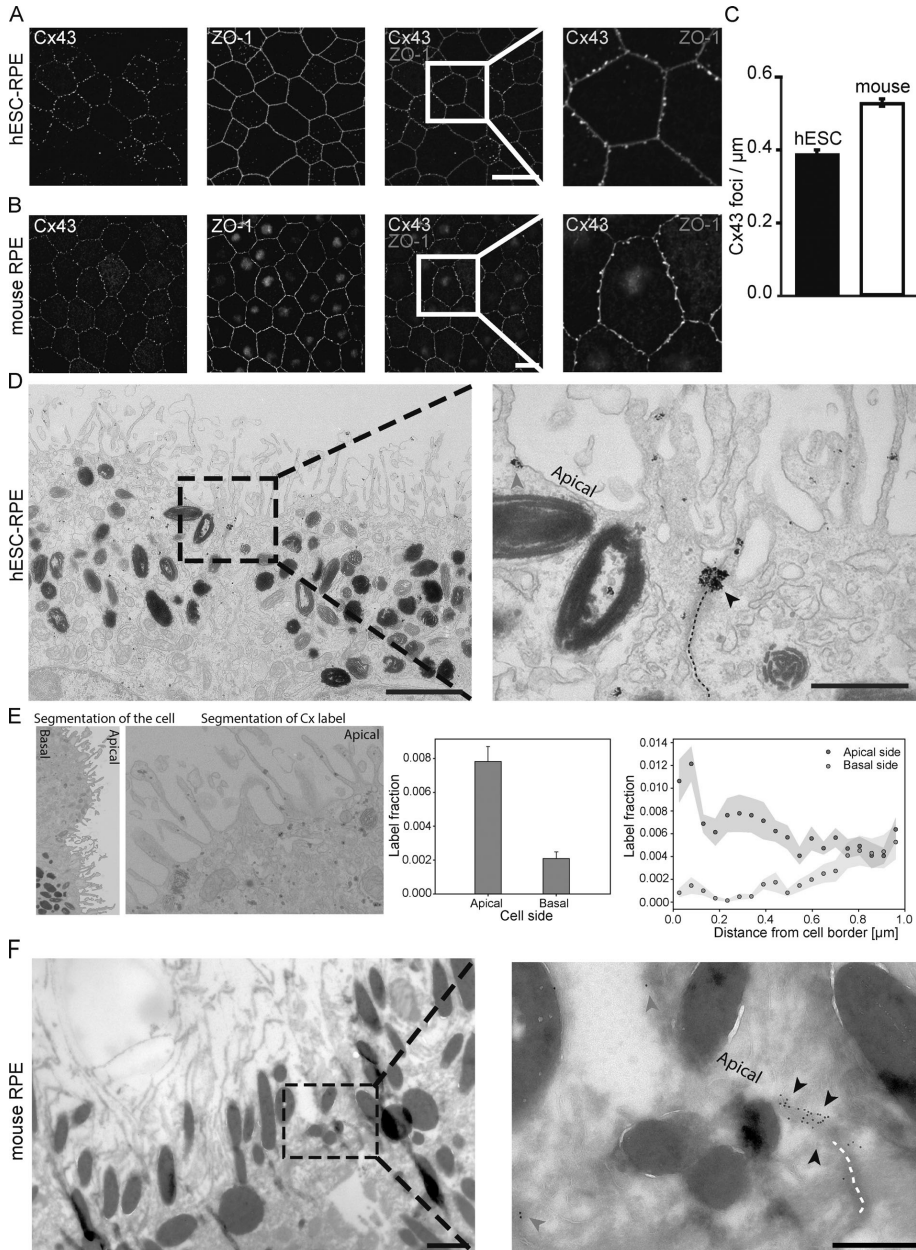


Figure 1. **Characterization of gap junction localization in RPE cells. (A and B)** Laser scanning confocal microscopy (LSCM) data as inverted greyscale Z-maximum intensity projections of hESC-RPE (A) and mouse RPE (B) stained against Cx43 (yellow) and cell-cell junction marker ZO-1 (magenta). Right panels show a higher magnification of the highlighted regions. Scale bars, 20 μm. **(C)** Quantitative analysis of the number of Cx43 positive puncta found per



micrometer of the cell perimeter. Data are shown as mean  $\pm$  SEM, number of cells  $n = 1,042$  for hESC-RPE and  $n = 160$  for mouse RPE. **(D)** Immunogold labeling and transmission electron microscopy images of hESC-RPE cells showing the clustering of Cx43 proteins at the cell-cell junctions (black arrowhead) and at the apical membrane (red arrowhead). Scale bars, 2  $\mu\text{m}$  (full image) and 500 nm (highlighted region). **(E)** Segmentation of the cells and Cx43 signal showed that the label density within 1  $\mu\text{m}$  from the cell border was at the highest on the apical membrane and very low at the basal side ( $n = 12$  cells). **(F)** Immunogold labeling of mouse cryosections showing the clustering of Cx43 proteins at the cell-cell junctions (black arrowheads) and the apical membrane (red arrowheads). Scale bars, 1  $\mu\text{m}$  (full image) and 500 nm (highlighted region).

input resistance of RPE cells. Thus, we hypothesized that blocking these channels would increase the cells' input resistance.

In whole-cell current-clamp recordings of RPE cells, we used a series of injected current pulses ( $-25$  and  $50$  pA for hESC-RPE

and  $-500$  and  $+1,500$  pA for mouse RPE) to measure input resistance (Fig. 3, A and B; see Materials and methods). The baseline resistance values were consistently higher in hESC ( $388 \pm 64$  M $\Omega$ ,  $n = 6$  cells) than in mouse RPE ( $21 \pm 3$  M $\Omega$ ,  $n = 10$  cells;

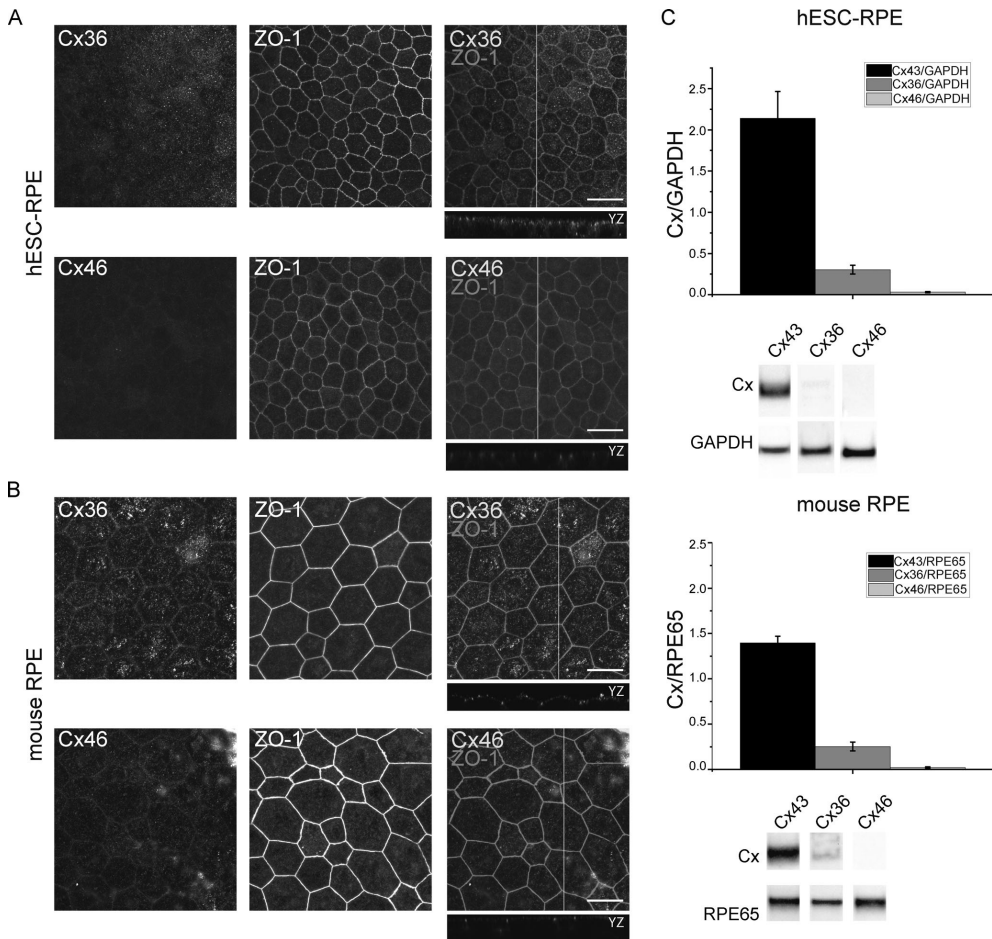


**Figure 2. Cx isoforms found in RPE. (A and B)** Laser scanning confocal microscopy (LSCM) data as inverted greyscale Z-maximum intensity projections and YZ-confocal sections (localization of the section highlighted with a white bar) of hESC-RPE (A) and mouse RPE (B) stained against either Cx36 or Cx46 (yellow) and cell-cell junction marker ZO-1 (magenta). Scale bars, 20  $\mu\text{m}$ . **(C)** Western blot analysis of different Cx isoforms. Whole cell lysates of hESC- or mouse RPE cells were analyzed by electroblotting and the band intensities for Cx43, Cx36, and Cx46 were analyzed against either GAPDH or RPE65 bands ( $n = 3$  for both hESC and mouse).

$P < 0.0001$ , two-tailed unpaired Student's *t* test). We applied the gap junction blocker MFA to the extracellular solution and re-measured input resistance (with smaller current pulses  $-10$  to  $25$  pA in hESC-RPE and  $-50$  to  $150$  pA in mouse). Input resistances increased nearly 5-fold (to  $1,900 \pm 310$  M $\Omega$ ) in hESC and  $>10$ -fold (to  $290 \pm 80$  M $\Omega$ ) in mouse RPE in the presence of MFA, and these values were significantly different from the control conditions ( $P = 0.0013$ ,  $n = 6$ , and  $P = 0.0067$ ,  $n = 10$ , for hESC and mouse respectively, two-tailed paired Student's *t* test). The effect was found in all recorded RPE cells in both preparations, and it was reversed with the washout of MFA (Fig. 3 C).

#### RPE gap junction coupling decreases exponentially over distance

Given that RPE expresses Cx's and its input resistance was affected by a gap junction blocker, we wanted to investigate their electrical coupling. We recorded pairs of adjacent RPE cells in dual patch-clamp configuration to measure the degree of electrical coupling and the effect of MFA (Fig. 4). With both cells in the current-clamp mode, we injected current into one cell (cell 1) and measured the resulting depolarization both in the injected cell (cell 1) and the coupled cell (cell 2). In all pairs, we also reversed the direction of current through the gap junction by injecting current in cell 2. To obtain a trans-junctional current-voltage relationship, we plotted the voltage change in the paired cell against the voltage change in the injected cell (Fig. 4 B). This relationship was linear and independent of the direction of current flow, consistent with a non-rectifying gap junction.

A coupling coefficient is defined as the ratio of the depolarization in the coupled cell to that in the injected cell. The coupling coefficients were  $0.13 \pm 0.013$  for hESC-RPE ( $n = 11$  pairs) and  $0.045 \pm 0.0070$  for mouse RPE ( $n = 7$  pairs), and MFA abolished the connectivity between RPE cells in both preparations (Fig. 4, A and C). This relationship was linear and independent of the direction of current flow (Fig. 4 B), consistent with a non-rectifying gap junction. There was no significant directional bias in either the hESC data ( $P = 0.071$  for control conditions and  $P = 0.088$  in MFA conditions) or the mouse RPE ( $P = 0.80$  for control conditions and  $P = 0.27$  for MFA conditions). In the presence of MFA, the voltage change in the recorded cell was no longer dependent on the voltage change in the injected cell in both hESC (coupling coefficient became  $0.026$ ) and mouse ( $0.022$ ) RPE (Fig. 4 C). This was significantly different from control conditions (hESC and mouse  $P < 0.001$ ). However, these coupling coefficients are relatively low as compared to other retinal cells (Trenholm and Awatramani, 2017), and thus small fluctuations in membrane voltage could be perceived as responses in the recorded cell and artificially inflate the coupling in MFA. Therefore, to measure how statistically significant the voltage changes were, we also calculated the standard score (*Z*-score) of the responses in the recorded cell (Fig. 4 C). In both hESC- and mouse RPE pairs, the *Z*-score was significantly affected by the application of MFA (hESC: control  $15.0 \pm 2.0$ , MFA  $3.4 \pm 0.9$ ,  $P < 0.001$ ; mouse: control  $6.2 \pm 1.0$ , MFA  $1.2 \pm 0.09$ ,  $P < 0.001$ ). Therefore, the coupling between neighbors in the RPE monolayer is significant and can be blocked with the application of MFA.

Next, we wanted to investigate the extent of coupling between RPE cells by analyzing the relationship of coupling coefficient to the inter-pair distance. This was carried out by patching hESC-RPE and mouse RPE cell pairs by increasing the number of cells between the pair (Fig. 5 A). The coupling was found to decay dramatically as the distance increased in hESC- and mouse RPE:  $0.12 \pm 0.024$  (adjacent cells between the pair,  $n = 5$ ),  $0.04 \pm 0.007$  (one cell between the pair,  $n = 7$ ),  $0.01 \pm 0.003$  (two cells between the pair,  $n = 4$ ), and  $0.01 \pm 0.005$  (three cells between the pair,  $n = 3$ ) for hESC-RPE; and  $0.09 \pm 0.015$  (adjacent cells between the pair,  $n = 21$ ),  $0.068 \pm 0.014$  (one cell between the pair,  $n = 3$ ),  $0.039 \pm 0.008$  (two cells between the pair,  $n = 3$ ), and  $0.036 \pm 0.008$  (three cells between the pair,  $n = 4$ ) for mouse RPE (Fig. 5 B). This phenomenon was also observed in dye coupling, where an individual cell in the monolayer was filled with a gap-junction permeable fluorescent dye, Alexa Fluor 488, that was allowed to diffuse to the adjacent cells for 45 min (Fig. 5 C). We observed that in both RPE preparations, the extent of the dye spread reached the adjacent cell layer but was not detectable past that; however, the diffusion was found more asymmetric in hESC-RPE. Therefore, we used a smaller marker neurobiotin that only required 15 min of incubation and investigated the diffusion in a population of hESC-RPE cells ( $n = 8$ ). The individual images were compiled into an averaged projection, but the asymmetry was still detected (Fig. 5 D). This showed that the gap junctions are capable of transporting small molecules across the monolayer, but the dye intensity dramatically decreased over distance.

#### Cx43 hemichannels influence input resistance

In addition to gap junctions, previous studies (Akanuma et al., 2018; Pearson et al., 2005) and our EM data (Fig. 1) indicated that Cx43 also assembles as hemichannels in the apical membrane of RPE cells. MFA blocks these hemichannels as well as gap junctions, and it can also have off-target effects on resistance through voltage-gated potassium channels by inhibiting hKv2.1 channels (Lee and Wang, 1999) and opening KNCQ2/Q3 channels (Peretz et al., 2005). However, due to the lack of functional evidence of either of these potassium channel types in RPE, we assume that the off-target (non-connexin blockade) effects of MFA on input resistance are likely to be negligible.

We wanted to determine whether the increase in input resistance that we measured in RPE cells with MFA (Fig. 3) was consistent with solely gap junction decoupling, or whether the blockade of additional conductances was required. We modeled a network of RPE cells consisting of a central cell and six connected neighbors, consistent with the hexagonal lattice of the monolayer (Figs. 1 A and 6 A; see Materials and methods; Liu et al., 2016; Ishii and Rohrer, 2017). This differential equations model calculated the input resistance of a cell in a network, given a measured input resistance with junctions intact and a junctional conductance (Fortier and Bagna, 2006). We evaluated the model at some example input resistances that align with our measurements (Fig. 3 C). By varying the resistance,  $R_j$ , of the gap junctions (see Eq. 4), we investigated the impact of junctional conductance on the resulting single cell input resistance ( $R$ ) of each cell (Fig. 6 B). Constraining the model to produce coupling

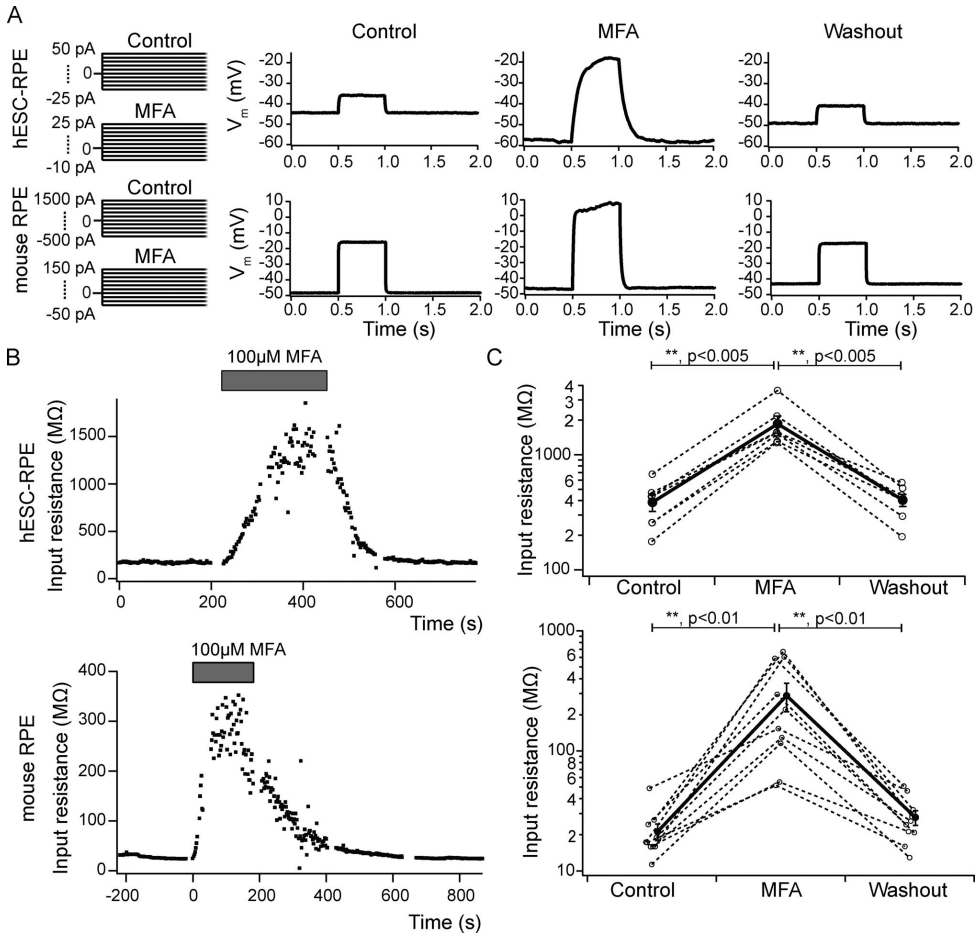


**Figure 3. Input resistance analysis of RPE cells. (A)** Representative current clamp recordings of hESC-RPE (top) and mouse RPE (bottom) cells showing the changes in their membrane potential ( $V_m$ ) in control conditions, in the presence of 100  $\mu$ M MFA, and after the washout of MFA. **(B)** Quantitative analysis of the input resistance before and after the addition of MFA in single recorded hESC-RPE (upper) and mouse RPE (lower) cell. The MFA application period is represented with a grey box. **(C)** Input resistance data in logarithmic scale for all the recorded cells before and after the MFA application. Open symbols and dashed lines represent individual cells and closed symbols and a solid black line show values as mean  $\pm$  SEM to demonstrate the averaged effect of MFA. Data are shown as mean  $\pm$  SEM, number of cells:  $n = 6$  hESC-RPE,  $n = 10$  mouse RPE.

coefficients in the measured range (0.15 with gap junctions open to 0.025 with them blocked by MFA; Fig. 4), we found that the input resistance did not increase as dramatically as we observed with the application of MFA (Fig. 3). MFA is known to have off-target effects, including blocking hemichannels. Thus, closing gap junctions alone could not account for the magnitude of the resistance increase that was measured with MFA.

These results suggest that a major component of the effect of MFA on the measured input resistance was instead due to the blockade of Cx43 hemichannels. To test this modeling result

experimentally, we carried out the patch-clamp recordings with a specific blocker, TAT-Gap19. This blocker is a Cx43 mimetic peptide, which specifically inhibits Cx43 hemichannels by preventing their opening, but importantly, does not interfere with gap junctions (Tarzemyan et al., 2017; Abudara et al., 2014). The peptide specificity is due to its direct binding to the C-terminal tail of Cx43, which prevents the interaction of cytoplasmic loop/C-terminal tail. This interaction is mandatory for hemichannel activity, while the gap junctions are unaffected (Ramadan et al., 2020). However, other similar peptides have been shown to also

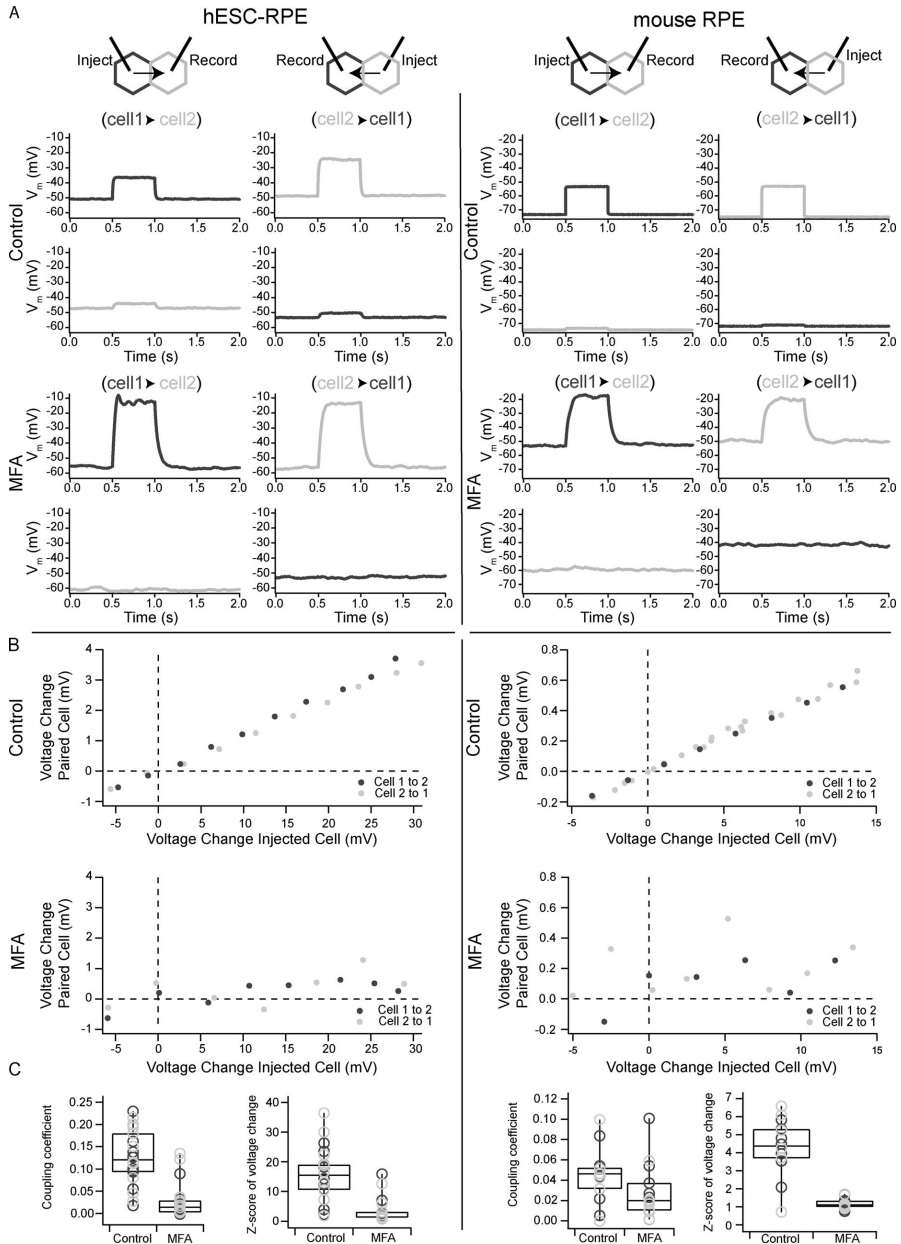


**Figure 4. Analysis of RPE electrical coupling.** The coupling was analyzed by injecting current pulses in one cell (blue) and recording the voltage responses in its adjacent cell (grey). The recordings were carried out in both directions (indicated by the black arrows), and both in the presence and absence of 100  $\mu$ M MFA. **(A)** Representative voltage responses are shown for both hESC-RPE (right) and mouse RPE (left). **(B)** Example of the voltage change in the injected cell versus the recorded voltage change in the response cell is shown in both directions with and without MFA over a range of responses. **(C)** Coupling coefficients

were calculated based on the ratio of voltage changes, and the linearity of the curve was assessed by analyzing the standard scores (Z-score) for control and MFA conditions. Center lines show the medians; box limits indicate the 25th and 75th percentiles for all cells (number of pairs:  $n = 11$  hESC-RPE,  $n = 7$  mouse RPE).

inhibit gap junctional communication, but importantly, the kinetics of this inhibition is much slower ( $\sim 30$  min; D'hondt et al., 2014). In a subset of experiments, we included TAT-Gap19 ( $90 \mu\text{M}$ ) in the intracellular solution while keeping the recording time under 15 min to prevent off-target effects (Fig. 6 C). Input resistances measured in the presence of TAT-Gap19 were significantly higher than those in control hESC-RPE cells ( $511 \pm 70 \text{ m}\Omega$  [ $n = 19$ ] versus  $301 \pm 28 \text{ m}\Omega$  [ $n = 23$ ],  $P = 0.012$ , Mann-Whitney  $U$  test; Fig. 6 C), suggesting that Cx43 hemichannels play a role in setting the input resistance of RPE cells. We also observed an increased input resistance in mouse RPE recordings, although the effect was more moderate ( $65 \pm 31 \text{ m}\Omega$  [ $n = 8$ ] versus  $18 \pm 4 \text{ m}\Omega$  [ $n = 8$ ],  $P = 0.05$ , Mann-Whitney  $U$  test).

In addition to electrophysiological characterization, the presence of functional hemichannels was investigated by a carboxyfluorescein dye uptake assay (Potter et al., 2021). Our results showed that both hESC- and mouse RPE preparations were able to uptake the dye after exposure to  $\text{Ca}^{2+}$  free extracellular solution for hemichannel opening, and that the label intensity varied between cells (Fig. 6 D). Previously, it has been suggested that a small subset of hemichannels may be open without the removal of  $\text{Ca}^{2+}$  (Potter et al., 2021). We wanted to analyze the fraction of spontaneously open hemichannels in RPE by incubating the monolayers in carboxyfluorescein without the initial step to remove  $\text{Ca}^{2+}$ . Our results showed a decrease in the relative intensity in both RPE preparations ( $-0.60 \pm -0.02$  for hESC- and  $-0.62 \pm -0.05$  for mouse RPE,  $n$  of experiments = 3). Taken together, the dramatic increases in input resistance we measured in MFA likely arose from the combination of this drug's blockade of Cx43 gap junctions and hemichannels.

## Discussion

A growing body of evidence has challenged the concept of RPE as the electrically passive partner for the retina that simply provides appropriate environmental conditions for maintaining visual function. Recent work by us and others have demonstrated that various essential tasks of RPE, such as renewal of photoreceptor membranes and growth factor secretion, depend on voltage, and that RPE cells express a family of voltage-gated calcium and sodium channels (Wimmers et al., 2007; Müller et al., 2014; Johansson et al., 2019; Korkka et al., 2019). Yet, the electrophysiological characteristics of RPE cells have not been thoroughly investigated, and studies are particularly lacking from mammalian species and intact monolayer preparations.

In this study, our goal was to examine the characteristics of the intercellular connectivity by analyzing input resistance in single (Fig. 3) and dual patch-clamp recordings (Fig. 4) from tissues that most accurately represent RPE cells in vivo. Due to the challenges related to recording from native mouse RPE tissue, previous physiological studies have focused on sub-confluent primary cultures (Wollmann et al., 2006) or isolated

cells (Cao et al., 2018). We have now developed a procedure for obtaining patch-clamp recordings from mouse RPE whole mounts, which opens possibilities for further studies on their physiology.

Our input resistance analysis demonstrates that mammalian RPE cells are physiologically coupled, and that this connectivity can be inhibited by blocking gap junctions and hemichannels with MFA (Fig. 3, B and C). Our results correlate with previous work from an immortalized cell line ARPE-19, although we found the effect of MFA to be reversible (Ning et al., 2013). While the MFA-induced increase in input resistance was similar both in hESC- and mouse RPE, our results show that mouse RPE cells display lower input resistance values than cultured cells. Mouse RPE had a higher number of Cx43 positive foci at the cell-cell junctions (Fig. 1 C), indicating a larger number of gap junctions in addition to having more extensive apical microvilli leading to a larger membrane area. Both factors would contribute to mouse RPE cells having a lower input resistance as compared to cultured cells.

The dual patch-clamp recordings showed that coupling coefficients (Figs. 4 C and 5 B) were lower in both of the RPE preparations compared to previously reported values in the retinal neuronal cells (Trenholm and Awatramani, 2017). It is worth noting that the low resistance of the RPE cells can cause variance in the coupling coefficient measurements. However, the values that were obtained in RPE cells were higher than the coupling ratios reported for astrocytes that are known to be able to form an electrical syncytium through gap junctional coupling (Xu et al., 2010; Ma et al., 2016). Similar to astrocytes (Xu et al., 2010), the coupling coefficients were found to decrease exponentially with increasing distance between the recorded RPE cell pair, and this was also observed in our dye coupling analysis (Fig. 5).

Our computational model (Fig. 6) showed that with coupling coefficients in the measured range, blocking gap junctions alone could not account for MFA's effect on input resistance. As MFA is a universal blocker for Cx43, we speculated that hemichannels might also influence the results as their presence has been previously shown by fluorescent dye diffusion and calcium imaging studies in immortalized ARPE-19 cell line (Akanuma et al., 2018) and developing RPE (Pearson et al., 2005). Indeed, the application of hemichannel inhibitor TAT-Gap19 in cultured RPE cells increased the input resistance significantly. This validated the results obtained from the computational model and confirmed that the Cx43 signal observed in our immuno-EM data originates from both gap junctions and hemichannels. The effect of the peptide was significant in mouse RPE as well, yet it appeared less potent. Our hemichannel finding is supported by the work of Akanuma et al. (2018), who demonstrate an increased dye uptake in ARPE-19 cells in calcium-deprived conditions that have been shown to activate the hemichannels. Furthermore, we observed an uptake of carboxyfluorescein dye

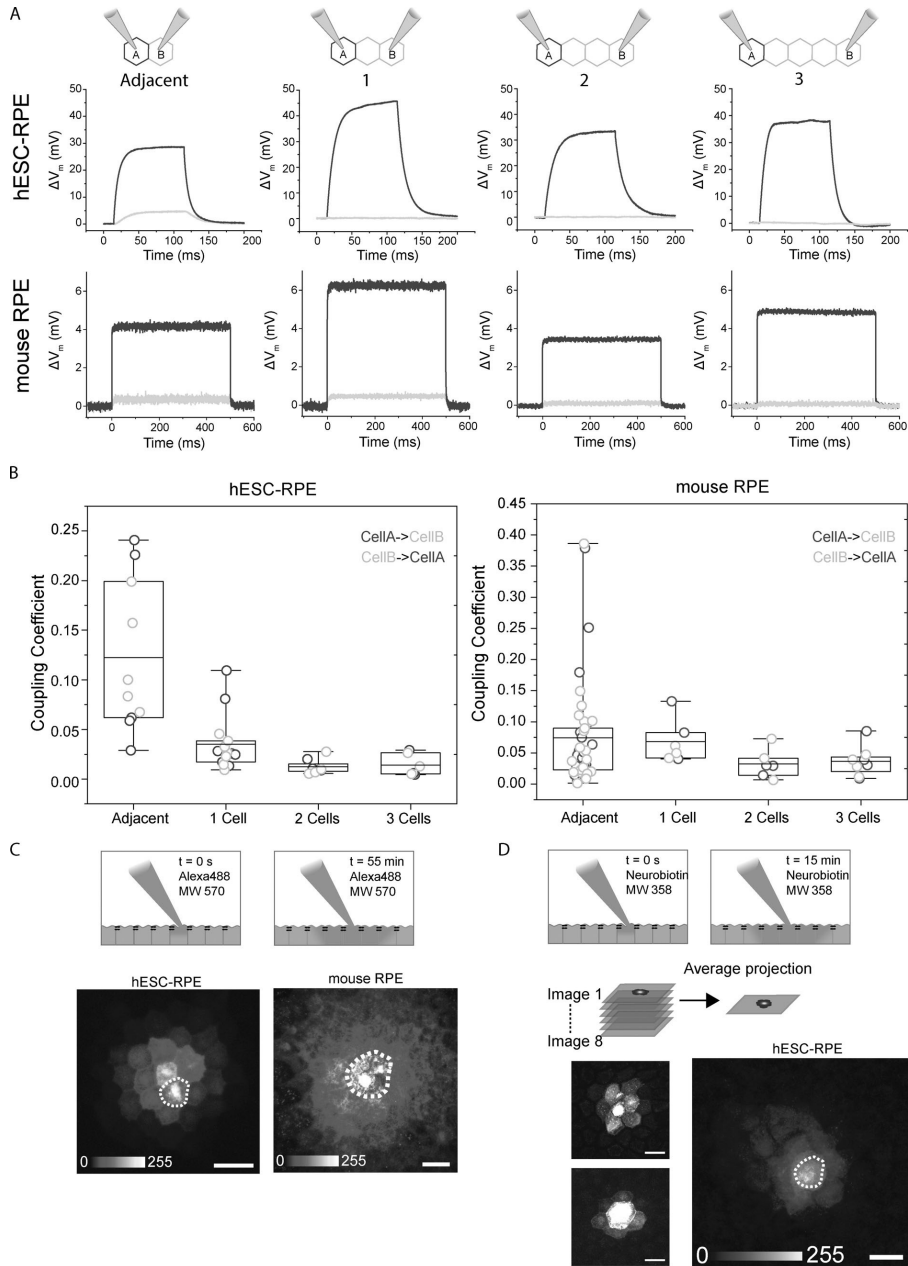


Figure 5. **RPE cell coupling decreases over distance.** (A) A schematic illustration of the paired recordings with an increasing number of inter-pair cells. The coupling was analyzed by injecting current pulses in one cell (blue) and recording the voltage responses in its adjacent cell (grey). Representative voltage responses are shown for both hESC-RPE (top) and mouse RPE (bottom). (B) Coupling coefficients were calculated based on the ratio of voltage changes for

each pair type. Center lines show the medians; box limits indicate the 25th and 75th percentiles, data points are plotted as open circles, number of pairs for hESC:  $n = 5$  adjacent;  $n = 7$ , 1 cell;  $n = 4$ , 2 cells;  $n = 3$ , 3 cells, number of pairs for mouse RPE:  $n = 21$  adjacent;  $n = 3$ , 1 cell;  $n = 3$ , 2 cells;  $n = 4$ , 3 cells. **(C and D)** A schematic illustration demonstrating the dye filling procedure. A single patched cell was loaded with gap junction permeable Alexa Fluor 488 for 45 min (C) or neurobiotin for 15 min (D) to allow the dye to fully diffuse to the adjacent RPE cells in the monolayer. Representative laser scanning confocal microscopy (LSCM) Z-maximum intensity projections of a hESC-RPE and a mouse RPE cell after the loading period for Alexa Fluor 488 (C) and an average projection of multiple hESC-RPE cells loaded with neurobiotin ( $n = 8$ ; D). The patched cell is highlighted in both RPE preparations, and the calibration bar reflects the intensity of the dye labeling. Scale bars, 20  $\mu\text{m}$ .

after calcium removal, demonstrating that hemichannels are functional in RPE cells (Fig. 6).

While the blockade of both gap junctions and Cx43 hemichannels by MFA together contributed to the increase in input resistance we observed, the effects were not additive. The full resistance increase we measured in MFA exceeded the sum of the modeled effects on gap junctions (Fig. 6) and the measured effects of Cx43 hemichannel blockade (Fig. 3). Factors contributing to this discrepancy could include off-target effects of MFA on ion channels other than Cx's (Peretz et al., 2005) and incomplete blockage of hemichannels by TAT-Gap19 (D'hondt et al., 2014). Future work may reveal other components that regulate the input resistance of RPE cells and how they might be influenced by MFA.

At this stage, it is not clear whether the variation between mouse and cultured RPE cells is due to differences between species. Our immunostainings and Western blot analyses had shown that a low level of Cx36 was present in RPE and, in particular, in the apical membrane. Hemichannels formed by this Cx isoform would not be affected by TAT-Gap19. While our immunoblots demonstrate that Cx43 comprises the highest fraction of the RPE Cx proteins, it is noteworthy that the lysis process was not specifically targeted for the extraction of membrane-bound proteins. Previous studies in HeLa transfectants have shown that biotinylated surface Cx proteins only comprise a small portion of the total Cx level (Schalper et al., 2008). Thus, the level of Cx36 could be higher than that shown by our data. The presence of Cx43 and Cx36 and the minimal expression of Cx46 in murine RPE has been previously reported by other groups on the mRNA level. Analysis of the GEO data set GSE172440 (Milićević et al., 2021) demonstrates that Gjal (encoding Cx43) is the most abundant Cx protein, while the expression of Gjd2 (Cx46) was found to be minimal. Gjd2 (encoding Cx36) was also expressed, albeit at lower levels than Gjal.

In addition to interspecies variation, the differences between cultured and mouse RPE could be caused by the culturing conditions of human RPE cells or due to a developmental issue as hESC-RPE typically resembles fetal tissue more than mature epithelium. As has been recognized before, the culture conditions can influence the expression patterns of ion channels and transporters (Reichhart and Strauss, 2014; Korkka et al., 2019). It is also worth noting that native RPE cells have been shown to exhibit intercellular heterogeneity in terms of their morphology and protein expression (Burke and Hjelmeland, 2005; Burke et al., 1996), and it has been suggested that this variability could cause phenotypically distinct subpopulations when propagated in vitro (Rizzolo, 2014; Campbell and Humphries, 2013). The mosaic-like behavior of RPE was also reflected in the baseline input resistance values (Fig. 3 C) and coupling coefficients (Fig. 4 C) obtained in this study.

While the integrity of tight junctions as a constituent of the blood-retina barrier has long been recognized as fundamentally important for visual health (Campbell and Humphries, 2013; Rizzolo, 2014), evidence suggests that gap junctions are also important for regulating the functions of RPE during development, such as the correct pacing of retinal organogenesis (Tibber et al., 2007) and calcium wave spreading (Pearson et al., 2004). However, less is known about the specific roles of gap junctions in mature RPE. In the retina, gap junctions are known to have myriad roles, such as receptive field size signal correlation (Devries, 1999) and motion detection (Murphy-Baum and Awatramani, 2018), and both light adaptation and circadian rhythm have been shown to alter the electrical coupling of the underlying neural circuits (Vasconcellos et al., 2005; Rassi Gabriel et al., 2011). As our results demonstrate that both gap junctions and Cx43 hemichannels can control the electrical excitability of RPE by altering the input resistance, it is plausible the connectivity could enable synchronization of the essential functions of RPE, particularly as the junctions facilitate signaling across wide regions. In other cell types, such as oligodendrocytes, astrocytes, and corneal endothelial cells, gap junctions and hemichannels have been implicated in potassium buffering, calcium wave propagation, as well as the release of signaling molecules such as ATP and nicotinamide-adenine dinucleotide (Belousov et al., 2017; D'hondt et al., 2014; Goodenough and Paul, 2003).

In addition to mediating signaling in the healthy tissues, gap junctions have also been implicated in cell death and survival, and hemichannels have been shown to open in response to metabolic stress (Belousov et al., 2017; Contreras et al., 2002). Therefore, a loss or malfunction in the regulation of Cx43 could impair the physiology of RPE. In fact, mutations in Cx43 have been implicated in a syndrome known as oculodentodigital dysplasia that causes abnormalities of the ocular, nasal, dental, and limb structures. Interestingly, developmental defects in RPE have been reported in some patients (Calera et al., 2009). Furthermore, conditional knockout of Cx43 has been shown to cause a reduction in aqueous humor production and complete loss of the vitreous chamber in mice (Pogoda et al., 2016). In the retina, photoreceptor degeneration has been shown to cause oscillatory electrical activity within the remaining electrically coupled retinal network (Biswas et al., 2014). Future studies may elucidate whether connectivity impairments also occur within the RPE in pathological conditions.

Both gap junctions and hemichannels are known to be regulated through posttranslational modifications, and interactions with various other cellular proteins can affect their gating and selectivity, trafficking, as well as assembly (Falk et al., 2014; Laird, 2006). Especially considering the short half-life of Cx

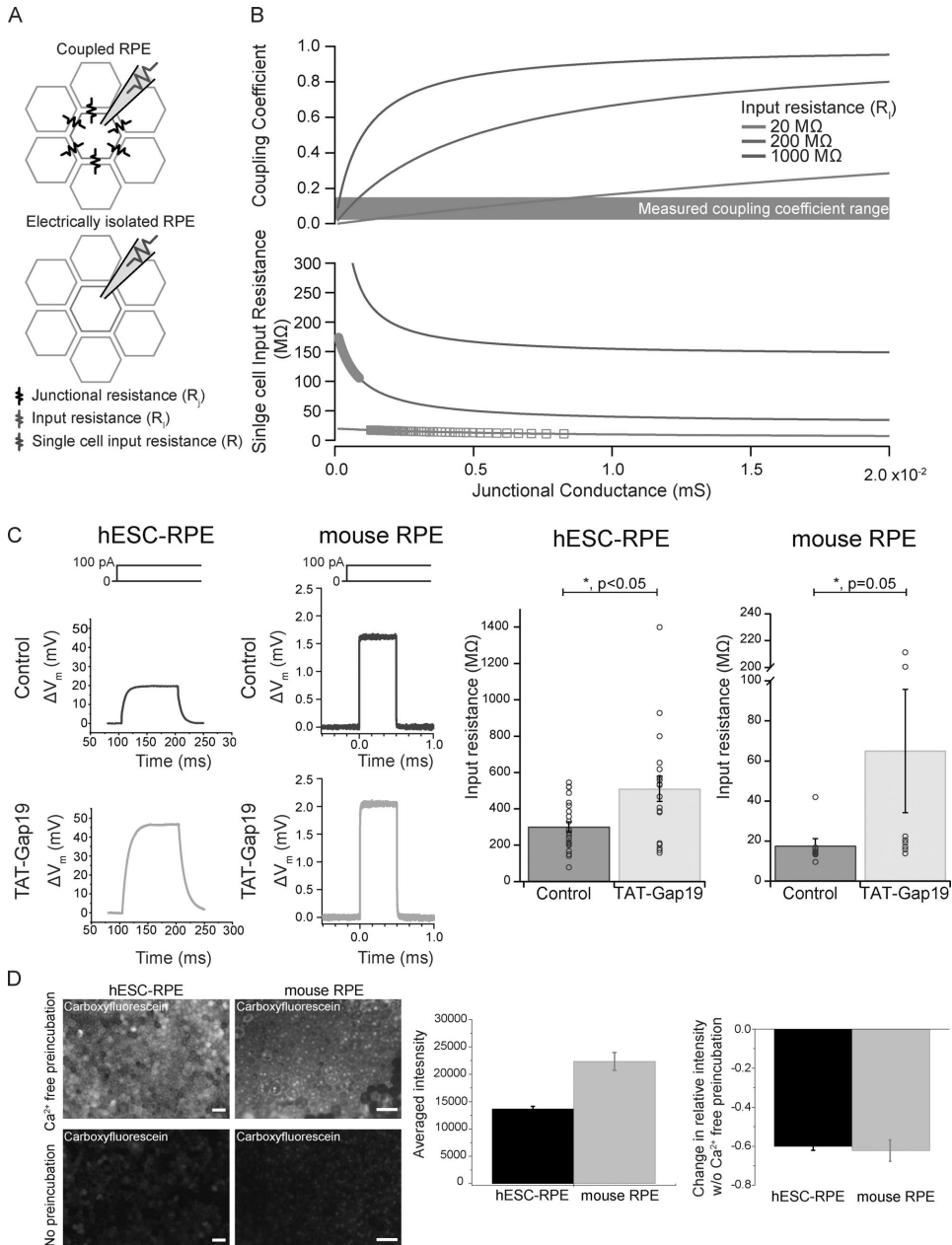


Figure 6. **Cx43 hemichannels modulate input resistance in RPE.** (A) Schematic model (see Materials and methods). (B) Top traces show the calculated coupling coefficients (Eq. 3), given a theoretically modeled total input resistance ( $R_i$ ), and junctional conductances (junctional conductance =  $1/R_j$ ). Bottom traces show the calculated single cell input resistances ( $R$ , see Eq. 4) of a given junctional connectivity. Grey shading indicates the values that correspond to our



experimentally measured values for coupling coefficients and grey markers show the corresponding input resistance values (R). (C) Representative current-clamp recordings of hESC- and mouse RPE cells in control conditions and with intracellular solution that has been supplemented with 90  $\mu\text{M}$  TAT-Gap19 and subsequent analysis. Quantitative analysis of the input resistance values obtained from control cells, and cells treated with TAT-Gap19, number of cells for hESC:  $n = 23$  control,  $n = 19$  TAT-Gap19, number of cells for mouse RPE:  $n = 8$  control,  $n = 8$  TAT-Gap19. (D) Confocal images of the 5(6)-carboxyfluorescein diacetate loading assay in hESC- and mouse RPE. The averaged intensity was analyzed from the monolayers with or without prior removal of extracellular calcium to open the hemichannels ( $n = 3$  in both hESC and mouse). Scale bars, 25  $\mu\text{m}$ .

proteins of 1–5 h (Laird, 2006; Falk et al., 2014), it is possible that natural variations in the state of Cx43 could play a role in regulating the excitability and physiological status of RPE. It is worth noting that in addition to a decrease in extracellular calcium, a modest increase in intracellular calcium can open the hemichannels by shifting their threshold for voltage activation toward the physiological range (D'hondt et al., 2014). Understanding the electrical coupling and its physiological regulation may help to elucidate the roles of various voltage-gated ion channels in RPE and other epithelial tissues. Taken together, these results demonstrate that while the baseline level of cellular coupling in RPE is low, gap junctions enable rapid changes in electrical properties and overall connectivity. This could facilitate the fast spreading of physiological signaling molecules and ions, such as ATP, cAMP, and calcium in RPE. Intriguingly, with our observation of hemichannels, this includes signaling within the monolayer as well as between RPE and the subretinal space.

## Acknowledgments

Jeanne M. Nerbonne served as editor.

We are grateful to Viivi Karema-Jokinen (Tampere University) for her technical assistance with the electron microscopy experiments and to Dr. Heli Skottmann (Tampere University) and Dr. Keijo Viiri (Tampere University) for kindly providing the hESCs for RPE differentiation and mouse tissue, respectively. We thank both Outi Heikkilä (Tampere University) and Susan Lynn Wohlgenant (Northwestern University) for their technical expertise and assistance. The authors acknowledge the Biocenter Finland (BF) and Tampere Imaging Facility (TIF) for their service. In addition, Tampere Facility of Electrophysiological Measurements, and Electron Microscopy Unit (University of Helsinki, Institute of Biotechnology) are gratefully acknowledged for their services. Part of the work was carried out with the support of Biocenter Oulu, Electron Microscopy Core Facility (University of Oulu).

This study was funded by the Academy of Finland (grant numbers 319257, 287287, 323507, 308315, and 330896), the Emil Aaltonen Foundation, the Jane and Aatos Erkko Foundation, and TUT on world tour mobility grant (Tampere University).

The authors declare no competing financial interests.

Author contributions: Conception and design of the study as well as data acquisition, analysis, and interpretation were performed by J. Fadjukov, S. Wienbar, G.W. Schwartz, and S. Nyman. The expertise on confocal microscopy and image analysis was provided by T.O. Ihalainen. S. Hakanen, V. Aho, and M. Vihinen-Ranta planned and conducted the electron microscopy sample preparation together with J. Fadjukov, and they conducted the electron microscopy imaging for the hESC-RPE. All

authors contributed to the writing of the manuscript and approved the final manuscript.

Submitted: 29 March 2021

Accepted: 17 February 2022

## References

- Abudara, V., J. Bechberger, M. Freitas-Andrade, M. de Bock, N. Wang, G. Bultynck, C.C. Naus, L. Leybaert, and C. Giaume. 2014. The connexin43 mimetic peptide Gap19 inhibits hemichannels without altering gap junctional communication in astrocytes. *Front. Cell. Neurosci.* 8:306. <https://doi.org/10.3389/fncel.2014.00306>
- Akanuma, S.I., H. Higashi, S. Maruyama, K. Murakami, M. Tachikawa, Y. Kubo, and K.I. Hosoya. 2018. Expression and function of connexin 43 protein in mouse and human retinal pigment epithelial cells as hemichannels and gap junction proteins. *Exp. Eye Res.* 168:128–137. <https://doi.org/10.1016/j.exer.2018.01.016>
- Bao, L. 2015. Trafficking regulates the subcellular distribution of voltage-gated sodium channels in primary sensory neurons. *Mol. Pain.* 11:61. <https://doi.org/10.1186/s12990-015-0065-7>
- Belousov, A.B., J.D. Fontes, M. Freitas-Andrade, and C.C. Naus. 2017. Gap junctions and hemichannels: communicating cell death in neurodevelopment and disease. *BMC Cell Biol.* 18:4. <https://doi.org/10.1186/s12860-016-0120-x>
- Beyer, E.C., and V.M. Berthoud. 2018. Gap junction gene and protein families: connexins, innexins, and pannexins. *Biochim. Biophys. Acta Biomembr.* 1860:5–8. <https://doi.org/10.1016/j.bbmem.2017.05.016>
- Biswas, S., C. Haseliter, A. Mataruga, G. Thumann, P. Walter, and F. Müller. 2014. Pharmacological analysis of intrinsic neuronal oscillations in rd10 retina. *PLoS One.* 9. e99075. <https://doi.org/10.1371/journal.pone.0099075>
- Bloomfield, S.A., and B. Völgyi. 2009. The diverse functional roles and regulation of neuronal gap junctions in the retina. *Nat. Rev. Neurosci.* 10: 495–506. <https://doi.org/10.1038/nrn2636>
- Bok, D. 1993. The retinal pigment epithelium: a versatile partner in vision. *J. Cell Sci.* 17:189–195. [https://doi.org/10.1042/jcs.1993.supplement\\_17.27](https://doi.org/10.1042/jcs.1993.supplement_17.27)
- Burke, J.M., and L.M. Hjelmeland. 2005. Mosaicism of the retinal pigment epithelium: seeing the small picture. *Mol. Interv.* 5:241–249. <https://doi.org/10.1124/mi.5.4.7>
- Burke, J.M., C.M. Skumatz, P.E. Irving, and B.S. McKay. 1996. Phenotypic heterogeneity of retinal pigment epithelial cells in vitro and in situ. *Exp. Eye Res.* 62:63–73. <https://doi.org/10.1006/exer.1996.0008>
- Calera, M.R., Z. Wang, R. Sanchez-Olea, D.L. Paul, M.M. Civan, and D.A. Goodenough. 2009. Depression of intraocular pressure following inactivation of connexin43 in the nonpigmented epithelium of the ciliary body. *Invest. Ophthalmol. Vis. Sci.* 50:2185–2193. <https://doi.org/10.1167/iovs.08-2962>
- Campbell, M., and P. Humphries. 2013. The blood-retina barrier tight junctions and barrier modulation. *Adv. Exp. Med. Biol.* 763:70–84. [https://doi.org/10.1007/978-1-4614-4711-5\\_3](https://doi.org/10.1007/978-1-4614-4711-5_3)
- Cao, X., B.R. Pattnaik, and B.A. Hughes. 2018. Mouse retinal pigment epithelial cells exhibit a thiocyanate-selective conductance. *Am. J. Physiol. Cell Physiol.* 315:C457–C473. <https://doi.org/10.1152/ajpcell.00231.2017>
- Chen, Y.S., C.R. Green, K. Wang, H.V. Danesh-Meyer, and I.D. Rupenthal. 2015. Sustained intravitreal delivery of connexin43 mimetic peptide by poly(D,L-lactide-co-glycolide) acid micro- and nanoparticles - Closing the gap in retinal ischaemia. *Eur. J. Pharm. Biopharm.* 95:378–386. <https://doi.org/10.1016/j.ejpb.2014.12.005>
- Contreras, J.E., H.A. Sánchez, E.A. Eugenin, D. Speidel, M. Theis, K. Willecke, F.F. Bukauskas, M.V.L. Bennett, and J.C. Sáez. 2002. Metabolic inhibition induces opening of unapposed connexin 43 gap junction

- hemichannels and reduces gap junctional communication in cortical astrocytes in culture. *Proc. Natl. Acad. Sci. USA.* 99:495–500. <https://doi.org/10.1073/pnas.012589799>
- Coulon, P., and C.E. Landisman. 2017. The potential role of gap junctional plasticity in the regulation of state. *Neuron.* 93:1275–1295. <https://doi.org/10.1016/j.neuron.2017.02.041>
- Decrock, E., M. Vinken, E. de Vuyst, D.V. Krysko, K. D’Herde, T. Vanhaecke, P. Vandenabeele, V. Rogiers, and L. Leybaert. 2009. Connexin-related signaling in cell death: to live or let die? *Cell Death Differ.* 16:524–536. <https://doi.org/10.1038/cdd.2008.196>
- Devries, S.H. 1999. Correlated firing in rabbit retinal ganglion cells. *J. Neurophysiol.* 81:908–920. <https://doi.org/10.1152/jn.1999.81.2.908>
- D’hondt, C., J. Iyyathurai, B. Himpens, L. Leybaert, and G. Bultynck. 2014. Cx43-hemichannel function and regulation in physiology and pathophysiology: insights from the bovine corneal endothelial cell system and beyond. *Front. Physiol.* 5:348. <https://doi.org/10.3389/fphys.2014.00348>
- Falk, M.M., R.M. Kells, and V.M. Berthoud. 2014. Degradation of connexins and gap junctions. *FEBS Lett.* 588:1221–1229. <https://doi.org/10.1016/j.febslet.2014.01.031>
- Fortier, P.A., and M. Bagna. 2006. Estimating conductances of dual-recorded neurons within a network of coupled cells. *J. Theor. Biol.* 240:501–510. <https://doi.org/10.1016/j.jtbi.2005.10.009>
- Goldberg, G.S., V. Valiunas, and P.R. Brink. 2004. Selective permeability of gap junction channels. *Biochim. Biophys. Acta.* 1662:96–101. <https://doi.org/10.1016/j.bbame.2003.11.022>
- Goodenough, D.A., and D.L. Paul. 2003. Beyond the gap: functions of unpaired connexon channels. *Nat. Rev. Mol. Cell Biol.* 4:285–294. <https://doi.org/10.1038/nrml072>
- Goodenough, D.A., and D.L. Paul. 2009. Gap junctions. *Cold Spring Harb. Perspect. Biol.* 1:a002576. <https://doi.org/10.1101/cshperspect.a002576>
- Goodenough, D.A., J.A. Goliger, and D.L. Paul. 1996. Connexins, connexons, and intercellular communication. *Annu. Rev. Biochem.* 65:475–502. <https://doi.org/10.1146/annurev.bi.65.070196.002355>
- Hudspeth, A.J., and A.G. Yee. 1973. The intercellular junctional complexes of retinal pigment epithelia. *Invest. Ophthalmol.* 12:354–365.
- Hutnik, C.M.L., C.E. Pocrnich, H. Liu, D.W. Laird, and Q. Shao. 2008. The protective effect of functional connexin43 channels on a human epithelial cell line exposed to oxidative stress. *Invest. Ophthalmol. Vis. Sci.* 49:800–806. <https://doi.org/10.1167/iov.07-0717>
- Ishii, M., and B. Rohrer. 2017. Mechanisms of bystander effects in retinal pigment epithelial cell networks. *Cell Death Dis.* 8:e3061. <https://doi.org/10.1038/cddis.2017.449>
- Janssen-Bienhold, U., R. Dermietzel, and R. Weiler. 1998. Distribution of Connexin43 immunoreactivity in the retinas of different vertebrates. *J. Comp. Neurol.* 396:310–321. [https://doi.org/10.1002/\(SICI\)1096-9861\(19980706\)396:3<310::AID-CNE3>3.0.CO;2-5](https://doi.org/10.1002/(SICI)1096-9861(19980706)396:3<310::AID-CNE3>3.0.CO;2-5)
- Johansson, J.K., V. Karema-jokinen, S. Hakanen, A. Jylha, H. Uusitalo, M. Vihinen-Ranta, H. Skottman, T.O. Ihalainen, and S. Nyman. 2019. Sodium channels enable fast electrical signaling and regulate phagocytosis in the retinal pigment epithelium. *BMC Biol.* 17:63. <https://doi.org/10.1186/s12915-019-0681-1>
- Kapur, J.N., P.K. Sahoo, and A.K.C. Wong. 1985. A new method for gray-level picture thresholding using the entropy of the histogram. *CVGIP.* 29: 273–285.
- Korkka, I., T. Viheriälä, K. Juuti-Uusitalo, H. Uusitalo-järvinen, H. Skottman, J. Hyttinen, and S. Nyman. 2019. Functional voltage-gated calcium channels are present in human embryonic stem cell-derived retinal pigment epithelium. *Stem Cells Transl. Med.* 8:179–193. <https://doi.org/10.1002/sctm.18-0026>
- Laird, D.W. 2006. Life cycle of connexins in health and disease. *Biochem. J.* 394:527–543. <https://doi.org/10.1042/BJ20051922>
- Lee, Y.T., and Q. Wang. 1999. Inhibition of hKv2.1, a major human neuronal voltage-gated K<sup>+</sup> channel, by meflofenamic acid. *Eur. J. Pharmacol.* 378: 349–356. [https://doi.org/10.1016/S0014-2999\(99\)00485-9](https://doi.org/10.1016/S0014-2999(99)00485-9)
- Liu, Z., O.P. Kocaoglu, and D.T. Miller. 2016. 3D imaging of retinal pigment epithelial cells in the living human retina. *Invest. Ophthalmol. Vis. Sci.* 57: OCT533. <https://doi.org/10.1167/IOVS.16-11016>
- Ma, B., R. Buckalew, Y. Du, C.M. Kiyoshi, C.C. Alford, W. Wang, D.M. Mctigue, J.J. Enearty, D. Terman, and M. Zhou. 2016. Gap junction coupling confers isopotentiality on astrocyte syncytium. *Glia.* 64:214–226. <https://doi.org/10.1002/glia.22924>
- Malfait, M., P. Gomez, T.A.B. van Veen, J.B. Parys, H. de Smedt, J. Vereecke, and B. Himpens. 2001. Effects of hyperglycemia and protein kinase C on Connexin43 expression in cultured rat retinal pigment epithelial cells. *J. Membr. Biol.* 181:31–40. <https://doi.org/10.1007/S0023200100082>
- Miličević, N., O. Ait-Hmyed Hakkari, U. Bagchi, C. Sandu, A. Jongejan, P.D. Moerland, J.B. ten Brink, D. Hicks, A.A. Bergen, and M.P. Felder-Schmittbuhl. 2021. Core circadian clock genes Per1 and Per2 regulate the rhythm in photoreceptor outer segment phagocytosis. *FASEB J.* 35: e21722. <https://doi.org/10.1096/fj.202100293RR>
- Müller, C., N. Más Gómez, P. Ruth, and O. Strauss. 2014. Cav1.3 L-type channels, maxiK Ca<sup>2+</sup>-dependent K<sup>+</sup> channels and bestrophin-1 regulate rhythmic photoreceptor outer segment phagocytosis by retinal pigment epithelial cells. *Cell Signal.* 26:968–978. <https://doi.org/10.1016/j.cellsig.2013.12.021>
- Murphy-Baum, B.L., and G.B. Awatramani. 2018. An old neuron learns new tricks: redefining motion processing in the primate retina. *Neuron.* 97: 1205–1207. <https://doi.org/10.1016/j.neuron.2018.03.007>
- Ning, N., Y. Wen, Y. Li, and J. Li. 2013. Meflofenamic acid blocks the gap junction communication between the retinal pigment epithelial cells. *Hum. Exp. Toxicol.* 32:1164–1169. <https://doi.org/10.1177/0960327112472997>
- Orellana, J.A. 2016. Physiological functions of Glial cell hemichannels. *Adv. Exp. Med. Biol.* 949:93–108. [https://doi.org/10.1007/978-3-319-40764-7\\_5](https://doi.org/10.1007/978-3-319-40764-7_5)
- Pearson, R.A., M. Catsicas, D.L. Becker, P. Bayley, N.L. Lüneborg, and P. Mobbs. 2004. Ca<sup>2+</sup> signalling and gap junction coupling within and between pigment epithelium and neural retina in the developing chick. *Eur. J. Neurosci.* 19:2435–2445. <https://doi.org/10.1111/j.0953-816X.2004.03338.x>
- Pearson, R.A., N. Dale, E. Llaudet, and P. Mobbs. 2005. ATP released via gap junction hemichannels from the pigment epithelium regulates neural retinal progenitor proliferation. *Neuron.* 46:731–744. <https://doi.org/10.1016/j.neuron.2005.04.024>
- Peretz, A., N. Degani, R. Nachman, Y. Uziyel, G. Gibor, D. Shabat, and B. Attali. 2005. Meflofenamic acid and diclofenac, novel templates of KCNQ2/Q3 potassium channel openers, depress cortical neuron activity and exhibit anticonvulsant properties. *Mol. Pharmacol.* 67:1053–1066. <https://doi.org/10.1124/MOL.104.007112>
- Pogoda, K., P. Kameritsch, M.A. Retamal, and J.L. Vega. 2016. Regulation of gap junction channels and hemichannels by phosphorylation and redox changes: a revision. *BMC Cell Biol.* 17:11. <https://doi.org/10.1186/s12860-016-0099-3>
- Potter, J.A., G.W. Price, C.L. Cliff, B.M. Williams, C.E. Hills, and P.E. Squires. 2021. Carboxyfluorescein dye uptake to measure connexin-mediated hemichannel activity in cultured cells. *Bio Protoc.* 11:e3901. <https://doi.org/10.21769/BIOPROT.3901>
- Quist, A.P., S.K. Rhee, H. Lin, and R. Lal. 2000. Physiological role of gap-junctional hemichannels: extracellular calcium-dependent isosmotic volume regulation. *J. Cell Biol.* 148:1063–1074. <https://doi.org/10.1083/JCB.148.5.1063>
- Ramadan, R., E. Vromans, D.C. Anang, I. Goetschalckx, D. Hoorelbeke, E. Decrock, S. Baatout, L. Leybaert, and A. Aerts. 2020. Connexin43 hemichannel targeting with TAT-Gap19 alleviates radiation-induced endothelial cell damage. *Front. Pharmacol.* 11:212. <https://doi.org/10.3389/fphar.2020.00212>
- Rassi Gabriel, L.A., R. Sachdeva, A. Marcotty, E.J. Rockwood, and E.I. Traubouli. 2011. Oculodentodigital dysplasia: new ocular findings and a novel connexin 43 mutation. *Arch. Ophthalmol.* 129:781–784. <https://doi.org/10.1001/archophthol.2011.113>
- Raviola, E., and N.B. Gilula. 1973. Gap junctions between photoreceptor cells in the vertebrate retina. *Proc. Natl. Acad. Sci. USA.* 70:1677–1681. <https://doi.org/10.1073/pnas.70.6.1677>
- Reichardt, N., and O. Strauss. 2014. Ion channels and transporters of the retinal pigment epithelium. *Exp. Eye Res.* 126:27–37. <https://doi.org/10.1016/j.exer.2014.05.005>
- Rizzolo, L.J. 2014. Barrier properties of cultured retinal pigment epithelium. *Exp. Eye Res.* 126:16–26. <https://doi.org/10.1016/j.exer.2013.12.018>
- Schalper, K.A., N. Palacios-Prado, J.A. Orellana, and J.C. Sáez. 2008. Currently used methods for identification and characterization of hemichannels. *Cell Commun. Adhes.* 15:207–218. <https://doi.org/10.1080/15419060802014198>
- Schneider, C.A., W.S. Rasband, and K.W. Eliceiri. 2012. NIH image to ImageJ: 25 years of image analysis. *Nat. Methods.* 9:671–675. <https://doi.org/10.1038/nmeth.2089>
- Sparrow, J.R., D. Hicks, and C.P. Hamel. 2010. The retinal pigment epithelium in health and disease. *Curr. Mol. Med.* 10:802–823. <https://doi.org/10.2174/156652410793937813>
- Strauss, O. 2005. The retinal pigment epithelium in visual function. *Physiol. Rev.* 85:845–881. <https://doi.org/10.1152/physrev.00021.2004>

- Tarzemany, R., G. Jiang, J.X. Jiang, H. Larjava, and L. Häkkinen. 2017. Connexin 43 hemichannels regulate the expression of wound healing-associated genes in human gingival fibroblasts. *Sci. Rep.* 7:14157. <https://doi.org/10.1038/s41598-017-12672-1>
- Tibber, M.S., D. Becker, and G. Jeffery. 2007. Levels of transient gap junctions between the retinal pigment epithelium and the neuroblastic retina are influenced by catecholamines and correlate with patterns of cell production. *J. Comp. Neurol.* 503:128–134. <https://doi.org/10.1002/cne.21388>
- Trenholm, S., and G.B. Awatramani. 2017. Dynamic Properties of Electrically Coupled Retinal Networks. In *Network Functions and Plasticity: Perspectives from Studying Neuronal Electrical Coupling in Microcircuits*. Elsevier, New York. pp. 183–208.
- Vaajasaari, H., T. Ilmarinen, K. Juuti-Uusitalo, K. Rajala, N. Onnela, S. Narkilahti, R. Suuronen, J. Hyttinen, H. Uusitalo, and H. Skottman. 2011. Toward the defined and xeno-free differentiation of functional human pluripotent stem cell-derived retinal pigment epithelial cells. *Mol. Vis.* 17:558–575.
- van Campenhout, R., A. Cooreman, K. Leroy, O.M. Rusiecka, P. van Brantegem, P. Annaert, S. Muyldermans, N. Devoogdt, B. Cogliati, B.R. Kwak, and M. Vinken. 2020. Non-canonical roles of connexins. *Prog. Biophys. Mol. Biol.* 153:35–41. <https://doi.org/10.1016/j.pbiomolbio.2020.03.002>
- Vasconcellos, J.P.C., M.B. Melo, R.B. Schimitti, N.C. Bressanim, F.F. Costa, and V.P. Costa. 2005. A novel mutation in the GJA1 gene in a family with oculodentodigital dysplasia. *Arch. Ophthalmol.* 123:1422–1426. <https://doi.org/10.1001/archophth.123.10.1422>
- Viheriala, T., J. Sorvari, T.O. Ihalainen, A. Sorkio, P. Gronroos, S. Schlie-Wolter, B. Chichkov, H. Skottman, S. Nymark, and T. Ilmarinen. 2021. Culture surface protein coatings affect the barrier properties and calcium signalling of hESC-RPE. *Sci. Rep.* 11:933. <https://doi.org/10.1038/s41598-020-79638-8>
- Wimmers, S., M.O. Karl, and O. Strauss. 2007. Ion channels in the RPE. *Prog. Retin. Eye Res.* 26:263–301. <https://doi.org/10.1016/j.preteyeres.2006.12.002>
- Wollmann, G., S. Lenzner, W. Berger, R. Rosenthal, M.O. Karl, and O. Strauss. 2006. Voltage-dependent ion channels in the mouse RPE: comparison with Norrie disease mice. *Vis. Res.* 46:688–698. <https://doi.org/10.1016/j.visres.2005.08.030>
- Xu, G., W.E.I. Wang, H.K. Kimelberg, and M.I.N. Zhou. 2010. Electrical coupling of astrocytes in rat hippocampal slices under physiological and simulated ischemic conditions. *Glia.* 58:481–493. <https://doi.org/10.1002/glia.20939>
- Zhang, Y.W., I. Morita, M. Ikeda, K.W. Ma, and S. Murota. 2001. Connexin43 suppresses proliferation of osteosarcoma U2OS cells through post-transcriptional regulation of p27. *Oncogene.* 20:4138–4149. <https://doi.org/10.1038/sj.onc.1204563>



# PUBLICATION

## III

**CDK5 activity in retinal pigment epithelium contributes to gap junction phosphorylation and dynamics during photoreceptor outer segment phagocytosis**

Fadjukov J., Wienbar S., Milićević N., Hakanen S., Vihinen-Ranta M., Ihalainen T.O., Schwartz G.W., Nymark S.

Manuscript

**Publication reprinted with the permission of the copyright holders**



